Ocean Engineering Studies

Compiled 1991

Volume IX: External Pressure Housing—Concrete

J. D. Stachiw

NAVAL OCEAN SYSTEMS CENTER

Ocean Engineering Studies

Compiled 1991

Volume IX: External Pressure Housings—Concrete

J. D. Stachiw

PUBLISHED BY
NAVAL OCEAN SYSTEMS CENTER
SAN DIEGO, CALIFORNIA

Foreword

Exploitation of the ocean floor for commercial or military use requires not only Remotely Operated Vehicles (ROVs), Autonomous Underwater Vehicles (AUVs), submersibles, and diving systems; it also requires 1-atmosphere enclosures permanently—or semipermanently—affixed to the ocean floor. These 1-atmosphere enclosures would serve as habitats for the crews, covers for mine shafts, and pressure-existent buildings for ore or food-processing plants. Bottom-mounted pressure-resistant enclosures must be negatively buoyant, instead of positively buoyant (as they are with pressure hulls for submersibles). This allows them to be constructed from inexpensive materials with low specific compressive strength.

The primary choice for such applications is Portland cement concrete, since it is inexpensive, can be cast in situ, does not deteriorate under long-term immersion, and has a fair specific compressive strength. In fact, its specific compressive strength is high enough to qualify the material as a viable candidate for use in constructing large submarine oil tankers that require pressure hulls with only marginal positive buoyancy.

Since concrete has not previously been used for constructing pressure–resistant shells for ocean engineering structures, there was a total absence of engineering data on which to base the design of any pressure–resistant concrete housings for U.S. Navy applications. To make up for this deficiency, the U.S. Navy initiated a research program whose objective was to generate sufficient data to enable formulation of design criteria to construct concrete pressure housings. The principal investigators were Dr. Stachiw, and Messrs. Haynes, Albertsen, Kahn, Highberg, and Hoofnagle. The reports these investigators produced effectively summarize the scope and results of the research program.

The results of the program were sufficiently encouraging and comprehensive to allow formulation of design criteria for use by U.S. Navy engineers. The performance of model scale concrete housings employed in the research program provided the data to use for confidently designing full-scale pressure–resistant concrete enclosures with an infinite lifetime.

Volume IX is a compilation of reports that summarize the studies on 15-inch diameter spherical test specimens to experimentally evaluate the effect of wall thickness, impregnation, reinforcement techniques, and penetrations on critical pressure, creep, and permeability.

Volume X is a compilation of reports that summarize the studies on (1) 15-inch diameter cylinders and (2) 66-inch diameter spheres under short-term and long-term loading. This volume also contains the design criteria and recommendations formulated at the conclusion of the research program on concrete external–pressure housings.

J. D. Stachiw
Marine Materials Office
Ocean Engineering
Division

TABLE OF CONTENTS: VOLUME IX

R 317

Technical Report

BEHAVIOR OF SPHERICAL CONCRETE HULLS UNDER HYDROSTATIC LOADING PART I. EXPLORATORY INVESTIGATION

March 1967

NAVAL FACILITIES ENGINEERING COMMAND

U. S. NAVAL CIVIL ENGINEERING LABORATORY

Port Hueneme, California

BEHAVIOR OF SPHERICAL CONCRETE HULLS UNDER HYDROSTATIC LOADING PART I. EXPLORATORY INVESTIGATION

Technical Report R-517

Y-F015-01-07-001

by

J. D. Stachiw and K. O. Gray

ABSTRACT

Hollow concrete spheres 16 inches in outside diameter have been tested to destruction by exposure to external hydrostatic pressure in seawater to determine the compressive strength and permeability of concrete under such loading. The testing has shown that for the particular mix used, the compressive strength of dry concrete in a spherical hull of 16-inch outside diameter and 1-inch wall thickness under biaxial loading (short-term hydrostatic pressurization to failure at a constant rate) is approximately 48% higher than for identical dry concrete in 3-inch-diameter by 6-inch-long solid test cylinders under uniaxial loading conditions. Concrete spheres in which the wall was thoroughly permeated by seawater failed at stress levels approximately 18% higher than 3-inch-diameter by 6-inch-long solid test cylinders. The permeability of uncoated spheres to seawater at simulated ocean pressure of 1,500 psi was approximately 6×10^{-3} milliliters per hour per square inch of area per 1 inch of thickness.

CONTENTS

INTRODUCTION

The Naval Facilities Engineering Command is responsible for the construction and maintenance of underwater structures attached to the ocean floor.

The conquest of hydrospace requires both mobile and fixed underwater structures capable of housing instruments and men for extended periods of time. There is a long history of research on the properties of materials and the design of hulls suitable for submarines; however, the research into materials and designs for static underwater hull structures is just beginning.

Although many materials developed for submarine or torpedo hulls are also applicable to fixed, ocean-bottom installations, there are many materials which have not received careful study because of their manifest inapplicability to submarines or torpedoes. One such material is concrete.

The purpose of this report is to describe a brief exploratory investigation into the applicability of concrete for the fabrication of structural hulls for deep submergence structures.* The scope of this series of experiments was limited to an examination of only three of the many performance characteristics of concrete in a deep ocean environment. These three study objectives were the short-term compressive strength, the long-term compressive strength, and the permeability of concrete (in the form of a hull model) to seawater under simulated deep ocean conditions.

BACKGROUND

Concrete has been used in harbor installations for many decades, but it has not been used for deep submergence structures. There are several reasons for this. Since concrete is not desirable for submarine hull construction, no research was done on its properties under seawater hydrostatic pressure prior to the recent interest in fixed, ocean-floor installations. Furthermore, the impetus of research has been directed towards the discovery of new materials that would give buoyancy to a deep submergence hull even at greatest depths in the ocean. The most potent argument used against concrete is that concrete hulls are limited by low compressive strength to depths less that 10,000 feet and therefore cannot satisfy depth requirements that may arise in the future. Thus the philosophy appears to have been that since concrete was definitely depth limited, there was no need to conduct research on its structural characteristics as a stop-gap solution to the problem of finding suitable materials for deep submergence structures.

---

* In this report "deep submergence" is used to refer to depths greater than 600 feet.

Recently, materials like glass and ceramics have been discovered to possess such high compressive strength, modulus of elasticity, and resistance to corrosion that deep submergence hulls for fixed or mobile installations can be built for any depth. Unfortunately, although glass and ceramics have the potential of providing man with hulls of ultimate depth capability, they are too expensive for applications in shallow depths where their use is not mandatory. Since currently available materials with the ultimate depth capability have been found impractical for general use because of their high costs of fabrication, the path has been cleared for other materials with limited depth capabilities, but with an attractive cost factor. Such a material is concrete, which is theoretically satisfactory for hulls with an operational depth requirement of 3,000 to 4,000 feet. In addition preliminary estimates indicate that it is more economical than other available metallic or nonmetallic materials when used in large structures.

The depth capability of 3,000 to 4,000 feet of buoyant concrete structures permits the utilization of such structures over large areas of the continental borderlands. About 12% to 14% of the ocean floor can be explored and settled using concrete as the primary hull construction material for the ocean floor installations. While the portion of ocean floor that could be made accessible through the use of concrete hulls is small in comparison to the total ocean area, in terms of importance, it is a most critical part of the total. The reason for its importance is found in the presence of large continental borderlands made up of shelves, and submerged banks in the 3,500-foot depth range. Since these shelves and banks are generally flat to gently sloping, and since they are also in the general vicinity of land, they make ideal construction sites.

The areas of primary interest to the United States are directly accessible from this country without traversing ocean floors that are under another country's sovereignty. By occupying the shelves and banks adjacent to the United States in the 0- to 3,500-foot depth range, the land area of the United States could be extended approximately 23% (Figures 1-3).

In summary, it can be stated that although there is a need to develop materials and structures with ultimate depth capability, development of materials and structures for depths to 3,500 feet is more important in terms of national defense and natural resources. Since concrete has been in many cases the most economical construction material on land, it should be investigated early in the search for undersea construction materials. It may also turn out to be one of the most economical materials for ocean-floor construction on continental shelves and submarine banks.

EXPERIMENT DESIGN

A literature search revealed studies of concrete for use in dams under low hydrostatic loading with fresh water. This search, however, failed to disclose any previous experimental work with concrete hulls under seawater hydrostatic loading

in excess of 100 psi. Therefore, it was decided first to conduct an exploratory investigation of the use of concrete hulls in seawater imposing a hydrostatic load of more than 100 psi to determine the avenues along which it would be most profitable to direct subsequent studies. Many lines of investigation are possible in such an exploratory study. Not only may different hull shapes be selected, but also their thickness and types of joints. In addition, once the hull shape has been selected, it can be tested for different properties, depending on the requirements of the study.

After considering the environmental conditions imposed on concrete structures on the ocean floor, it was decided to design the hull test models for a maximum operational depth of 3,500 feet and a maximum collapse depth of 7,000 feet. In addition, the models were to possess at least a 0.75 weight-to-displacement ratio. Thus, the exploratory study would be oriented to the continental shelf depth zone and the structures would be in a buoyant structure class and could be towed afloat to a construction site for emplacement on the sea floor. If desired, they could subsequently be retrieved by flotation.

A spherical hull shape was selected for all the test models because it was the only configuration that would meet design criteria (Figures 4 and 5). A big advantage of using a spherical hull for the test model is its inherent uniform distribution of stresses. The stresses encountered in a relatively thin sphere are primarily biaxial, and the magnitudes of the meridional and equatorial membrane stresses are equal and of a compressive nature. Such a stress distribution has previously been found to be beneficial for brittle materials like glass and ceramics and appears to be desirable for concrete — which is also a brittle material, though one with a unique physical structure.

Because of the uniformity of stress distribution, the maximum compressive stress calculated for the spherical hull at implosion can be safely considered to be the actual maximum stress that existed anywhere in the hull. Knowledge of the magnitude of the maximum compressive strength of concrete under equal compressive biaxial membrane stresses, and the smaller compressive radial stress will be extremely useful in the evaluation of future concrete hull models where the presence of discontinuities in the walls will create stress risers that will reduce the ultimate load capacity. Also, in future NCEL studies, the strength of concrete under biaxial membrane stresses of equal magnitudes and radial stress of smaller magnitudes will be compared to the strength of concrete under biaxial stresses of different magnitudes, as in a column. From the comparison of ultimate compressive strengths of concrete under different biaxial and triaxial stress distributions, resulting from hydrostatic loading of the model, NCEL investigators will attempt to formulate a general theory of concrete failure under hydrostatic loading.

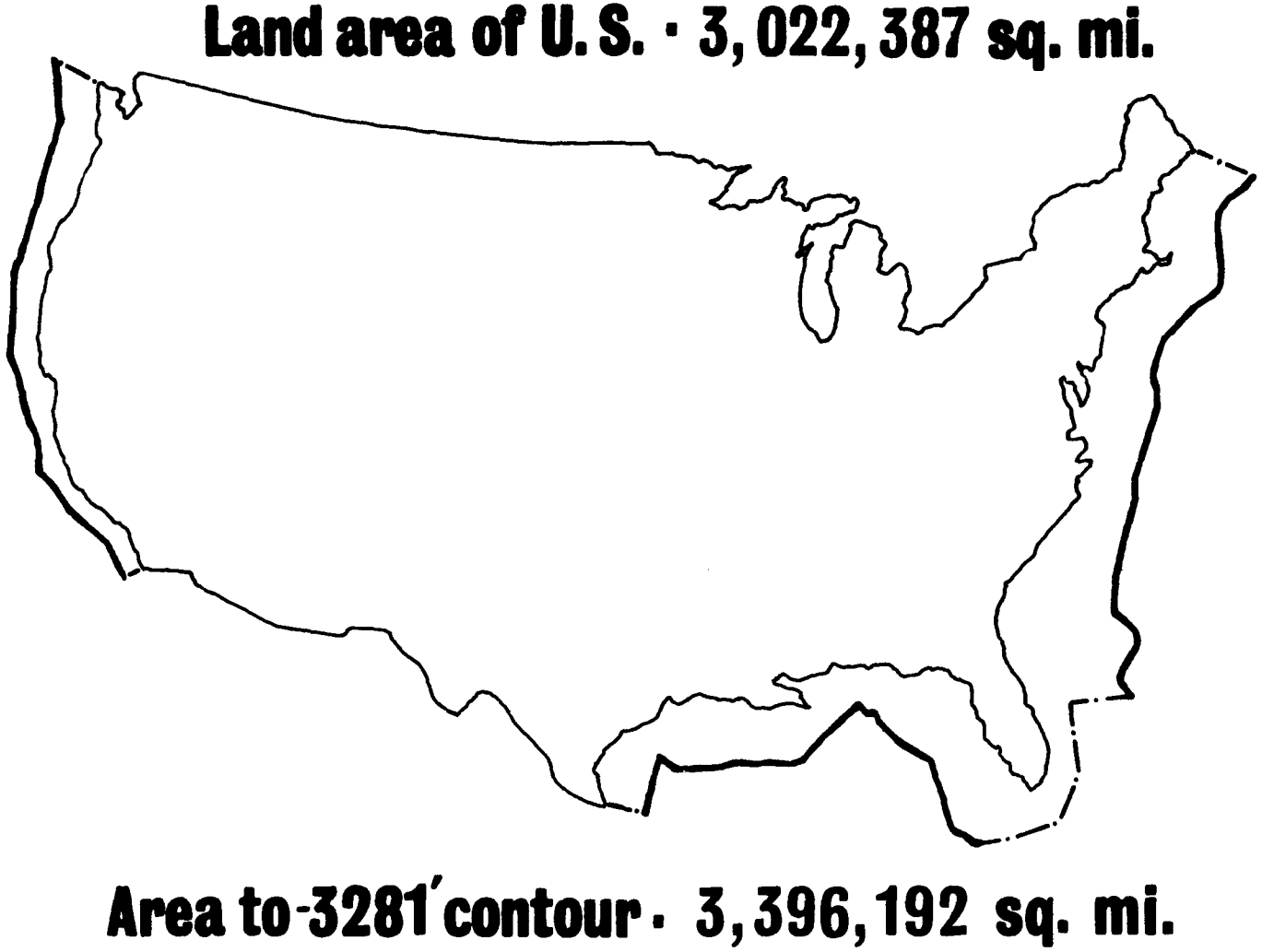

Figure 1. Continental United States, showing the extent of the continental margins lying in the 0- to 3,281-foot depth range.

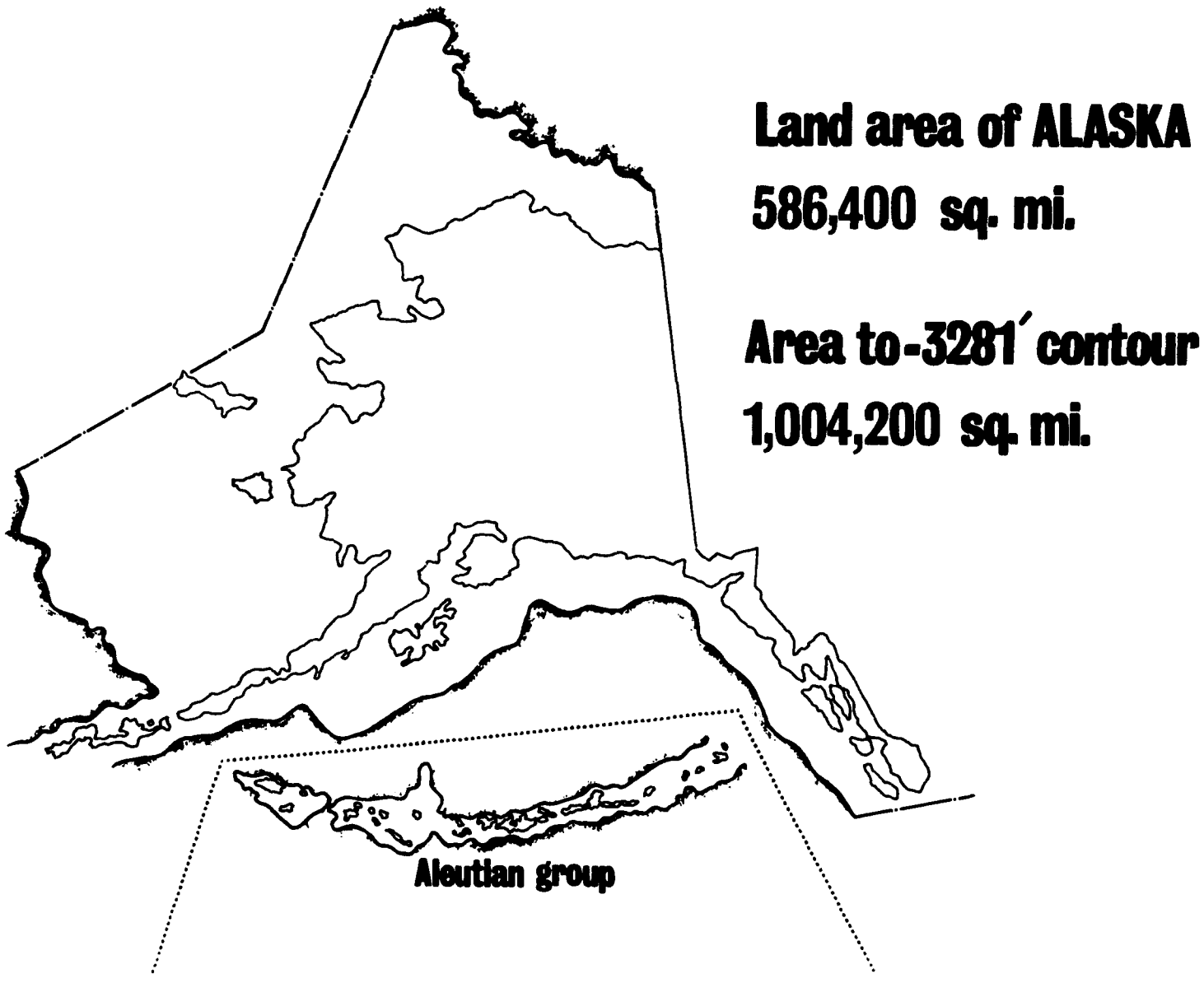

Figure 2. Alaska, showing the extent of the continental margins lying in the 0- to 3,281-foot depth range.

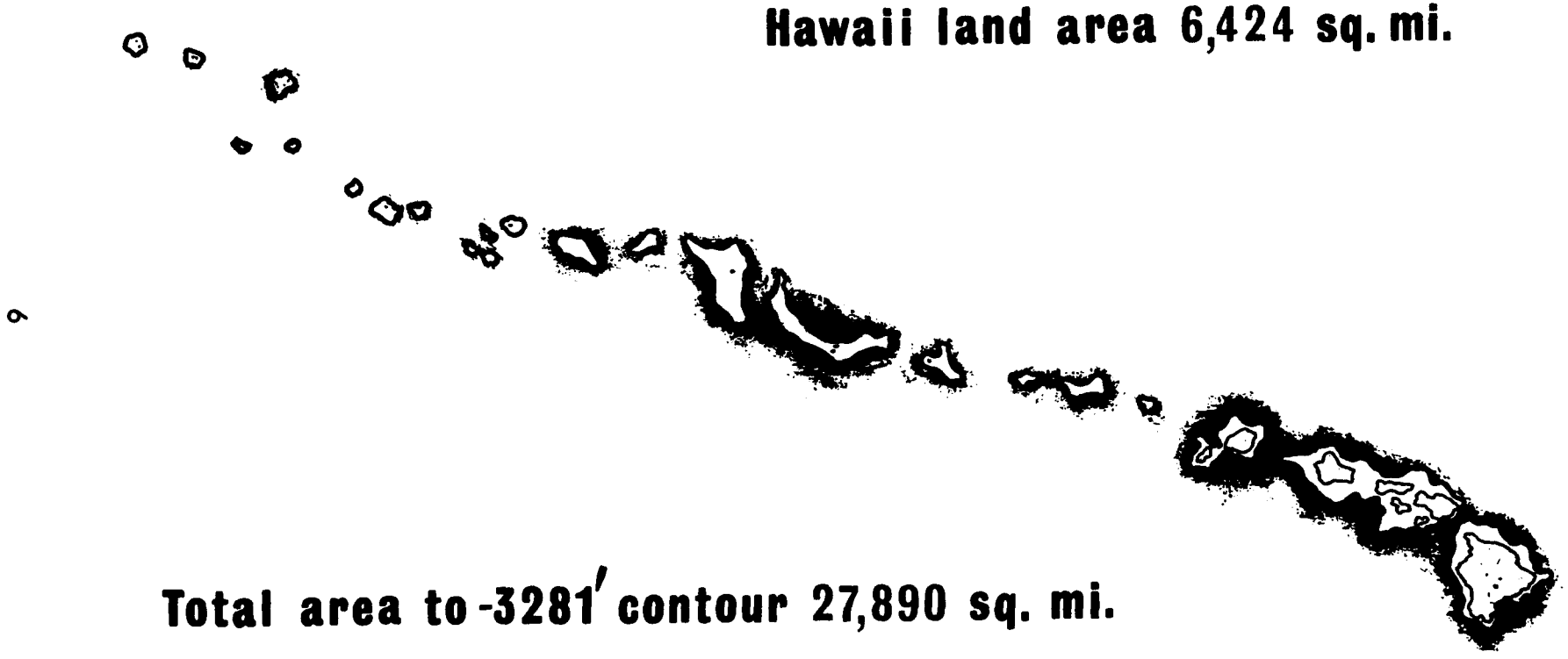

Figure 3. The Hawiian Archipelago, showing the extent of the adjacent insular shelves lying in the 0- to 3,281-foot depth range.

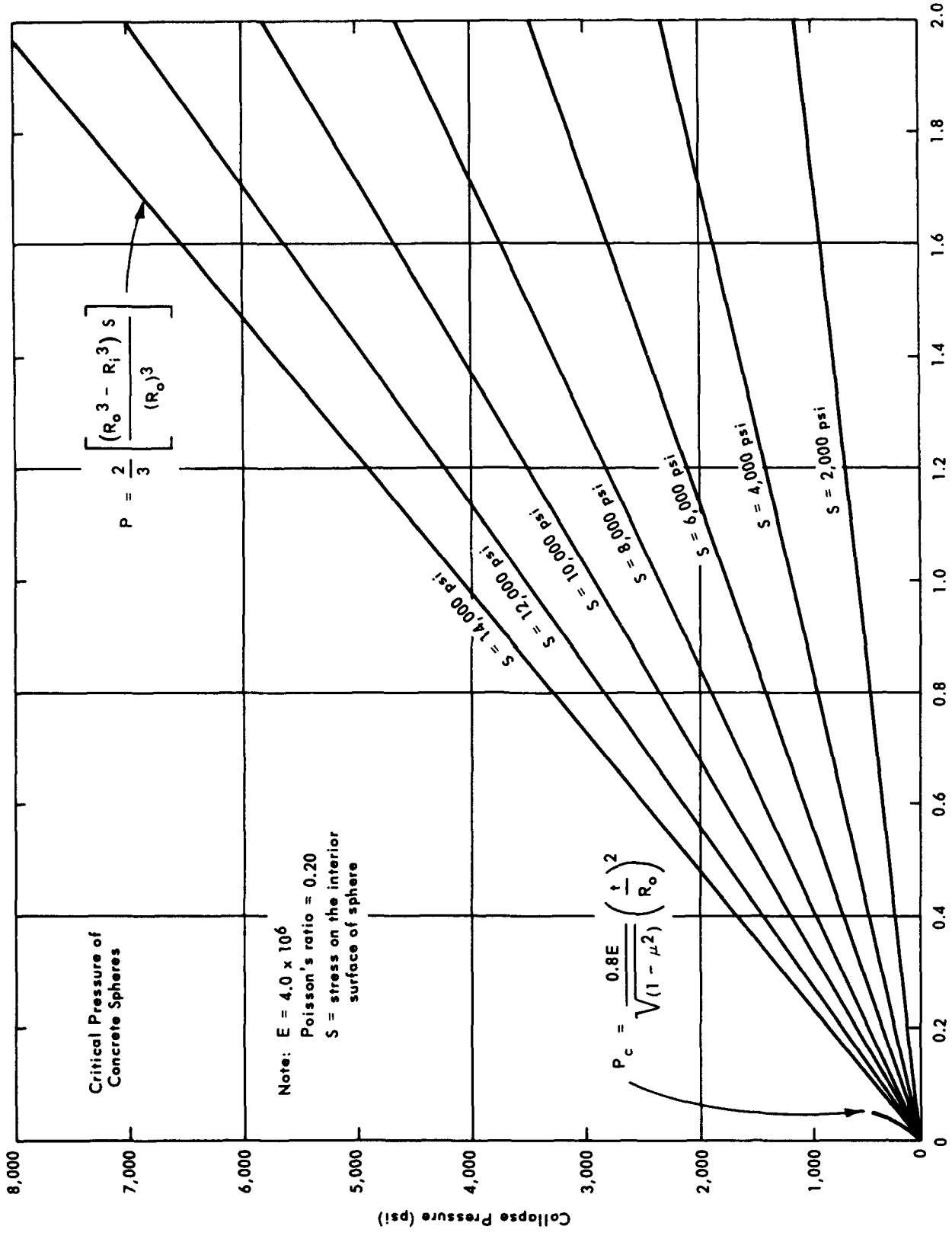

Figure 4. Buoyancy of spherical concrete hulls for undersea applications.

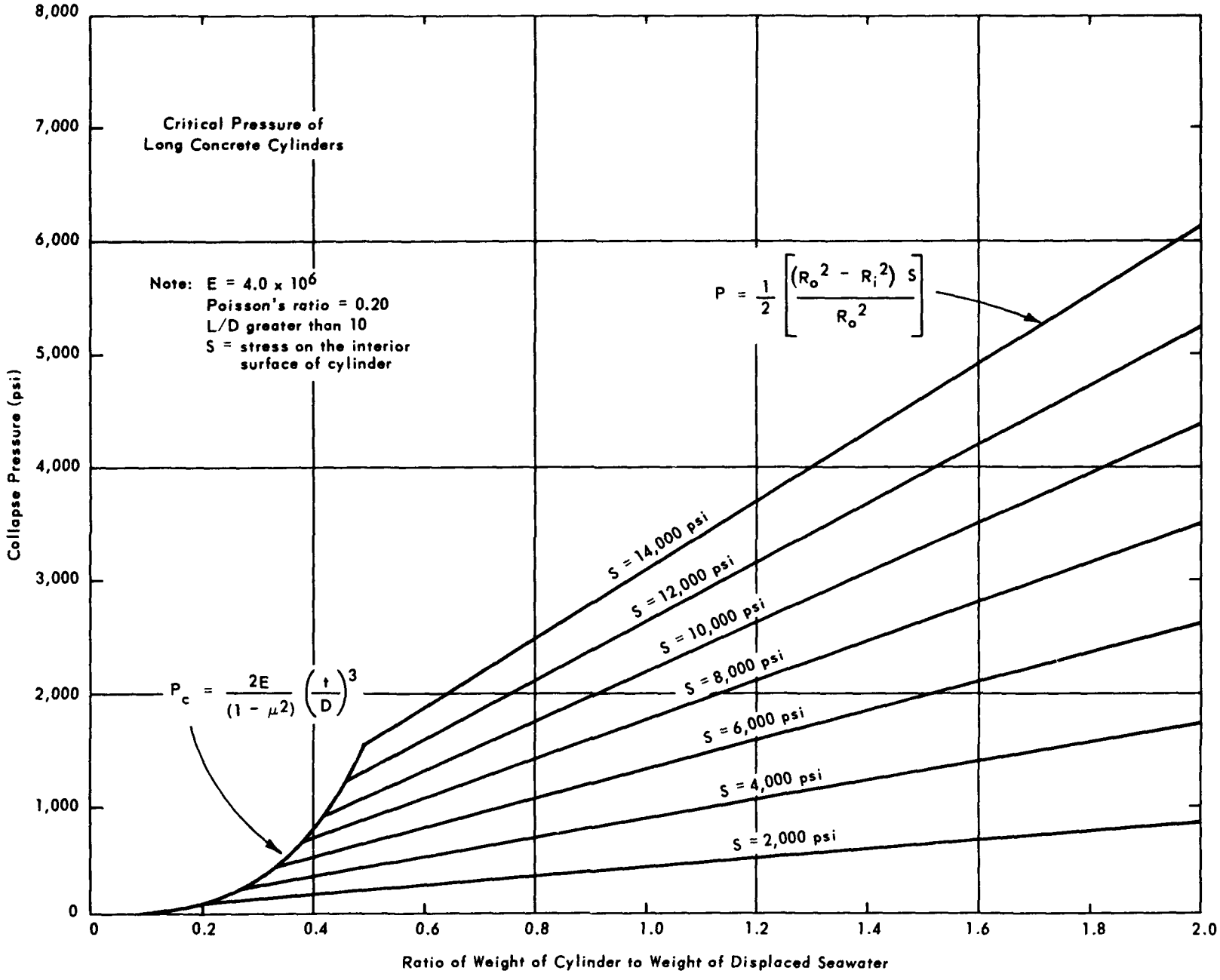

Figure 5. Buoyancy of cylindrical concrete hulls for undersea applications.

The spherical shape is also advantageous for the determination of concrete's permeability under different levels of hydrostatic pressure. Since permeability of concrete is probably related to stress, uniformity of stress in the sphere eliminates any side effects that could be associated with the nonuniform distribution of stresses. A spherical hull also eliminates any anomalies caused by edge effects of the test sample, as would be found, for example, in a flat specimen mounted in some sort of a flange. Furthermore, since in a spherical hull there is also continuity of curvature, a reasonable assumption can be made that the leakage of water through the walls of the sphere will be uniform throughout, and thus only the level of water in the sphere must be known in order to determine a nominal rate of leakage through the given concrete mix.

In view of the lack of previous research in the undersea use of concrete hulls, it was decided to use the exploratory study with concrete spheres to touch upon several facets of the field rather than research any one of them exhaustively. Thus, in this study hydrostatic tests on 12 concrete spheres have been employed to explore the ultimate compressive strength of concrete under short-term and long-term loading — the latter at hydrostatic pressures approaching the critical pressure. Experiments were also conducted to investigate the leakage of water through unprotected concrete at different hydrostatic pressure levels. Because of the exploratory nature of these tests, only one to three spheres were tested in each type of experiment. Experimental data from such a small number of test samples are considered to be indicators of the general level of magnitude of the parameters studied, but not conclusive and final evidence of these parameters. Once the general magnitude of the parameters investigated is known, an accurate plan can be drawn up for future experiments to more thoroughly evaluate and define the physical and mechanical properties of concrete under the external hydrostatic pressure of seawater.

SPECIMEN DESIGN

The concrete spheres (fabricated from two hemispheres joined equatorially) were designed to fail as a result of material failure rather than elastic instability. The 16-inch outside diameter of the sphere was set by the 18-inch internal diameter of the largest pressure vessel available at NCEL's Deep Ocean Simulation Laboratory. The minimum shell thickness required to have the sphere fail both by material fracture and elastic instability was established by equating the pressures from the elastic stability and the maximum compressive stress formulas and solving both equations for the shell thickness at which the sphere fails simultaneously by material fracture and elastic instability. Once that thickness is determined it is considered the minimum shell thickness. If the sphere is made with a shell thinner than this minimum dimension, it will fail by buckling due to elastic instability, while if it is made with a thicker shell it will fail by material fracture or plastic instability.

Using (1) the formula for membrane stresses in thick spheres[1]

$$S = - P \frac{R_o^3 \left(R_i^3 + 2R^3\right)}{2R^3 \left(R_o^3 - R_i^3\right)} \qquad (1)$$

where P = external hydrostatic pressure, psi

R_o = external radius, inches

R_i = internal radius, inches

R = radius for which membrane stresses are calculated, inches

S = meridional, or hoop membrane stress, psi

and (2) the elastic stability equation for spheres[2]

$$P_c = \frac{0.8E\left(\frac{R_o - R_i}{R_o}\right)^2}{\sqrt{1 - \mu^2}} \qquad (2)$$

where E = modulus of elasticity, psi

P_c = external hydrostatic pressure at which critical pressure buckling of the hull occurs, psi

μ = Poisson's ratio

By equating $P = P_c$ one obtains a set of equations that can be satisfied only by one particular R_i for a given R_o, maximum S at R_i, and E of a given material. Solving the set of equations for $R_o = 8$ inches (assumed maximum $S = 10{,}000$ psi at R_i, $E = 4 \times 10^6$, and Poisson's ratio 0.2) the minimum shell thickness is calculated to be approximately 0.05 inch. The wall thickness selected for the spheres actually fabricated was 1 inch. This dimension insured not only that the failure of the sphere will take place by material fracture in case E was substantially less than 4×10^6 psi at higher stress levels but also that the spheres will be easy to cast, since commercially available aggregate can be used.

Besides wall thickness, the deviation from nominal sphericity also plays a considerable role in determining whether the sphere will fail in the elastic instability mode, or in the fracture-of-material mode. Although accurate and conclusive analytical relationships between the deviation in sphericity and the decrease in the elastic stability of the sphere are not known, some hypotheses[2,3] have been postulated that give at least an approximate relationship between these two parameters. The

accepted hypothesis at the present time is that so long as the deviation from sphericity is less than 3% of shell thickness, no allowances for out of roundness have to be made. To avoid the complications from the presence of spherical deviations larger than 3% of shell thickness, the dimensional tolerance on the sphere's radius was kept within ±1/32 inch. No further calculations were made to determine what decrease in elastic stability resulted from any spherical deviation in the structure.

The discussion of sphere design would be incomplete without mention of the equatorial joint between the two hemispheres that make up the sphere. Although only a seamless sphere can be assumed to have no stress concentrations, it is very difficult and uneconomical to build such a sphere. There are many methods for assembling the sphere from structural components in such a manner that the assembly is virtually free of stress concentrations. To mention a few, there is the hemisphere assembly, the orange peel assembly, the dodecahedron, icosahedron, octahedron, and tetrahedron spherical polygon family of assemblies, and other assemblies consisting of irregular spherical structural modules. Since the hemisphere assembly requires the least number of joints, and the dimensional joint tolerances are the easiest to maintain, it was selected for the test spheres.

FABRICATION OF CONCRETE SPHERES

Concrete hemispheres were cast in a mold and cemented together with an epoxy bonding agent. Depending on the type of test, the exterior and interior surfaces were either left untreated or coated with a waterproofing material. A complete discussion of the concrete mix used, the casting, joining and waterproofing techniques is presented in Appendix A.

The treatment of the exterior surface depended upon the type of test for which the given sphere was intended. For the permeability tests, where the rate of water flow through concrete under hydrostatic pressure was under investigation, the exterior surface of the sphere was left untreated, the way it emerged from the mold. For the strain determination tests, on the other hand, where the prime objective of the test was to protect the electric strain gages from seawater, the external surface of the spheres was either protected by a thin coat of Epocast 8288, Epocast Wes-Top 415 polyurethane varnish, or RTV 501 silicone rubber.

HYDROSTATIC TESTING

Instrumentation

Two different types of instrumentation were employed on the concrete spheres. The permeability experiments required instrumentation designed to measure rate of permeability, while the short- and long-term stress investigations needed only strain measuring instruments.

A discussion of the instrumentation techniques utilized is contained in Appendix B.

Testing Procedure

The testing of the concrete spheres under hydrostatic pressure was conducted in the 18-inch pressure vessel of the Deep Ocean Simulation Laboratory (Appendix C summarizes procedures followed in all hydrostatic tests of spheres and contains tabulated data from each test). The spheres were placed in a retaining cage prior to testing so that they would not float in the vessel and strike the end closure (Figure 6) when the vessel was filled with water. The vessel was pressurized by air-operated, positive-displacement pumps that elevated the pressure inside the vessel at a rate of 1,000 psi per minute until implosion occurred. Pressure and temperature sensors located inside the pressure vessel permitted recording of these two parameters on a strip chart recorder. Upon implosion of the concrete spheres, manifesting itself by a loud noise, the end closure was removed and the fragments of the concrete structure were inspected. Figure 7 illustrates the typical fragment size resulting from failure by implosion.

During some of the long-term hydrostatic pressure tests where continuous permeation of concrete took place, a hydraulic circuit was connected to the pressure vessel so that a continuous supply of seawater at the required hydrostatic pressure was available to replace the water (which penetrated into the sphere) and thereby maintain a uniform pressure in the vessel. The level of water collecting in the interior of the sphere was checked three times daily, either by means of the electronic water level detector, or by measuring the volume of water ejected by compressed air from the interior of the sphere through a drainage tube.

Each sphere inserted into the pressure vessel was accompanied by several concrete test cylinders cast from the same mix, and at the same time as the sphere. Upon completion of the test, these test cylinders were removed from the pressure vessel and tested to destruction under uniaxial compression in a constant-strain test machine. Other test cylinders, not exposed to hydrostatic pressure, were divided into two groups, one of which was immersed in a pan of seawater; the other group was left dry. Cylinders from these two groups were also tested to destruction at the same time and in the same manner, and their failure stress used for comparison with the failure stresses obtained from testing the hydrostatically pressurized cylinders.

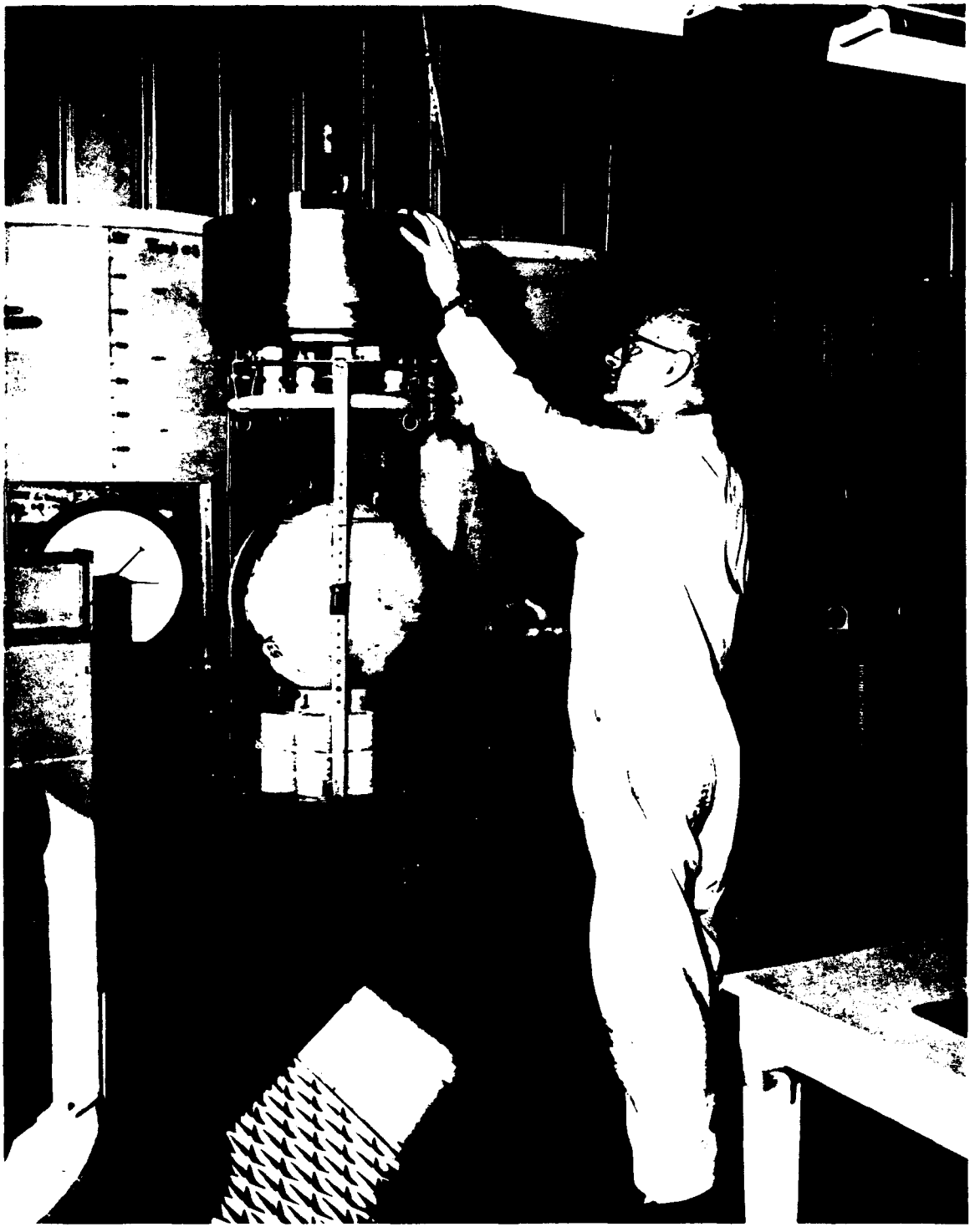

Figure 6. Test assembly including concrete sphere, accompanying test cylinders and pressure vessel end closure.

Figure 7. Fragments of concrete sphere after failure by implosion at 3,100 psi. Size of pieces is typical of all sphere failures except for sphere 7.

DISCUSSION OF TESTS AND RESULTS

Short-Term Strength of Dry Concrete Spheres

The first group of exploratory experiments concerned itself with the ultimate compressive strength of dry concrete under short-term hydrostatic loading. For this purpose, spheres 1, 2, and 3, waterproofed with a heavy coat of epoxy, were imploded; the corresponding 3-inch-diameter by 6-inch-long test cylinders were crushed in uniaxial compression machines, and the resulting data analyzed.

It may be noted from Table 1 that the average ultimate strength of the concrete spheres under hydrostatic loading is approximately 48% higher than for the 3 x 6-inch control cylinders tested under standard conditions. How much of this increase in concrete strength is due to disparity between the size of the test cylinder and the size of the hull is unknown.

In order to obtain some data on the decrease of strength of control cylinders when permeated by water at the implosion pressure of the spheres, several concrete control cylinders were subjected to hydrostatic pressure together with the parent sphere. In an attempt to insure that the test cylinders became permeated, they

were not protected with a waterproof coating. Upon implosion of the concrete sphere, the test cylinders were immediately removed from the pressure vessel and tested to failure under uniaxial compression. Observation of the fractured test cylinders revealed that the water had not penetrated them completely in the short time period (approximately 5 minutes) that it took to pressurize the concrete spheres to their critical pressure. Therefore, the compressive strength of concrete obtained from testing to failure of the partially wetted test cylinders is not representative of the strength of completely wetted concrete. The compressive strength of the partially wetted concrete cylinders, is as a matter of fact, barely distinguishable from the strength of dry test cylinders of the same mix, not subjected to hydrostatic pressure in the vessel.

Table 1. Implosion Pressure and Calculated[1/] Stresses in spheres 1, 2, and 3; and Average Compressive Strength of Test Cylinders Associated With These Spheres

Item	Sphere 1	Sphere 2	Sphere 3	Average
Implosion pressure	3,100 psi	3,050 psi	3,200 psi	3,110 psi
Compressive stress[1/] on the interior of the sphere	14,080 psi	13,860 psi	14,540 psi	14,160 psi
Compressive stress[1/] on the exterior of the sphere	12,530 psi	12,330 psi	12,940 psi	12,600 psi
Average compressive strength of 3 x 6-inch dry test cylinders under uniaxial compression	8,990 psi	9,750 psi	9,930 psi	9,560 psi

1/ Stress calculated with Equation 1.

Short-Term Strength of Wet Concrete Spheres

The second group of exploratory experiments dealt with ultimate compressive strength of wet concrete under short-term hydrostatic loading. Spheres 5 and 12 served as uncoated test specimens (the results of the tests are tabulated in Appendix C). To wet the spheres thoroughly, they were exposed to high hydrostatic pressure until the leakage detectors indicated that water was passing through the wall. After

thorough wetting, the spheres were further pressurized until they failed, and the corresponding test cylinders crushed under uniaxial compression in a constant-strain test machine. This information is summarized in Table 2.

Table 2. Implosion Pressure, Calculated Stress, and Wetting Periods for Spheres 5 and 12; and Average Compressive Strength for the Corresponding Wet and Dry Test Cylinders

Item	Sphere 5	Sphere 12	Average
Implosion pressure	2,850 psi	2,750 psi	2,800 psi
Compressive stress[1] on the interior of the sphere	12,950 psi	12,500 psi	12,720 psi
Compressive stress[1] on the exterior of the sphere	11,550 psi	11,100 psi	11,320 psi
Average compressive strength of 3 x 6-inch dry test cylinders[2]	10,500 psi	11,060 psi	10,780 psi
Average compressive strength of 3 x 6-inch wet test cylinders[2]	8,160 psi	7,790 psi	7,970 psi
Wetting period at 1,500 psi hydrostatic pressure	4 days	13 days	

1/ Calculated stress with Equation 1.
2/ Under uniaxial compression.

Although it is definitely known that the spheres were completely permeated by seawater at the time of implosion, it is not known to what degree the corresponding test cylinders, exposed to the same pressure, were permeated. The thickness of the test cylinders (3 inches, versus 1 inch for the spheres) and the cylinders' lack of an internal cavity into which the displaced air from the concrete pores could escape support the hypothesis that the cylinders were only partially permeated by seawater. Because of this, their compressive strength cannot with certainty be considered as representative of the compressive strength of completely wet concrete under uniaxial compression. Still, the lower compressive strength of these cylinders, which were probably only partially wetted, indicates that the compressive strength of wet concrete under uniaxial compression would decrease at least 20%, and probably more, if complete wetting of the test cylinders were achieved.

There is one additional variable, which was not evaluated, that makes the test results obtained from crushing of wet test cylinders questionable. This variable is the possible micro-cracking of the concrete which occurs during the instantaneous depressurization of the pressure vessel upon implosion of the sphere. This variable may be eliminated in the future by crushing the test cylinders inside the pressure vessel with a uniaxial loading frame while the hydrostatic pressure is held constant.

In general, the comparison between the average stress of 12,720 psi on the interior of the completely wet spheres imploding at the average pressure of 2,800 psi and uniaxial compressive stress of 10,780 psi at the failure of dry test cylinders has shown that the short-term strength of wet concrete under biaxial compression on the interior of a sphere is approximately 18% higher than the compressive strength of identical dry concrete in 3 x 6-inch test cylinders under uniaxial compression. This is considerably less than the 48% increase in strength of dry concrete on the interior of spheres 1, 2, and 3. Thus, it can be concluded that the short-term strength of wet concrete under biaxial compression on the interior of a sphere is approximately 20% less than the strength of dry concrete under biaxial compression on the interior of a sphere. In both cases the yardstick of comparison is the compressive strength of dry 3 x 6-inch concrete cylinders under uniaxial compression. How much of this decrease was caused by the length and magnitude of previous pressurization required to permeate the spheres with seawater is at the present time unknown.

Permeability of Concrete Spheres to Seawater

The third group of exploratory experiments concerned itself with the permeability of unprotected concrete to seawater under hydrostatic pressure. Spheres 6, 11, and 12 served as test specimens (the results of these permeability tests are tabulated in Appendix C). After the permeability tests were completed, all of the spheres were subjected to sufficiently high hydrostatic pressure to cause failure by implosion. In this manner, the same spheres also provided data on the strength of wet concrete.

The rate of seawater seepage into sphere 6 at 750 psi has been measured to be approximately 2.5 milliliters per hour, while for sphere 12 pressurized to 1,500 psi the rate was approximately 5 milliliters per hour. When the leakage rate is divided by the surface area of the sphere, it can be expressed as 6×10^{-3} milliliters per hour per square inch of area per inch of thickness. In both cases the salinity of water siphoned from the interior of the sphere was about 20% lower than the salinity of the pressurization medium. Sphere 11, which was pressurized to 2,000 psi did not show any seepage after 5 days of pressurization. It is also interesting that sphere 6, after pressurization to 750 psi for 20 days and subsequent pressure release and drying did not show any water in its interior when it was repressurized to 1,500 psi and held at that pressure for 7 days.

From this rather sparse data it would appear that permeability of concrete to seawater under high hydrostatic pressure is quite low, and that some chemical or physical phenomena, which occur in the concrete, result in a decrease in the salinity of the water that passes through the concrete sphere wall.

Long-Term Strength of Wet and Dry Concrete Spheres

Although only one sphere was specifically tested for its long-term strength under hydrostatic pressure, some of the data collected from the other spheres is also applicable to this parameter. Since the compressive strength of wet concrete is lower than the strength of dry concrete, an additional variable has been introduced into the tests dealing with the behavior of dry concrete spheres under long-term hydrostatic loading. When waterproofed spheres are subjected to a long-term pressure (equal to 80 to 90% of short-term critical pressure) they may collapse after some period of time and it is never certain whether the collapse was due to a loss of compressive strength caused by wetting of the concrete through a pin hole in the waterproof coating, or was due to static fatigue of dry concrete. Of the coated spheres tested, only those that were coated with epoxy or silicone rubber remained dry to the moment of implosion. This dryness of the sphere walls is inferred from observations of similarly coated test cylinders which were examined after being crushed in the test machine.

This uncertainty does not exist when uncoated spheres are subjected to long-term hydrostatic pressure, since in this case it can be experimentally arranged to have the walls of the sphere completely permeated by water at a lower pressure prior to subjecting the sphere to the actual long-term pressure test. Although the data collected on wetted concrete spheres is sparse, an inference can be drawn that static fatigue does take place at hydrostatic pressures that are close to short-term critical pressure.

The performance of the single concrete sphere (number 8) that definitely was not permeated during the long-term pressure application shows that the resistance of dry concrete to static fatigue is superior to that of wet concrete. (See Table 3.)

Deformation of Concrete Spheres Under Short-Term Loading

Although five spheres were instrumented to some degree with electric resistance strain gages, only sphere 8 had a sufficient number of gages to permit comparison of strains measured by several strain gages.

In general, it can be stated, that the measured strains (Figures 8-13) both on the outside and inside of the sphere were uniform and that the difference between individual strain readings at various locations on the same surface was less than 10%. This relative lack of variation in strain reading between individual gages on the same sphere surface indicates true sphericity and uniform wall thickness.

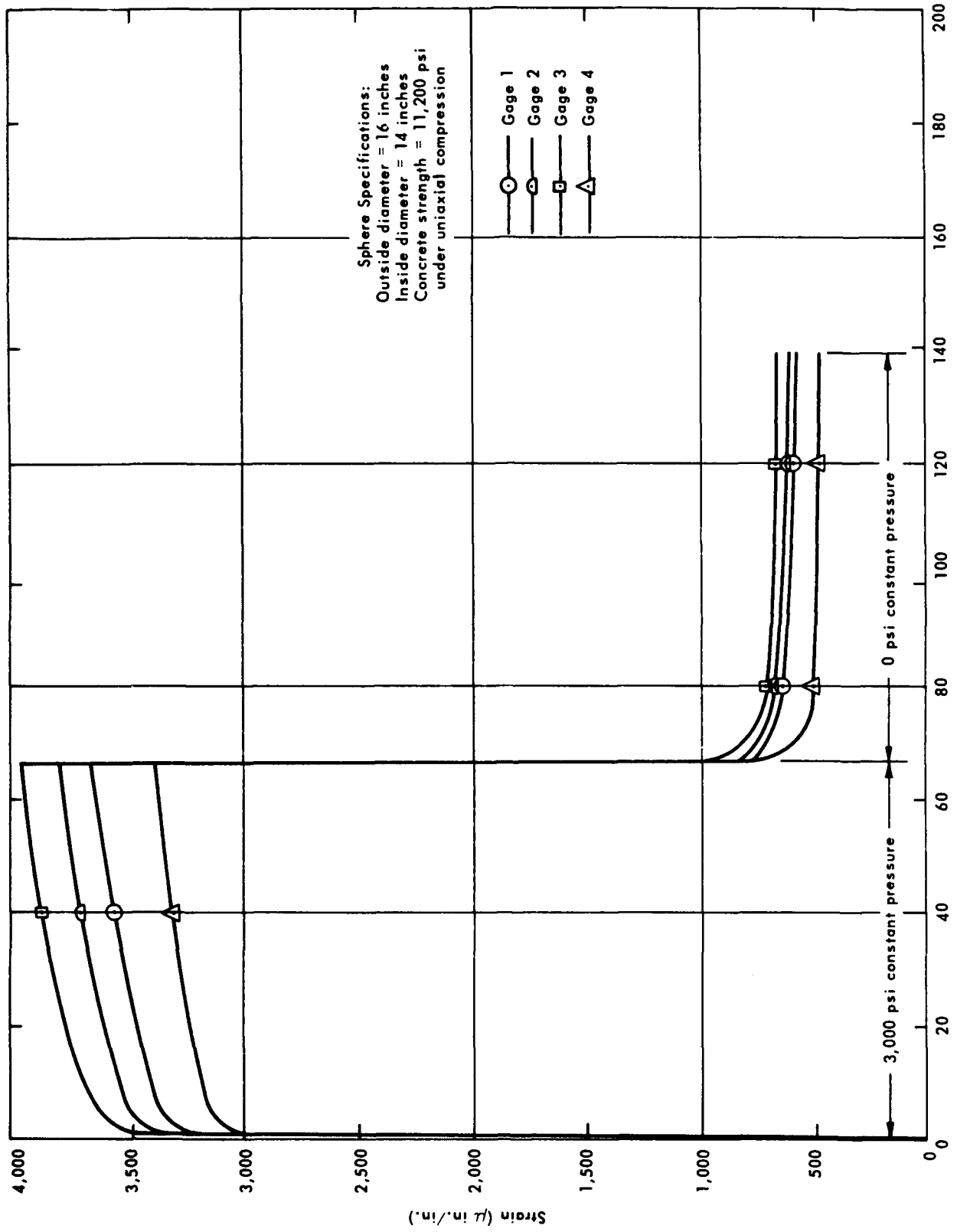

Figure 8. Strains on the interior surface of sphere 8 during a single, long-term, external hydrostatic pressure cycle (first pressurization).

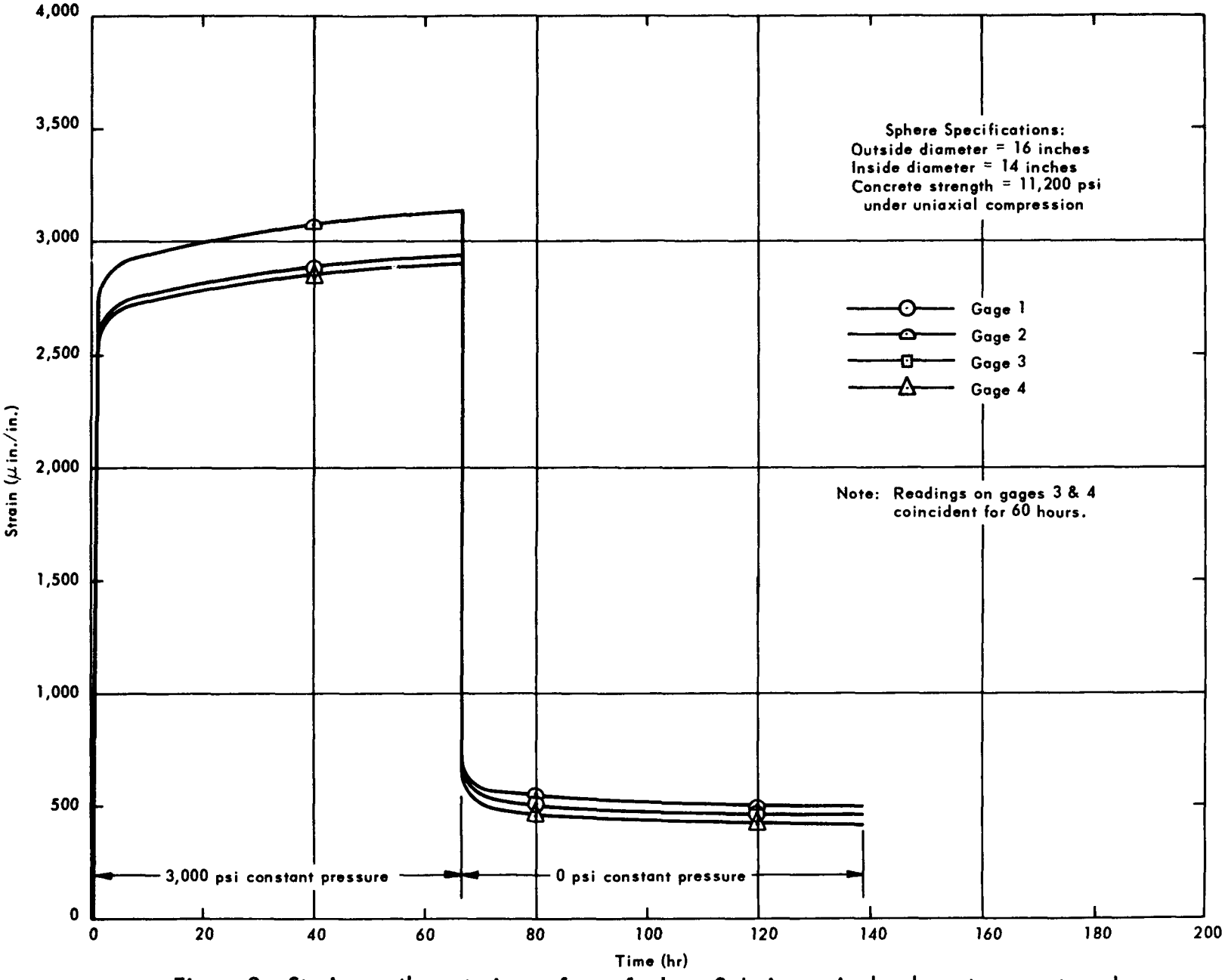

Figure 9. Strains on the exterior surface of sphere 8 during a single, long-term, external hydrostatic pressure cycle (first pressurization).

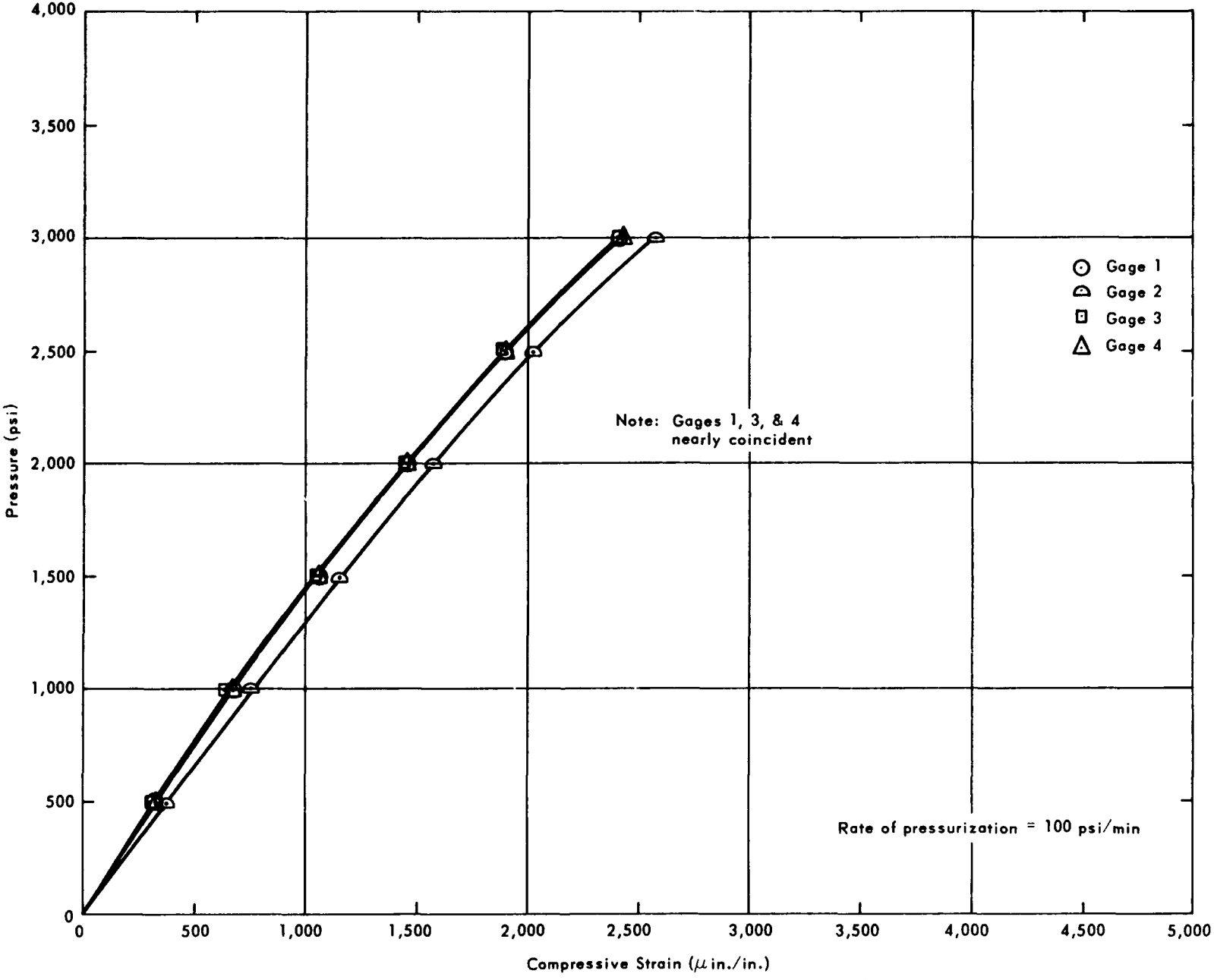

Figure 10. Strains on exterior surface of sphere 8 during external hydrostatic pressure cycle (first pressurization, outside gage locations).

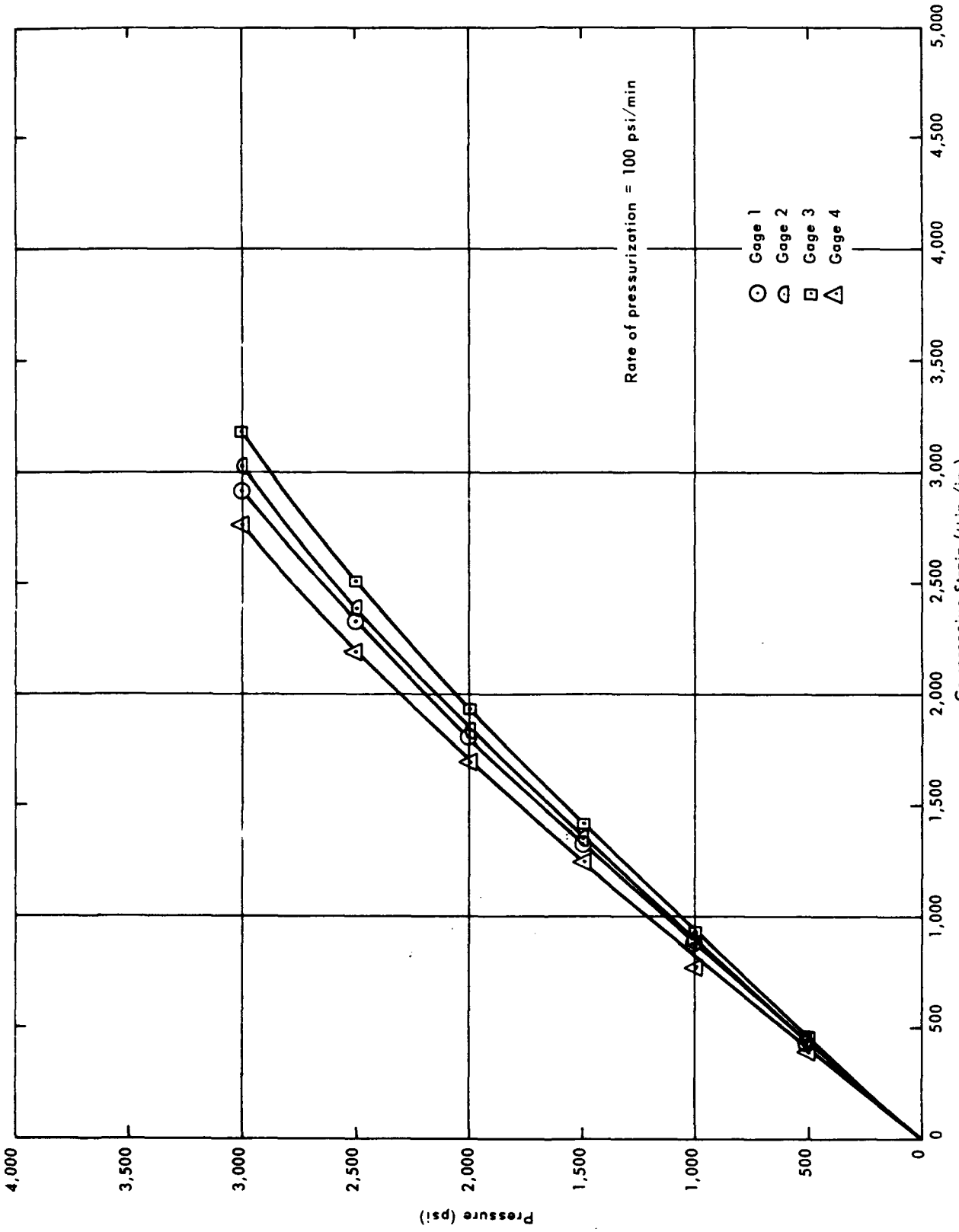

Figure 11. Strains on interior surface of sphere 8 during external hydrostatic pressure cycle (first pressurization, inside gage locations).

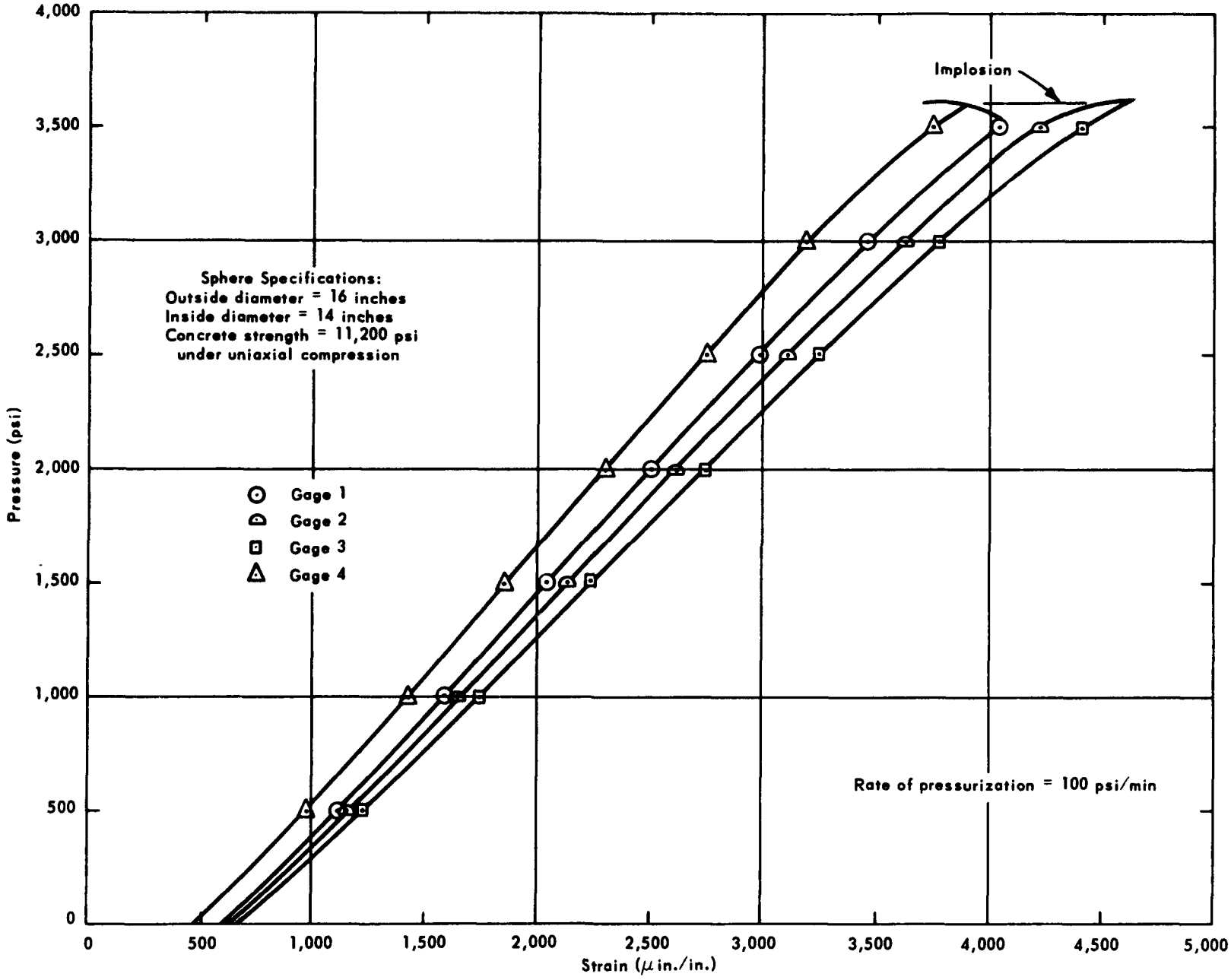

Figure 12. Strains on the interior surface of sphere 8 during external hydrostatic pressure cycle (second pressurization, sphere pressurized to implosion).

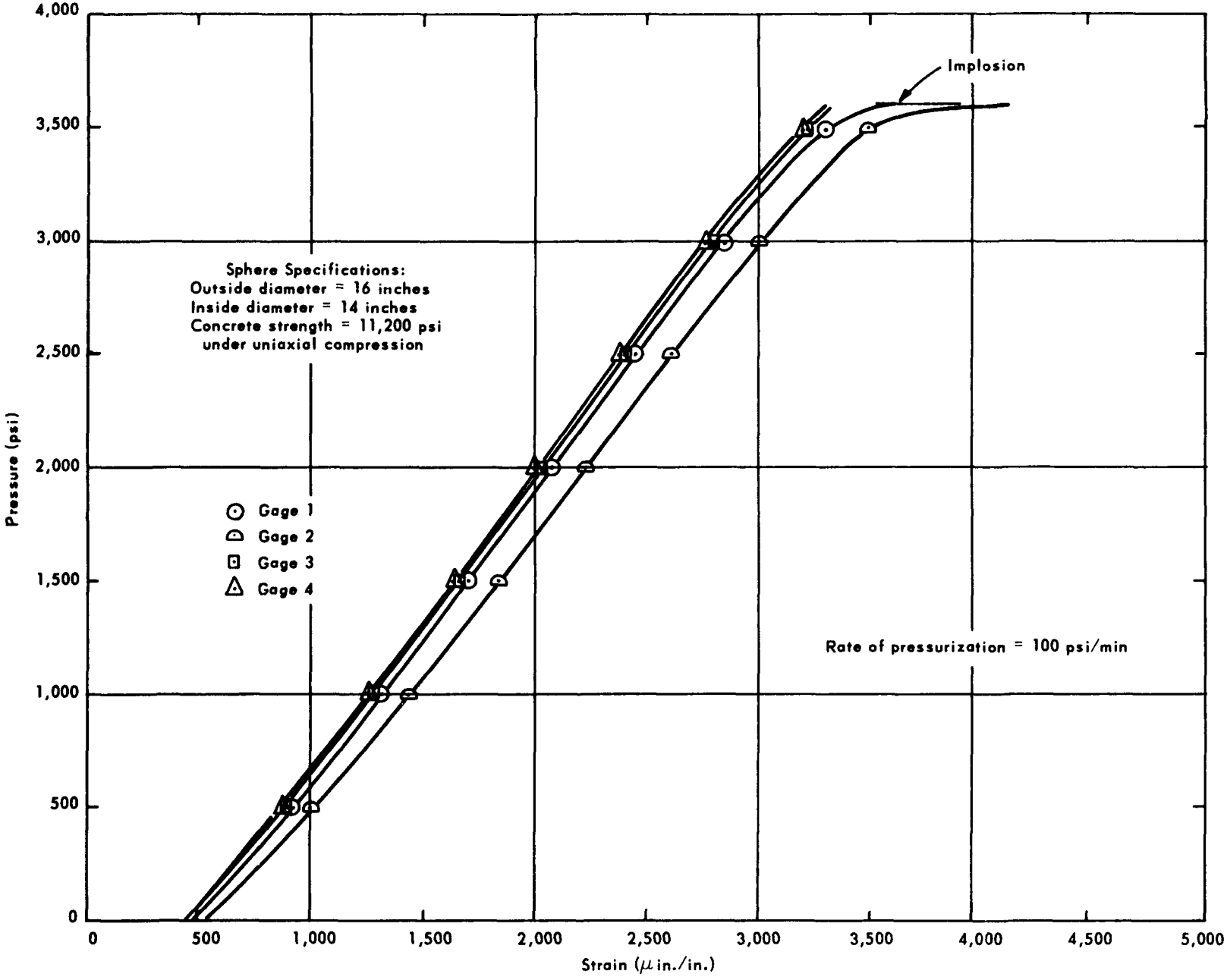

Figure 13. Strains on the exterior surface of sphere 8 during external hydrostatic pressure cycle (second pressurization, sphere pressurized to implosion).

The difference between the average strain readings on the outside and the inside of the sphere did not correspond to the difference in calculated strains for the exterior and interior of the sphere. The magnitude of the difference between the average strain on the exterior and on the interior of the sphere was approximately 20% of the strain on the sphere's exterior, while the difference in calculated strains is only 11% of the stress on the sphere's exterior. This could be an indication that the classical formula for calculations of strains on the surfaces of a thick-walled concrete sphere does not predict strains accurately because the material's tangential modulus of elasticity is not constant, but depends on the magnitude of stress at a given location in or on the structure.

Table 3. Hydrostatic Pressure and Duration of Loading of Spheres 11, 6, 10, and 8 in Static Fatigue Test; and the Average Compressive Strength of the Corresponding Wet and Dry Test Cylinders

Item	Sphere 11	Sphere 6	Sphere 10	Sphere 8
Condition of concrete in sphere	wet	wet	partially wet	dry
Hydrostatic pressure	2,000 psi	2,500 psi	2,500 psi	3,000 psi
Compressive stress[1/] on the interior of the sphere	9,089 psi	11,361 psi	11,361 psi	13,633 psi
Duration of loading prior to implosion	6 days	10 minutes	5 hours	3 days[2/]
Average compressive strength of 3 x 6-inch dry test cylinders	10,890 psi	10,610 psi	11,110 psi	11,200 psi
Average compressive strength of 3 x 6-inch wet test cylinders	7,530 psi	8,140 psi	8,210 psi	7,230 psi

1/ Stress calculated with Equation 1.
2/ No implosion occurred during 3-day test.

Deformation of Concrete Spheres Under Long-Term Loading

Only one strain-gage-instrumented sphere (number 8) was subjected to long-term hydrostatic pressure loading. To accelerate the acquisition of data on the behavior of dry concrete in a spherical hull under long-term hydrostatic pressure, the sphere was pressurized to 3,000 psi, or approximately 80% of its short-term critical pressure. The measured strains (Figures 8 and 9) showed that dry concrete under biaxial compressive stresses has a time-dependent strain rate, which is very large immediately after load application, but which decreases with time. That the time-dependent strain is a function of both the compressive stress level as well as time was shown by the difference of time-dependent strain rates measured on the exterior and interior surfaces of the sphere. The interior surface of the sphere, which was under a higher stress, showed a considerably higher time-dependent strain rate than the exterior of the sphere, which was under a lesser stress.

The long-term hydrostatic loading of sphere 8 was conducted for only 3 days, and thus it is not known how much the time-dependent strain rate decreases after loading duration of several months, or years. The data generated indicates that even at the 13,633-psi compressive-stress level to which the concrete on the interior of the sphere was subjected, the time-dependent strain rate of dry concrete decreased to 0.01 microinch/inch/minute after 3 days. This would lead one to believe that at lower stress levels, corresponding to shallower depths in the ocean, time-dependent strain would not pose any serious engineering problems for concrete spheres with a 0.0625 wall-thickness to diameter ratio.

Upon depressurization, a time-dependent relaxation strain was observed whose rate decreased to a very small value after only 3 days. The difference between the strain level at the beginning of pressurization, and the strain after 3 days of relaxation at zero pressure shows that a nonrecoverable deformation of concrete in the sphere occurred.

Since literature search failed to discover sources discussing data on time-dependent strain of concrete under biaxial compression at 80% stress level of ultimate strength, no comparison could be made between the data generated by this study and other data. Even when a comparison is attempted with work done previously[4] on time-dependent strain of concrete under uniaxial loading, no meaningful correlation can be found as the concrete specimens used in the other studies underwent a distinctly different curing cycle previous to testing. Because of this, new studies will have to be conducted before the phenomenon of time-dependent strain in spherical concrete hulls is well understood.

FINDINGS

1. Dry concrete in a 1-inch-thick spherical hull of 0.0625 wall-thickness to diameter ratio under short-term hydrostatic loading failed at an average compressive stress 48% higher than identical dry concrete in 3-inch-diameter by 6-inch-long solid test cylinders under uniaxial compressive loading.

2. Seawater-permeated concrete in a 1-inch-thick spherical hull of 0.0625 wall-thickness to diameter ratio under short-term hydrostatic loading fails at compressive stresses 18% higher than identical dry concrete in 3x6-inch-long solid test cylinders under uniaxial compressive loading.

3. Permeability of unprotected 1-inch-thick concrete spherical hull of 0.0625 wall-thickness to diameter ratio under long-term hydrostatic loading of 1,500 psi in seawater was approximately 6×10^{-3} milliliters per hour per square inch of area per inch of thickness.

4. The collapse pressure under short-term hydrostatic loading of 1-inch-thick concrete spherical hulls with 0.0625 wall-thickness to diameter ratios and having 10,000 - 11,000 psi compression strength (as determined by dry testing 3x6-inch solid test cylinders under uniaxial loading) is in the 6,000- to 8,000-foot depth range.

CONCLUSIONS

Concrete appears to be an acceptable material for the construction of positively buoyant fixed ocean-floor hull structures in the 0- to 3,500-foot depth range. It possesses sufficient compressive strength in a buoyant spherical hull structure to withstand the external hydrostatic pressure at that depth — whether the concrete is wet, or dry. The exploratory experiments have shown, however, that many parameters like creep, permeability, and long-term strength of concrete under hydrostatic loading must be thoroughly investigated and understood before concrete hulls for underwater structures can be designed with confidence.

ACKNOWLEDGMENTS

The concrete mix used in the fabrication of the spheres was designed by Mr. W. R. Lorman of NCEL's Materials Division.

The mixing of the concrete, the molding of the hemispheres and the task of developing a suitable bonding material for joining the hemispheres was conducted under the personal supervision of D. F. Griffin, Director of the Materials Division. He was also a coauthor of Appendix A "Fabrication of Concrete Spheres."

The initial exploratory work on instrumentation of the spheres was done by V. Hernandez of the NCEL Materials Division. He was also a coauthor of Appendix A.

The electronic leak detector system was developed by F. E. Nelson of NCEL's Instrumentation Division.

The instrumentation, assembly, coating, and testing of most of the spheres was done by J. V. Graham, Senior Technician of the Ocean Engineering Division.

Appendix A

FABRICATION OF CONCRETE SPHERES

by D. F. Griffin and Val Hernandez

FABRICATION OF CONCRETE SPHERES

The hemispherical shells from which the concrete spheres were assembled, were cast in aluminum molds (Figures A-1 through A-4) using a microconcrete specifically designed for this particular purpose. San Gabriel aggregate was used as the basis for all batches in the sizes and proportions shown below in Table A-1.

Table A-1. Composition of the San Gabriel Aggregate Portion of the Microconcrete Used in Casting Hemispherical Shells

Screen Size		Percent Retained on Each Sieve	Amount in Pounds	
Passing	Retained		Individual	Cumulative
no. 4	no. 8	29.6	17.4	17.4
no. 8	no. 16	20.8	12.2	29.6
no. 16	no. 30	14.7	8.6	38.2
no. 30	no. 50	10.3	6.1	44.3
no. 50	no. 100	7.3	4.3	48.6
no. 100	on pan	17.3	10.2	58.8
Total		100.0	58.8	58.8

The first trial batch of concrete included 17.8 pounds of type I portland cement and 10 pounds of Port Hueneme tap water. Technically, this is a mortar rather than concrete, the no. 4 sieve being the dividing line between concrete and mortar.

The relative size of the aggregate to the wall thickness can be clearly seen in Figure A-5.

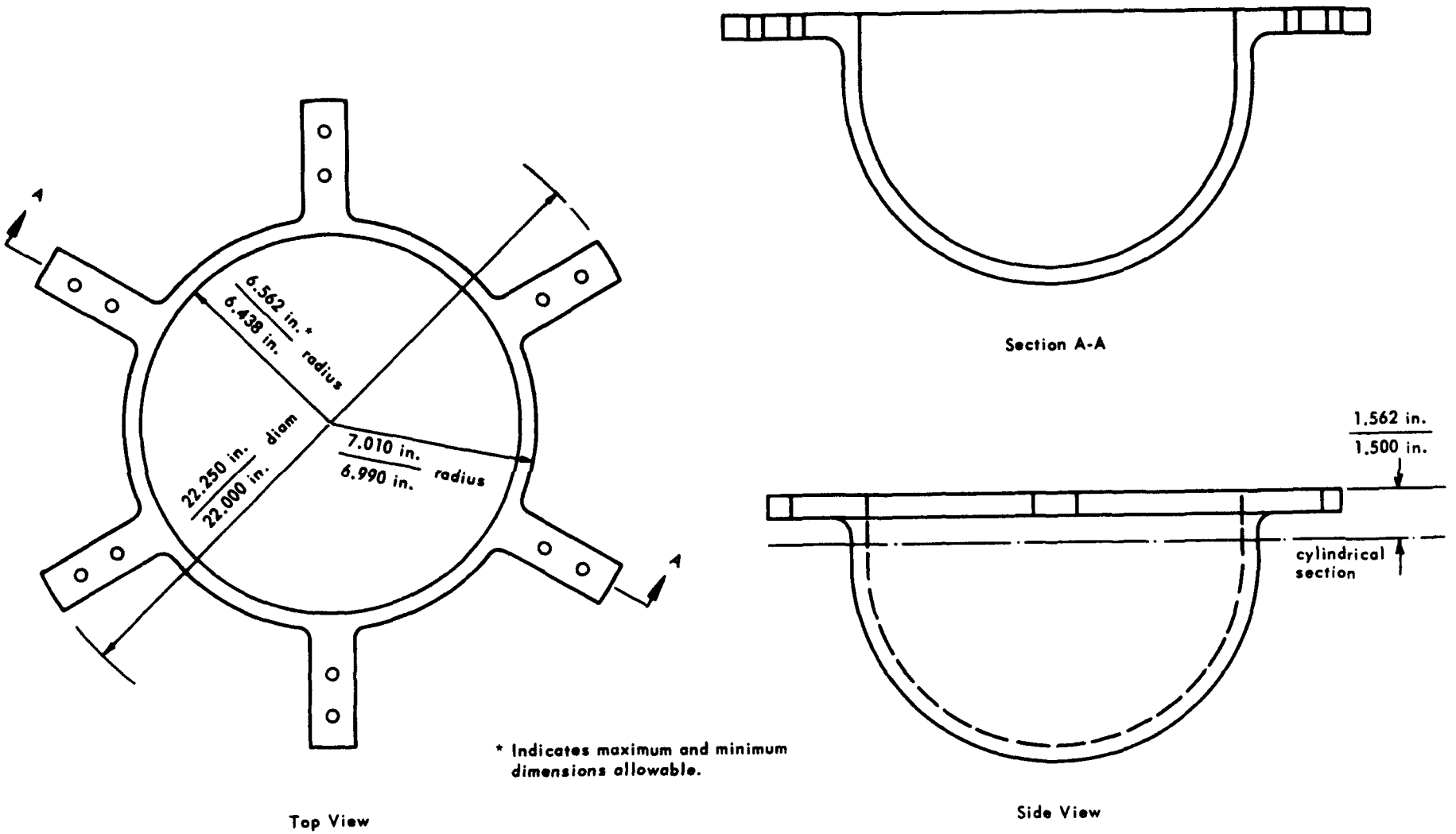

Figure A-1. Concrete hemisphere mold, male insert.

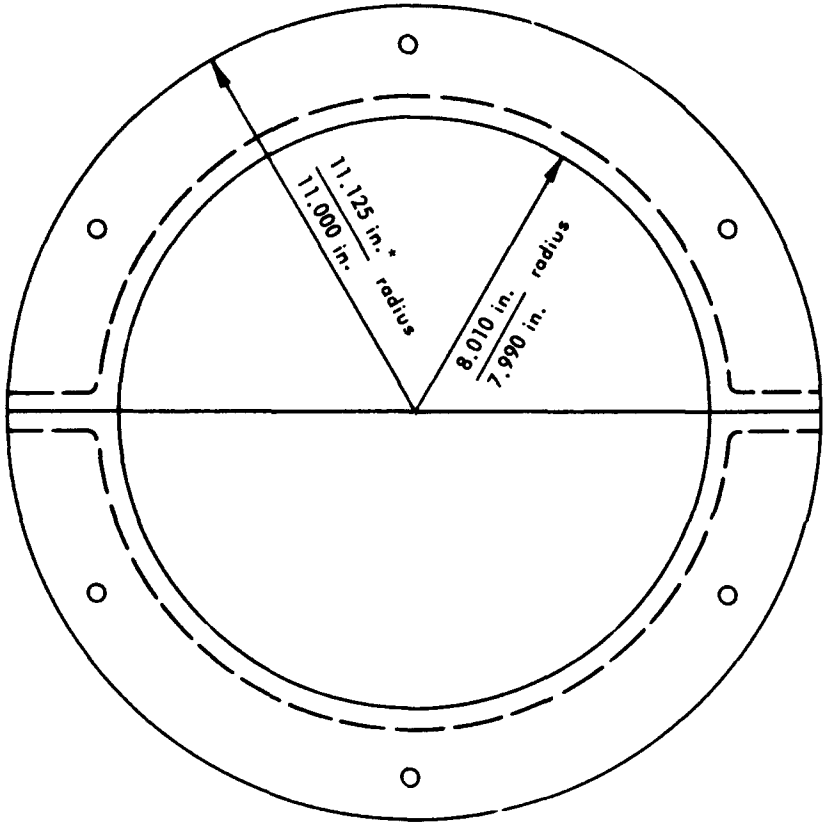

Top View

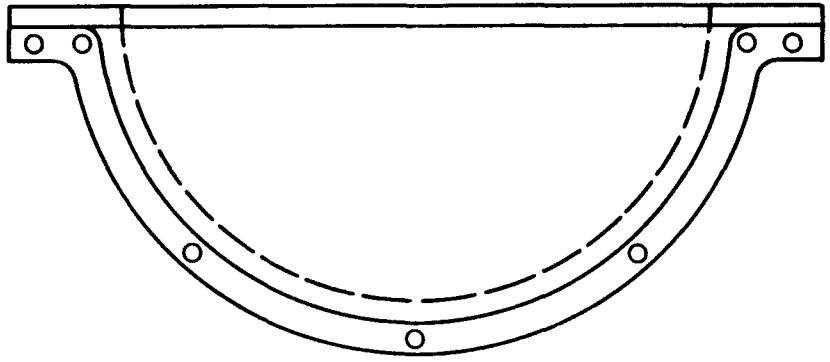

Side View

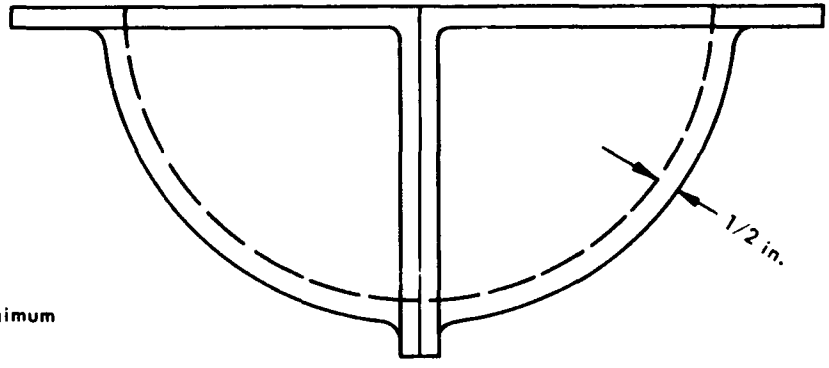

End View

* Indicates maximum and minimum dimensions allowable.

Figure A-2. Concrete hemisphere mold, female shell.

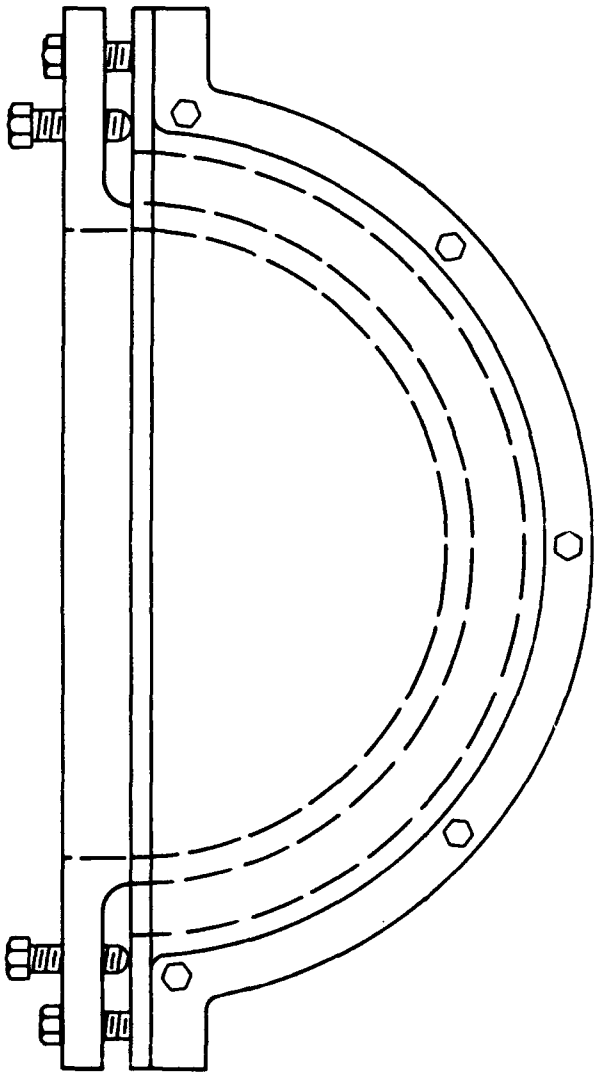

Figure A-3. Concrete hemisphere mold, assembly.

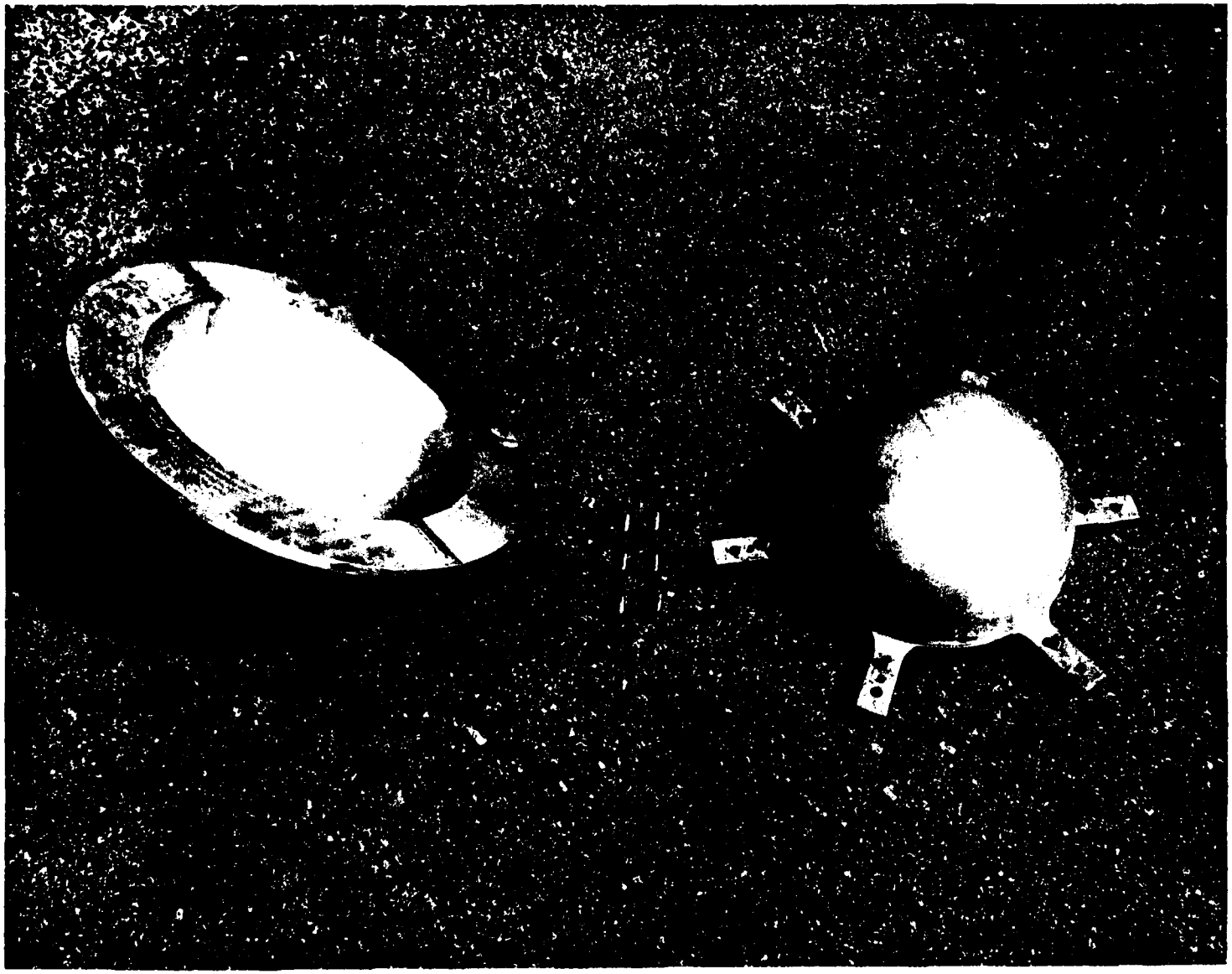

Figure A-4. Concrete hemisphere mold, disassembled.

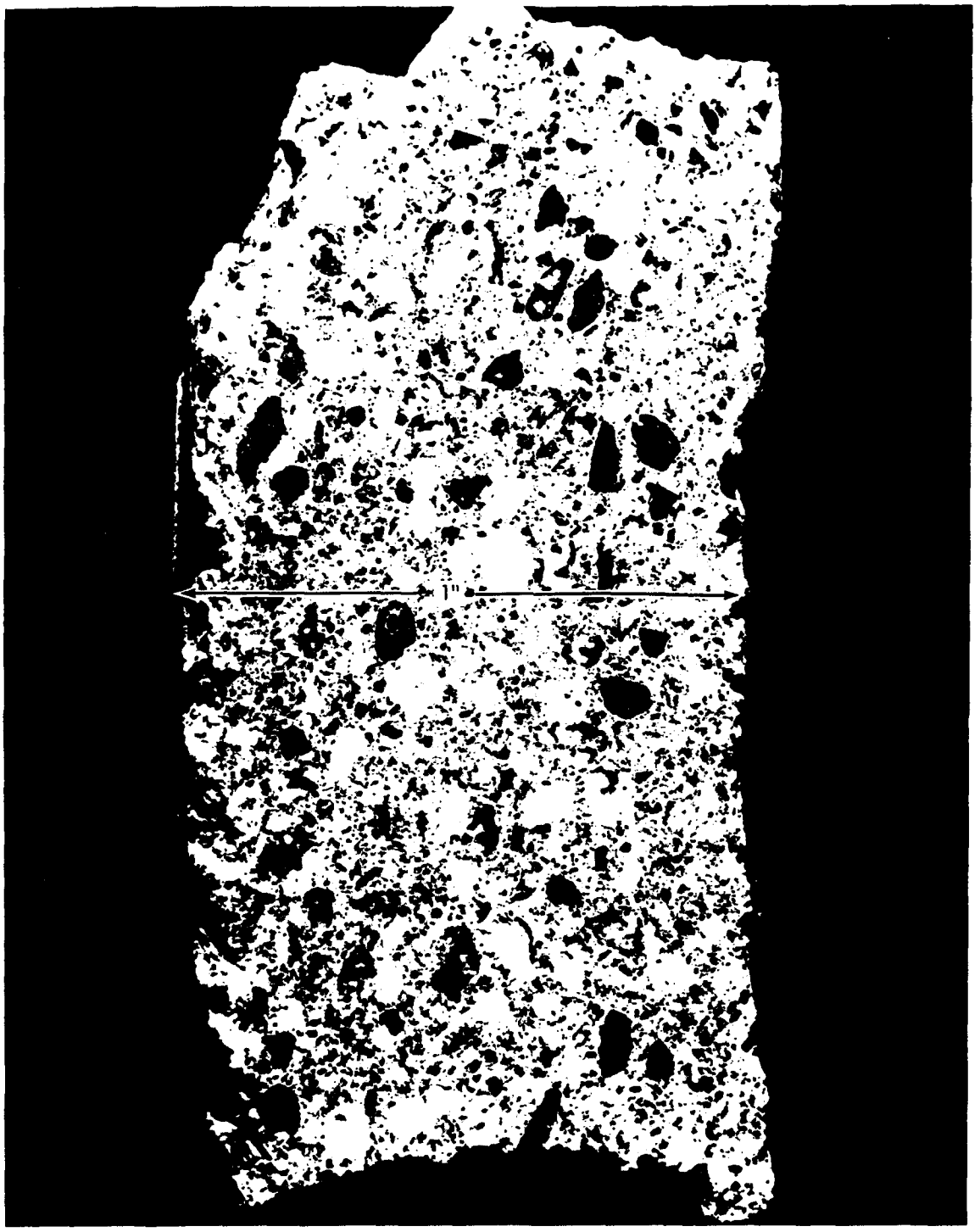

Figure A-5. Cross section of a typical wall fragment from an imploded sphere.

Concrete Mixing

Concrete was mixed in a pan type mixer of 1.75-cubic-foot capacity. The following sequential operations were followed:

1. Aggregate added
2. Mixed dry for 30 seconds
3. Water (73°F) added with mixer running
4. Mixed for 150 seconds (total of 3 minutes including step 2)

The batch, as designed, called for less water than 10 pounds; however, 10 pounds proved to give optimum workability and plasticity. Taking into account 1.8% water absorption of the aggregate, the water-to-cement ratio was 0.50.

Concrete Placement

The surfaces of the hemispherical mold were first sprayed with acrylic spray and then coated with form oil. The mortar was poured into the mold from one side only in order to avoid entrapment of large air bubbles. A spud vibrator was held against the wooden framework supporting the mold; however, the mortar did not flow into place easily because the vibration was not adequate. A 1/4-inch flexible acrylic tube was used to help rod the mortar into the mold.

Because the first hemispherical shell could not be removed from the mold without breaking, it was decided to use type III portland cement to provide higher early strength to reduce possibility of breakage in subsequent castings. It was concluded in the case of the first casting, that form oil had been wiped clean by pouring mortar into the mold from one side, thereby allowing hardened mortar to stick to the form. In addition, the acrylic tube used to compact the mortar had abraded the acrylic spray from the form; this resulted in some lightly corroded marks on the aluminum.

Following the above experience, the mold surfaces were thoroughly cleaned and smoothed with fine emery paper. They were then coated with a release agent and allowed to dry. A thin layer of vaseline was then applied to the form surfaces, the form was assembled and then filled with fresh mortar. In addition, a form vibrator was attached to the flange of the form as shown in Figure A-6. In Figure A-6, a nylon cord is being fixed in place. The cord is to provide an air bleeder line to facilitate removal of the internal form.

Figure A-7 illustrates the method used to remove the inner form after the concrete hardened (24 hours after casting). The inner circle of bolts was set to hold the form at the correct height above the lower form. The outer circle of bolts screw into holes in the flange of the lower form. When the upper form is to be removed, the outer bolts are removed, small metal plates are placed over the threaded holes

in the flange, the bolts are replaced in the upper unthreaded holes and a nut is attached to each bolt just below each of the arms. Each nut was held with a wrench while the bolt was tightened against the small plate thus operating like a screw jack. Torque was applied to each bolt in stages until the form broke loose.

Figure A-8 shows a close-up of the inner surface of the hemisphere. No way has been found to eliminate the entrapped air bubbles. One set of hemispheres was cast using an air-entraining agent in hopes entrapped air could escape; however, the result was about the same as shown in Figure A-8.

Figure A-9 shows the exterior of a hemisphere as cast. The exterior surfaces always were good. The interior surfaces always had some bubble holes, sometimes more, sometimes less. For each casting, the hemisphere forms were completely cleaned, the form film being stripped with acetone. A fresh coating of release agent was then applied followed by a coating of vaseline.

Interior Surface Treatment

Shortly after the molds were stripped, the interior surface of each concrete hemisphere was rubbed down by hand with steel wool. This removed all traces of vaseline and broke through any thin films of mortar covering air bubbles. In addition, the annular surface where two hemispheres join was smoothed with an abrasive block and also with steel wool to remove uneven portions and laitance. A cement mortar consisting of 50% type II portland cement and 50% aggregate passing a no. 100 sieve and enough water to make it plastic, was then hand worked into all the open pores of the interior of the concrete hemispheres, leaving a smooth surface finish. Type II portland cement was used to minimize shrinkage.

Bonding the Hemispheres

Before bonding, the annular edges of the hemispheres had been etched with 10% hydrochloric acid solution and thoroughly dried. All hemispheres were first cured in 100% relative humidity and then cleaned and stored in 20% relative humidity for a week or so. Immediately prior to bonding the annular surfaces were cleaned lightly with acetone. The epoxy bonding formulation (8288-A Epocast furane epoxy) was thoroughly mixed and a copious supply of the mixture was placed on the annular surface of the lower hemisphere. The upper hemisphere was seated and pressed down to refusal, the excess bonding material was spread around the joint with a spatula. This material can be easily washed from the hands and utensils with soap and water.

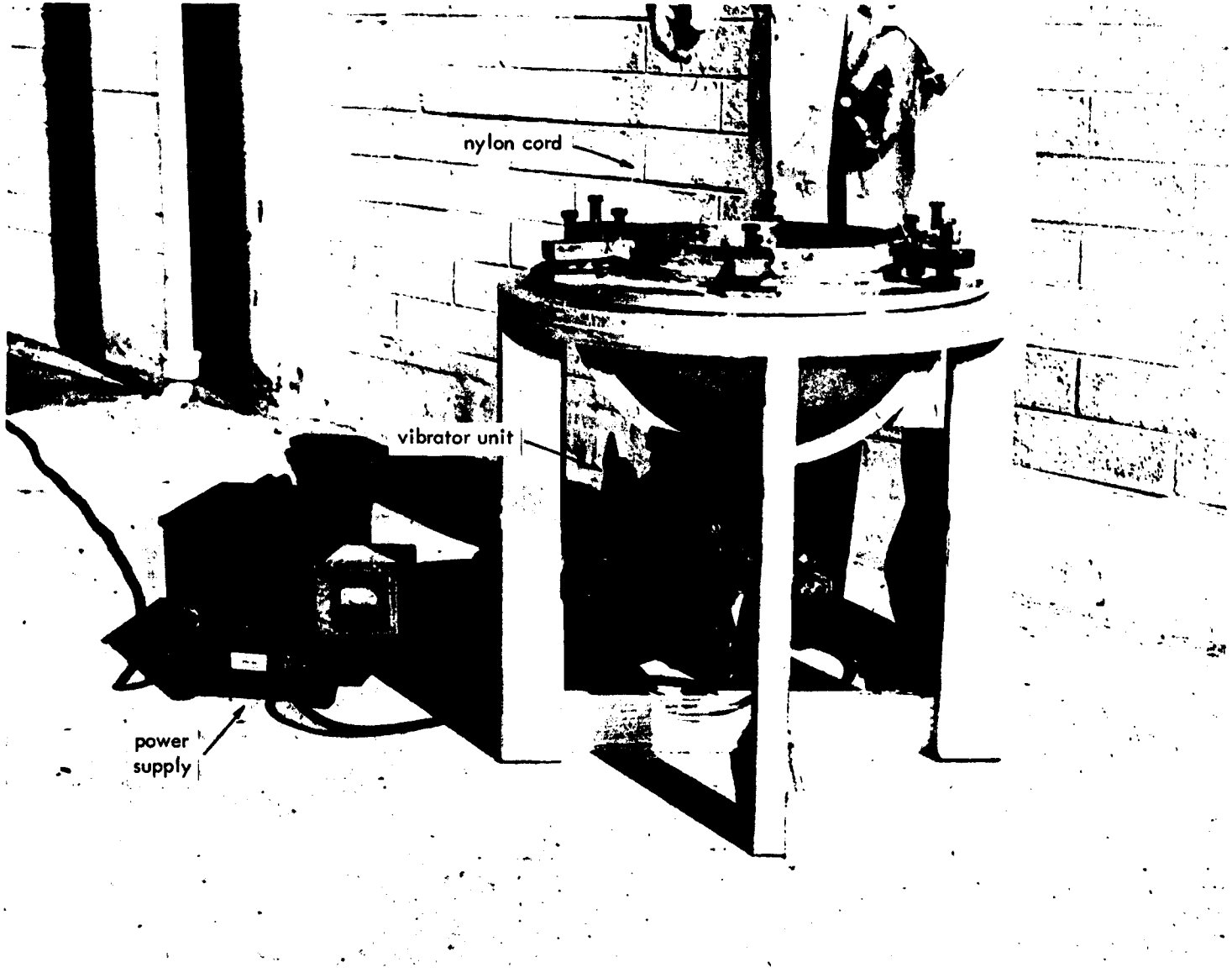

Figure A-6. Hemisphere mold showing external vibrator clamped to bottom of form and the nylon cord used to form an annular air bleed groove to assist in releasing the concrete from the form.

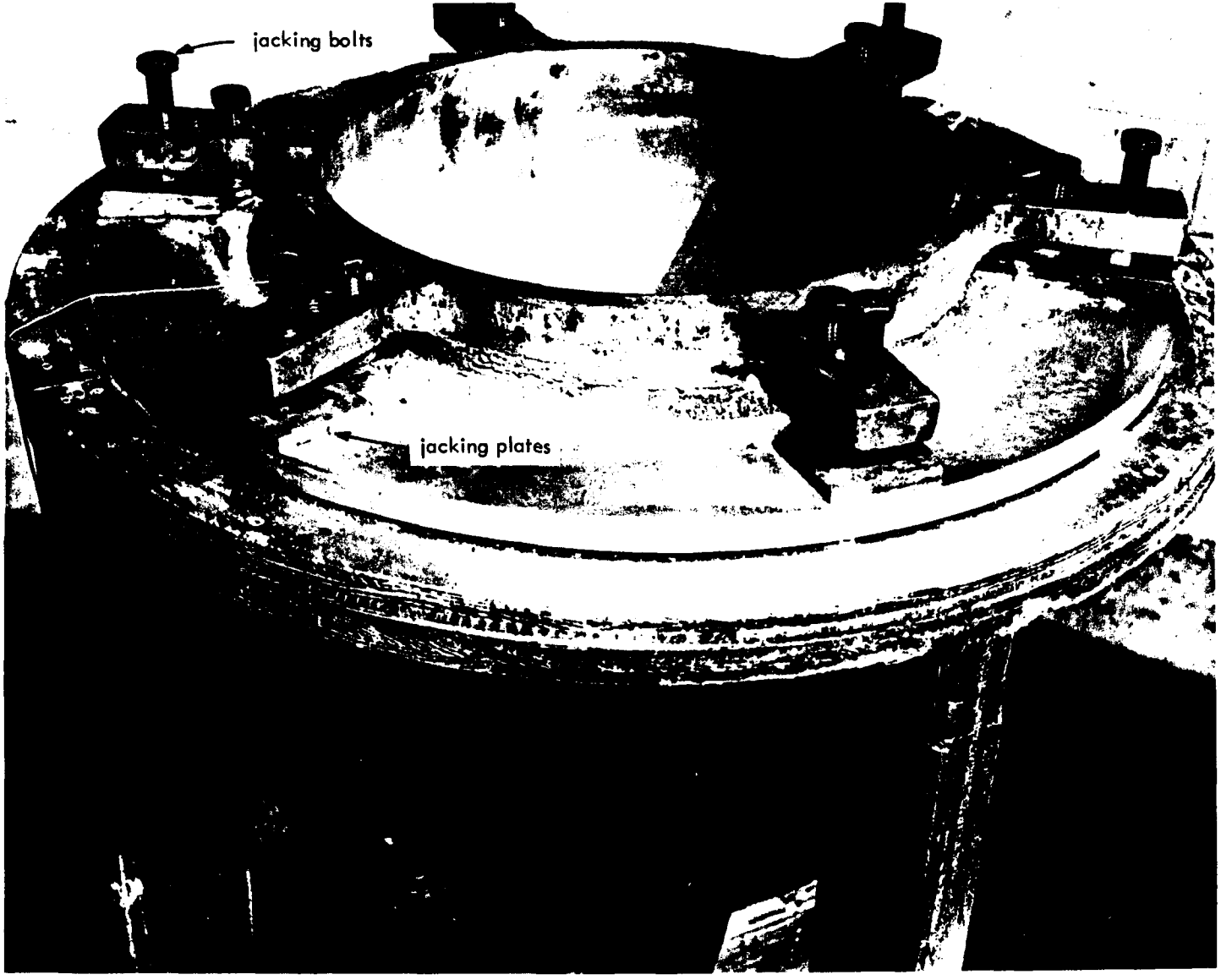

Figure A-7. Configuration for jacking the male insert portion out of the form after concrete has set.

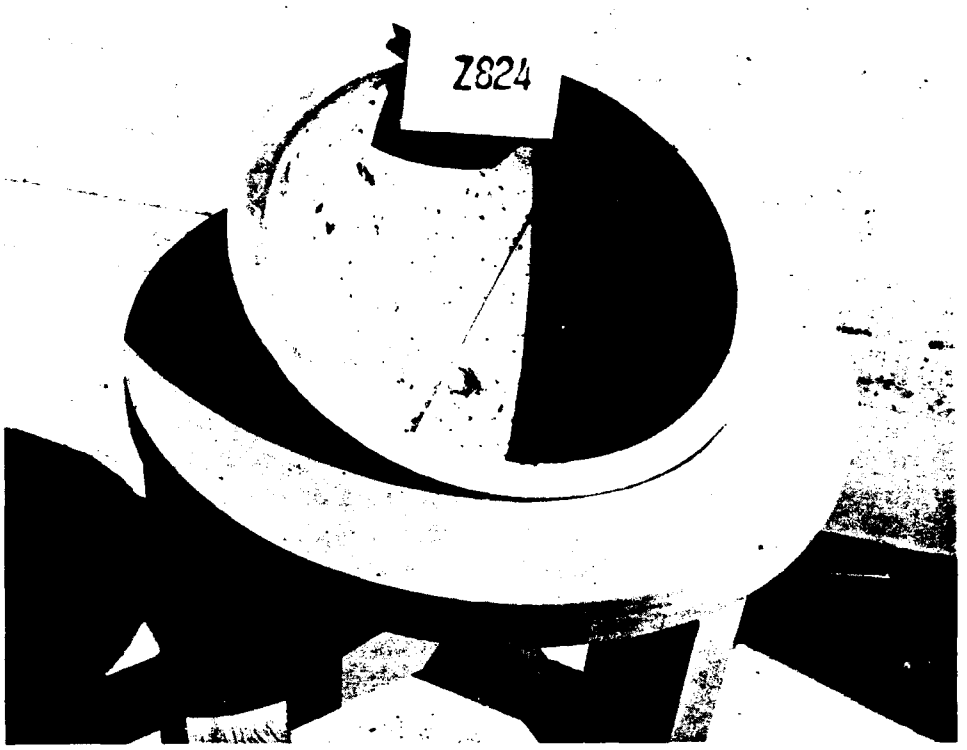

Figure A-8. Air cavities and air bleed groove in interior surface of concrete hemisphere before patching treatment.

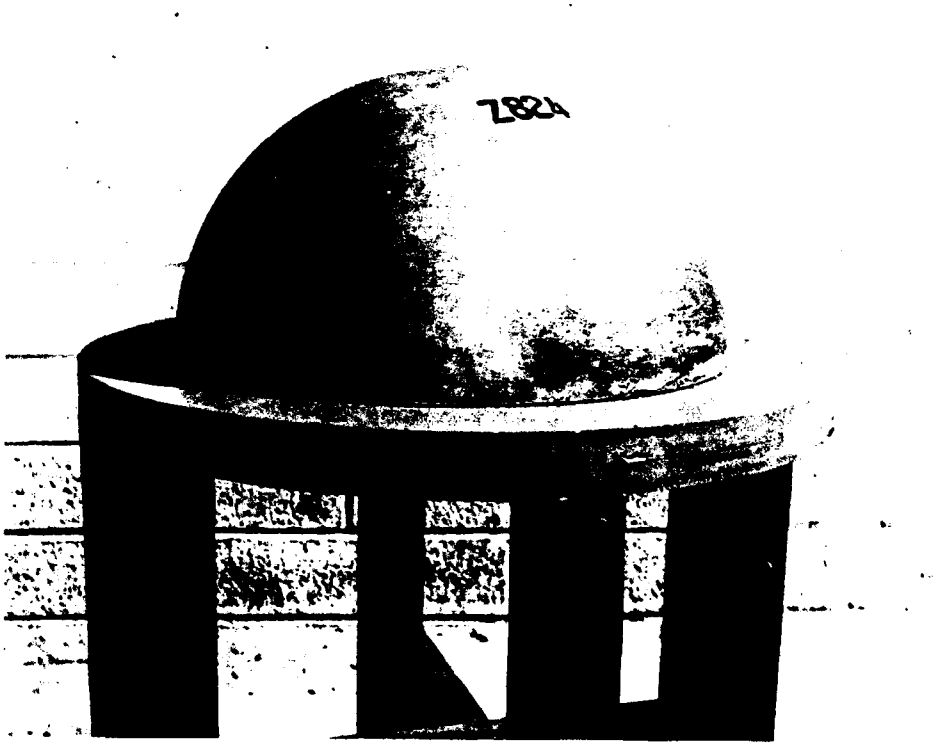

Figure A-9. Exterior surface of a hemisphere as cast.

Appendix B

INSTRUMENTATION OF THE SPHERES

INSTRUMENTATION OF THE SPHERES

Strain Instrumentation

The instrumentation for the determination of strains consisted of electric resistance strain gages attached to the concrete sphere, and a manual strain switch and read-out unit. Two different methods were used to attach the strain gages to the concrete surface. One method was by adhesive bonding, and the other consisted of bonding the gages first to a metallic transducer hoop, which in turn was attached by two screws to the concrete (Figure B-1). The instrumentation leads were conducted to the strain switch and read-out unit outside the pressure vessel, either by means of waterproof electric cables and bulkhead connectors, or through a waterproof conduit attached to both the sphere and the vessel end closure (Figures B-2 and B-3).

Permeability Instrumentation

Two different approaches were used to measure the rate of permeability through concrete in the experimental spheres. One approach relied exclusively on electronic transducers and read-out equipment, while the other utilized only mechanical or hydraulic components. The electronic water detector (Figure B-4) specially designed for this study operated on the principle that a rising water level in the sphere would markedly change the resistance between two separated rods placed inside the sphere cavity (Figures B-5 and B-6). As the water rose in the sphere it would wet more and more of the two vertical rods, decreasing the resistance between them. This voltage change could be amplified, measured, and recorded to provide a resistance versus time record. Since the salinity of water seeping into the sphere is not constant, but varies as time passes due to reaction of the dissolved salts in seawater with the concrete, precalibration is relatively of little value. Anticipating this problem, reference bench marks were provided on the two rods wetted by water inside the sphere. When the water level rose it wetted the bench marks in sequence, which in turn led to generation of special electronic signals that showed up on the recording paper as vertical marks bisected by the trace from the general detector rods. Since the elevation of the bench marks above the lowest point of the sphere's interior was known, the vertical marks on the general resistance trace provided check marks for the computation of rate at which water permeated the sphere. With their aid the general resistance trace between them could also be interpolated, furnishing precise information on the rate at which water rose in the concrete sphere.

The other approach used in the measurement of permeability rate consisted of tubing inserted into the sphere, through which accumulated water in the sphere's interior could be ejected at desired time intervals. The plumbing for this permeability detector system consisted of two tubes (Figure B-7). One tube was placed with its opening at the top of the concrete sphere specimen, and its was used to pressurize the interior of the sphere with 10 to 20 psi of compressed air. The other tube was placed with its opening at the bottom of the sphere, and its function was to drain the water pushed through it with compressed air from the interior of the sphere at prescribed time intervals.

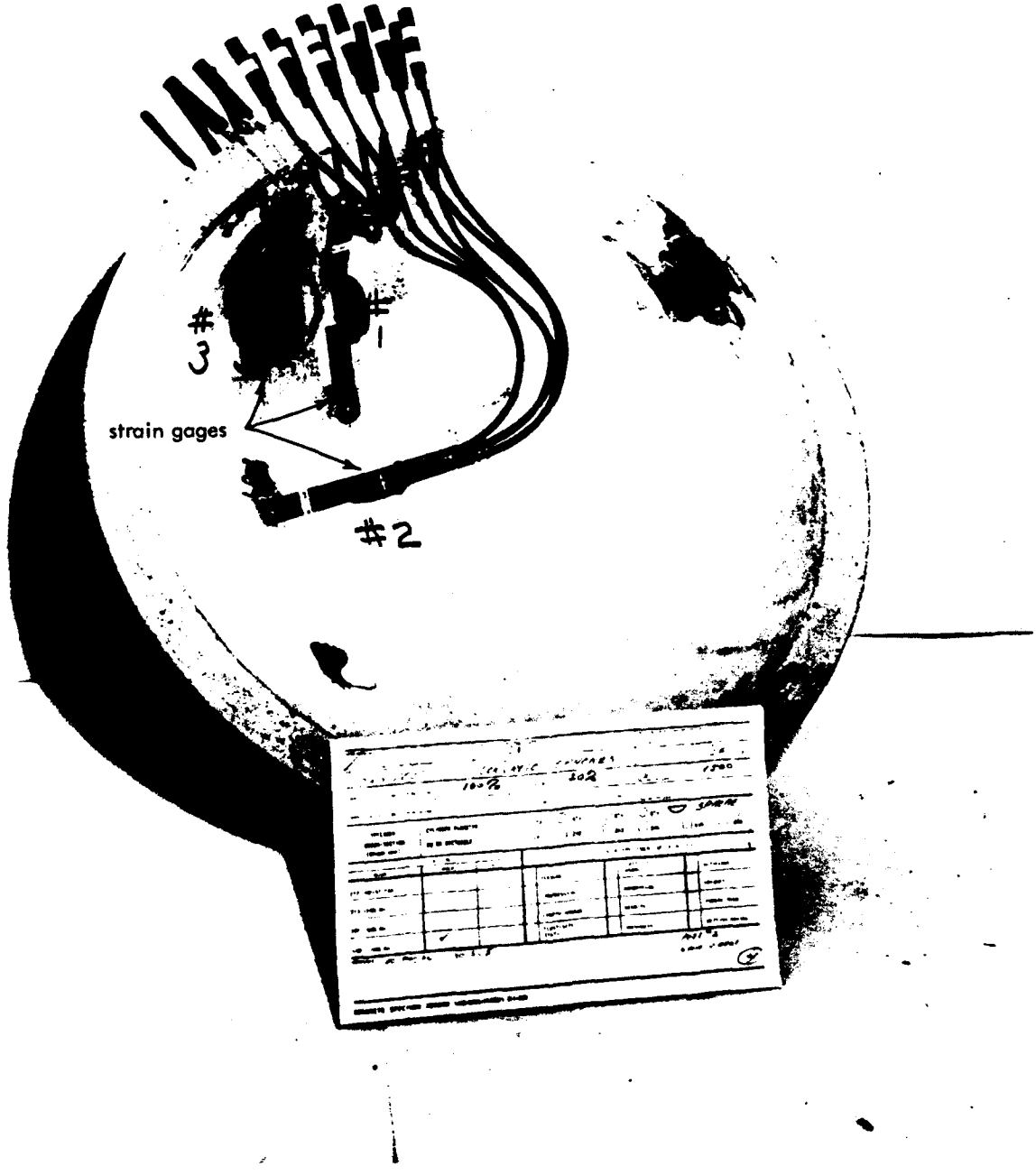

Figure B-1. Instrumentation leads passed through saw cuts in hemisphere rim.

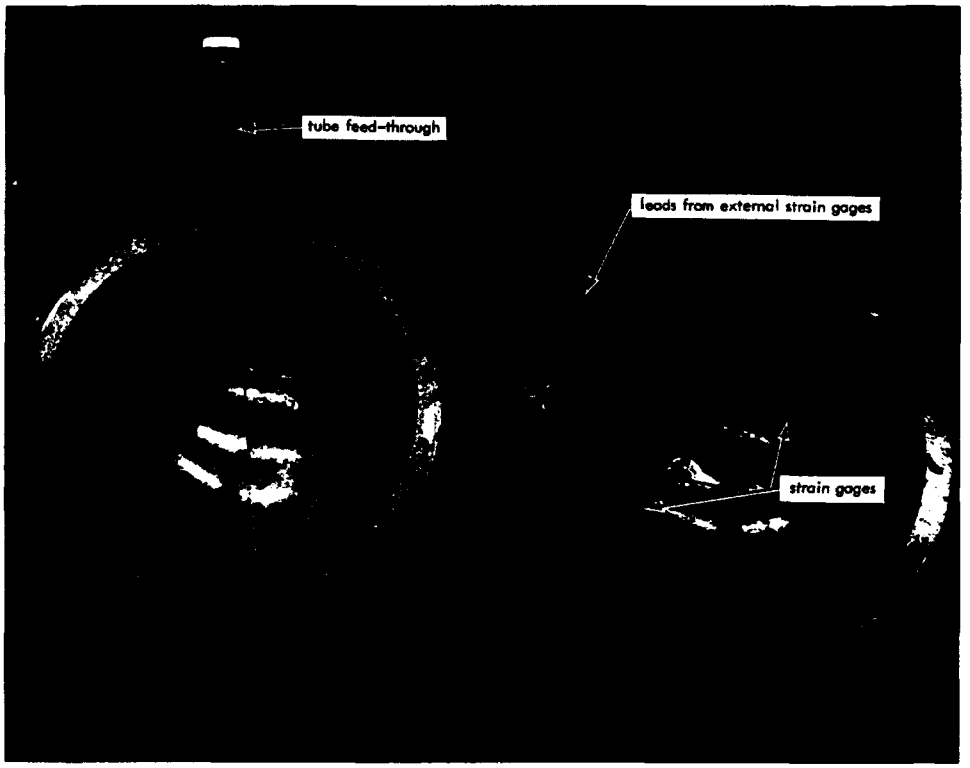

Figure B-2. Concrete hemispheres showing tube feed-through (for passing leads through pressure vessel head) and internal strain gages.

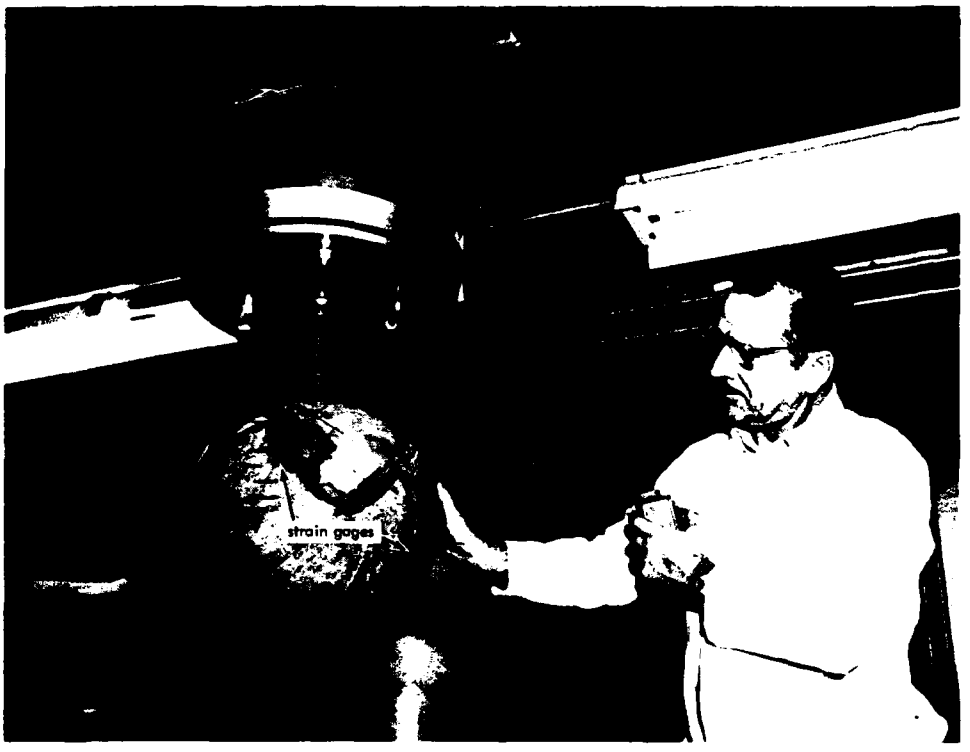

Figure B-3. Instrumented and coated concrete sphere attached to the 18-inch pressure vessel head.

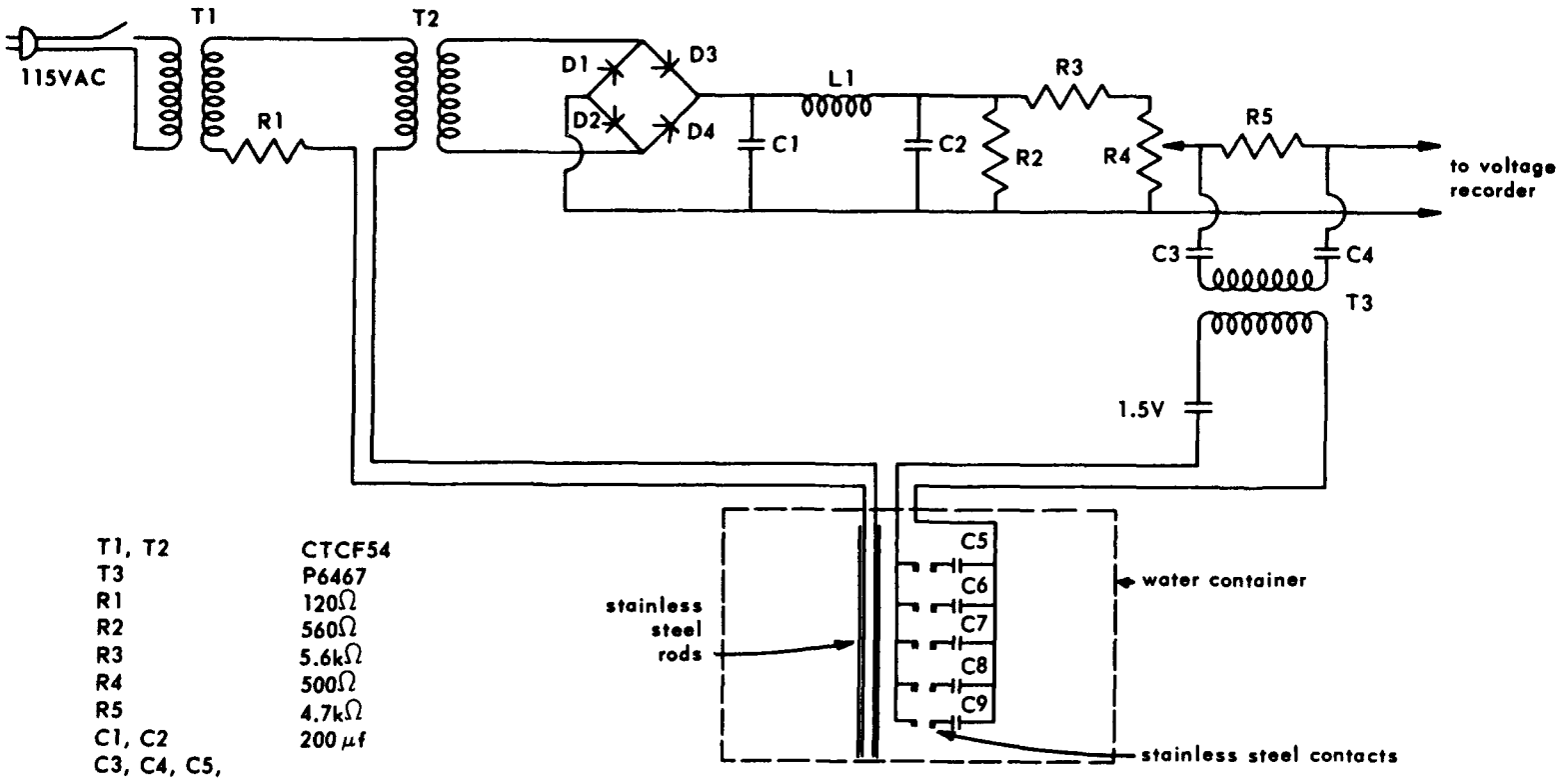

T1, T2	CTCF54
T3	P6467
R1	120Ω
R2	560Ω
R3	5.6kΩ
R4	500Ω
R5	4.7kΩ
C1, C2	200 μf
C3, C4, C5, C6, C7, C8, C9	47 μf
D1, D2, D3, D4	1N91
L1	6h

Note: The output of the leak detector is nonlinear. No attempt was made to make it linear because a large signal was desired when the water shorts the leads the first time.

Figure B-4. Schematic diagram of leak detector circuit.

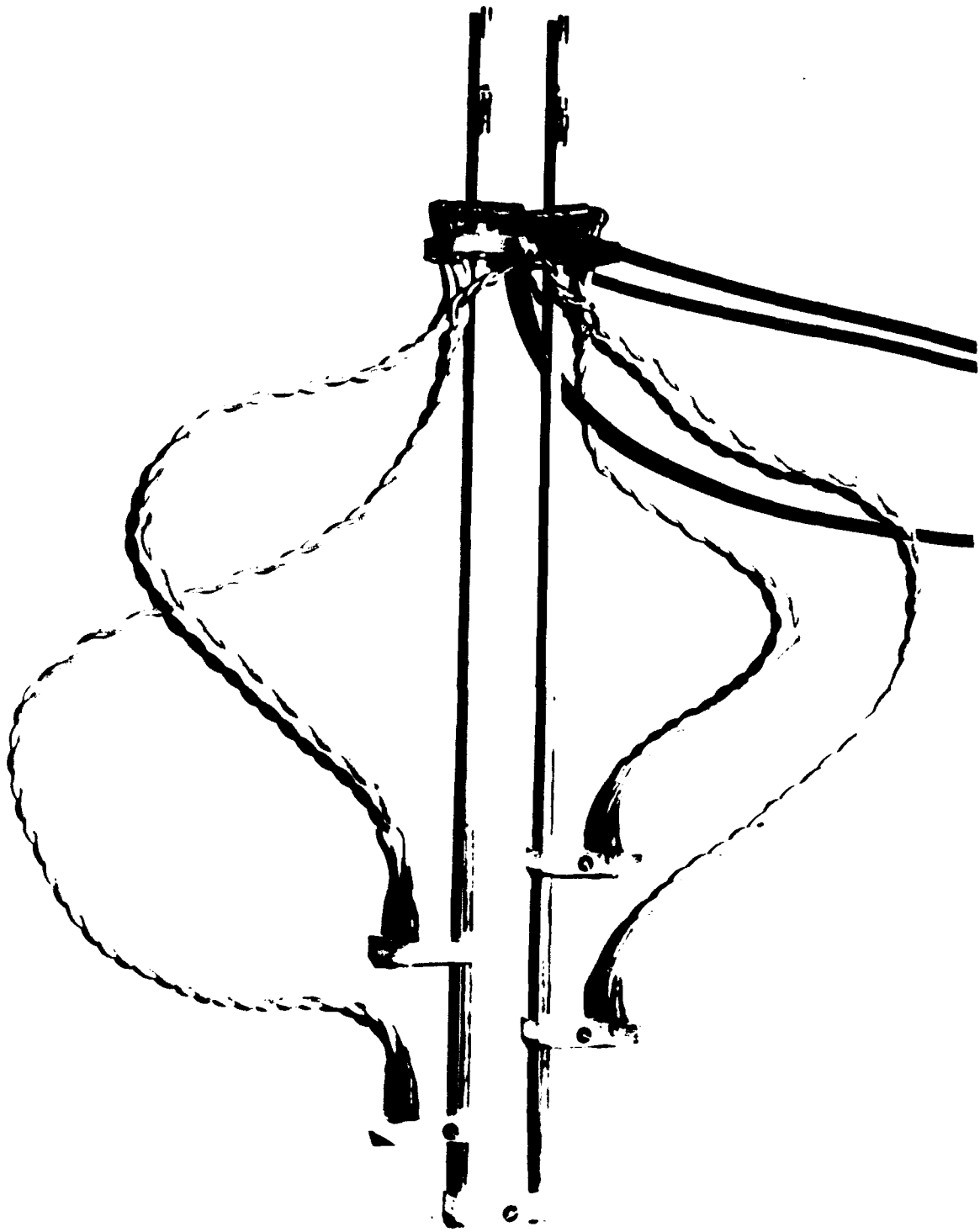

Figure B-5. Electronic leak detector sensing assembly.

Figure B-6. Electronic leak detector sensing assembly installed in concrete hemisphere.

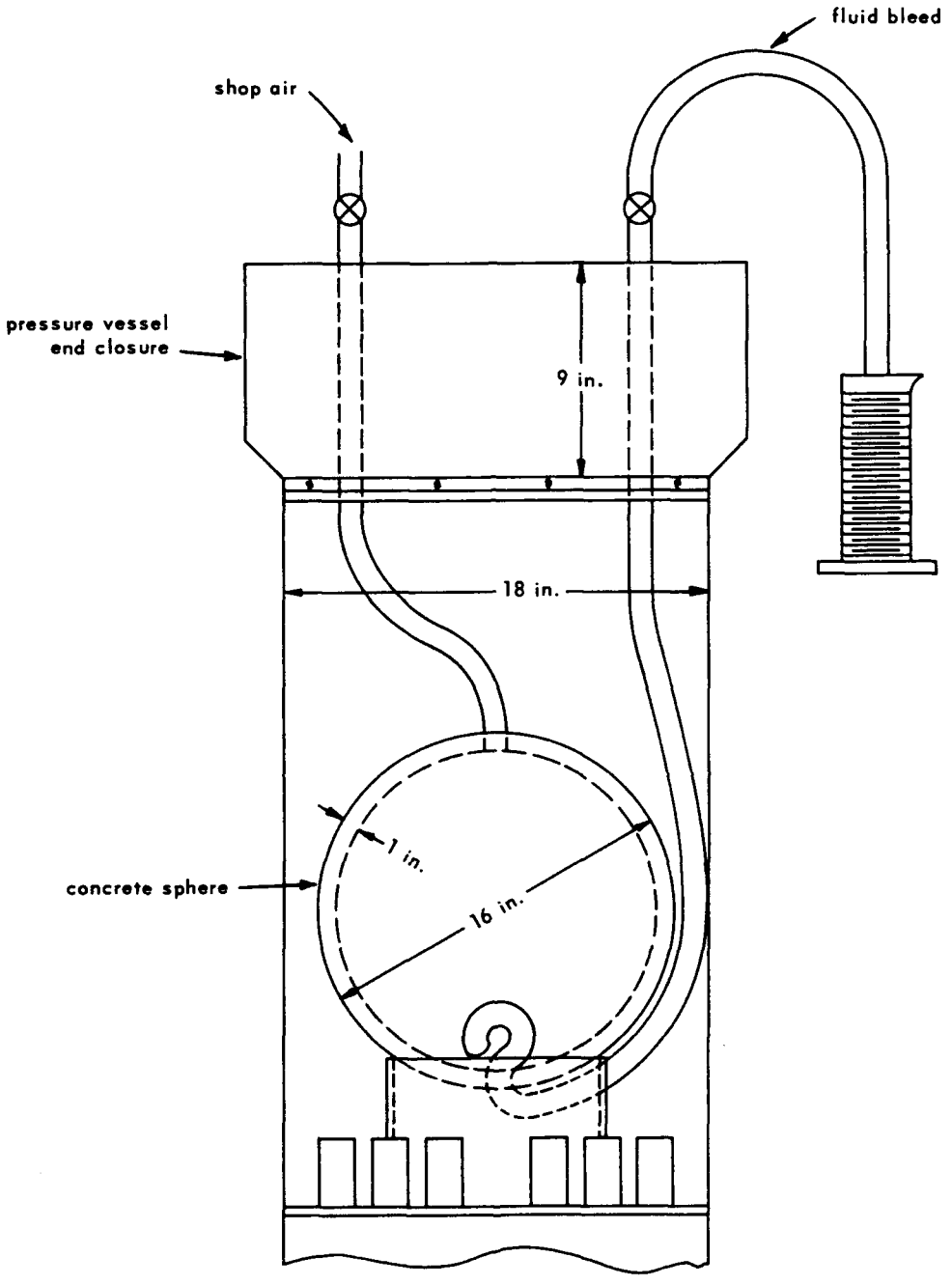

Figure B-7. Diagram of hydraulic leak detection system installed in pressure vessel.

Appendix C

TEST DESCRIPTIONS AND DATA

Summary of Tests on Concrete Spheres

Sphere No.	Type of Test	Surface Coating	Instrumentation	Test 1	Test 2	Test 3	Test 4	Description of Sphere Test (Summary No.)	Test Cylinder Data (Table No.)
1	Short-term strength	Epoxy	SR-4 gages	Pressurized at rate of 1,000 psi/min to failure	None	None	None	C-1	C-1
2	Short-term strength	Epoxy	SR-4 gages	Pressurized at rate of 1,000 psi/min to failure	None	None	None	C-2	C-2
3	Short-term strength	Epoxy	SR-4 gages	Pressurized at rate of 1,000 psi/min to failure	None	None	None	C-3	C-3
4	Permeability	None	Leak detector	Pressurized to 3,000 psi and held	None	None	None	C-4	C-4
5	Permeability	None	Leak detector	Pressurized to 1,500 psi and held	Pressurized at rate of 100 psi/min to failure	None	None	C-5	C-5
6	Permeability	None	Leak detector	Pressurized to 750 psi and held	Pressurized to 1,500 psi and held	Pressurized to 2,000 psi and held	Pressurized to 2,500 psi and held	C-6	C-6
7	Long-term strength	Varnish	None	Pressurized to 2,850 psi and held	None	None	None	C-7	C-7
8	Long-term strength	Epoxy rubber	SR-4 gages	Pressurized to 3,000 psi and held	Pressure dropped to 0 psi and held	Pressurized at rate of 100 psi/min to failure	None	C-8	C-8
9	Long-term strength	Epoxy	SR-4 gages	Pressurized to 3,000 psi and held	None	None	None	C-9	C-9
10	Permeability	None	Leak detector	Pressurized to 2,500 psi and held	None	None	None	C-10	C-10
11	Permeability	None	Leak detector	Pressurized to 2,000 psi and held	None	None	None	C-11	C-11
12	Permeability	None	Leak detector	Pressurized to 1,500 psi and held	Pressurized at rate of 100 psi/min to failure	None	None	C-12	C-12

Summary C-1. Test Procedures for Sphere 1

Type of Test. Critical pressure of concrete sphere under short-term external hydrostatic loading.

Test Procedures. Pressurized externally with seawater at 1,000 psi/min rate till implosion occurred. The surface of the sphere was first coated with Epocast 8288 and then with polyurethane varnish. The implosion occurred at 3,100 psi of hydrostatic pressure. The concrete in the sphere walls was dry at the time of implosion.

Instrumentation. The sphere was instrumented with electric resistance strain gages bonded to its exterior and interior surfaces with Shell Epon 815 which was also used for waterproofing of gages.

Data. Only one strain gage on the exterior of the shell functioned during the test. At 3,000 psi the strain was 2,870 microinches/inch.

Summary C-2. Test Procedures for Sphere 2

Type of Test. Critical pressure of concrete sphere under short-term external hydrostatic loading.

Test Procedures. Pressurized with seawater at 1,000 psi/min rate till implosion occurred. The surface of the sphere was first coated with Epocast 8288 and then with polyurethane varnish. Imploded at 3,050 psi of external hydrostatic pressure. The concrete in the sphere wall was dry at the time of implosion.

Instrumentation. The sphere was instrumented with electric resistance strain gages bonded to its exterior and interior surfaces, and to a metallic hoop attached with two screws to the interior of the sphere. Shell Epon 815 was used for the bonding and waterproofing of gages.

Data. Only one strain gage mounted directly on the interior surface of the sphere, and two gages mounted on a hoop strain transducer attached to the sphere's interior functioned during the test. The hoop transducer data was erratic. At 3,000 psi the strain on the interior of the sphere was 2,940 microinches/inch.

Summary C-3. Test Procedures for Sphere 3

Type of Test. Critical pressure of concrete sphere under short-term external hydrostatic loading.

Test Procedures. Pressurized with seawater at 1,000 psi/min rate till implosion occurred. The surface of the sphere was coated with Epocast 8288, and thereafter coated with polyurethane varnish. Imploded at 3,200 psi of external hydrostatic pressure. The concrete in the sphere wall was dry at the time of implosion.

Instrumentation. The sphere was instrumented with electric strain gages bonded to its exterior and interior surfaces with Shell Epon 815, which was also used for the waterproofing of gages.

Data. Only one strain gage which was mounted on the exterior of the sphere remained functional during the test. At 3,000 psi the strain on the exterior of the sphere was 3,050 microinches/inch.

Summary C-4. Test Procedures for Sphere 4

Type of Test. Permeability of concrete under external hydrostatic pressure.

Test Procedures. The uncoated sphere was to be pressurized with seawater to 3,000 psi and then held at that pressure while the rate of water flow through concrete was monitored. The sphere, however, imploded at 2,950 psi during the pressurization process. The sphere was being pressurized at 1,000 psi/min rate when the implosion occurred. Concrete in the sphere wall was partially permeated with water at time of implosion.

Instrumentation. The sphere was instrumented with an electronic water level monitor placed inside the sphere whose exterior was not coated with any waterproofing compound.

Data. No water leaked into the interior of the sphere prior to implosion.

Summary C-5. Test Procedures for Sphere 5

Type of Test. Permeability of concrete under external hydrostatic pressure.

Test Procedures. The uncoated sphere was pressurized with seawater to 1,500 psi and held under that pressure for 4 days. Subsequently the sphere was subjected to additional pressure at 1,000 psi/min rate till implosion occurred. The implosion occurred at 2,850 psi. The concrete in the sphere wall was thoroughly permeated with water at the time of implosion.

Instrumentation. The sphere was instrumented with an electronic level indicator mounted inside the sphere.

Data. After 21 hours at 1,500 psi of hydrostatic pressure, permeating seawater reached the interior surface of the sphere. Malfunctioning of the chart recorder made the determination of the subsequent flow rate into the vessel impossible.

Summary C-6. Test Procedures for Sphere 6

Type of Test. Permeability of concrete under external hydrostatic pressure.

Test Procedures. The uncoated sphere was pressurized with seawater to 750 psi, held at that pressure for 20 days, and then removed from the pressure vessel for inspection. After drying out for 20 days it was repressurized with seawater to 1,500 psi and held at that pressure for 7 days. After removal for inspection and drying for 9 days it was pressurized to 2,000 psi and held at that pressure for 8 days. The 2,000 psi pressurization test was concluded with pressurization of the sphere to 2,500 psi and holding it at that pressure till failure occurred after 10 minutes. The concrete in the sphere wall was wet at the time of implosion.

Instrumentation. The sphere was instrumented with an electronic and hydraulic water-level indicator placed inside the sphere.

Data. During the first pressurization at 750 psi, the water penetrated to the inside of the sphere after 11 days and then leaked in at a rate of 2.5 milliliters/hour. The salinity of the water reaching the inside of the sphere was approximately 20% less than that of the water surrounding the sphere. After the sphere was dried for 20 days, the second pressurization (1,500 psi) was instituted. This pressure was held for 7 days without detectable leakage. Following a 9-day drying period the third pressurization period (2,000 psi) was started. After holding at this pressure for 8 days without detectable leakage, the pressure was increased at a rate of 100 psi/min until 2,500 psi was reached. This pressure level was maintained until the sphere failed by implosion after a period of 10 minutes.

Summary C-7. Test Procedures for Sphere 7

Type of Test. Critical pressure of concrete sphere under long-term external hydrostatic loading.

Test Procedures. The sphere, coated with polyurethane varnish, was pressurized to 2,850 psi and held at that pressure till implosion occurred after 25 hours. The concrete in the sphere was wet at the time of implosion.

Instrumentation. No instrumentation was used with this sphere.

Data. The failure of the sphere was of the local type (see Figure C-1) creating a small hole in the sphere's wall. The test cylinders (Table C-7) that were coated with polyurethane varnish and tested in the pressure vessel together with sphere 7 were also found to be permeated with seawater. This is reflected in their compressive strength which was the same as of uncoated cylinders subjected to the same test conditions.

Summary C-8. Test Procedures for Sphere 8

Type of Test. Critical pressure of concrete sphere under long-term external hydrostatic loading.

Test Procedures. The exterior of the sphere was coated with Epocast 8288, and subsequently covered with a 1/16-inch-thick layer of RTV 501 silicone rubber. The sphere was pressurized to 3,000 psi and held at that pressure for 3 days. It was then depressurized and allowed to relax at zero pressure for 3 days. The second pressurization applied at a rate of 100 psi/min resulted in failure by implosion at 3,600 psi. The concrete in the sphere walls was dry at the time of implosion.

Instrumentation. The sphere was instrumented with electric resistance strain gages attached to the exterior and interior surfaces.

Data. The strains measured on the exterior and interior of the sphere during the initial pressurization, relaxation, and repressurization periods are plotted in Figures 8 through 13. During the second pressurization cycle, when the sphere was imploded, strains were measured that indicate plastic buckling of the sphere occurred. The accompanying concrete test cylinders, coated with polyurethane varnish and a top coat of RTV 501 silicon rubber were found to be partially permeated with water after pressurization due to local failure of the coating system over collapsed, near-surface cavities in the concrete.

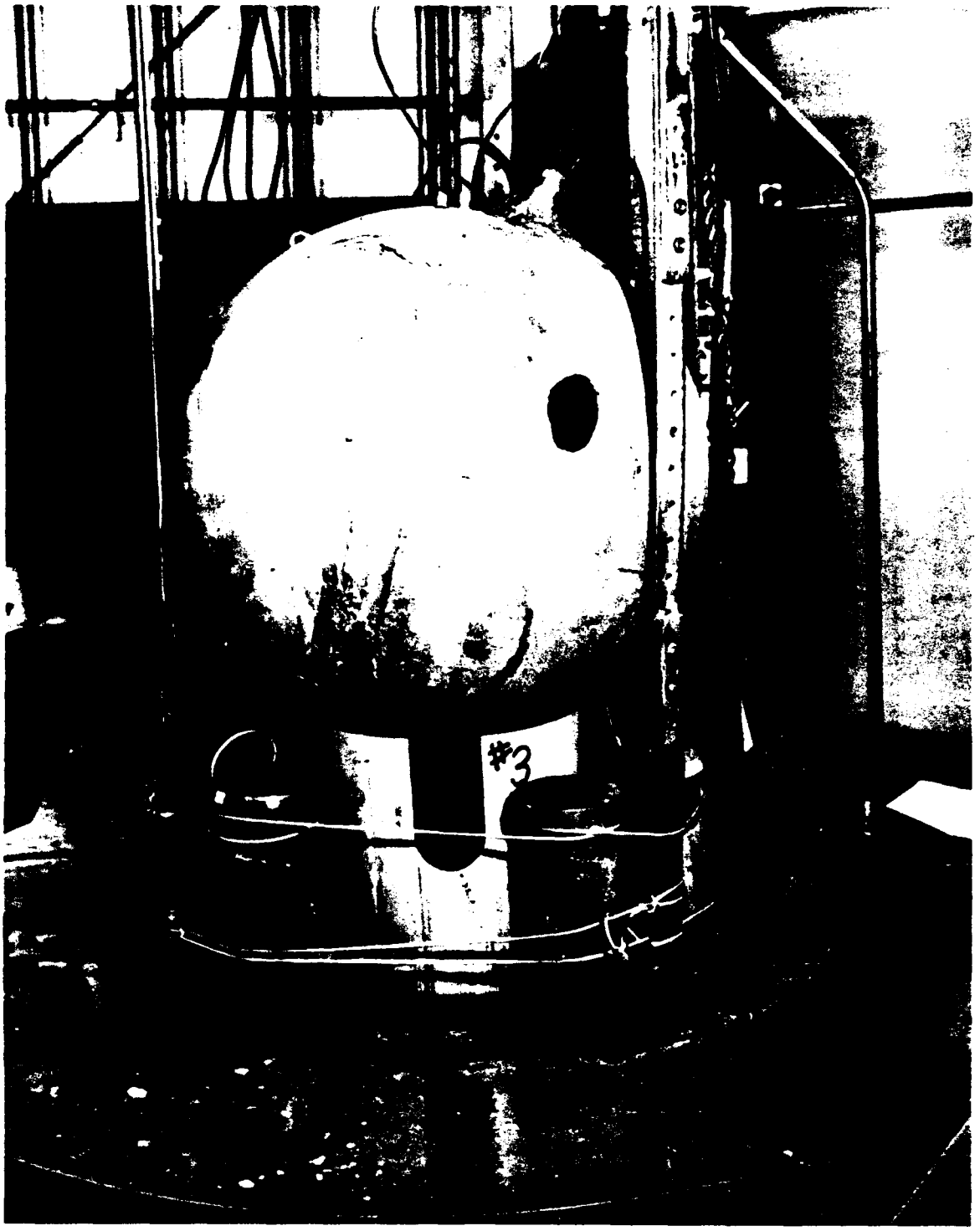

Figure C-1. Localized failure of sphere 7.

Summary C-9. Test Procedures for Sphere 9

Type of Test. Critical pressure of concrete sphere under long-term external hydrostatic loading.

Test Procedures. The sphere, coated with Epocast Wes-Top 415, was pressurized to 3,000 psi at 1,000 psi/min rate and was held at that pressure till implosion, which occurred after 24 minutes. The concrete in the sphere was partially permeated with seawater at the time of implosion.

Instrumentation. The sphere was instrumented with electric resistance strain gages located on the exterior and interior of the sphere.

Data. Strains on the interior surface of the sphere, after rapid pressurization to a pressure of 3,000 psi, averaged 3,170 microinches/inch, while those on the outside surface averaged 2,710 microinches/inch. The average compressive creep in the concrete that occurred during the 24 minutes that the sphere withstood the 3,000 psi hydrostatic pressure, was 240 microinches/inch for the outside surface and 340 microinches/inch for the inside surface. The concrete test cylinders which had been treated with Epocast Wes-Top 415 were found to be partially permeated with seawater after pressurization.

Summary C-10. Test Procedures for Sphere 10

Type of Test. Permeability of concrete under external hydrostatic pressure.

Test Procedures. The uncoated sphere was pressurized to 2,500 psi and then held at that pressure till collapse of the sphere occurred after 5 hours. The concrete in the sphere was partially permeated with seawater at the time of implosion.

Instrumentation. The sphere was instrumented with a hydraulic water level indicator only.

Data. There was no water collected in the sphere cavity at the time of implosion. The concrete test cylinders coated with polyurethane varnish were found to be partially permeated with seawater after pressurization.

Summary C-11. Test Procedures for Sphere 11

Type of Test. Permeability of concrete under external hydrostatic pressure.

Test Procedures. The uncoated sphere was pressurized to 2,000 psi in seawater and was held at that pressure for 6 days. The concrete in the sphere was found to be totally permeated by seawater.

Instrumentation. The sphere was instrumented with hydraulic water level indicators only.

Data. No water was found in the sphere cavity prior to its implosion at 2,000 psi after being pressurized with seawater for 6 days. Concrete test cylinders coated with polyurethane varnish were found to be almost totally permeated with seawater after pressurization. Test cylinder coated with Dow Corning's 92.018 was only partially permeated with seawater after pressurization.

Summary C-12. Test Procedures for Sphere 12

Type of Test. Permeability of concrete under external hydrostatic pressure.

Test Procedures. The uncoated sphere was pressurized to 1,500 psi in seawater, and was held at that pressure for 13 days. Subsequently the sphere was pressurized at 1,000 psi/min rate till implosion occurred at 2,750 psi. The concrete in the sphere was totally permeated with seawater at the time of implosion.

Instrumentation. The level of water inside the sphere was determined by draining it at regular time intervals through a tube inserted into the sphere.

Data. After 32 hours at 1,500 psi water penetrated to the interior of the sphere. Flow continued at approximately 5 milliliters/hour rate for additional 11 days till pressure was raised to 2,750 psi and the sphere imploded. The concrete itself contained approximately 2 grams of water per cubic inch of concrete. The concrete test cylinders coated with polyurethane varnish were almost totally permeated by seawater after pressurization.

Table C-1. Test Parameters and Results for Cylinders Tested With Sphere 1
(All cylinders uncoated)

Test Cylinder No.	Days Cured at Relative Humidity of:		Duration of Pretest Immersion in Seawater at:		Age at Test (days)	Uniaxial Compressive Strength (psi)
	100%	20%	3,100 psi	0 psi		
Hemisphere Z824						
Z825	23	18	—	—	41	8,950
Z826	23	18	5 min	1 hr	41	8,750
Z827	23	18	—	—	41	9,100
Z828	23	18	5 min	1 hr	41	8,050
Z829	23	0	—	—	23	7,330
Z830	23	0	—	—	23	7,220
Hemisphere Z837						
Z838	22	18	—	—	40	9,410
Z839	22	18	5 min	1 hr	40	9,255
Z840	22	18	—	—	40	9,510
Z841	22	18	5 min	1 hr	40	8,750
Z842	22	0	—	—	22	7,840
Z843	22	0	—	—	22	7,720

Table C-2. Test Parameters and Results for Cylinders Tested With Sphere 2
(All cylinders uncoated)

Test Cylinder No.	Days Cured at Relative Humidity of:		Duration of Pretest Immersion in Seawater at:		Age at Test (days)	Uniaxial Compressive Strength (psi)
	100%	20%	3,050 psi	0 psi		
Hemisphere Z892						
Z893	24	0	—	—	24	5,670
Z894	24	0	—	—	24	5,750
Z895	24	26	—	—	50	9,900
Z896	24	26	—	—	50	9,620
Z897	24	26	—	—	50	9,590
Z898	24	26	5 min	1 hr	50	9,140
Z899	24	26	5 min	1 hr	50	9,000
Z900	24	26	5 min	1 hr	50	9,000
Hemisphere Z902						
Z903	23	0	—	—	23	5,730
Z904	23	0	—	—	23	6,790
Z905	23	26	—	—	49	9,870
Z906	23	26	—	—	49	9,660
Z907	23	26	—	—	49	9,800
Z908	23	26	5 min	1 hr	49	9,120
Z909	23	26	5 min	1 hr	49	7,870

Table C-3. Test Parameters and Results for Cylinders Tested With Sphere 3
(All cylinders uncoated)

Test Cylinder No.	Days Cured at Relative Humidity of:		Duration of Pretest Immersion in Seawater at:		Age at Test (days)	Uniaxial Compressive Strength (psi)
	100%	20%	3,200 psi	0 psi		
Hemisphere Z915						
Z916	35	0	—	—	35	8,670
Z917	35	0	—	—	35	8,590
Z918	35	0	—	—	35	8,560
Z919	35	13	—	—	48	10,100
Z920	35	13	—	—	48	9,900
Z921	35	13	—	—	48	9,900
Z922	35	13	5 min	1 hr	48	9,850
Z923	35	13	5 min	1 hr	48	9,690
Hemisphere Z925						
Z926	34	0	—	—	34	8,350
Z927	34	0	—	—	34	8,460
Z928	34	0	—	—	34	8,330
Z929	34	13	—	—	47	10,000
Z930	34	13	—	—	47	9,960
Z931	34	13	—	—	47	9,820
Z932	34	13	5 min	1 hr	47	9,690
Z933	34	13	5 min	1 hr	47	9,800
Z934	34	13	5 min	1 hr	47	9,680

Table C-4. Test Parameters and Results for Cylinders Tested With Sphere 4
(All cylinders uncoated)

Test Cylinder No.	Days Cured at Relative Humidity of:		Duration of Pretest Immersion in Seawater at:		Age at Test (days)	Uniaxial Compressive Strength (psi)
	100%	20%	3,000 psi	0 psi		
Hemisphere 43A						
44A	71	92	1 day	1 day	165	7,890
45A	71	92	1 day	1 day	165	7,710
46A	71	92	1 day	1 day	165	6,680
47A	71	92	—	2 days	165	10,240
48A	71	92	—	2 days	165	10,380
49A	71	92	—	2 days	165	10,540
50A	71	94	—	—	165	10,510
51A	71	94	—	—	165	10,710
52A	71	94	—	—	165	10,240
Hemisphere 53A						
54A	70	92	1 day	1 day	164	7,800
55A	70	92	1 day	1 day	164	7,640
56A	70	92	1 day	1 day	164	7,900
57A	70	92	—	2 days	164	10,510
58A	70	92	—	2 days	164	10,380
59A	70	92	—	2 days	164	10,500
60A	70	94	—	—	164	10,950
61A	70	94	—	—	164	10,500
62A	70	94	—	—	164	10,820

Table C-5. Test Parameters and Results for Cylinders Tested With Sphere 5
(All cylinders uncoated)

Test Cylinder No.	Days Cured at Relative Humidity of:		Duration of Pretest Immersion in Seawater at:		Age at Test (days)	Uniaxial Compressive Strength (psi)
	100%	20%	1,500 psi	285 psi		
Hemisphere Z982						
Z983	71	21	4 days	3 min	96	8,180
Z984	71	21	4 days	3 min	96	8,120
Z985	71	21	4 days	3 min	96	8,080
Z986	71	21	4 days	3 min	96	8,240
Z987	71	25	—	—	96	10,200
Z988	71	25	—	—	96	10,480
Z989	71	25	—	—	96	10,800
Z990	71	25	—	—	96	10,480
Z991	71	25	—	—	96	10,550
Hemisphere Z992						
Z993	70	21	4 days	3 min	95	8,100
Z994	70	21	4 days	3 min	95	8,190
Z995	70	21	4 days	3 min	95	8,260
Z996	70	21	4 days	3 min	95	8,100
Z997	70	25	—	—	95	10,600
Z998	70	25	—	—	95	10,550
Z999	70	25	—	—	95	10,200
1A	70	25	—	—	95	10,500
2A	70	25	—	—	95	10,720

Table C-6. Test Parameters and Results for Cylinders Tested With Sphere 6 (All cylinders uncoated; age at test 186 days)

Test Cylinder No.	Days Cured at Relative Humidity of:		Duration (days) of Pretest Immersion in Seawater at:		Drying Period at 20% RH (days)	Duration (days) of Pretest Immersion in Seawater at:		Drying Period at 20% RH (days)	Duration (days) of Pretest Immersion in Seawater at:		Drying Period at 20% RH (days)	Duration of Pretest Immersion in Seawater at:		Uniaxial Compressive Strength (psi)
	100%	20%	750 psi	0 psi		1,500 psi	0 psi		2,000 psi	0 psi		2,500 psi	0 psi	
Hemisphere 83A														
84A	74	46	20	—	22	7	—	8	8	—	—	10[1]	2[2]	8,560
85A	74	46	20	—	22	7	—	8	8	—	—	10	2	8,330
86A	74	46	20	—	22	7	—	8	8	—	—	10	2	8,060
87A	74	46	—	20	22	—	7	8	—	8	—	—	2	10,100
88A	74	46	—	20	22	—	7	8	—	8	—	—	2	10,380
89A	74	46	—	20	22	—	7	8	—	8	—	—	2	10,280
90A	74	66	—	—	22	—	—	15	—	—	10	—	2	10,610
91A	74	66	—	—	22	—	—	15	—	—	10	—	—	10,750
92A	74	66	—	—	22	—	—	15	—	—	10	—	—	10,740
Hemisphere 93A														
94A	73	46	20	—	22	7	—	8	8	—	—	10	2	7,940
95A	73	46	20	—	22	7	—	8	8	—	—	10	2	8,040
96A	73	46	20	—	22	7	—	8	8	—	—	10	2	7,950
97A	73	46	—	20	22	—	7	8	—	8	—	—	2	9,700
98A	73	46	—	20	22	—	7	8	—	8	—	—	2	7,500
99A	73	46	—	20	22	—	7	8	—	8	—	—	2	10,090
100A	73	66	—	—	22	—	—	8	—	—	10	—	—	10,540
101A	73	66	—	—	22	—	—	8	—	—	10	—	—	10,520
102A	73	66	—	—	22	—	—	8	—	—	10	—	—	10,550

1/ Minutes.
2/ Days.

Table C-7. Test Parameters and Results for Cylinders Tested With Sphere 7

Test Cylinder No.	Days Cured at Relative Humidity of:		Duration of Pretest Immersion in Seawater at:		Age at Test (days)	Uniaxial Compressive Strength (psi)	Surface Coating
	100%	20%	2,850 psi	0 psi			
Hemisphere 23A							
24A	71	183	15 days	—	269	8,320	None
25A	71	183	15 days	—	269	8,400	Polyurethane varnish
26A	71	183	15 days	—	269	8,350	None
27A	71	183	—	15 days	269	9,280	None
28A	71	183	—	15 days	269	11,300	Polyurethane varnish
29A	71	183	—	15 days	269	9,900	None
30A	71	198	—	—	269	11,900	None
31A	71	198	—	—	269	11,550	Polyurethane varnish
32A	71	198	—	—	269	11,550	None
Hemisphere 33A							
34A	70	183	15 days	—	268	7,420	None
35A	70	183	15 days	—	268	7,550	Polyurethane varnish
36A	70	183	15 days	—	268	7,520	None
37A	70	183	—	15 days	268	10,900	None
38A	70	183	—	15 days	268	10,500	Polyurethane varnish
39A	70	183	—	15 days	268	8,850	None
40A	70	198	—	—	268	10,100	None
41A	70	198	—	—	268	11,150	Polyurethane varnish
42A	70	198	—	—	268	11,000	None

Table C-8. Test Parameters and Results for Cylinders Tested With Sphere 8

Test Cylinder No.	Days Cured at Relative Humidity of:		Duration of Pretest Immersion in Seawater at:		Age at Test (days)	Uniaxial Compressive Strength (psi)	Surface Coating
	100%	20%	3,000 psi	0 psi			
Hemisphere Z935							
Z936	69	245	3 days	3 days	320	7,250	None
Z937	69	245	3 days	3 days	320	8,100	First coat, polyurethane varnish; second coat, RTV 501 silicone rubber
Z938	69	245	3 days	3 days	320	7,150	None
Z939	69	245	—	6 days	320	9,850	None
Z940	69	245	—	6 days	320	10,600	First coat, polyurethane varnish; second coat, RTV 501 silicone rubber
Z941	69	245	—	6 days	320	11,300	None
Z942	69	251	—	—	320	11,500	None
Z943	69	251	—	—	320	11,400	None
Hemisphere Z945							
Z946	70	245	3 days	3 days	321	7,150	None
Z947	70	245	3 days	3 days	321	8,150	First coat, polyurethane varnish; second coat, RTV 501 silicone rubber
Z948	70	245	3 days	3 days	321	7,380	None
Z949	70	245	—	6 days	321	9,850	None
Z950	70	245	—	6 days	321	10,450	First coat, polyurethane varnish; second coat, RTV 501 silicone rubber
Z951	70	245	—	6 days	321	10,500	None
Z952	70	251	—	—	321	11,000	None
Z953	70	251	—	—	321	10,900	None

Table C-9. Test Parameters and Results for Cylinders Tested With Sphere 9

Test Cylinder No.	Days Cured at Relative Humidity of:		Duration of Pretest Immersio in Seawater at:		Age at Test (days)	Uniaxial Compressive Strength (psi)	Surface Coating
	100%	20%	3,000 psi	0 psi			
Hemisphere A3							
4A	70	205	24 min	1 day	276	8,750	None
5A	70	205	24 min	1 day	276	9,170	Epocast Wes-Top 415
6A	70	205	24 min	1 day	276	8,750	None
7A	70	205	—	1 day	276	9,150	None
8A	70	206	—	—	276	10,350	Epocast Wes-Top 415
9A	70	205	—	1 day	276	8,950	None
10A	70	206	—	—	276	10,600	None
11A	70	205	—	1 day	276	10,100	Epocast Wes-Top 415
12A	70	206	—	—	276	10,500	None
Hemisphere A13							
14A	69	205	24 min	1 day	275	8,725	None
15A	69	205	24 min	1 day	275	9,730	Epocast Wes-Top 415
16A	69	205	24 min	1 day	275	8,570	None
17A	69	205	—	1 day	275	9,140	None
18A	69	205	—	1 day	275	10,900	Epocast Wes-Top 415
19A	69	205	—	1 day	275	9,360	None
20A	69	206	—	—	275	10,900	None
21A	69	206	—	—	275	10,900	Epocast Wes-Top 415
22A	69	206	—	—	275	10,900	None

Table C-10. Test Parameters and Results for Cylinders Tested With Sphere 10

Test Cylinder No.	Days Cured at Relative Humidity of:		Duration of Pretest Immersion in Seawater at:		Age at Test (days)	Uniaxial Compressive Strength (psi)	Surface Coating
	100%	20%	2,500 psi	0 psi			
Hemisphere A63							
64A	71	196	5 hr	30 hr	270	8,050	None
65A	71	196	5 hr	30 hr	270	9,000	Polyurethane varnish
66A	71	196	5 hr	30 hr	270	8,550	None
67A	71	196	—	36 hr	270	10,500	None
68A	71	196	—	36 hr	270	11,400	Polyurethane varnish
69A	71	196	—	36 hr	270	10,500	None
70A	71	199	—	—	270	11,200	None
71A	71	199	—	—	270	11,600	Polyurethane varnish
72A	71	199	—	—	270	11,500	None
Hemisphere A73							
74A	70	196	5 hr	30 hr	269	8,000	None
75A	70	196	5 hr	30 hr	269	9,000	Polyurethane varnish
76A	70	196	5 hr	30 hr	269	8,230	None
77A	70	196	—	36 hr	269	10,000	None
78A	70	196	—	36 hr	269	10,900	Polyurethane varnish
79A	70	196	—	36 hr	269	10,200	None
80A	70	199	—	—	269	10,900	None
81A	70	199	—	—	269	10,600	Polyurethane varnish
82A	70	199	—	—	269	10,900	None

Table C-11. Test Parameters and Results for Cylinders Tested With Sphere 11

Test Cylinder No.	Days Cured at Relative Humidity of:		Duration of Pretest Immersion in Seawater at:		Age at Test (days)	Uniaxial Compressive Strength (psi)	Surface Coating
	100%	20%	2,000 psi	0 psi			
Hemisphere A103							
104A	127	155	6 days	1 day	289	7,250	None
105A	127	155	6 days	1 day	289	8,100	Polyurethane varnish
106A	127	155	6 days	1 day	289	8,075	None
107A	127	155	—	7 days	289	7,300	None
108A	127	155	—	7 days	289	10,450	Polyurethane varnish
109A	127	155	—	7 days	289	10,250	None
110A	127	162	—	—	289	11,150	None
111A	127	162	—	—	289	10,800	Polyurethane varnish
112A	127	162	—	—	289	10,900	None
Hemisphere A113							
114A	126	155	6 days	1 day	288	7,550	None
115A	126	155	6 days	1 day	288	9,100	Dow Corning 92.018
116A	126	155	6 days	1 day	288	7,275	None
117A	126	155	—	7 days	288	10,400	None
118A	126	155	—	7 days	288	11,100	Polyurethane varnish
119A	126	155	—	7 days	288	10,200	None
120A	126	162	—	—	288	10,800	None
121A	126	162	—	—	288	11,000	Polyurethane varnish
122A	126	162	—	—	288	10,700	None

Table C-12. Test Parameters and Results for Cylinders Tested With Sphere 12

Test Cylinder No.	Days Cured at Relative Humidity of:		Duration of Pretest Immersion in Seawater at:		Age at Test (days)	Uniaxial Compressive Strength (psi)	Surface Coating
	100%	20%	1,500 psi	0 psi			
Hemisphere 123A							
124A	190	70	13 days	—	273	7,650	None
125A	190	70	13 days	—	273	7,500	Polyurethane varnish
126A	190	70	13 days	—	273	7,600	None
127A	190	70	—	13 days	273	10,200	None
128A	190	70	—	13 days	273	10,850	Polyurethane varnish
129A	190	70	—	13 days	273	10,350	None
130A	190	83	—	—	273	11,000	None
131A	190	83	—	—	273	11,100	Polyurethane varnish
132A	190	83	—	—	273	10,750	None
Hemisphere 133A							
134A	189	70	13 days	—	272	7,800	None
135A	189	70	13 days	—	272	8,280	Polyurethane varnish
136A	189	70	13 days	—	272	7,900	None
137A	189	70	—	13 days	272	10,050	None
138A	189	70	—	13 days	272	11,000	Polyurethane varnish
139A	189	70	—	13 days	272	10,400	None
140A	189	83	—	—	272	11,050	None
141A	189	83	—	—	272	11,200	Polyurethane varnish
142A	189	83	—	—	272	11,250	None

REFERENCES

1. R. J. Roark. Formulas for stress and strain, 3rd ed. New York, McGraw-Hill, 1954.

2. U. S. Navy. David W. Taylor Model Basin. Report 1759: The elastic buckling strength of spherical glass shells, by M. A. Krenzke and R. M. Charles. Washington, D. C., Sept. 1963. (AD 423 588)

3. ———. Report 1757: The effect of initial imperfections on the collapse strength of deep spherical shells, by M. A. Krenzke and T. J. Kiernan. Washington, D. C., Feb. 1965. (AD 612 100)

4. U. S. Naval Civil Engineering Laboratory. Technical Report R-333-I: Study of creep in concrete — Phase 1 (I-beam), by J. R. Keeton. Port Hueneme, Calif., Jan. 1965. R-333-II: Study of creep in concrete — Phase 2 (Hollow-box beam), by J. R. Keeton. Port Hueneme, Calif., Feb. 1965. R-333-III: Study of creep in concrete — Phases 3, 4, and 5, by J. R. Keeton. Port Hueneme, Calif., May 1965.

U. S. Naval Civil Engineering Laboratory
BEHAVIOR OF SPHERICAL CONCRETE HULLS UNDER HYDROSTATIC LOADING — PART I. EXPLORATORY INVESTIGATION
by J. D. Stachiw and K. O. Gray
R-517 69 p. illus March 1967 Unclassified

1. Undersea structures — Spherical concrete hulls I. Y-F015-01-07-001

Hollow concrete spheres 16 inches in outside diameter have been tested to destruction by exposure to external hydrostatic pressure in seawater to determine the compressive strength and permeability of concrete under such loading. The testing has shown that for the particular mix used, the compressive strength of dry concrete in a spherical hull of 16-inch outside diameter and 1-inch wall thickness under biaxial loading (short-term hydrostatic pressurization to failure at a constant rate) is approximately 48% higher than for identical dry concrete in 3-inch-diameter by 6-inch-long solid test cylinders under uniaxial loading conditions. Concrete spheres in which the wall was thoroughly permeated by seawater failed at stress levels approximately 18% higher than 3-inch-diameter by 6-inch-long solid test cylinders. The permeability of uncoated spheres to seawater at simulated ocean pressure of 1,500 psi was approximately 6×10^{-3} milliliters per hour per square inch of area per 1 inch of thickness.

U. S. Naval Civil Engineering Laboratory
BEHAVIOR OF SPHERICAL CONCRETE HULLS UNDER HYDROSTATIC LOADING — PART I. EXPLORATORY INVESTIGATION
by J. D. Stachiw and K. O. Gray
R-517 69 p. illus March 1967 Unclassified

1. Undersea structures — Spherical concrete hulls I. Y-F015-01-07-001

Hollow concrete spheres 16 inches in outside diameter have been tested to destruction by exposure to external hydrostatic pressure in seawater to determine the compressive strength and permeability of concrete under such loading. The testing has shown that for the particular mix used, the compressive strength of dry concrete in a spherical hull of 16-inch outside diameter and 1-inch wall thickness under biaxial loading (short-term hydrostatic pressurization to failure at a constant rate) is approximately 48% higher than for identical dry concrete in 3-inch-diameter by 6-inch-long solid test cylinders under uniaxial loading conditions. Concrete spheres in which the wall was thoroughly permeated by seawater failed at stress levels approximately 18% higher than 3-inch-diameter by 6-inch-long solid test cylinders. The permeability of uncoated spheres to seawater at simulated ocean pressure of 1,500 psi was approximately 6×10^{-3} milliliters per hour per square inch of area per 1 inch of thickness.

U. S. Naval Civil Engineering Laboratory
BEHAVIOR OF SPHERICAL CONCRETE HULLS UNDER HYDROSTATIC LOADING — PART I. EXPLORATORY INVESTIGATION
by J. D. Stachiw and K. O. Gray
R-517 69 p. illus March 1967 Unclassified

1. Undersea structures — Spherical concrete hulls I. Y-F015-01-07-001

Hollow concrete spheres 16 inches in outside diameter have been tested to destruction by exposure to external hydrostatic pressure in seawater to determine the compressive strength and permeability of concrete under such loading. The testing has shown that for the particular mix used, the compressive strength of dry concrete in a spherical hull of 16-inch outside diameter and 1-inch wall thickness under biaxial loading (short-term hydrostatic pressurization to failure at a constant rate) is approximately 48% higher than for identical dry concrete in 3-inch-diameter by 6-inch-long solid test cylinders under uniaxial loading conditions. Concrete spheres in which the wall was thoroughly permeated by seawater failed at stress levels approximately 18% higher than 3-inch-diameter by 6-inch-long solid test cylinders. The permeability of uncoated spheres to seawater at simulated ocean pressure of 1,500 psi was approximately 6×10^{-3} milliliters per hour per square inch of area per 1 inch of thickness.

U. S. Naval Civil Engineering Laboratory
BEHAVIOR OF SPHERICAL CONCRETE HULLS UNDER HYDROSTATIC LOADING — PART I. EXPLORATORY INVESTIGATION
by J. D. Stachiw and K. O. Gray
R-517 69 p. illus March 1967 Unclassified

1. Undersea structures — Spherical concrete hulls I. Y-F015-01-07-001

Hollow concrete spheres 16 inches in outside diameter have been tested to destruction by exposure to external hydrostatic pressure in seawater to determine the compressive strength and permeability of concrete under such loading. The testing has shown that for the particular mix used, the compressive strength of dry concrete in a spherical hull of 16-inch outside diameter and 1-inch wall thickness under biaxial loading (short-term hydrostatic pressurization to failure at a constant rate) is approximately 48% higher than for identical dry concrete in 3-inch-diameter by 6-inch-long solid test cylinders under uniaxial loading conditions. Concrete spheres in which the wall was thoroughly permeated by seawater failed at stress levels approximately 18% higher than 3-inch-diameter by 6-inch-long solid test cylinders. The permeability of uncoated spheres to seawater at simulated ocean pressure of 1,500 psi was approximately 6×10^{-3} milliliters per hour per square inch of area per 1 inch of thickness.

Unclassified

Security Classification

DOCUMENT CONTROL DATA - R & D

Security classification of title, body of abstract and indexing annotation must be entered when the overall report is classified)

1 ORIGINATING ACTIVITY (Corporate author) U. S. Naval Civil Engineering Laboratory Port Hueneme, California 93041	2a. REPORT SECURITY CLASSIFICATION Unclassified 2b. GROUP

3 REPORT TITLE

Behavior of Spherical Concrete Hulls Under Hydrostatic Loading
Part I. Exploratory Investigation

4 DESCRIPTIVE NOTES (Type of report and inclusive dates)

Not final; April 1965 to May 1966

5 AUTHOR(S) (First name, middle initial, last name)

J. D. Stachiw and K. O. Gray

6 REPORT DATE	7a. TOTAL NO OF PAGES	7b. NO OF REFS
March 1967	69	4

8a CONTRACT OR GRANT NO b PROJECT NO Y-F015-01-07-001 c d	9a. ORIGINATOR'S REPORT NUMBER(S) R-517 9b. OTHER REPORT NO(S) (Any other numbers that may be assigned this report)

10 DISTRIBUTION STATEMENT

Distribution of this report is unlimited.
Copies of this document available at CFSTI $3.00.

11 SUPPLEMENTARY NOTES	12 SPONSORING MILITARY ACTIVITY
	Naval Facilities Engineering Command

13 ABSTRACT

Hollow concrete spheres 16 inches in outside diameter have been tested to destruction by exposure to external hydrostatic pressure in seawater to determine the compressive strength and permeability of concrete under such loading. The testing has shown that for the particular mix used, the compressive strength of dry concrete in a spherical hull of 16-inch outside diameter and 1-inch wall thickness under biaxial loading (short-term hydrostatic pressurization to failure at a constant rate) is approximately 48% higher than for identical dry concrete in 3-inch-diameter by 6-inch-long solid test cylinders under uniaxial loading conditions. Concrete spheres in which the wall was thoroughly permeated by seawater failed at stress levels approximately 18% higher than 3-inch-long solid test cylinders. The permeability of uncoated spheres to seawater at simulated ocean pressure of 1,500 psi was approximately 6×10^{-3} milliliters per hour per square inch of area per 1 inch of thickness.

DD FORM 1 NOV 65 1473 (PAGE 1)

S/N 0101-807-6801

Unclassified

Security Classification

14 KEY WORDS	LINK A		LINK B		LINK C	
	ROLE	WT	ROLE	WT	ROLE	WT
Undersea structures						
Spherical hulls						
Concrete hulls						
Hydrostatic loading						
Permeability of concrete						
Deformation of concrete						

Technical Report **R 547**

BEHAVIOR OF SPHERICAL CONCRETE HULLS UNDER HYDROSTATIC LOADING

PART II. Effect of Penetrations

October 1967

NAVAL FACILITIES ENGINEERING COMMAND

NAVAL CIVIL ENGINEERING LABORATORY

Port Hueneme, California

BEHAVIOR OF SPHERICAL CONCRETE HULLS UNDER HYDROSTATIC LOADING – PART II. Effect of Penetrations

Technical Report R-547

Y-F015-01-07-001

by

J. D. Stachiw

ABSTRACT

The objective of the study was (1) to show that concrete hulls with window and hatch penetrations for ocean bottom habitats can be built, and (2) to determine if the collapse pressure of such hulls is degraded by the incorporation of properly designed penetrations. All of the experimental work was performed on six concrete spheres (16-inch outside diameter and 14-inch inside diameter) cast from concrete with a uniaxial compressive strength of 10,000 psi. The concrete sphere models failed under hydrostatic pressures ranging from 2,675 psi to 3,400 psi, depending on the type of penetration insert. It was found that the collapse pressure of a concrete hull equipped with properly designed operational windows and hatches was the same as that of a similar concrete hull without penetrations.

CONTENTS

INTRODUCTION

There has been relatively little investigation of concrete hulls for fixed ocean-bottom manned and unmanned installations. There have been two primary reasons for this lack of interest: no immediate need existed for ocean-bottom installations with large enclosed areas under atmospheric pressure, and concrete was dismissed as a material for fixed hulls because of its inapplicability to underwater vehicle hull construction. Thus, so long as the requirements for underwater vehicles dominated the underwater engineering scene, there was little interest in concrete as material for external pressure hulls.

It is only very recently that serious thought has been given to utilizing concrete in compartmented underwater structures for fixed ocean-bottom installations. Recent exploratory studies with models of hollow concrete spheres[1] have shown that buoyant concrete spherical hulls are feasible for depths to 3,500 feet, while negatively buoyant spherical hulls could conceivably operate at depths of 10,000 feet. Thus, this study is initiated against a general background of need for ocean-bottom structures and proven feasibility of employing concrete for such structures.

Almost all designs for fixed underwater hulls rely on different types of penetrations for access to the interior of the structure, supply of power to equipment located in it, communication with shore-based personnel, and observation of hydrospace. Most of the penetrations in the hull are equipped with metallic or plastic insert assemblies that permit the access to the hull's interior, feeding in of wires and pipes, and insertion of transparent viewing panes without the leakage of water into the sphere's interior.

The presence of the penetrations with different types of bulkhead feedthrough assemblies in the hull wall causes stress concentrations in the hull structure that may result in failure of the hull at lower pressure than if the wall were solid. Thus, it is of paramount importance to know the magnitudes of stress concentrations around penetrations so that their effect on the hull's critical pressure can be accounted for.

The objective of the study reported here was to explore experimentally the relationship between (1) the rigidity of the penetration inserts, (2) the magnitude of stress concentrations generated by the presence of inserts in the concrete hull, and (3) the implosion pressure of the hull assembly.

Data from this exploratory study will serve two purposes: they will permit concrete hull designers to design underwater structures with a higher degree of confidence, and will serve as a guideline for further studies that will have as their objective the detailed investigation of stress concentrations in underwater concrete structures.

SCOPE OF INVESTIGATION

The study of the effect of penetrations on critical pressures of concrete hulls was limited to two areas of experimental investigation. One concerned itself with the design, fabrication, and testing of a working model of a habitat with a 16-inch outside diameter (OD) and 14-inch internal diameter (ID), representing a spherical underwater concrete structure with scaled operational windows and wire feedthroughs. The other area of investigation was limited to the testing of 16-inch-OD/14-inch-ID concrete spherical hull models having solid penetration inserts of different rigidities. Only two sizes of inserts, and three kinds of insert materials were experimentally evaluated. The aluminum, steel, and polyvinyl chloride (PVC) plastic inserts had spherical angle tapers of either 8 degrees, or 32 degrees 30 minutes. The two selected sizes of model penetration inserts were considered representative of the penetration inserts required for a full-sized spherical structure. The 32 degree 30 minute insert simulated a penetration insert required for man-sized hatches or windows, while the 8 degree insert simulated an electrical wiring or hydraulic piping feedthrough on an underwater hull structure of 10 to 20 feet in diameter.

EXPERIMENT DESIGN

The objective of designing, fabricating, and testing the spherical habitat model (Figure 1) was to prove the feasibility of concrete hulls with usable windows, hatches, and wire feedthroughs for service at an ocean depth of 3,500 feet. The model's dimensions, composition of the concrete mix, and method of casting were selected to be the same as in the previous feasibility study of concrete spherical hulls.[1] Thus, the critical pressure of the model with penetrations could be directly compared to the critical pressure of models without penetrations. The difference between the critical pressure of the habitat model and of the concrete spheres without penetrations would serve as a quantitative indicator of the decrease in hull strength resulting from the use of the particular type of window, hatch, and feedthrough insert designs. Since only one type of habitat model was designed and built, no variation of design parameters was contemplated.

The concrete spherical hull models (Table 1) had solid penetration inserts (Figure 2) of different rigidities; they were cast from the same mix and had the same dimensions as the habitat model. Since it is known that the magnitude of the stress concentration around a penetration in the hull is to a large degree dependent on the mismatch between the rigidity of the penetration insert and that of the hull material, a series of insert materials was selected

that represented a wide range of rigidity properties. The most rigid inserts selected were made of steel, while the least rigid inserts were made from polyvinyl chloride plastic; other inserts used were made from aluminum. It was planned that during the hydrostatic testing to destruction of the insert-equipped models, strains would be measured around the inserts and compared to strains existing in the same sphere away from the penetration inserts. Some quantitative measure of the stress concentration factors produced by inserts of different rigidities would thus be obtained.

Table 1. Description of Concrete Sphere Models and Test Procedures

(16-inch OD/14-inch ID; spheres 13 through 17 had 1- and 4-inch openings, sphere 18 had 1-inch opening)

Sphere No.	Type of Insert	Number of Strain Gage Rosettes	Procedure
13[1]	Functional acrylic windows and steel hatches	3	Hold for 8 days at 1,500 psi, then pressurize to implosion at 100 psi/min
14	Functional acrylic windows and steel hatches	3	Short-term implosion testing; pressurize at 100 psi/min
15	Solid steel inserts	4	Short-term implosion testing; pressurize at 100 psi/min
16	Solid aluminum inserts	4	Short-term implosion testing; pressurize at 100 psi/min
17	Solid PVC plastic inserts	4	Short-term implosion testing; pressurize at 100 psi/min
18	1-inch pipe instrumentation feedthrough	3	Short-term implosion testing; pressurize at 100 psi/min

[1] Tests on sphere specimens 1 through 12 were reported in Reference 1.

HULL MODELS

Fabrication

The six concrete spheres (16-inch OD/14-inch ID) were cast from a specially designed concrete mix in a hemispherical aluminum mold (Figures 3 and 4) used for casting similar spheres in previous NCEL concrete hull studies.[1] One of the spheres that served as a control for this study was cast without any penetrations, except for the instrumentation feedthrough. The five other spheres had the penetrations cast in (Figure 5). This was accomplished by providing dummy mold inserts that were inserted into the annular space between the male and female portions of the mold, and were subsequently bolted in place. After hardening of the concrete, the bolts holding the mold inserts to the mold were unscrewed and the concrete hemispherical shell was removed together with the inserts from the mold. Once the hemisphere was removed from the mold and dummy inserts were knocked out, the concrete was cured in a 100% relative humidity (RH) atmosphere for approximately 2 months.

After curing, the hemispheres were dried in 20% RH atmosphere. When dry, they were instrumented with electrical resistance strain gages (Figure 6), waterproofed with several coats of epoxy resin, and joined together into spheres by bonding with epoxy adhesive. When the adhesive had set, the spheres were equipped with penetration inserts (Figures 7 and 8), which were also set in place with epoxy adhesive. A detailed description of individual models and the penetration inserts used in them appears in Appendix A.

Instrumentation

The six concrete spherical hull models were each instrumented with 45-degree strain gage rosettes bonded to the interior surface of the sphere (Figures 9 and 10), and one 45-degree rosette bonded to one of the penetration inserts. One of the rosettes was located at the edge of the small penetration, the second was placed at the edge of the large penetration, the third was placed midway between them away from the penetrations, while the fourth was placed in the center of the penetration insert. With this strain gage arrangement it was planned to measure the strain concentration around the penetration inserts. The 45-degree rosette bonded to the low-pressure face of one of the large penetration inserts would measure the strain generated in the insert. Since the measurement of strain in concrete requires electrical resistance strain gages of at least 3/4-inch length, determination of the absolute value of the strain concentration was considered to be not feasible because the 3/4-inch

length of the strain gages would cause the gage to average out the strain reading. Thus, only a qualitative indication of the strain concentration around penetration inserts would be obtained. Still, it was hoped that by comparing the measured strains around penetration inserts differing in rigidity, some conclusion could be drawn on the relationship between the insert's rigidity and the strain increase in its vicinity. Planned investigation by NCEL employing photoelastic analysis of models of external pressure hulls with penetration inserts will determine with great precision not only the actual value of the strain concentration around inserts, but also the strain gradient around them.

Testing

Before they were tested to destruction in simulated hydrospace, the models were equipped with special feedthroughs for the instrumentation wiring (Figure 11). The specially designed feedthrough not only permitted the instrumentation leads to pass from the model to the recording equipment without being in contact with the pressurized seawater surrounding the model in the pressure vessel, but also made it possible to attach the model rigidly to the pressure vessel's end closure (Figures 12 and 13). With this type of arrangement the integrity of the sensitive strain gage circuits was assured, and the model was kept in the center of the pressure vessel without danger of striking the sides of the pressure vessel interior during lowering of the vessel head.

After placement of the sphere in the pressure vessel, the pressure vessel end closure was locked in place and the strain gage leads were connected to a strain recorder. During short-term implosion tests the test specimen (Figure 14) was pressurized at a rate of 100 psi/min, with strain readings being taken every 100 psi until implosion of the sphere occurred. After implosion, the fragments were removed from the pressure vessel and inspected to determine, if possible, how the fracture was initiated (Figures 15 through 22). Concurrently with the testing to destruction of the concrete sphere, the associated concrete test cylinders were taken from the 20% RH storage room and were crushed in a standard test fixture under uniaxial compressive loading.

For the long-term pressure testing of concrete spheres at a pressure of 1,500 psi, pressurization took place at a rate of 100 psi/min until 1,500 psi was reached. This pressure level was then maintained for the 200-hour duration of the long-term test. Upon termination of the long-term test, the pressurization was again restarted at a rate of 100 psi/min until implosion of the spherical hull model took place.

DISCUSSION

The experimental data from this study consist of recorded critical pressures at which implosions took place (Table 2) and strains measured at four different locations (Figures 9 and 10) on the sphere as 100 psi external hydrostatic pressure increments were applied (Figures 23 through 48). In general, test results indicate that the implosion strength of concrete hollow spheres was not decreased by the incorporation of properly designed penetration flanges. Also, it appears that the use of solid penetration inserts had no deleterious influence on the implosion strength of spheres, so long as the compressive modulus of elasticity of an insert was equal to, or higher than that of the concrete. The long-term pressurization of the concrete hull model shows that ocean bottom habitat models with a factor of safety of two are practical to an operational depth of 3,500 feet. During testing, no windows or hatches failed or were permanently deformed prior to implosion of the concrete habitat models.

When the implosion pressures of the concrete hull models with operational windows and hatches (spheres 13 and 14) were compared to the implosion pressure of the concrete hull model without such penetrations (sphere 18), no significant difference was found between them (Table 2). It was also found that there is no significant difference between critical pressures of concrete hull models with solid penetration inserts (spheres 15, 16, and 17) and the model without penetrations (sphere 18), so long as the rigidity of the insert was equal to, or greater than, the rigidity of the concrete hull model.

The strains measured at the small penetrations (Figures 23, 26, 29, 33, 37, 41) in the concrete hull models were not found to be significantly different from strains measured at locations in the sphere remote from penetrations (Figures 24, 27, 30, 34, 42, 43, 44). Whether this indicates that there are no stress concentrations around the small penetrations in the concrete hull could not be positively proven with the 3/4-inch-long strain gage used, as the distance from the center of the 3/4-inch strain gage rosette to the edge of the penetration was 1/2 inch. The 3/4-inch length of the individual rosette legs tended to average out the high strains possibly present at the edge of the penetration with the lower strains away from the penetration. The fairly large distance from the center of the rosette to the edge of penetration caused the gage to miss the strain peak generally present at the very edge of a penetration.

The strains measured at the large penetrations (Figures 25, 28, 31, 35, 39) in the concrete hull models were found to be significantly higher (Figure 39) than strains measured at locations in the sphere away from penetrations (Figure 38) only in sphere No. 17, which had solid plastic inserts in the penetrations. The strains measured by the strain gage rosette 1/2 inch

away from the edge of the penetration with a plastic insert were approximately 40% higher than the strains in the same sphere not in close proximity to penetrations. Significantly, as already mentioned, this is also the sphere that failed at a hydrostatic pressure approximately 20% lower than the average implosion pressure of spheres 13, 14, 15, 16 and 18. The higher strains at the large penetration, as well as the lower implosion pressure of sphere 17 with the plastic inserts, are valid indications that stress concentrations exist at penetrations filled with inserts whose rigidity is less than that of concrete. In this case the mismatch in the rigidities of the PVC plastic insert and the concrete wall is in the ratio of approximately 1:8.

The tangent modulus of elasticity (E_t) of concrete under short-term uniaxial compression (2,100-psi/min loading rate) was found to decrease with increasing stress level. Analysis of the axial strains on the exterior surface of concrete test cylinders under uniaxial compression (Figure 44) shows that the average tangent modulus of elasticity for the concrete mix employed in the casting of spheres 13 through 18 (Figure 45) is 3.68×10^6 psi in the 0- to 4,500-psi stress range, but decreases rapidly at higher stress levels. Thus, at the 10,000-psi stress level, the same concrete mix shows a decrease of the average tangent modulus of elasticity to 1.48×10^6. At 11,000 psi, just prior to failure of concrete test cylinders, the average tangent modulus of elasticity becomes less than 0.5×10^6 psi. It is not known what the magnitude of the tangent modulus of elasticity is at stress levels above 10,000 psi inside the sphere under triaxial loading at the moment of implosion, but it appears that it is more than under uniaxial loading at comparable stress level. Still in absence of information describing E_t under biaxial and triaxial loading as found in the sphere, experimentally determined E_t for uniaxial loading was utilized in calculation of stresses from strains measured on the sphere (Figure 49).

Failure of spheres appeared to have taken place due to plastic buckling of the hull, as evidenced by the presence of many large fragments after implosion. No major spalling of interior or exterior hull surfaces seems to have taken place since the original epoxy coating that had been applied to the surfaces of the spheres prior to testing was adhering firmly everywhere to the surfaces of the sphere fragments. The hydrostatic implosion was observed to be relatively slow, on the order of 1 to 2 seconds.

When the strains on the interior of the 0.0625 t/D ratio concrete hull models are translated into stresses utilizing the E_t (Figure 45) measured on the exterior of uniaxially tested cylinders (Figure 44), it is found that the measured stresses at locations remote from the penetrations (Figure 49) are of the same magnitude as stresses derived analytically for the interior of a 0.0625 t/D ratio thick sphere in the 0- to 5,000-psi stress range, corresponding to the linear range of E_t under uniaxial loading. For example, at 1,000 psi external hydrostatic loading the average stress measured on the interior of the sphere (using $E_t = 3.68 \times 10^6$ psi) is 4,420 psi, while the stress calculated on

the basis of thick-wall sphere expression[1] (Figure 49) is 4,550 psi. At calculated stress levels above 6,000 psi considerable difference exists between calculated and experimentally determined stresses on the interior of the sphere, regardless of whether a constant $E_t = 3.68 \times 10^6$ psi, or E_t varying according to Figure 45, is utilized in the equation converting measured strains to stresses. Using constant E_t the experimentally determined stresses are found to be higher than the calculated ones, while using variable E_t the experimentally determined stresses are found to be lower than calculated ones (Figure 49).

Table 2. Summary of Test Results

Sphere No.	Type of Insert	Procedure	Implosion Pressure (psi)	Age of Concrete (days)	Strength of Concrete (psi)[1]	Modulus of Elasticity of Concrete (psi)[2]
13	Functional acrylic windows and steel hatches	Held at 1,500 psi for 8 days, then pressurized to implosion at 100 psi/min	3,300	350	10,840	3.45×10^6
14	Functional acrylic windows and steel hatches	Short-term implosion test; 100 psi/min pressurization	3,300	310	9,640	3.64×10^6
15	Solid steel inserts $E = 27 \times 10^6$ psi	Short-term implosion test; 100 psi/min pressurization	3,485	330	11,205	3.85×10^6
16	Solid aluminum inserts $E = 10 \times 10^6$ psi	Short-term implosion test; 100 psi/min pressurization	3,400	335	11,165	3.62×10^6
17	Solid PVC plastic inserts $E = 0.5 \times 10^6$ psi	Short-term implosion test; 100 psi/min pressurization	2,675	330	11,150	3.55×10^6
18	1-inch pipe instrumentation feedthrough	Short-term implosion test; 100 psi/min pressurization	3,375	320	11,480	3.48×10^6

[1] Strength and modulus of elasticity of concrete were determined by subjecting 3 x 6-inch test cylinders of the same mix and age as the associated concrete sphere to compression testing in an uniaxial test machine. The compressive strength shown is the average of 18 test cylinders loaded to destruction at 2,100 psi/min.

[2] Modulus of elasticity in a concrete test cylinder under 2,500 psi uniaxial compressive stress.

The strains measured on the interior surface of the solid inserts (Figures 32, 36, 40) were found to vary inversely with the modulus of elasticity of the given insert material, which for steel is 27×10^6 psi, for aluminum 10.4×10^6 psi, and for PVC plastic 0.5×10^6 psi. Thus at 1,000-psi external hydrostatic pressure loading, the strains in steel, aluminum, and plastic inserts were 225, 450, and 650 μin./in., respectively. When these strains are translated into stresses they are found to be 8,680 psi for steel (Figure 50), 6,700 psi for aluminum (Figure 51), and 460 psi for plastic inserts (Figure 52). When the stresses in inserts are compared to the 950-μin./in. strain and 4,420-psi stress on the interior of concrete sphere at locations away from the penetrations, it is found that when the rigidity of the insert is higher than that of the surrounding concrete, the stresses at the center of the insert are found to be higher than in concrete. When the rigidity of the insert is less than of the concrete, the stresses in the insert are also found to be less than in concrete.

Time-dependent strains measured on the interior of concrete sphere 13, which was subjected to external hydrostatic pressure of 1,500 psi for 200 hours, show four distinct levels of strain rates (Figures 46, 47, and 48). The magnitude of the strain rates is inversely related to elapsed time from application of the sustained load. The four strain-rate levels are:

a. 0 to 15 minutes after pressurization to 1,500 psi: 5 μin./in./min.
b. 15 minutes to 2 hours after pressurization to 1,500 psi: 0.2 μin./in./min.
c. 2 to 140 hours after pressurization to 1,500 psi: 0.015 μin./in./min.
d. 140 to 200 hours after pressurization to 1,500 psi: 0.001 μin./in./min.

The critical pressure of sphere 13, which was subjected to sustained hydrostatic pressure of 1,500 psi for 200 hours, is the same as the critical pressure of identical sphere 14, which was subjected only to implosion testing. This would seem to indicate that prior pressurization at the 1,500-psi level sustained for 200 hours did not decrease the short-term critical pressure of the spherical concrete habitat model.

FINDINGS

1. Properly designed penetration inserts for 0.0625-thickness-to-diameter-ratio concrete spheres do not decrease the critical pressure of such spheres under short-term hydrostatic loading.

2. The magnitude of strains around the penetrations, strains in the inserts, and the critical pressure of concrete spheres is a function of the penetration insert rigidity.

3. The strains on the interior of 0.0625-thickness-to-diameter-ratio concrete spheres can be calculated only for stress levels below 5,000 psi on the basis of thick-wall analytical expression. At higher stress levels, values for experimental and calculated strains diverge markedly.

CONCLUSIONS

1. Concrete pressure hulls for ocean bottom habitats with penetrations and inserts in the form of windows and hatches can be so designed and built that the presence of penetrations will not markedly decrease the critical pressure of the concrete hull.

2. Ocean-bottom habitats of spherical shape require a minimum safety factor of two, based on their short-term critical pressure, in order for the concrete hull to safely withstand the hydrostatic loading found at 3,500-foot depth for long periods of time.

FUTURE STUDIES

Various other studies in the continuing program for investigation of factors which affect the performance of concrete underwater habitats are in progress or being planned. At the present time there is only one study in progress, and its objective is the exploratory determination of stresses, strains, and permeability rates in concrete spherical hull models of 16-inch outside diameter and 1-, 2-, 3-, and 4-inch wall thickness. In this study the relationship between the thickness-to-diameter ratio and the behavior of the concrete spheres will be investigated.

ACKNOWLEDGMENTS

The concrete mix used in the fabrication of the spheres was designed by Mr. W. R. Lorman of NCEL's Materials Division.

The mixing of the concrete, the molding of the hemispheres and the curing of the spheres were under the personal supervision of Mr. D. F. Griffin, Director of Materials Division.

The assembly, instrumentation, coating, testing, and data reduction were done by Mr. J. V. Graham, Senior Technician of the Ocean Engineering Division.

The detail design of the ocean-bottom habitat model was done by Mr. G. P. McMahan of the Design Division.

The test arrangements reflect many ideas of Mr. K. O. Gray, Senior Project Scientist, for which the author is grateful.

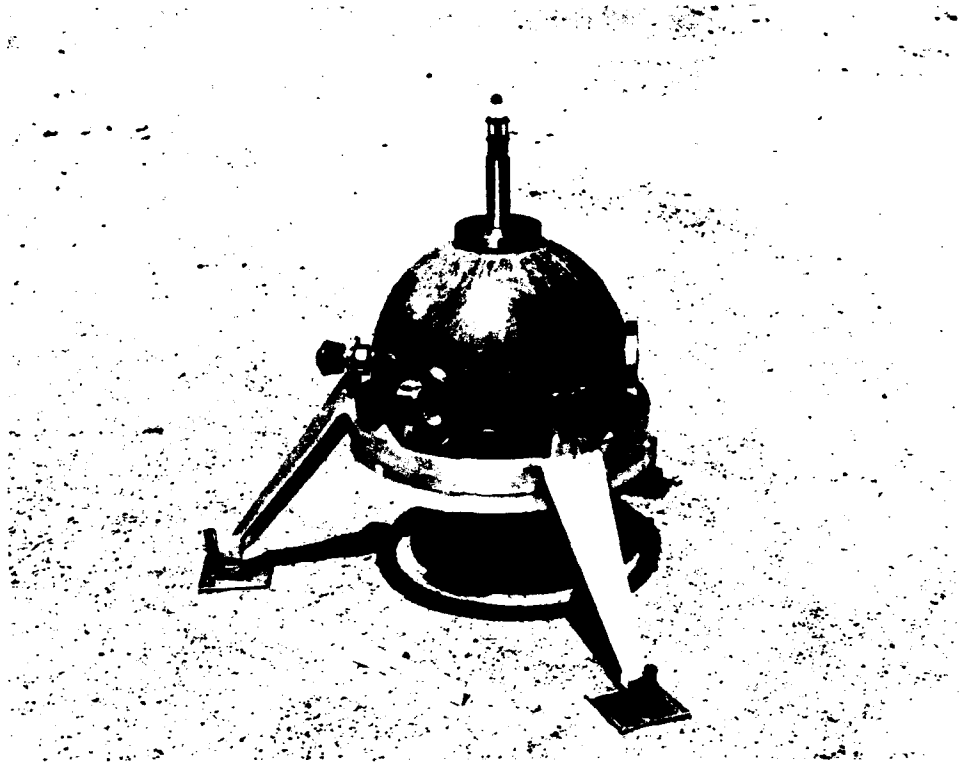

Figure 1. Model of 16-inch-OD spherical concrete hull equipped with scaled operational windows, hatches, and feedthroughs.

Figure 2. Model of 16-inch-OD spherical concrete hull equipped with solid penetration inserts.

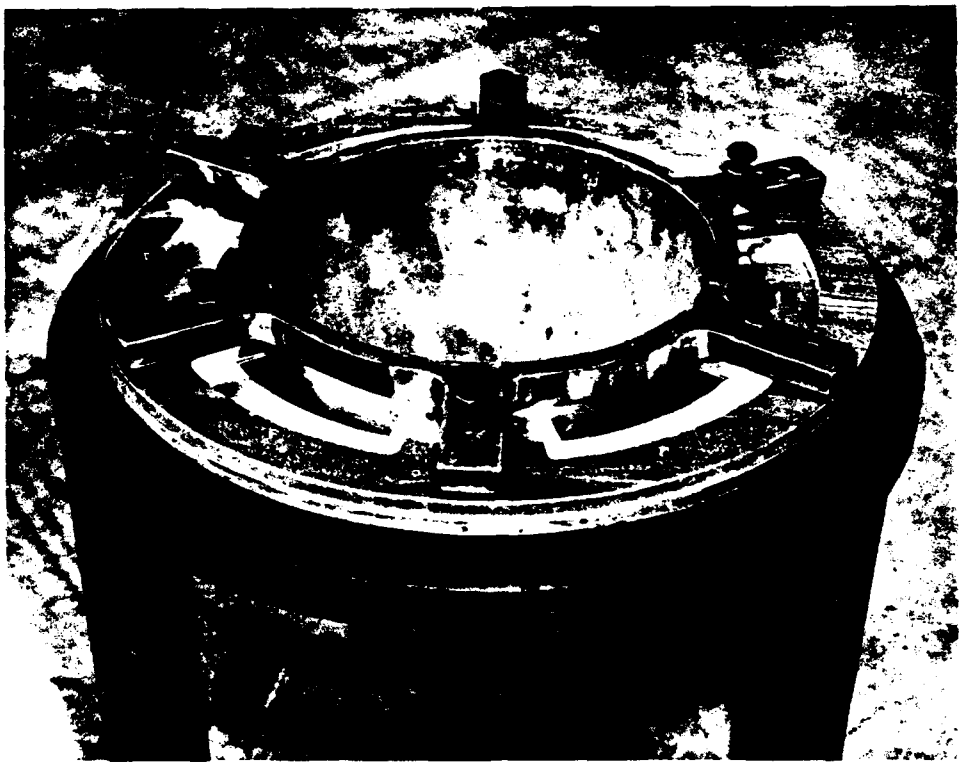

Figure 3. Assembled mold and rack used for casting 16-inch-OD/14-inch-ID concrete spheres.

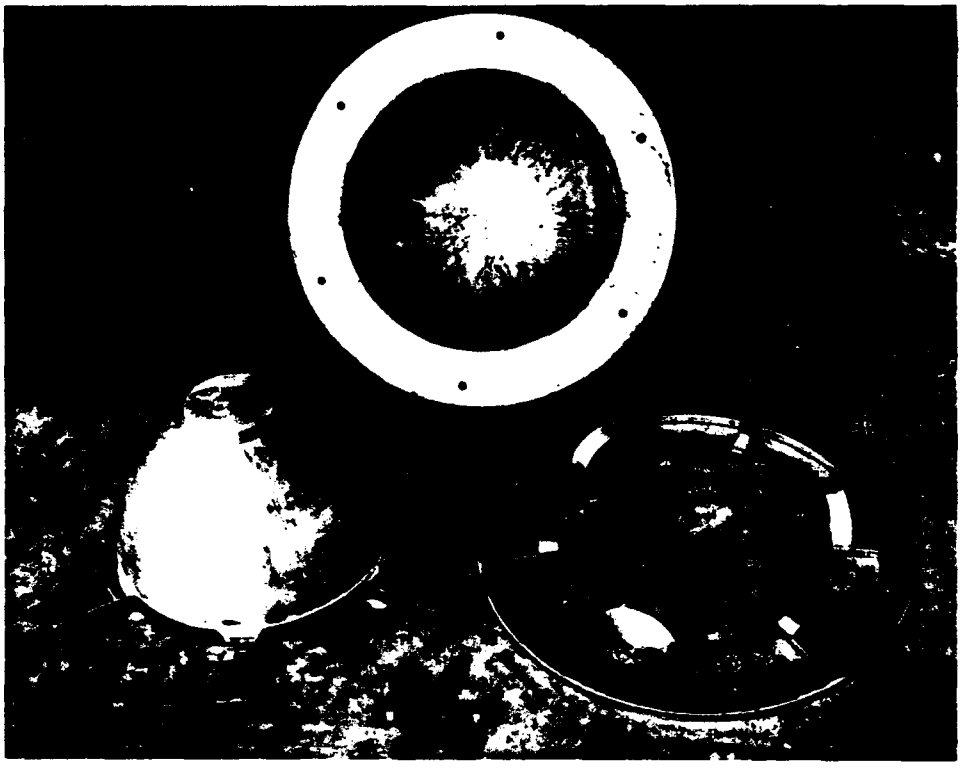

Figure 4. Disassembled mold used for casting concrete spheres.

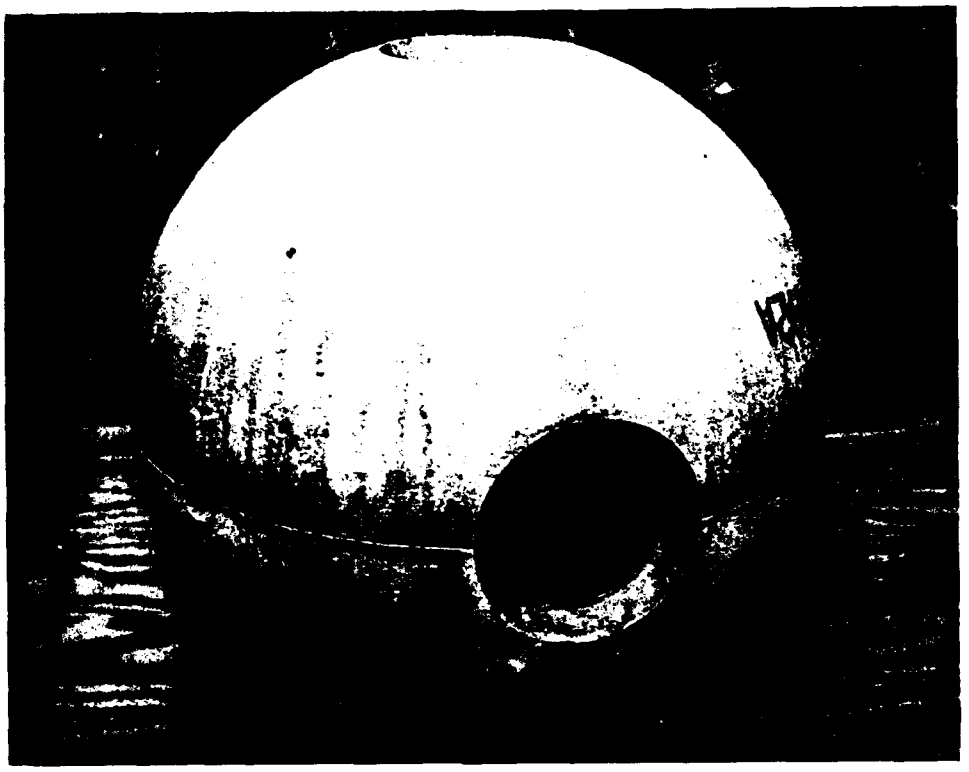

Figure 5. Typical 16-inch-OD concrete sphere prior to bonding of hemispheres and placement of penetration inserts.

Figure 6. Interior of typical 16-inch-OD concrete sphere with electric resistance strain gages in place.

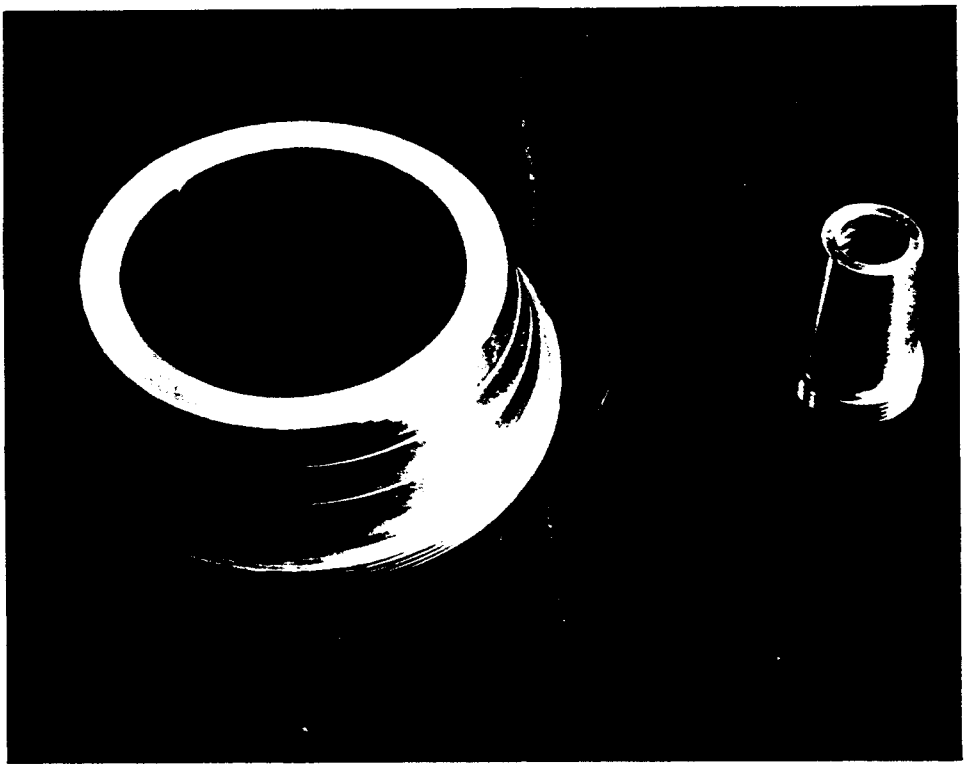

Figure 7. Penetration inserts for mounting scaled operational windows and wire feedthroughs in the concrete sphere models.

Figure 8. Solid penetration inserts for concrete sphere models.

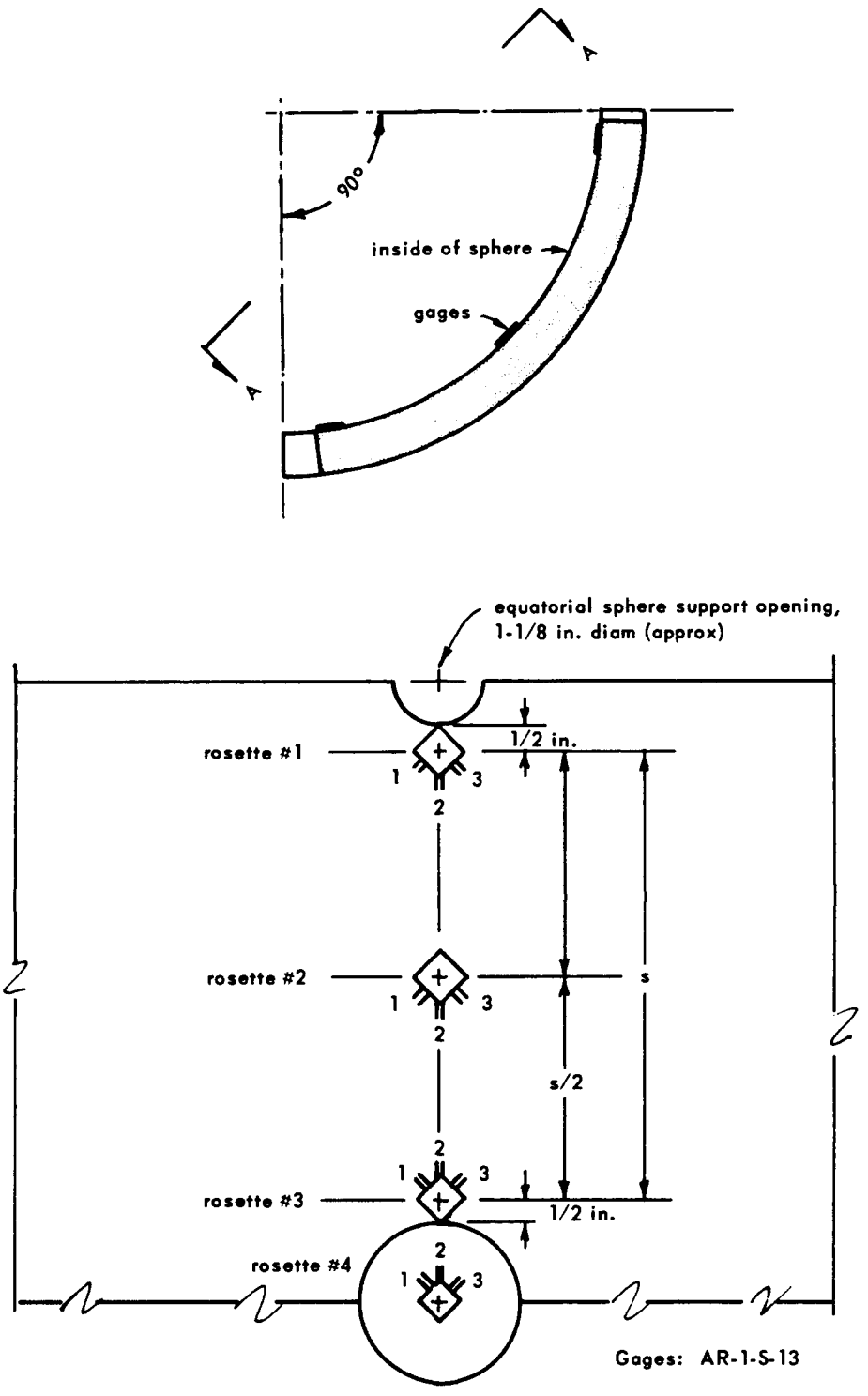

View A-A

Figure 9. Location of strain gages on the inside surface of concrete spheres with window penetrations.

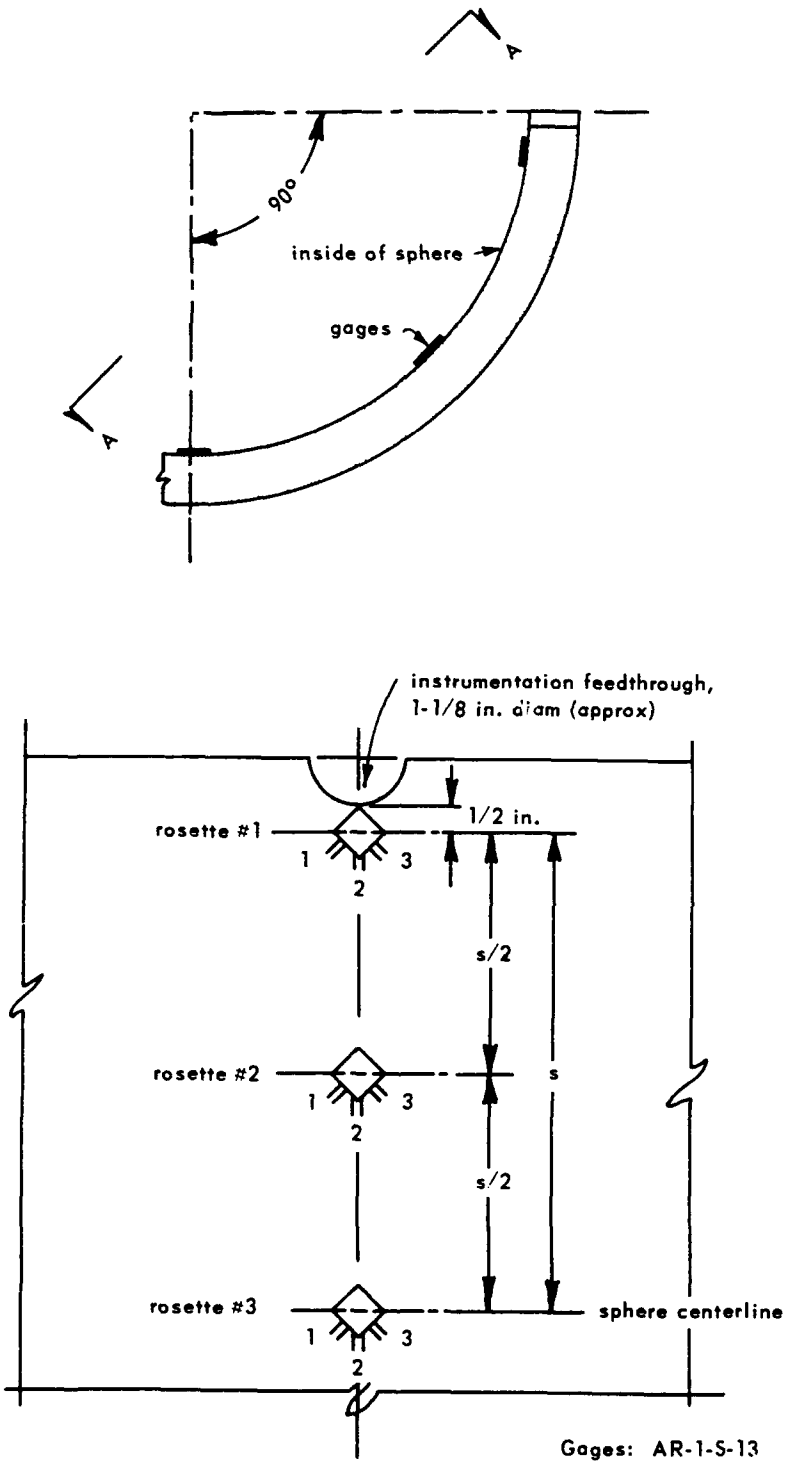

View A-A

Figure 10. Location of strain gages on the inside surface of the concrete sphere without window penetrations.

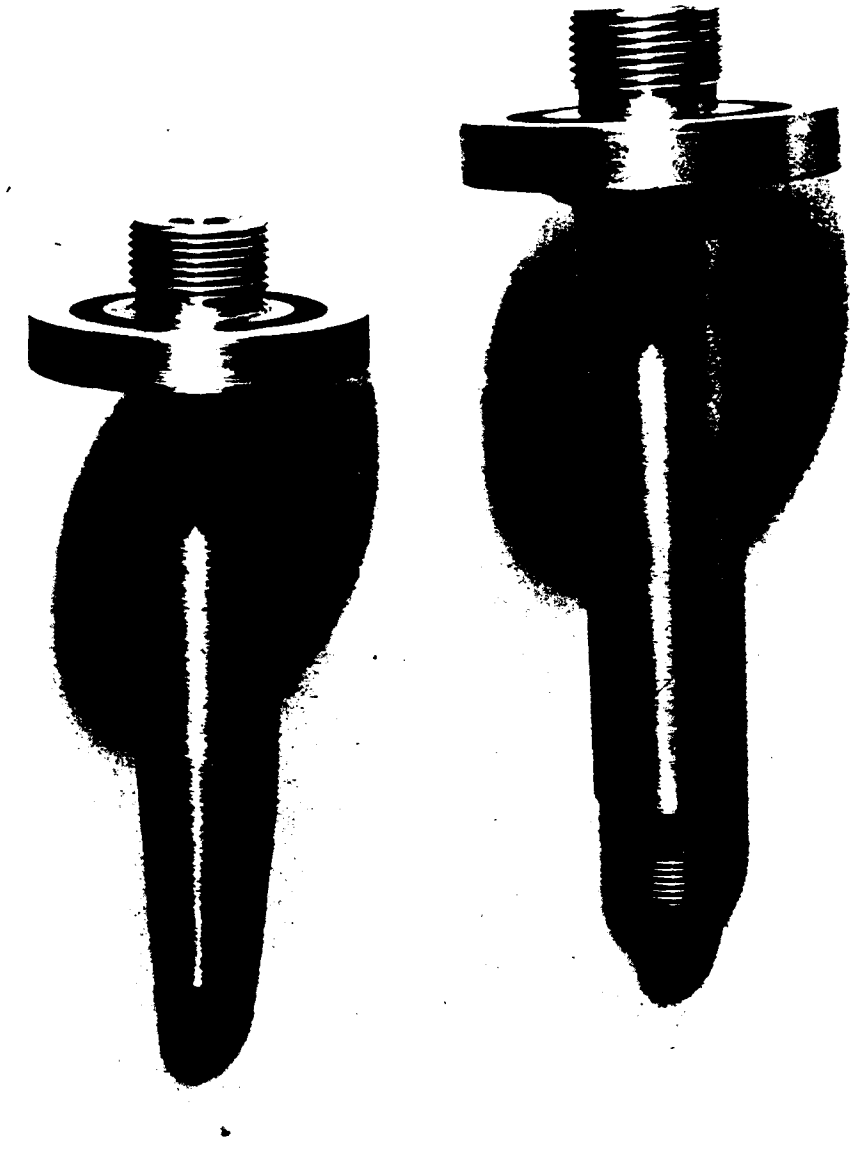

Figure 11. Feedthroughs for strain gage instrumentation; the flanged end is screwed into the pressure vessel head.

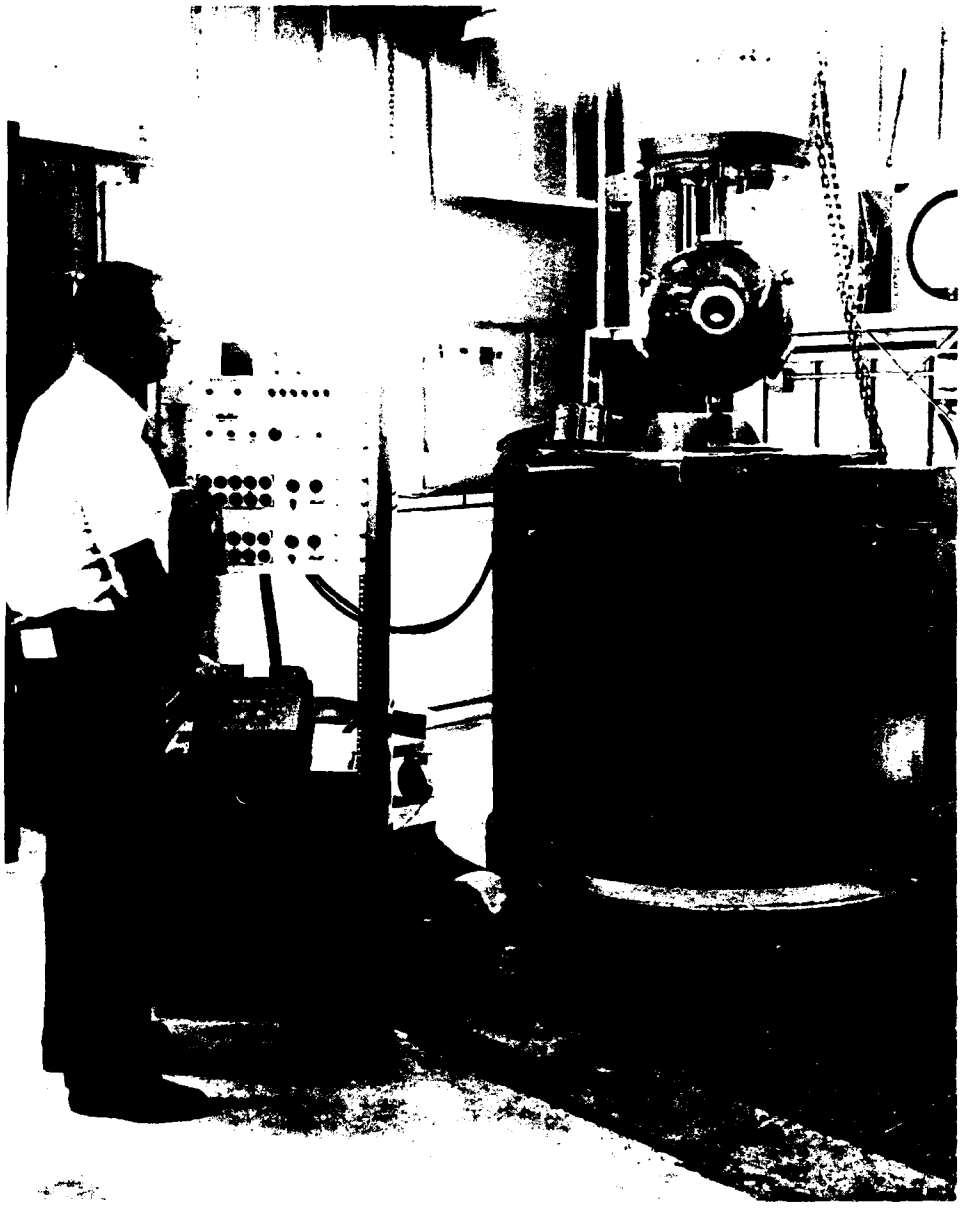

Figure 12. Concrete sphere with operational windows ready for placement in the NCEL 18-inch-ID pressure vessel.

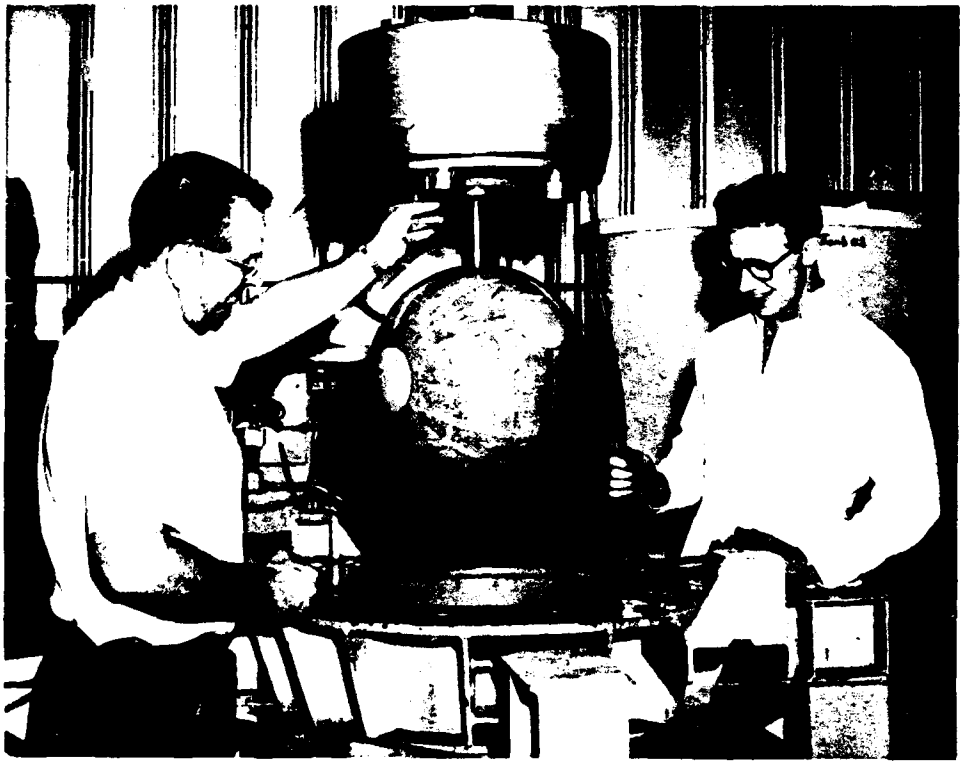

Figure 13. Concrete sphere with solid penetration inserts ready for testing in the NCEL 18-inch-ID pressure vessel.

Figure 14. Pressurizing concrete sphere to destruction with seawater pumped by air-powered, positive-displacement pumps.

Figure 15. Remnants of sphere 14 with operational windows and hatch after implosion at 3,300 psi.

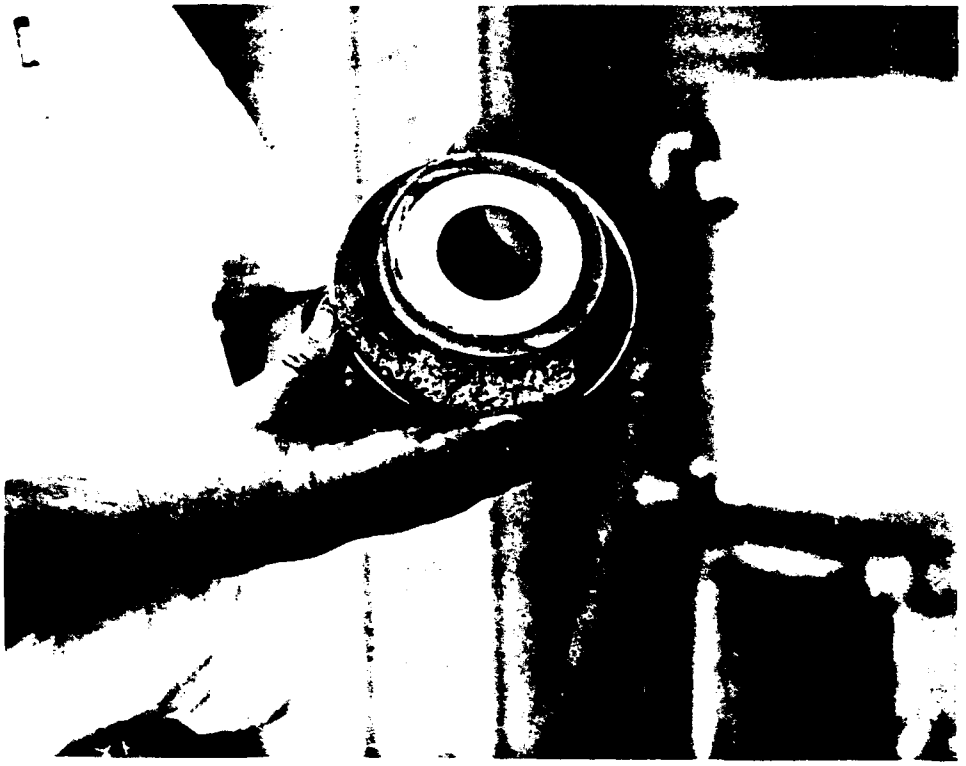

Figure 16. Penetration insert with operational window after implosion of the concrete sphere model at 3,300 psi.

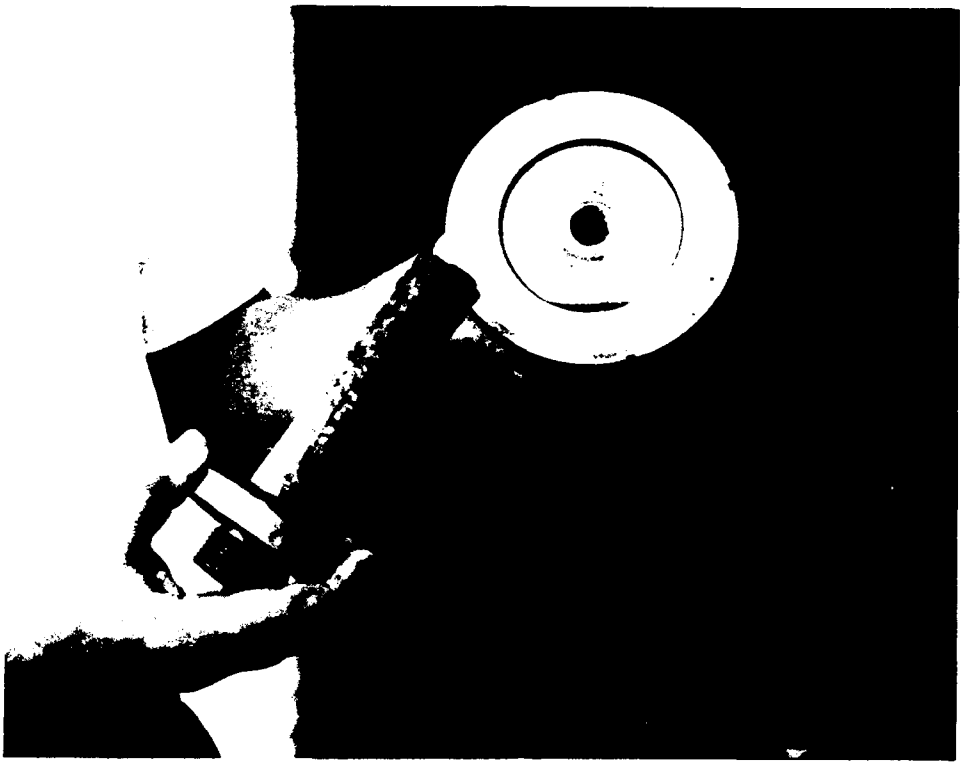

Figure 17. Penetration insert with hatch from which the feedthrough has broken off during implosion of the concrete sphere at 3,300 psi.

Figure 18. Fragments of sphere with steel inserts after implosion at 3,485 psi.

Figure 19. Fragments of sphere with solid aluminum inserts after implosion at 3,400 psi.

Figure 20. Fragments of sphere with polyvinyl chloride plastic inserts after implosion at 2,675 psi.

Figure 21. Fragments of sphere without inserts except for the instrumentation lead feedthrough after implosion at 3,375 psi.

Figure 22. Fragments of sphere with window inserts after 5-day pressurization at 1,500 psi with subsequent pressurization to implosion at 3,300 psi.

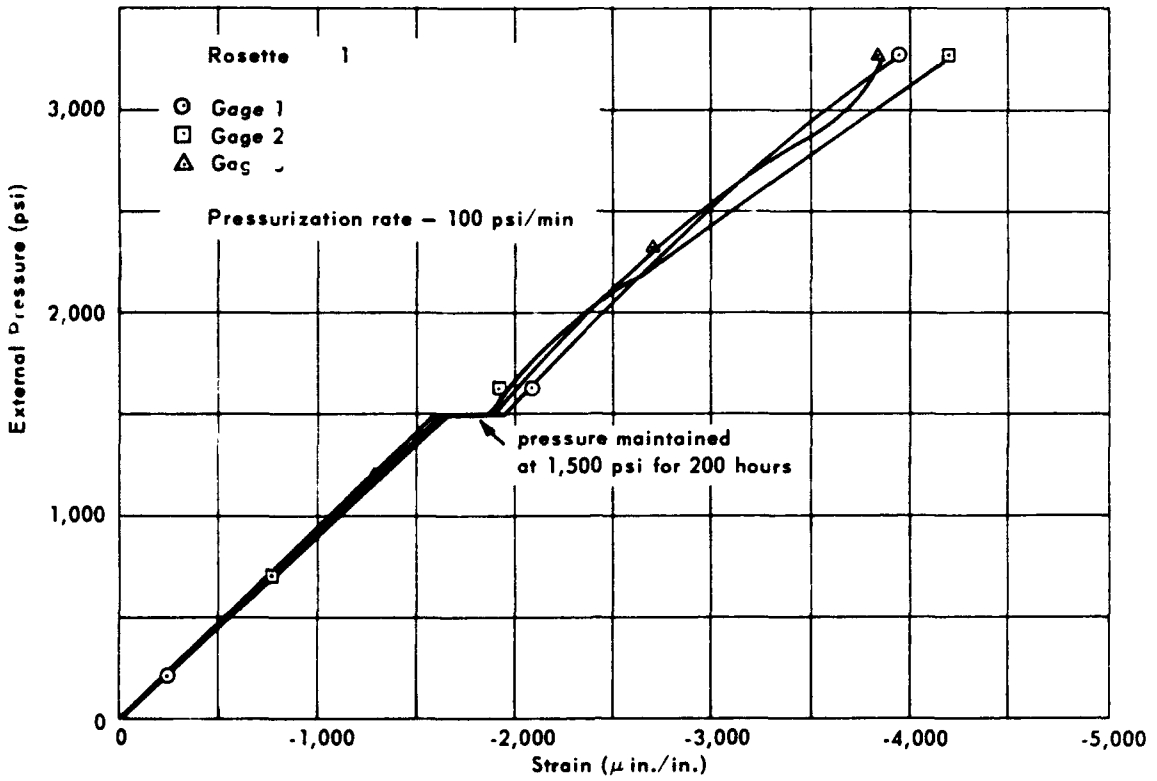

Figure 23. Strains on the interior of sphere 13 at the small penetration.

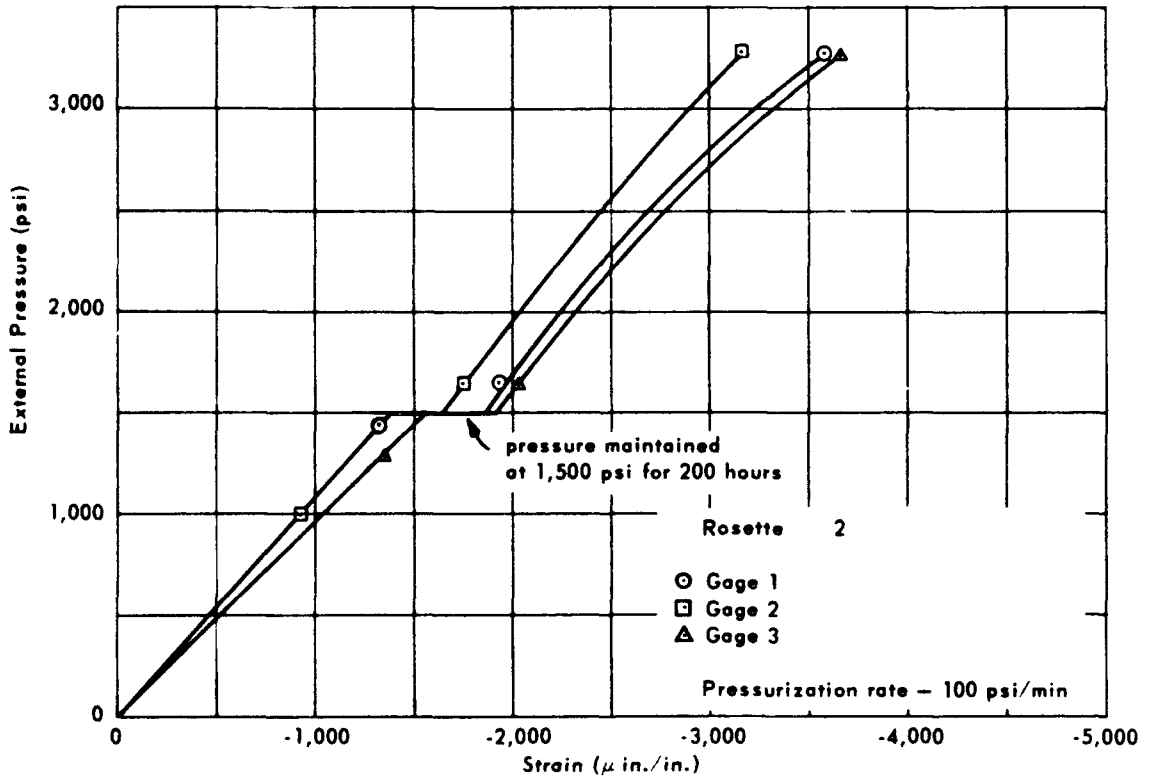

Figure 24. Strains on the interior of sphere 13 midway between small and large penetrations.

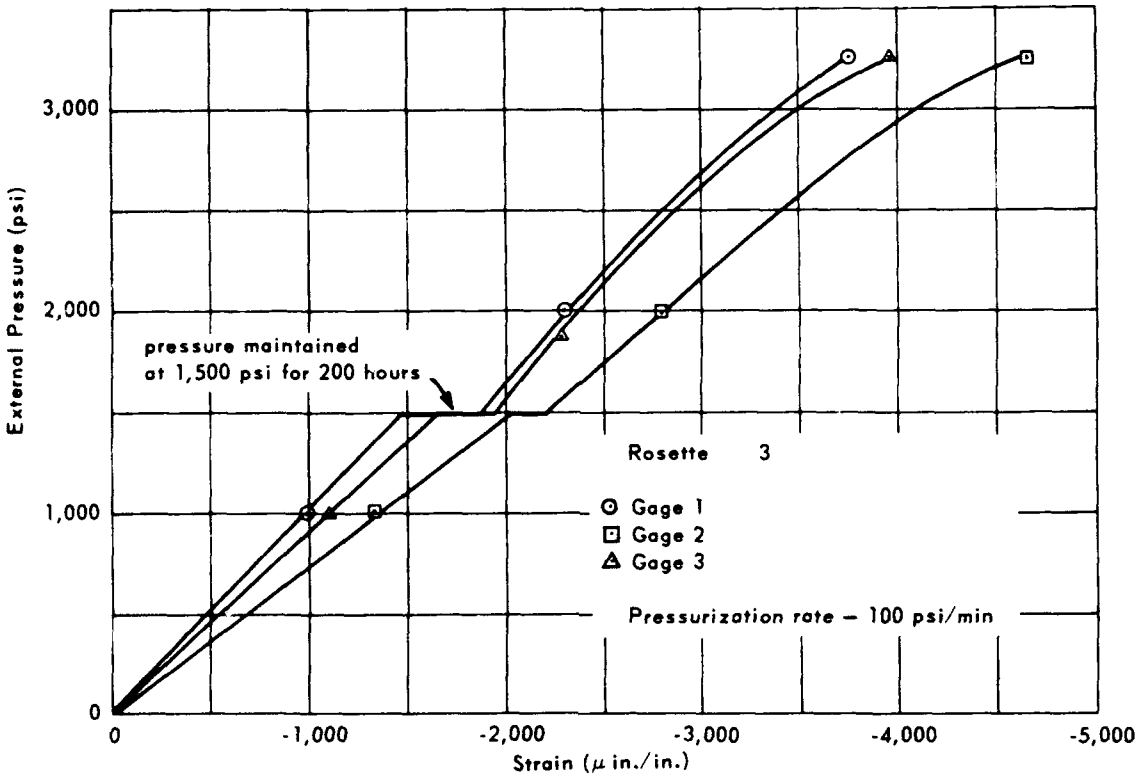

Figure 25. Strains on the interior of sphere 13 at the large penetration.

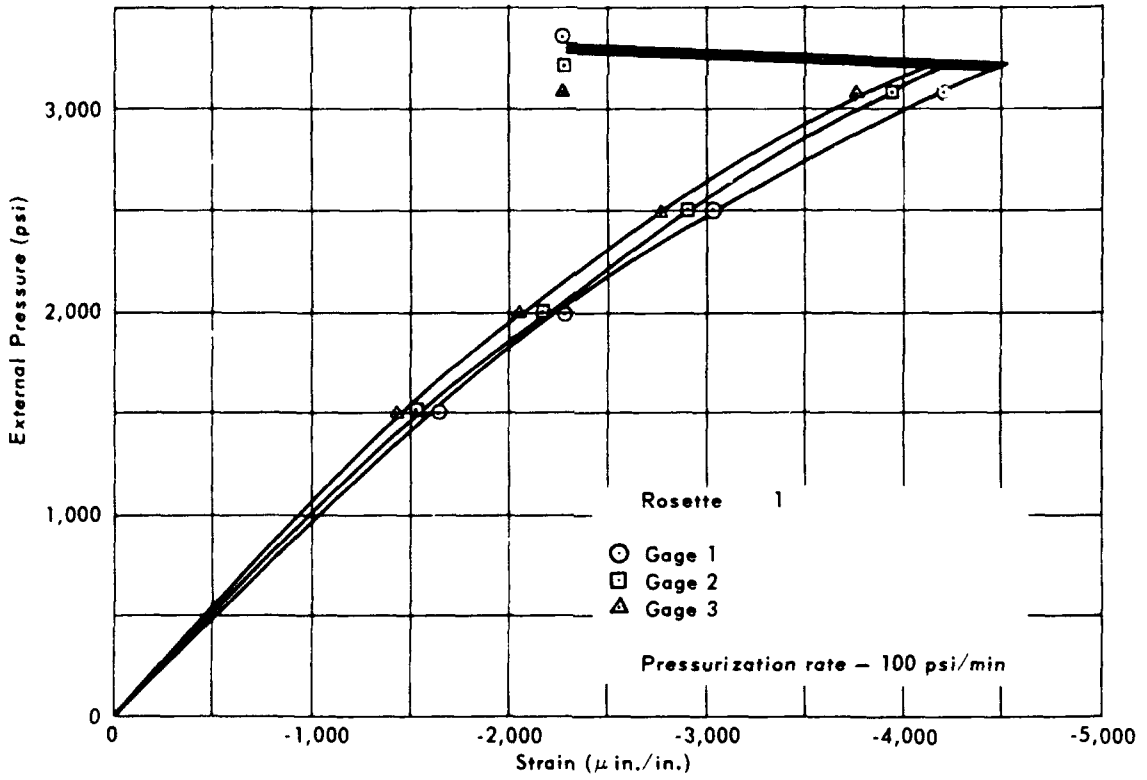

Figure 26. Strains on the interior of sphere 14 under short-term hydrostatic loading at the small penetration.

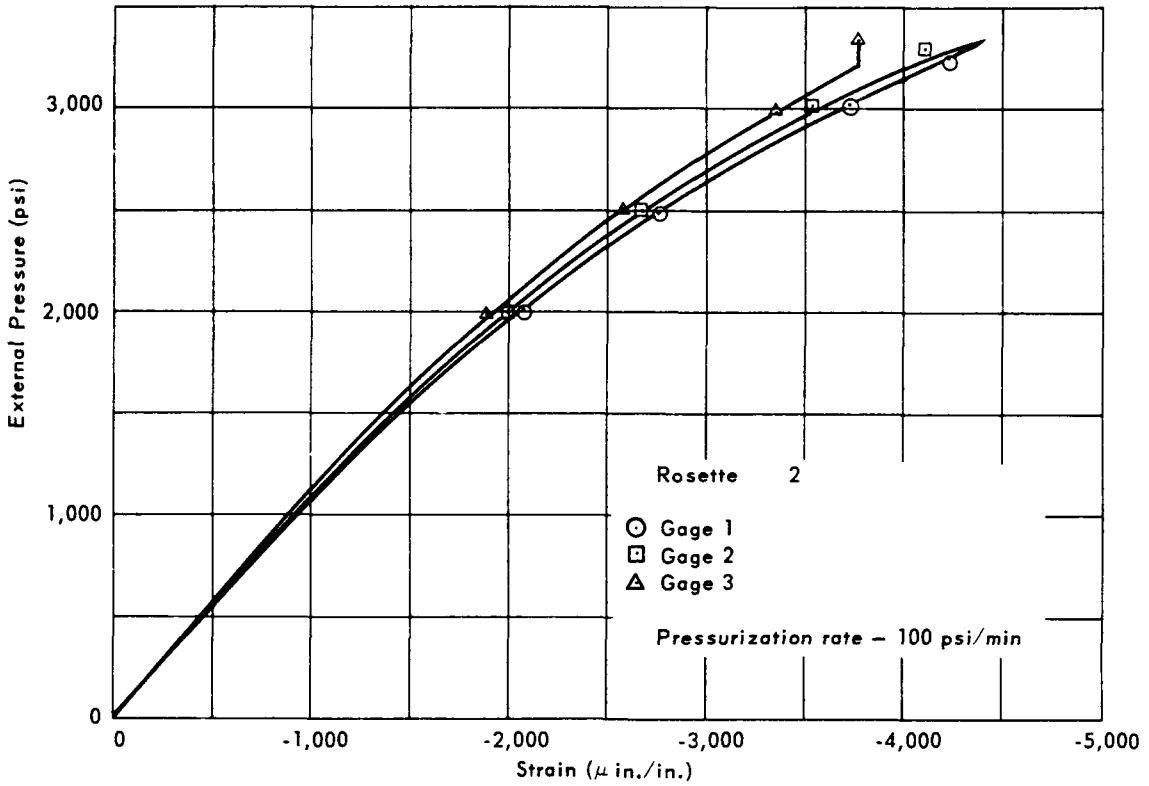

Figure 27. Strains on the interior of sphere 14 under short-term hydrostatic loading midway between large and small penetration.

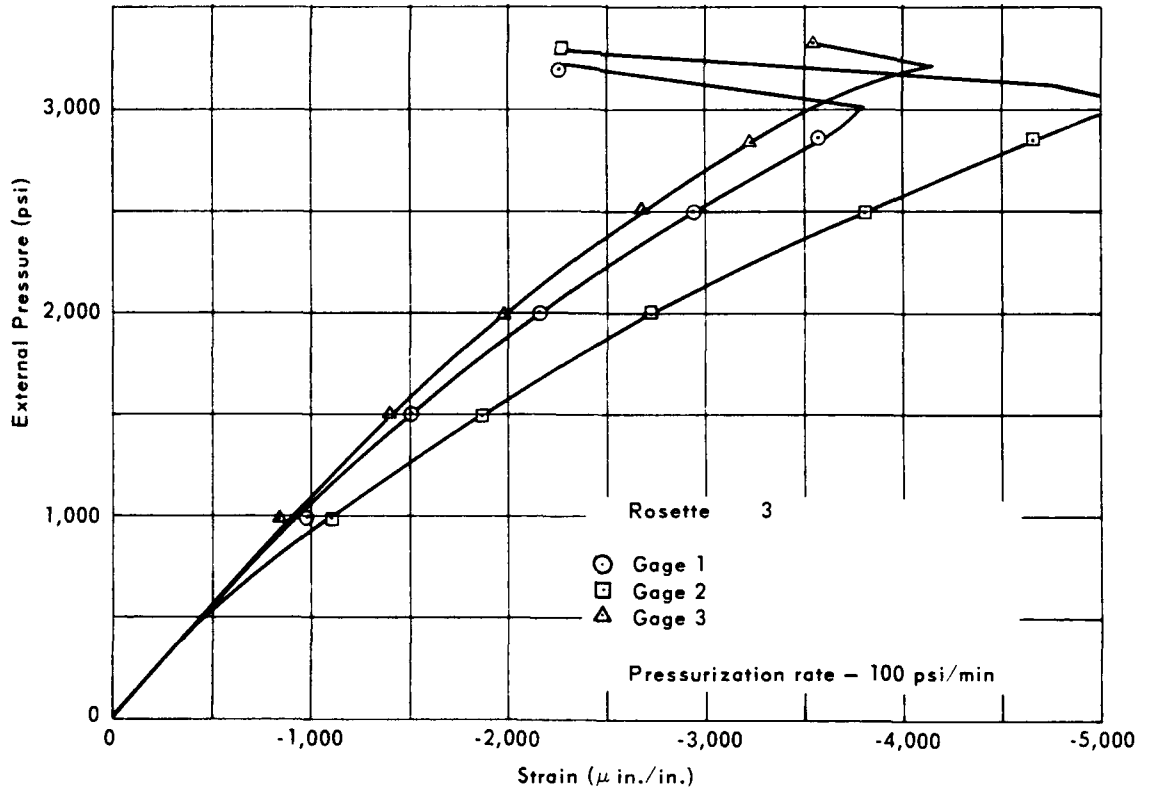

Figure 28. Strains on the interior of sphere 14 under short-term hydrostatic loading at the large penetration.

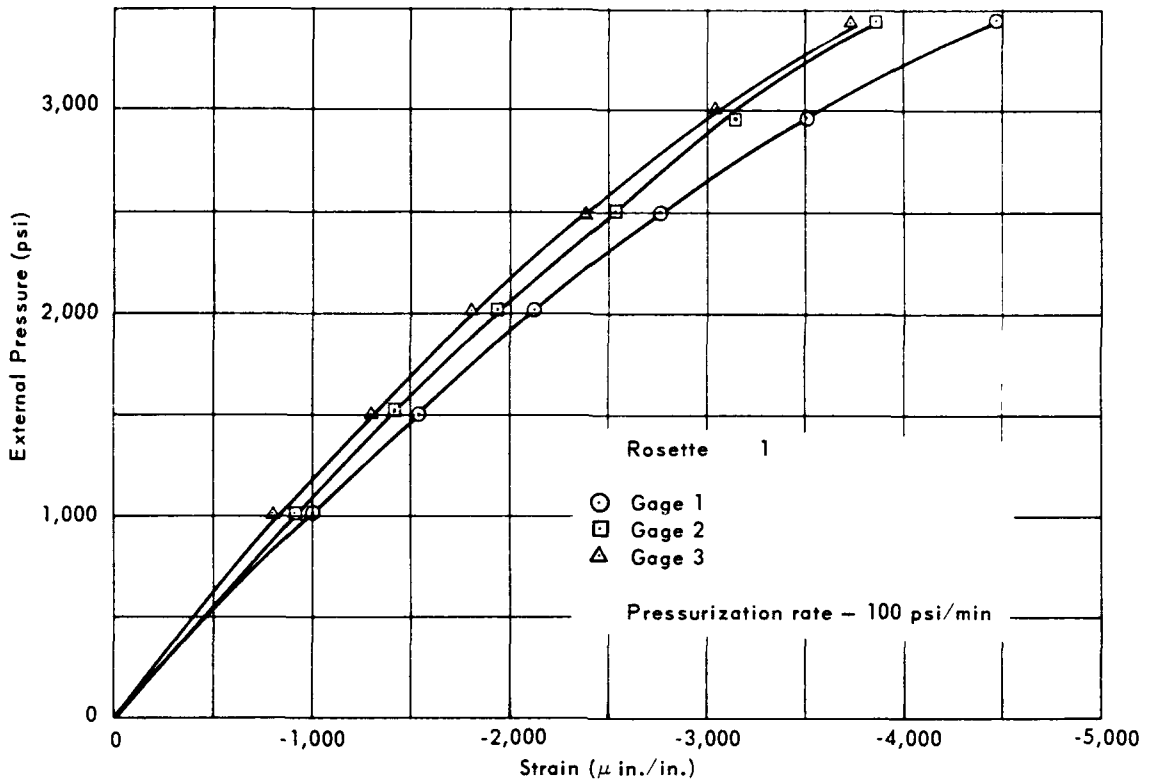

Figure 29. Strains on the interior of sphere 15 under short-term hydrostatic loading at the small penetration.

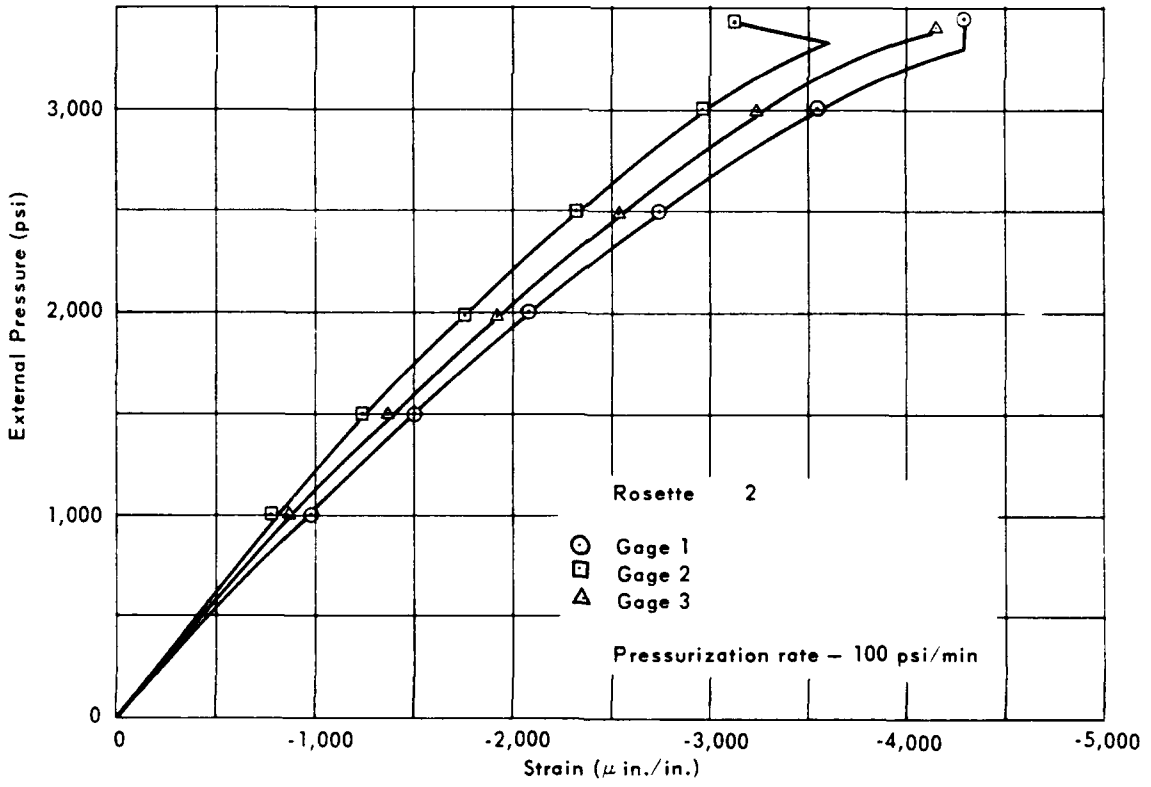

Figure 30. Strains on the interior of sphere 15 under short-term hydrostatic loading midway between large and small penetrations.

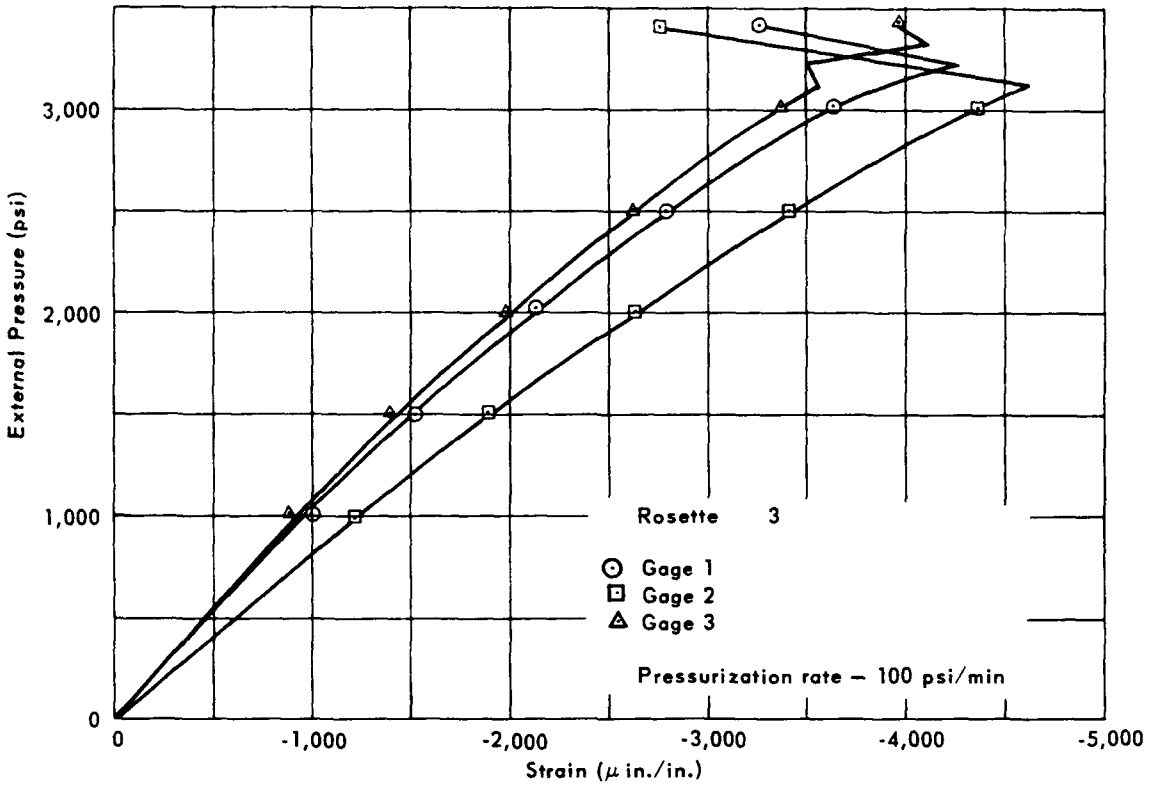

Figure 31. Strains on the interior of sphere 15 under short-term hydrostatic loading at the large penetration.

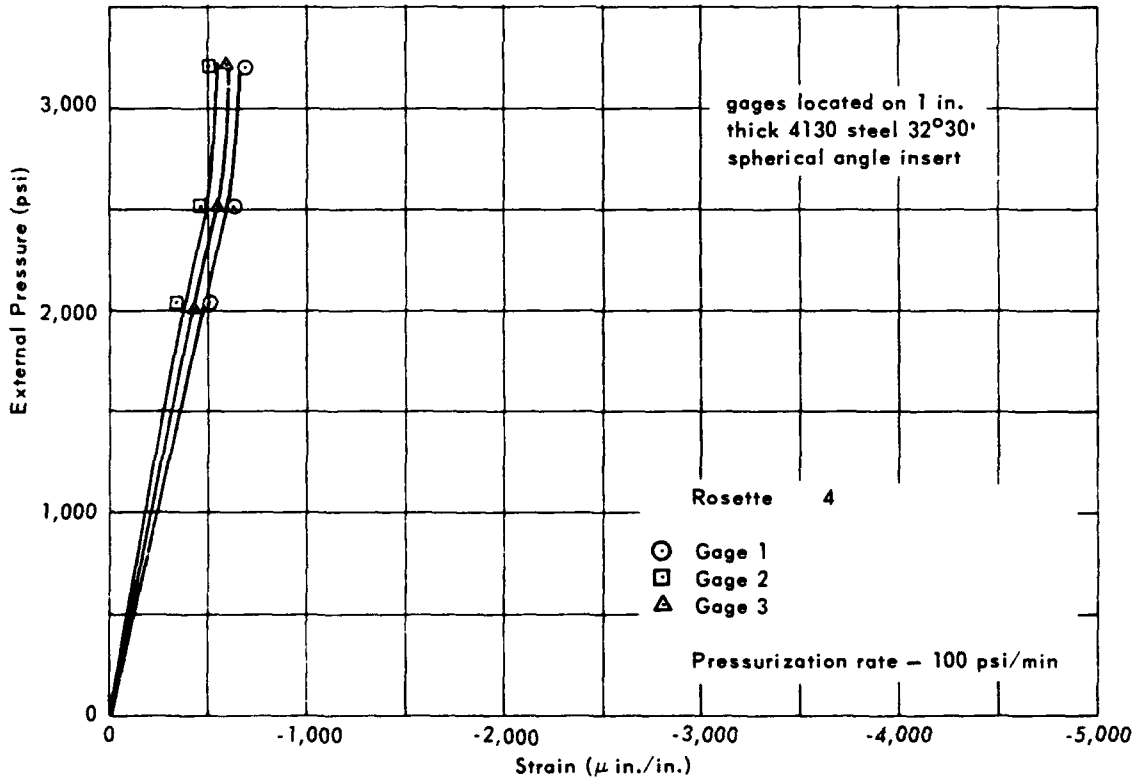

Figure 32. Strains on the interior of sphere 15 under short-term hydrostatic loading in the center of large steel insert.

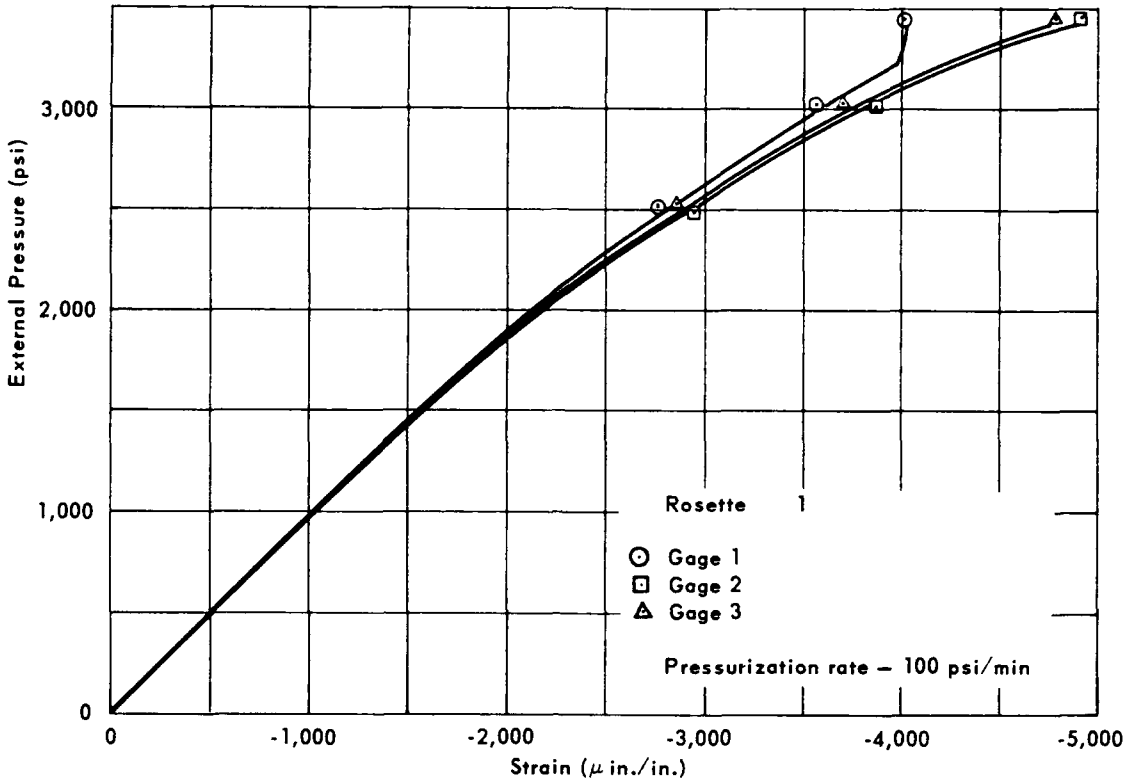

Figure 33. Strains on the interior of sphere 16 under short-term hydrostatic loading at the small penetration.

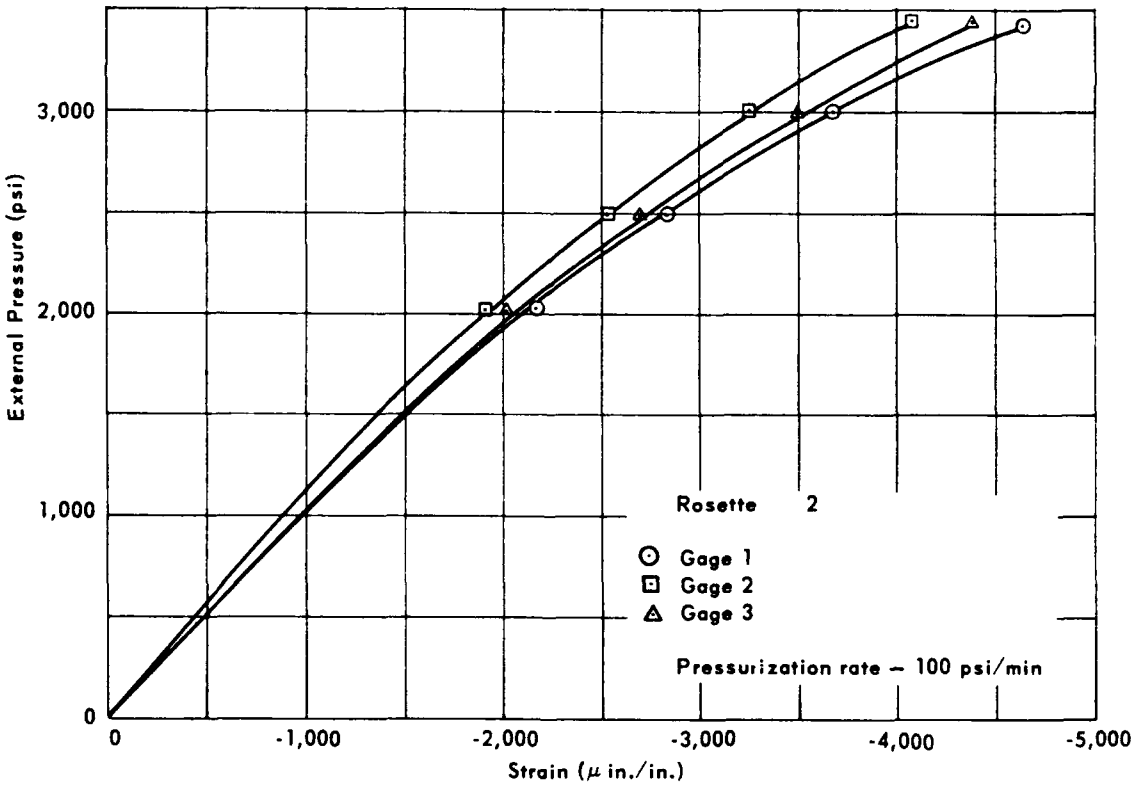

Figure 34. Strains on the interior of sphere 16 under short-term hydrostatic loading midway between large and small inserts.

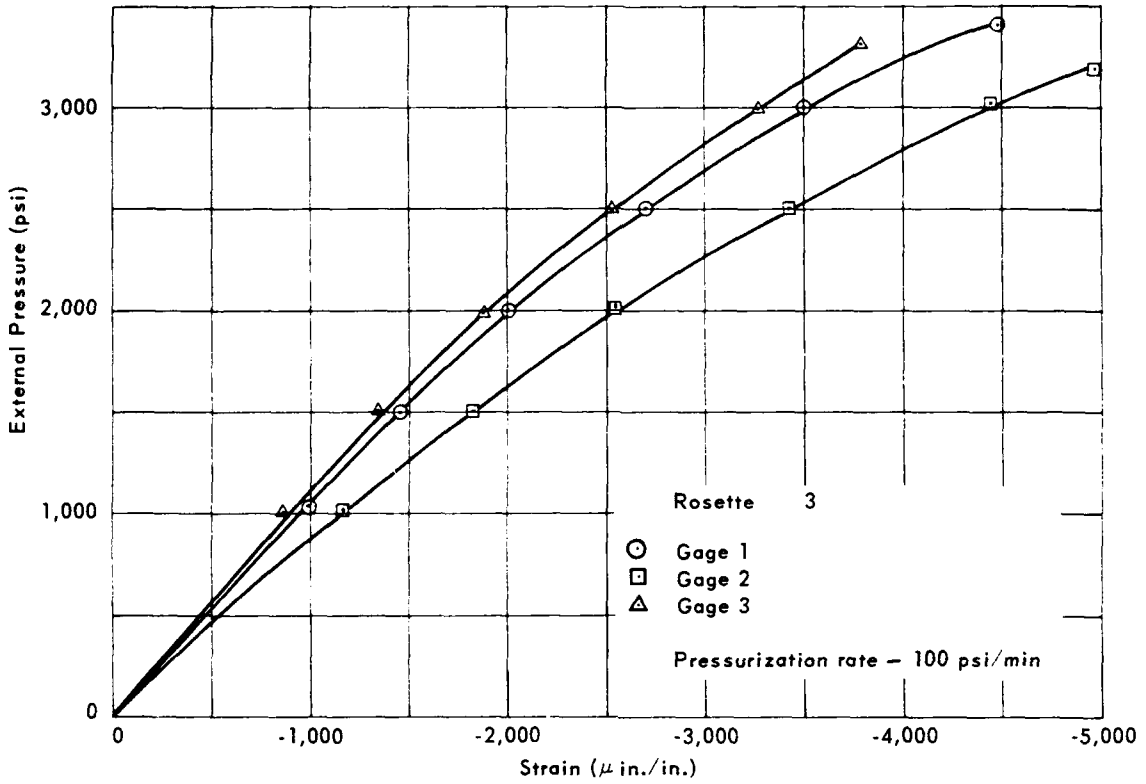

Figure 35. Strains on the interior of sphere 16 under short-term hydrostatic loading at the large penetrations.

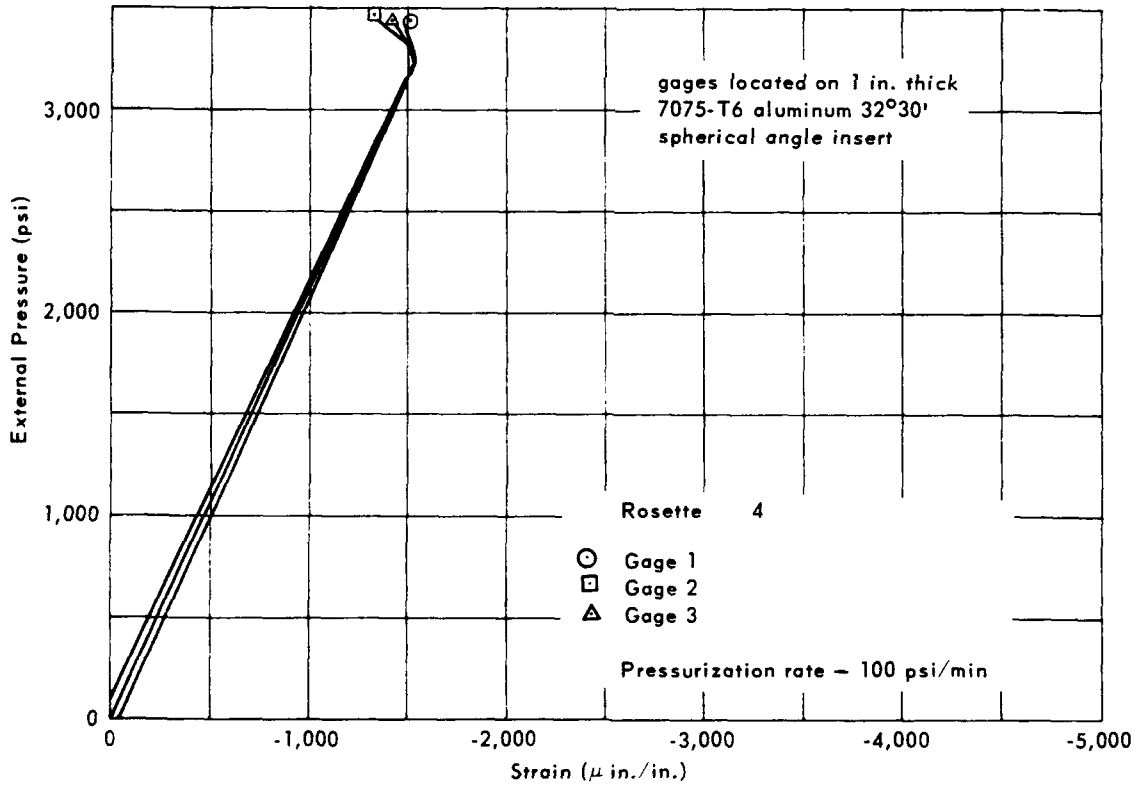

Figure 36. Strains on the interior of sphere 16 under short-term hydrostatic loading at center of large aluminum insert.

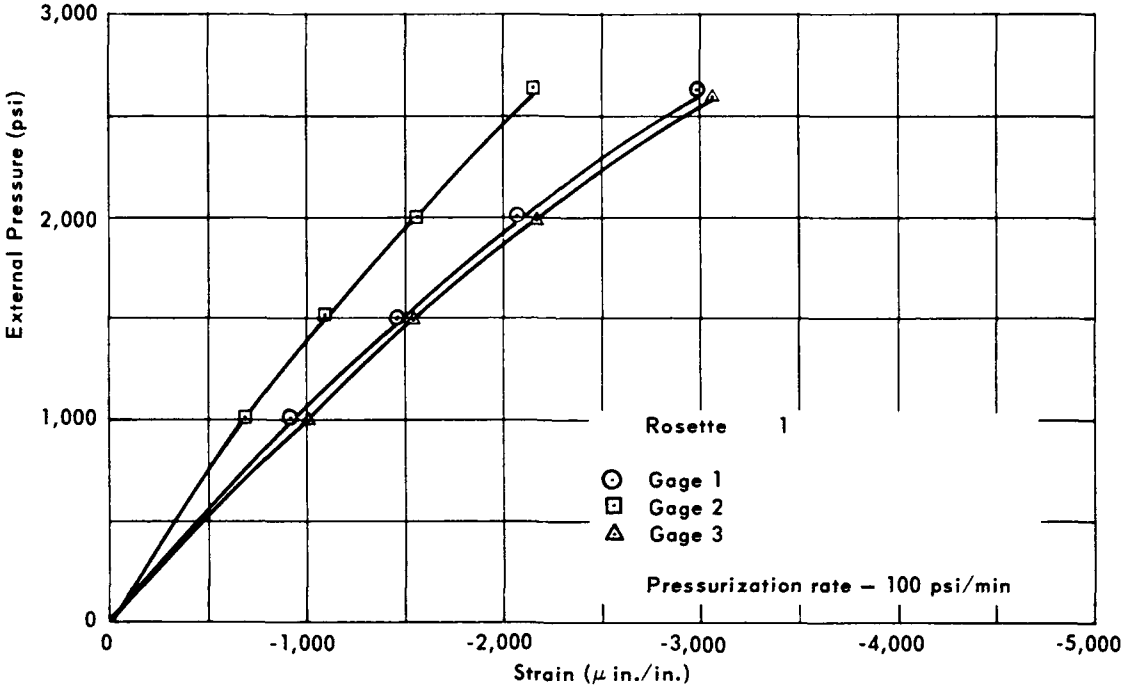

Figure 37. Strains on the interior of sphere 17 under short-term hydrostatic loading at the small penetration.

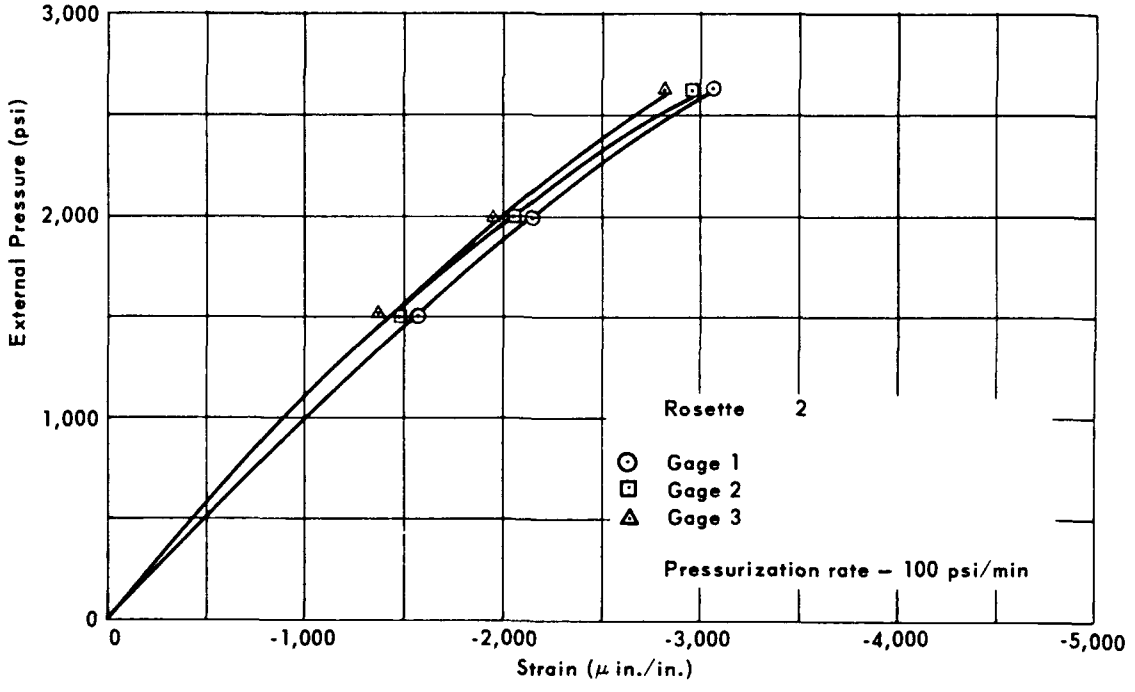

Figure 38. Strains on the interior of sphere 17 under short-term hydrostatic loading midway between large and small penetrations.

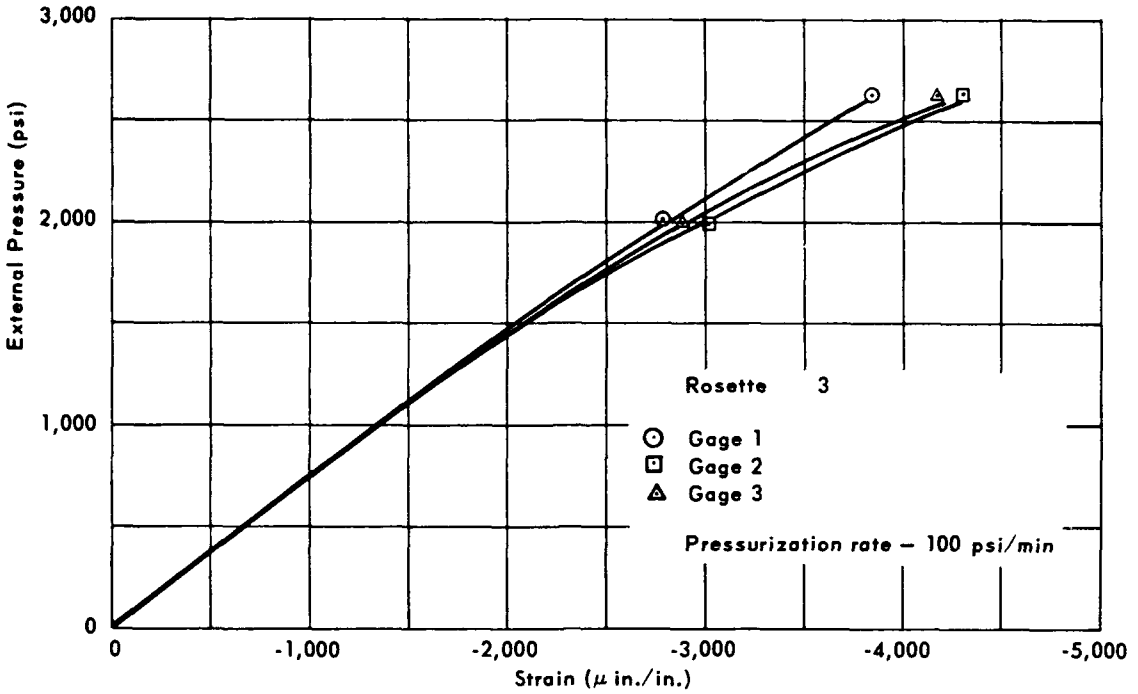

Figure 39. Strains on the interior of sphere 17 under short-term hydrostatic loading at the large penetration.

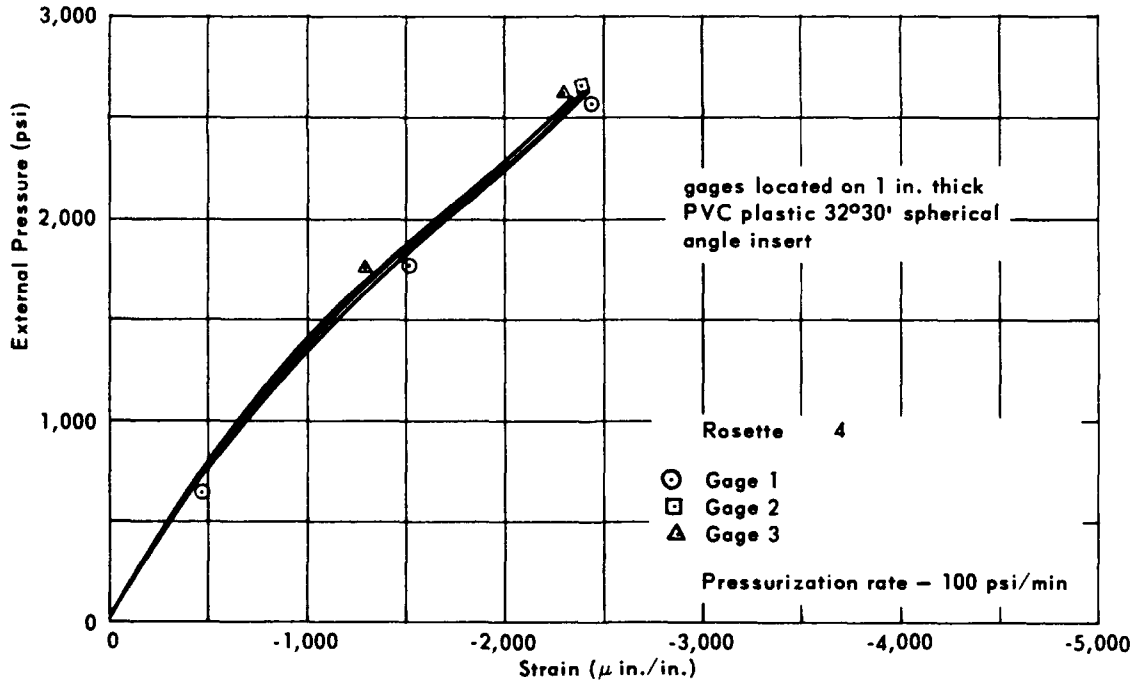

Figure 40. Strains on the interior of sphere 17 under short-term hydrostatic loading in the center of large plastic insert.

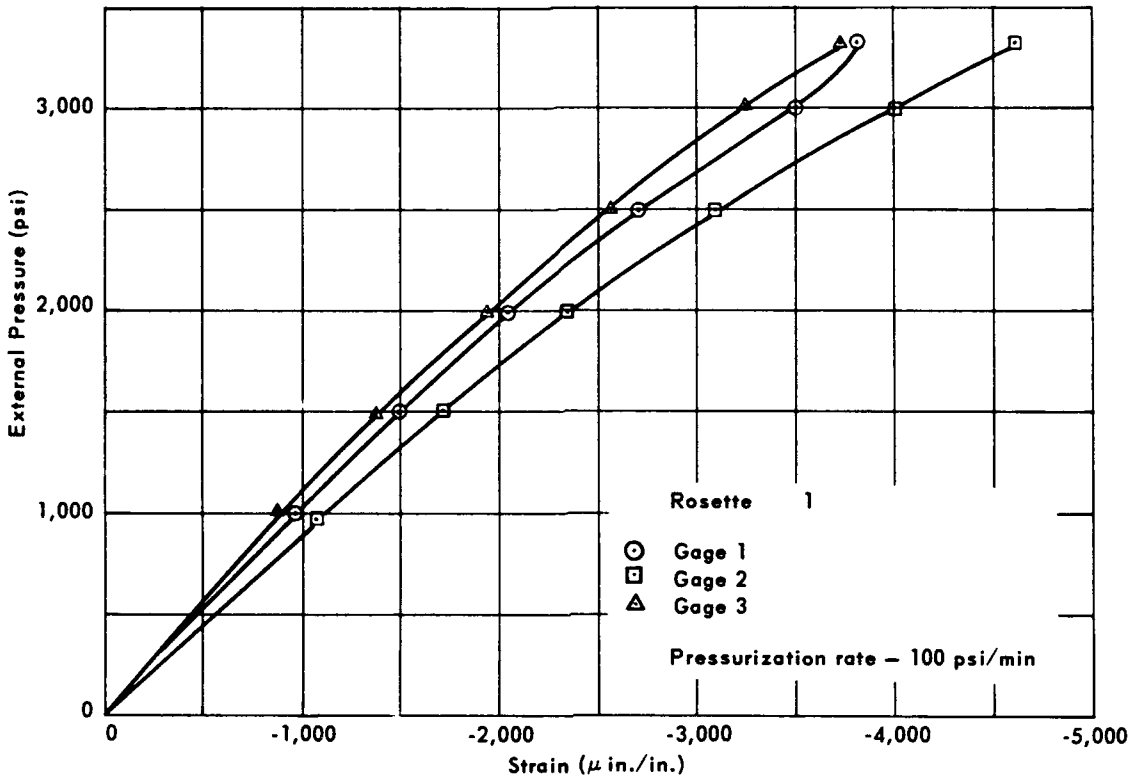

Figure 41. Strains on the interior of sphere 18 under short-term hydrostatic loading at the small penetration.

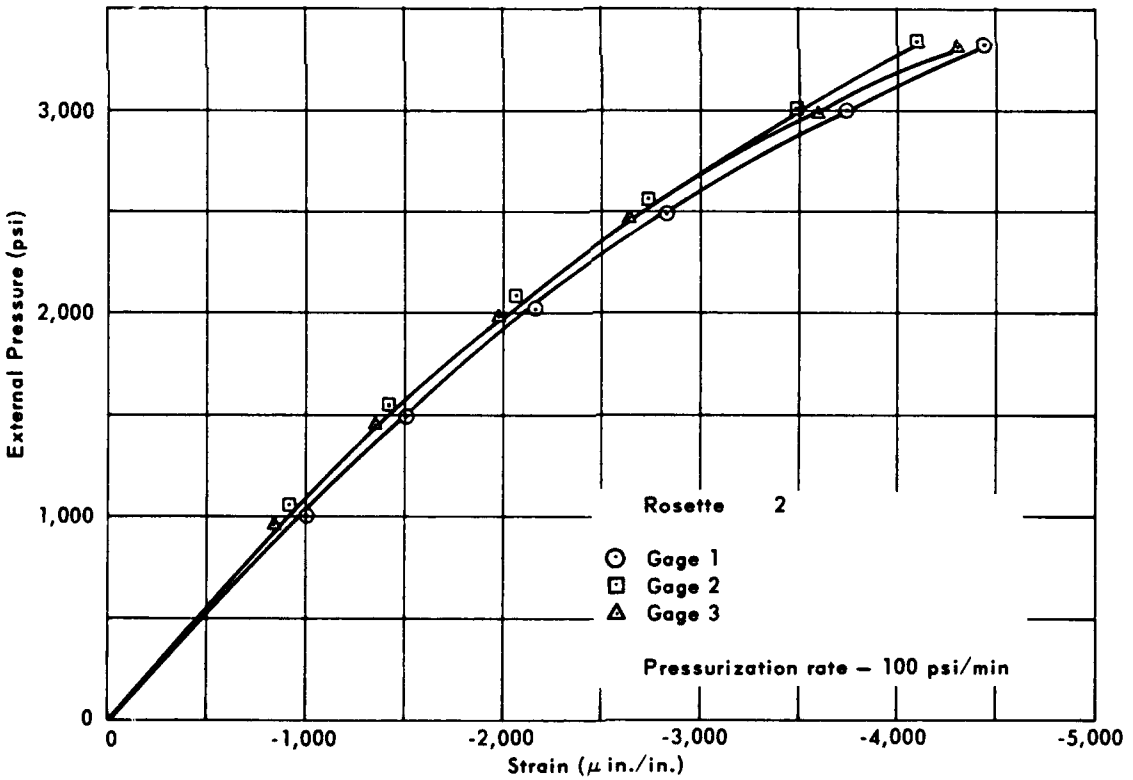

Figure 42. Strains on the interior of sphere 18 under short-term hydrostatic loading $\pi D/8$ radians away from small penetration.

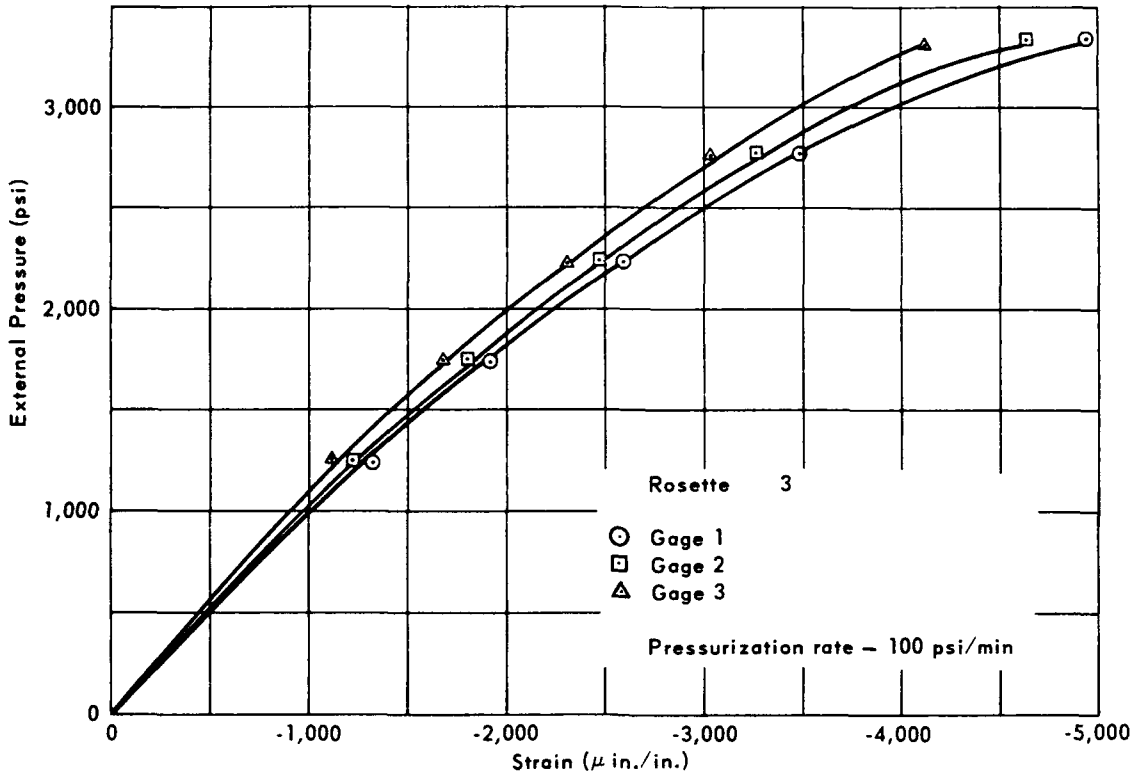

Figure 43. Strains on the interior of sphere 18 under short-term hydrostatic loading $\pi D/4$ radians away from small penetration.

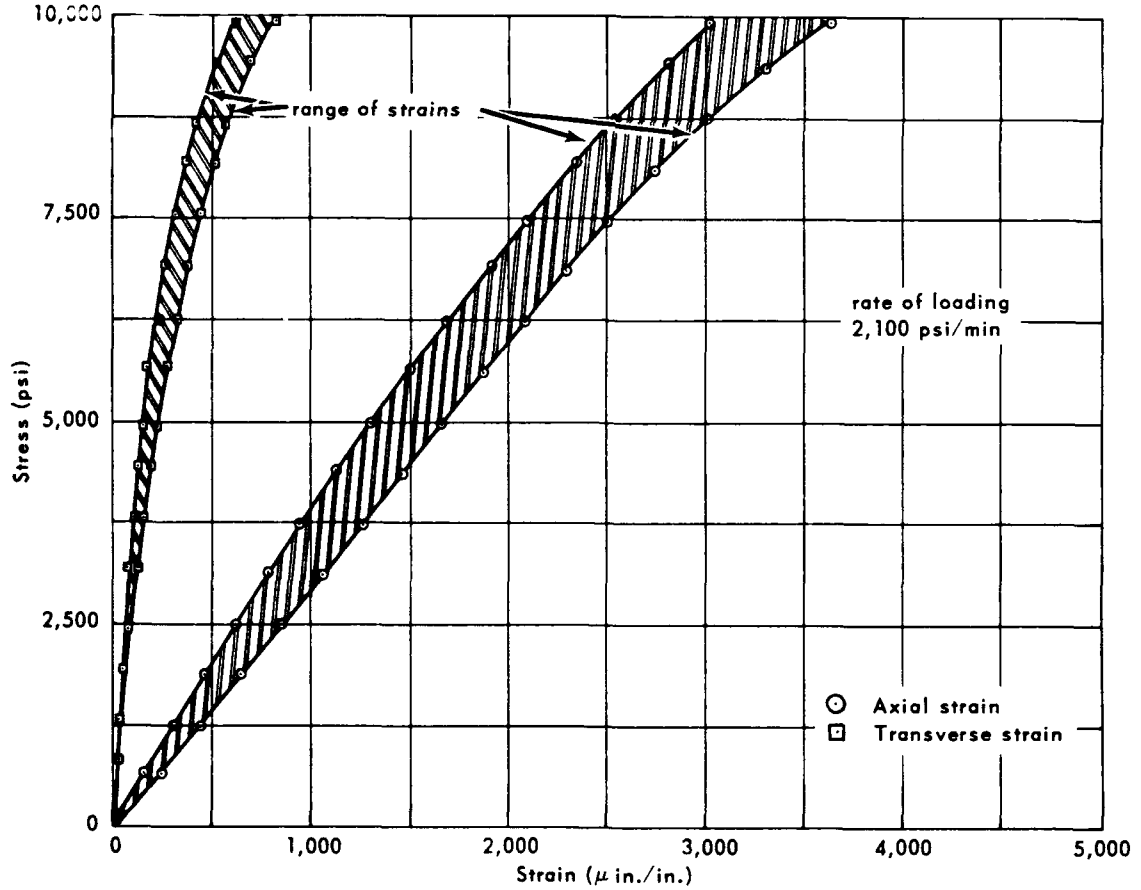

Figure 44. Strains on the exterior of 3 x 6-inch test cylinders under uniaxial compression.

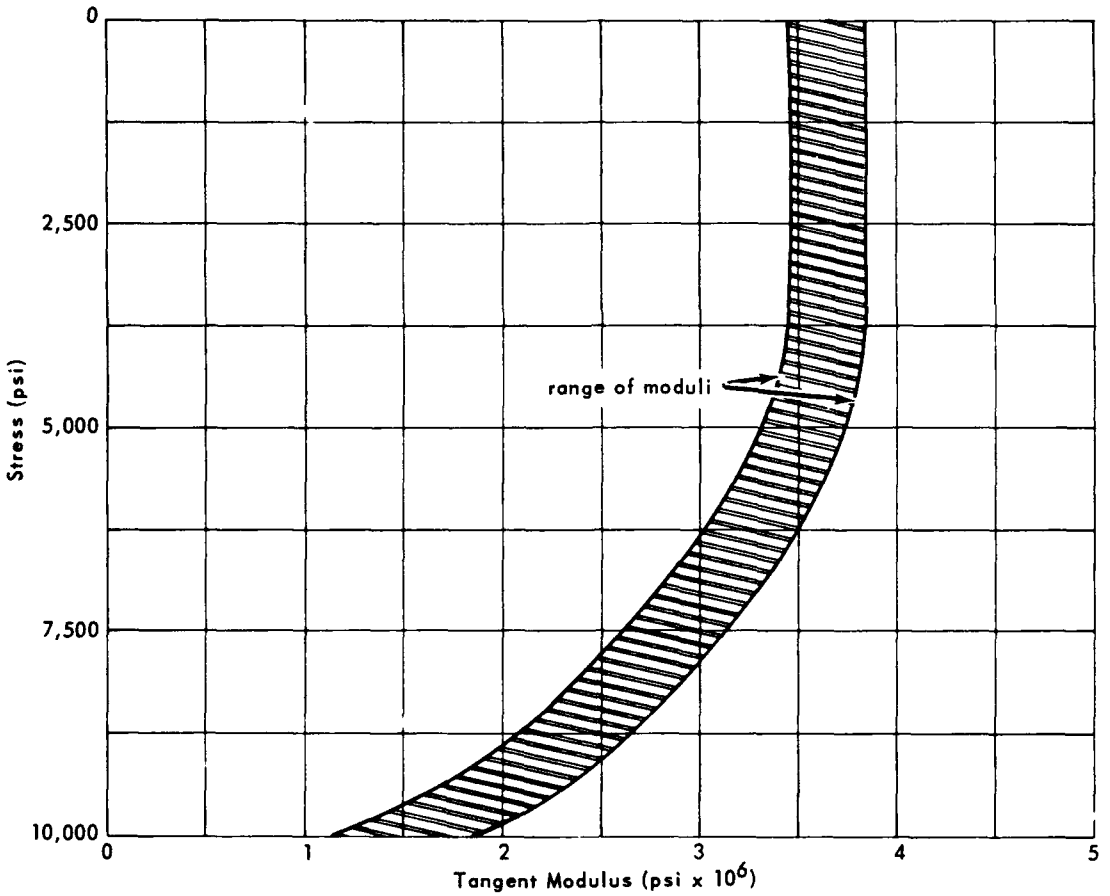

Figure 45. Tangent modulus of elasticity of concrete in 3 x 6-inch test cylinders under uniaxial compression.

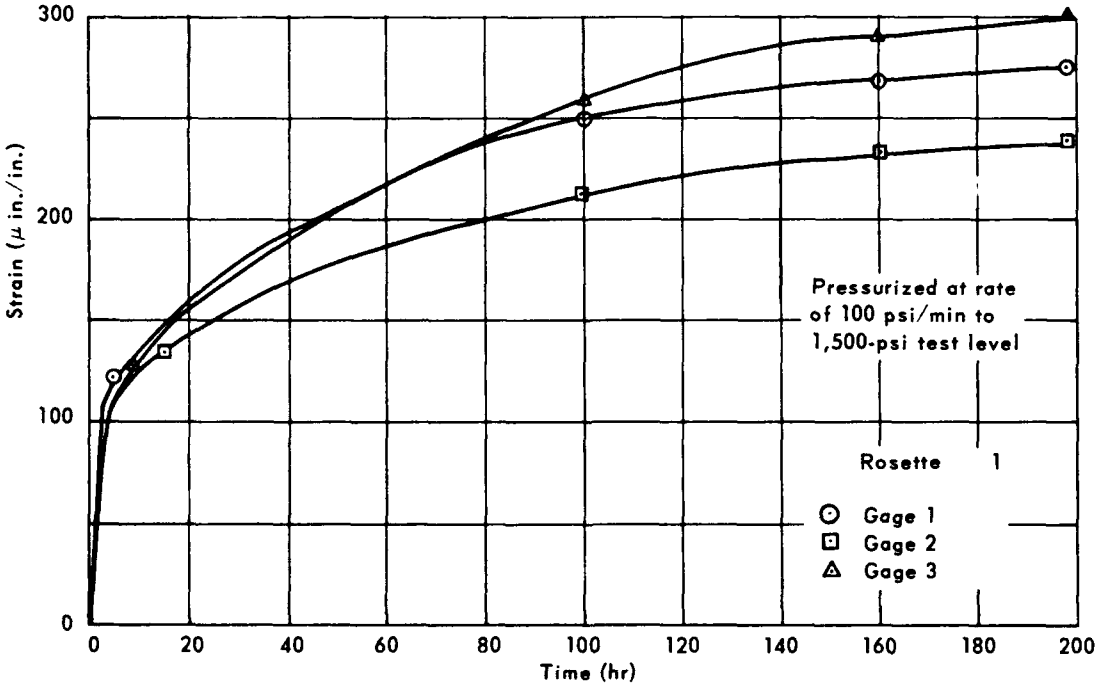

Figure 46. Time-dependent strain on the interior of sphere 13 at the small penetration under 1,500-psi external pressure.

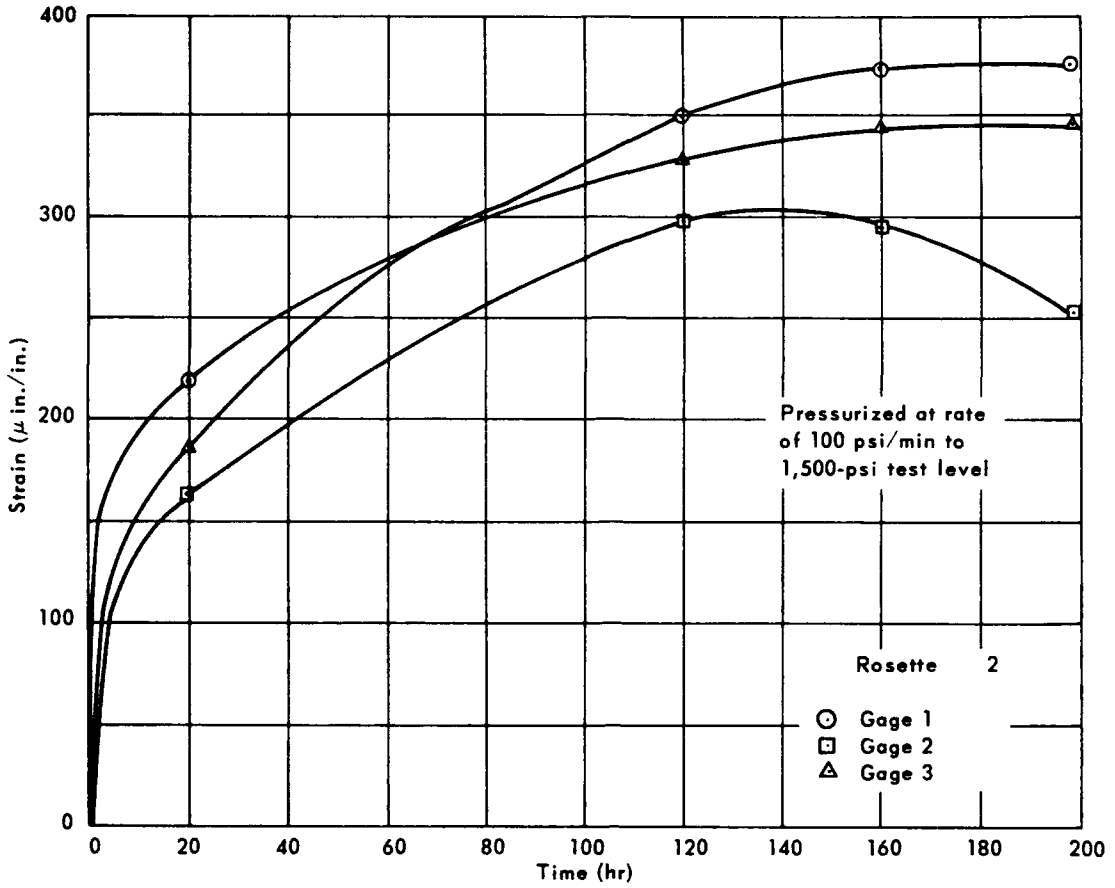

Figure 47. Time-dependent strain on the interior of sphere 13 midway between small and large penetrations under 1,500-psi external pressure.

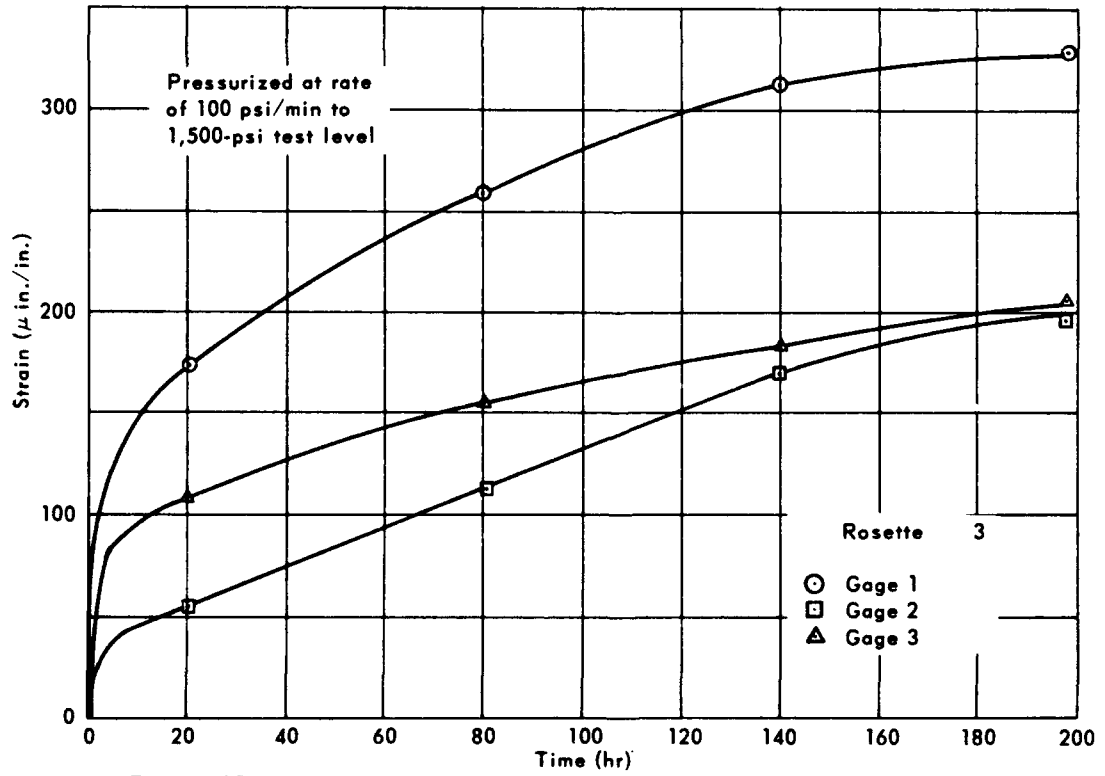

Figure 48. Time-dependent strain on the interior of sphere 13 at the large penetration under 1,500-psi external pressure.

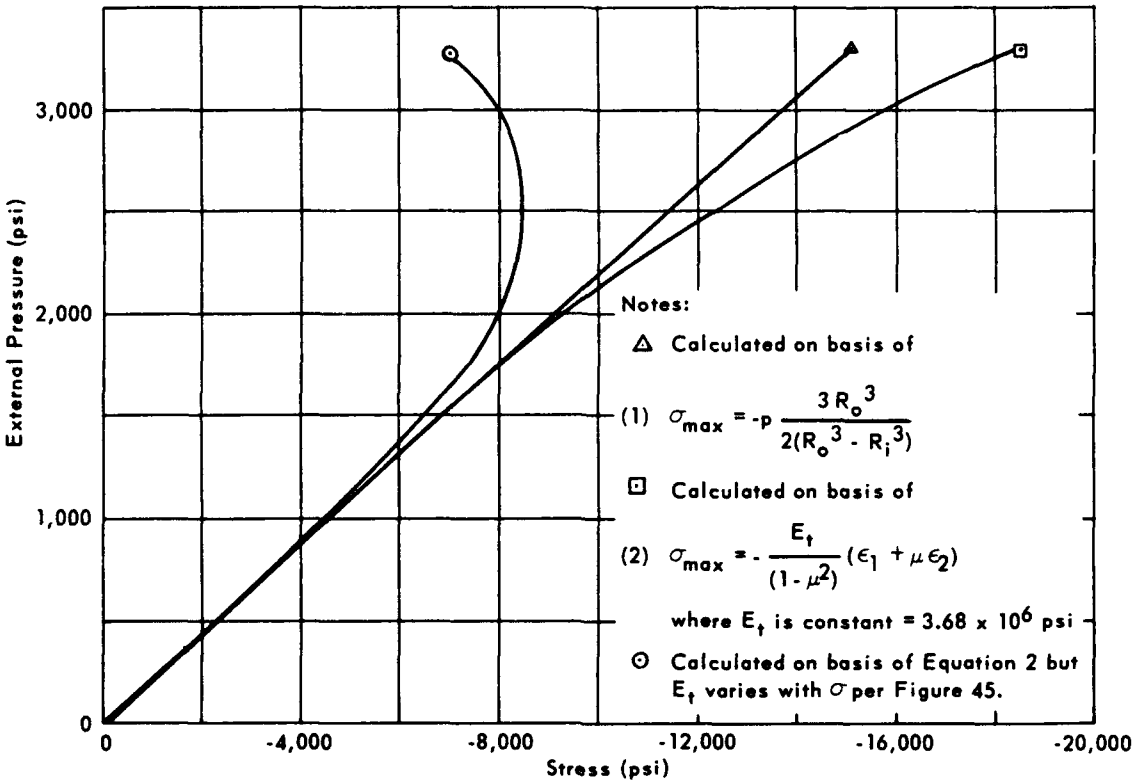

Figure 49. Typical stress levels on the interior surface of a concrete sphere midway between small and large penetrations under 1,500-psi external pressure.

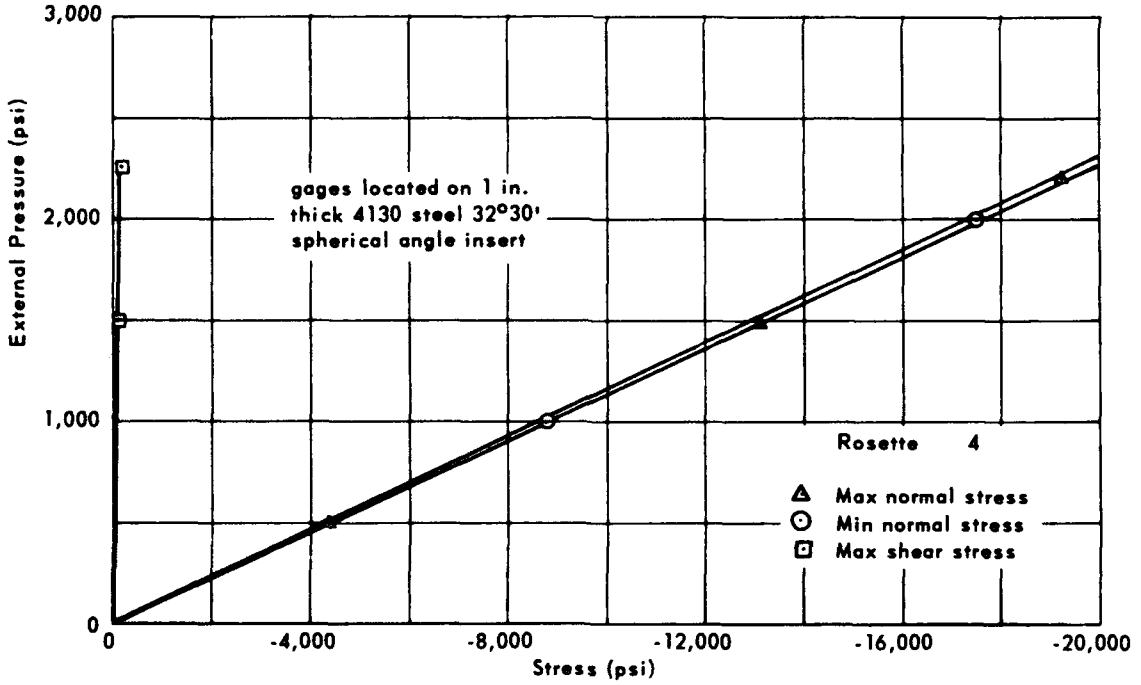

Figure 50. Typical stress level on the interior surface of large steel insert flush with the internal diameter of sphere 15.

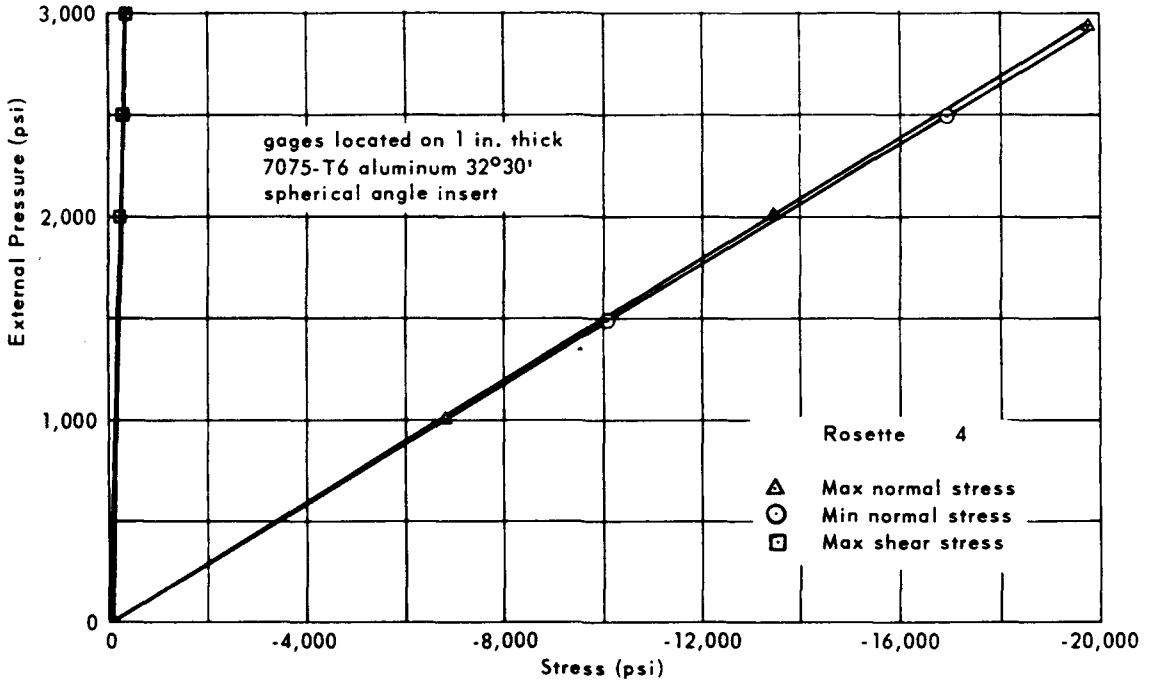

Figure 51. Typical stress levels on the interior surface of large aluminum insert flush with the internal diameter of sphere 16.

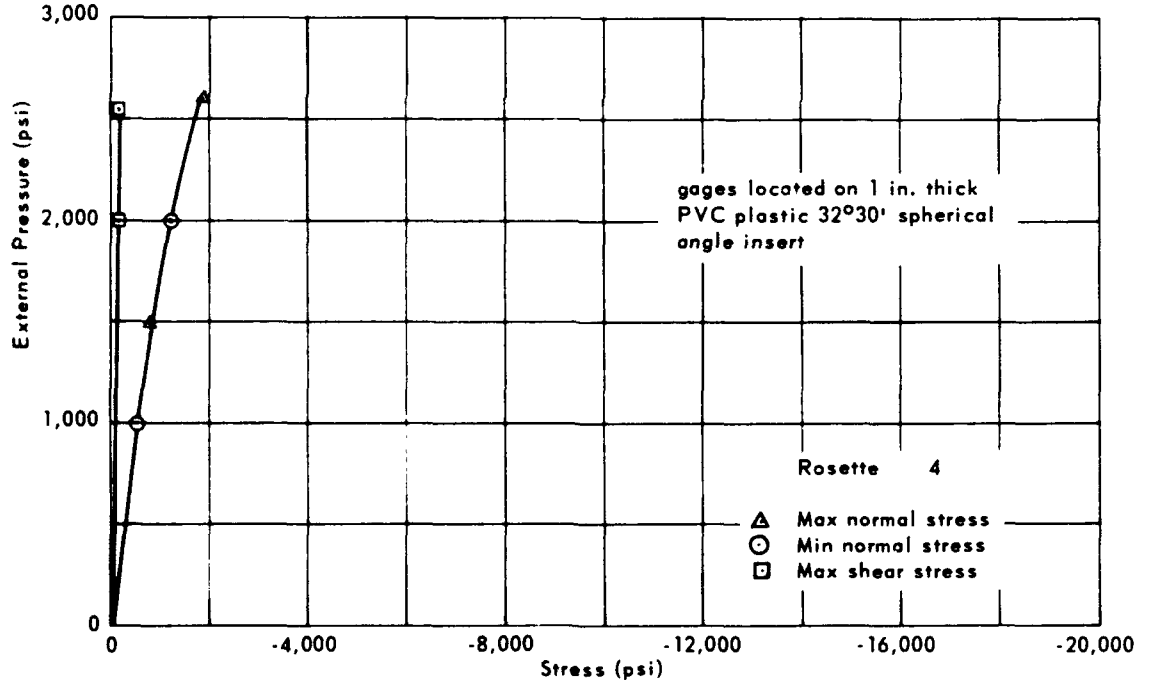

Figure 52. Typical stress levels on the interior surface of large plastic insert flush with the internal diameter of sphere 17.

Appendix A

OCEAN-BOTTOM CONCRETE HABITAT CONCEPT 1

INTRODUCTION

Although the objective of this study was only to gather exploratory experimental data that would prove the feasibility of using concrete external pressure hulls with penetrations for windows, hatches and feedthroughs at depths to 3,350 feet, it was thought desirable to perform the necessary experiments with working models of such hulls, rather than simulated models. For this reason, a working model of a typical ocean-bottom concrete habitat was designed (Figures A-1, A-2, A-3) for testing in this feasibility study.

The objective was to design a simple, ocean-bottom concrete habitat that could be considered typical of first generation concrete habitats to be emplaced on the ocean bottom.

The ocean-bottom concrete habitat was to be designed as a model that could be tested within the 18-inch-ID by 36-inch-long pressure vessel available for hydrospace simulation testing at the Deep Ocean Laboratory. The model was to represent a scaled-down version of a 20-foot-diameter unmanned oceanographic data collection station serviced from time to time by divers or by underwater vehicles capable of transferring personnel. The maximum operational depth of the habitat was to be 3,350 feet; at this depth there would be a minimum safety factor of two according to calculations based on the implosion pressure of the concrete habitat at a dive rate of 224 ft/min.

The unmanned oceanographic data collection station was conceived as a monocoque concrete sphere (Figure A-4) resting on an aluminum cradle supported by three pad-equipped legs (Figure A-5). Three large windows placed around the circumference, and one located at the bottom of the sphere (Figure A-6) would permit television or photographic cameras to observe and record the behavior of the ocean floor, hydrospace, and its inhabitants. To make the habitat adaptable to different missions, it could be selectively equipped with an array of specialized subassemblies, fitting into the large hull penetrations. Such subassemblies as a glass observation dome, diver transfer chamber, vehicle transfer hatch, or oceanographic instrument tower would make the basic concept of the ocean-bottom concrete habitat adaptable to an almost unlimited number of mission requirements.

For the design resulting from this study to be clearly understood, the underlying design philosophy must be stated:

1. To permit the evaluation of the behavior of concrete under hydrostatic pressure, the habitat hull will not be a steel-concrete composite, but will be made entirely of concrete without any reinforcements. If the hull performs satisfactorily under hydrostatic pressure without steel reinforcements, none will be used in the full-scale hulls except where necessary for attachment of internal and external appendages and to prevent damage to the structure during casting, handling, and transportation to its site on the ocean floor.

2. The components of the ocean-bottom habitat would be so proportioned that a maximum operational depth of 3,350 feet can be achieved safely without making the complete habitat assembly more than 10% negatively buoyant. In such a manner the whole habitat assembly, when equipped with auxiliary floats, could be towed to its location and then lowered after removal of auxiliary floats.

3. All the penetrations of the hull should be standardized in a single size, or at the most two sizes, so that the specialized subassemblies can be placed in any penetration on the spherical hull.

4. All special subassemblies that are used interchangeably in the many hull penetrations are not to vary the reinforcing effect that they exert on the penetration flanges even if their own rigidity varies from one subassembly to another.

5. Although concrete alone is sufficiently dense to prevent serious leakage of seawater into the interior of the habitat at 1,500 psi of external pressure, an external waterproof membrane is to be employed.

6. The interior of the habitat will be at all times at atmospheric pressure.

DESIGN

The dimensions of the small-scale concrete hull were selected after testing to implosion a series of hollow concrete spheres under external hydrostatic pressure.[1] The data resulting from testing 16-inch-OD/14-inch-ID concrete spheres without any penetrations indicated that spheres of such dimensions, when cast from concrete whose strength is at least 10,000 psi at testing time, will successfully withstand 3,000 psi of external pressure before failing.

When testing had determined that the strength of the spheres was satisfactory for 1,500-psi operational pressure, the penetration flanges were designed to be of such rigidity that they approximated the rigidity of concrete

removed from the penetration. Such penetration flanges were designed in two basic sizes. The larger one, 3 inches in diameter (full scale, 45 inches), was to be used for incorporation of windows, hatches, instrumentation tower mounting plates, or observation cupolas. The smaller penetration, 1/2 inch in diameter (full scale, 7.5 inches), was provided for the housing of electrical wire and hydraulic line feedthroughs. The external portion of the small penetration flange was also to serve as one of the trunnions for the whole concrete sphere.

The penetration flanges were designed to have a spherical angle taper on the exterior surface of the flange so that shear stresses between the penetration flange and the concrete would be minimized. The taper on the interior of the flange was identical to that on the exterior. To eliminate one source of variation in the rigidity of the penetration flanges, all insert subassemblies were designed to fit loosely in the penetration flanges so that a known clearance existed at all times between the exterior taper of the insert and the interior taper of the penetration flange. The only point of contact between the penetration flange and the insert subassembly is at the O-ring sealing surfaces. At this location the insert lip and the flange lip bear against each other when hydrostatic loading is applied, and the magnitude of the bearing stress is directly proportional to the hydrostatic pressure. The rigidity of the insert assembly affects the rigidity of the penetration flange only slightly through the friction existing between the flange and insert assembly lips at the O-ring sealing surfaces. Because the magnitude of reinforcement afforded the penetration flange by the friction forces at the lip bearing surfaces is small, these forces have been disregarded.

Several penetration insert subassemblies were conceived and designed. One that could be placed on top of the concrete structure when it was utilized as an oceanographic data collection station was an oceanographic instrumentation tower (Figure A-7) in which current-velocity, current-direction, and temperature-magnitude transducers were located. A sonar transducer and light beacon capped off the tower. The electric signals generated by these instruments would be fed to recorders situated inside the habitat. The recordings would be either read out upon interrogation, or retrieved by service personnel during one of the regular service calls.

Another insert was the window subassembly (Figures A-8 and A-9) with a 60-degree conical acrylic window. Both the insert and the window were designed for operation at 1,500-psi hydrostatic pressure for an unlimited period of time. The sealing of the window in the insert was accomplished by means of a low-pressure and a high-pressure seal. The purpose of the low-pressure seal, consisting of a thin rubber gasket compressed between the acrylic window and the retaining ring, was to seal the window while the structure is towed in

the ocean, and to generate an axial force on the window so that the greased window seat would act as a high-pressure seal. Miniature lights (Figure A-10) were placed on each tripod leg and below the framework ring to simulate underwater lights for illumination of hydrospace in close proximity to the habitat model (Figure A-11). For applications requiring 360-degree visibility around the sphere, a glass cupola assembly was designed to fit the penetration flange (Figures A-12 and A-13). A photographic or television camera mounted on a 360-degree pan head inside the glass cupola would permit continuous visual surveillance of hydrospace around the habitat. Although in the small-scale model the glass cupola was a cylinder with hemispherical end closure, other types of cupolas could be used for the full-scale habitat. The selection of the cylindrical cupola for the small-scale model was dictated by the fact that such small enclosures with a 40,000-foot depth rating are readily available as off-the-shelf items while hemispheres are not. When full-scale habitats are built, glass hemispheres of as much as 44 inches in diameter with a 5,000-foot depth rating, which are commercially available, will be utilized.

An insert subassembly in the form of a vehicle mating transfer hatch was also provided (Figure A-1) so that the full-scale habitat placed in depths beyond diver's capability could be serviced by a submarine. The exterior of the transfer hatch housing is hemispherical to permit mating with the DSRV type submarine hatch skirt, even though the habitat may not be in a perfectly vertical position.

Similarly, an insert subassembly can be designed to permit divers to go back and forth between habitats and hydrospace. This subassembly would have to be placed at the bottom penetration of the habitat to permit easy entry and egress. This would be also a good location for transfer of personnel from bottom-crawling vehicles.

Besides the rather typical subassemblies mentioned, there are many insert assemblies that could be designed for a specific mission of the habitat — for example, subassemblies for a hydrophone, mechanical arm, soil bearing strength plate, seawater sampler, torpedo tube, or releasing mines. The only requirement that applies to them all is that their mounting plates fit over the penetration opening, and that their mounting lip bearing surfaces match the lip of the penetration flanges.

FABRICATION

All efforts were made to make the habitat components from materials resistant to corrosion. The structural components that in addition to carrying loads had to perform mechanical functions requiring noncorroded surfaces for their success were fabricated from type 316 stainless steel. Other metallic structural components whose surface condition was not of primary importance for the fulfullment of their mission were made of type 6061-T6 aluminum.

The concrete hull itself was cast from a mix especially designed for this application.[1] The strength of this concrete when tested under uniaxial compression was above 7,000 psi after 28 days of curing in a 100% relative humidity environment. The strength of this concrete mix increased to the 10,000- to 11,000-psi strength level after 250 days of curing, of which 220 days were spent in 20% relative humidity. Previously conducted experiments have shown that the permeability of an unprotected 1-inch-thick concrete hull under 1,500 psi of seawater pressure is only about 6×10^{-3} ml/hr/in.^{2} of surface, and thus not of such magnitude that a sump pump located on the interior of the hull could not handle it. Since the continuous dampness on the interior of the hull would be quite detrimental to performance of electronic equipment, a waterproof coating was applied to the exterior of the hull to eliminate this problem completely. The waterproof coating in this case was epoxy resin applied approximately 0.015 inch thick.

The penetration inserts were also bonded to the concrete hull penetration surfaces by means of Epocast 8288-A epoxy adhesive. The thickness of the adhesive layer between the penetration flange and the concrete surface of the penetration ranged between 0.015 and 0.060 inch. The joint between the two hemispheres that form the hull sphere was also filled with epoxy adhesive 0.015 to 0.030 inch thick.

DESIGN EVALUATION

The design was evaluated experimentally by subjecting the small-scale model habitat in its support frame (Figure A-14) to tests in simulated hydrospace environment. The tests were either operational, to determine whether the whole system performed as designed, or structural, in which only the load-carrying ability of the structure was checked. In the operational tests, the small-scale model habitat complete with subassemblies was subjected to 1,500 psi of seawater pressure and checked for leaks, operation of lights, and similar factors. In the structural tests only the hull was subjected to destructive testing while strains on its interior were monitored.

Both the operational and the structural tests showed that the small-scale concrete habitat model performed as specified. The many insert subassemblies were found to fit interchangeably into the penetration flanges and not to leak under 1,500 psi of external hydrostatic pressure. The hull assembly was found to withstand safely 1,500 psi of external pressure with maximum measured stresses of only 4,000 to 5,000 lb/in.^{2}. Collapse of the two habitat models tested occurred at 3,300 psi of hydrostatic pressure. This gives the small-scale models an apparent safety factor of two – which is probably more than sufficient for hydrospace structures.

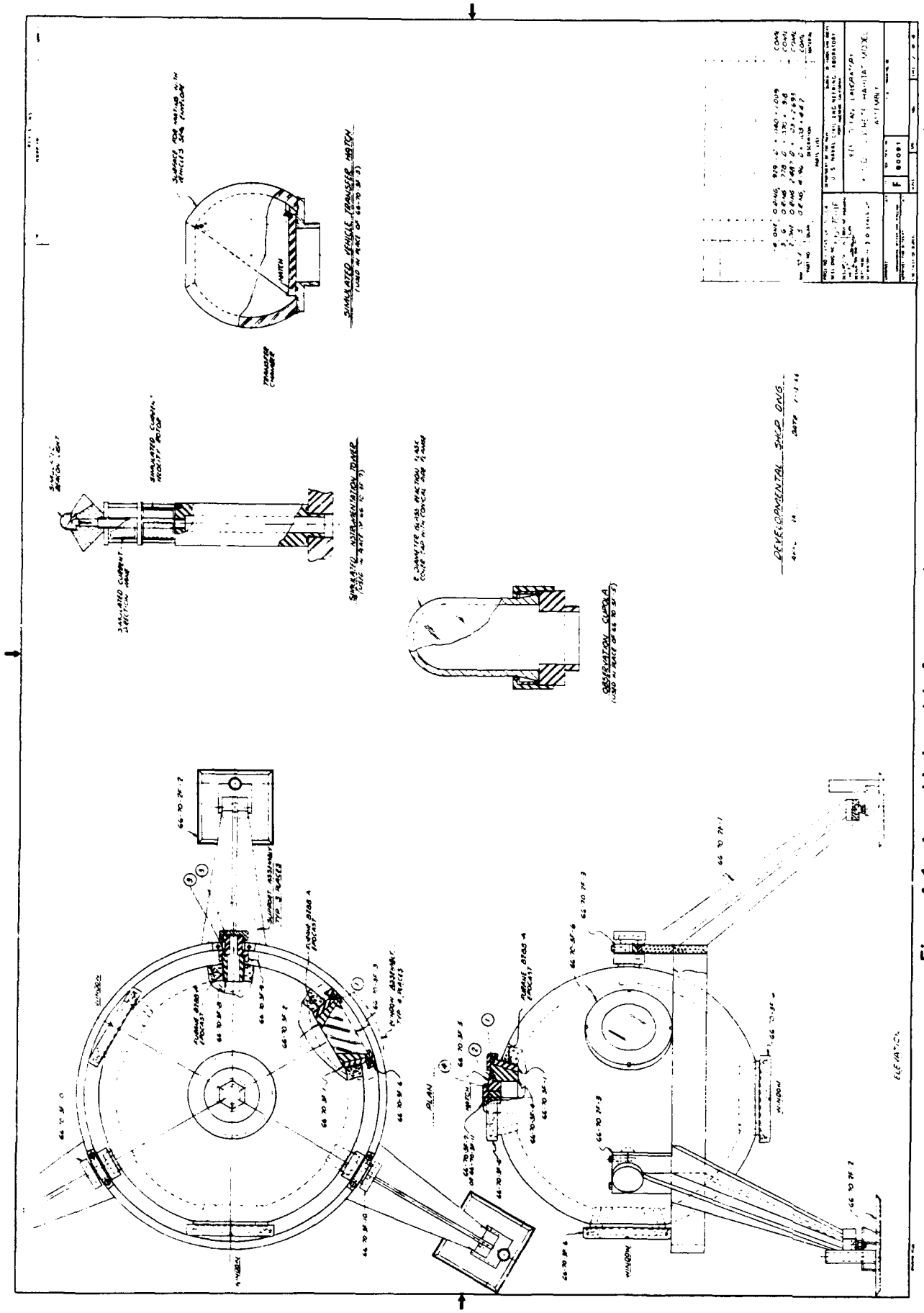

Figure A-1. Assembled model of an ocean-bottom concrete habitat.

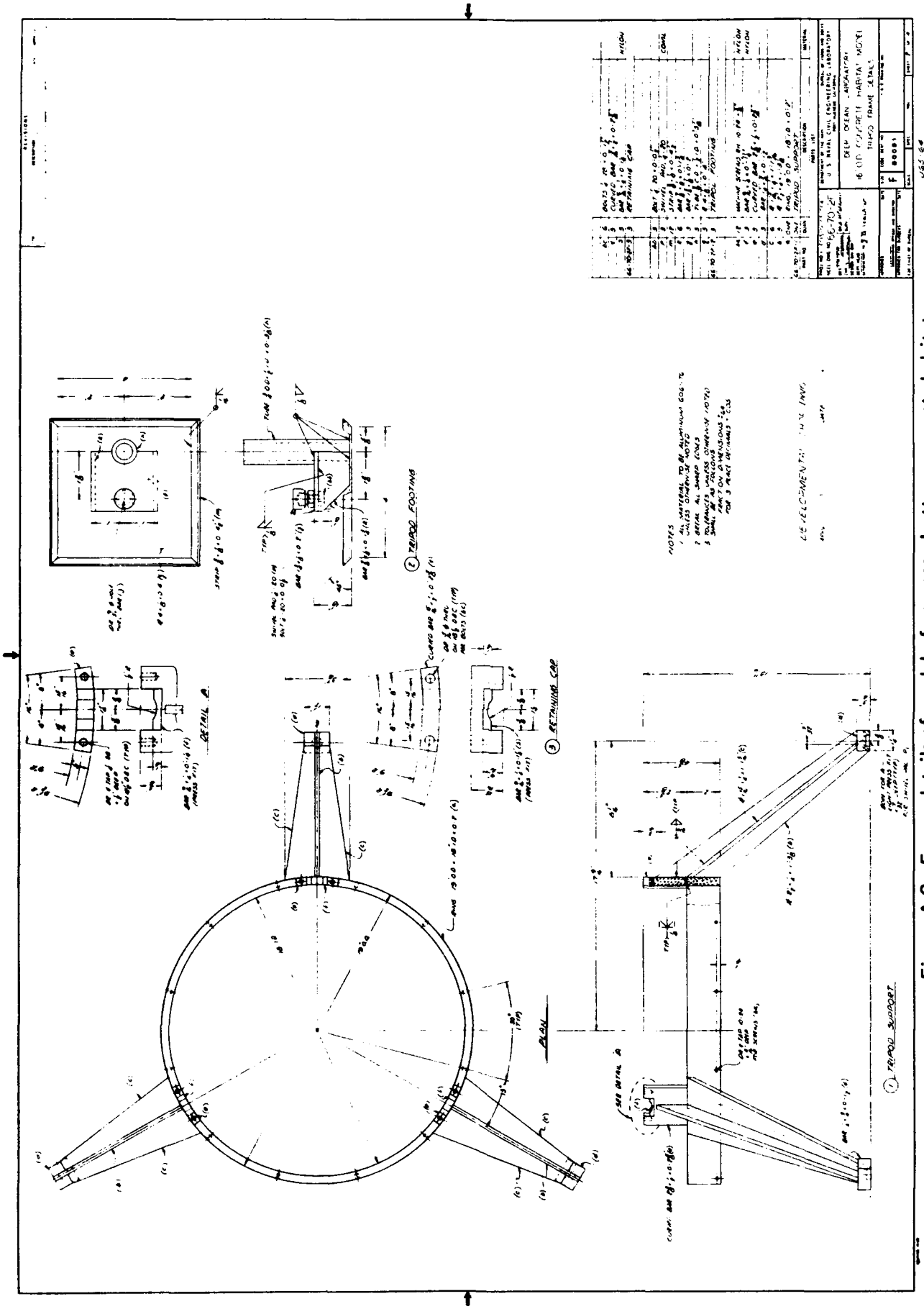

Figure A-2. Frame details of model of an ocean-bottom concrete habitat.

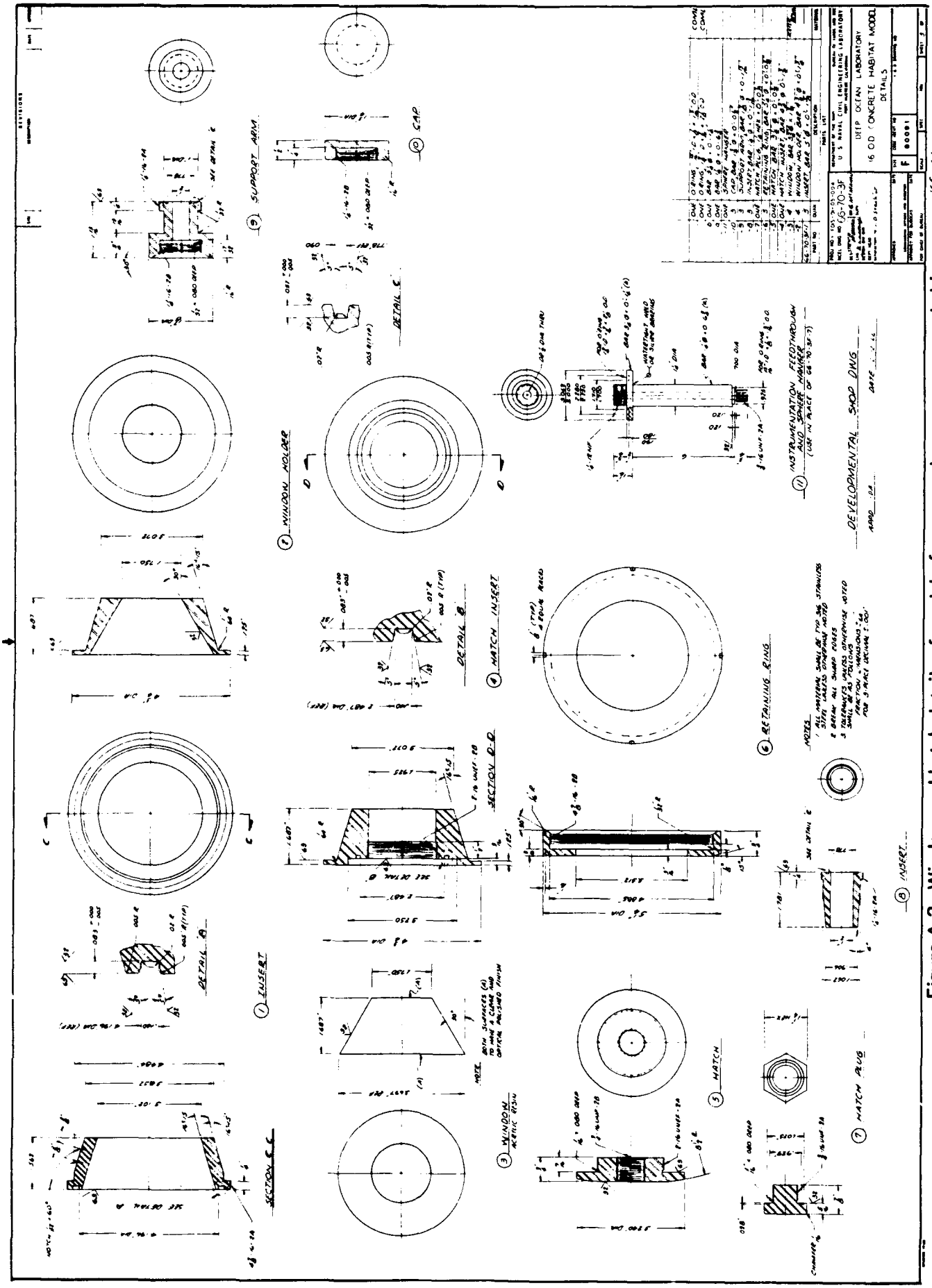

Figure A-3. Window and hatch details of model of an ocean-bottom concrete habitat.

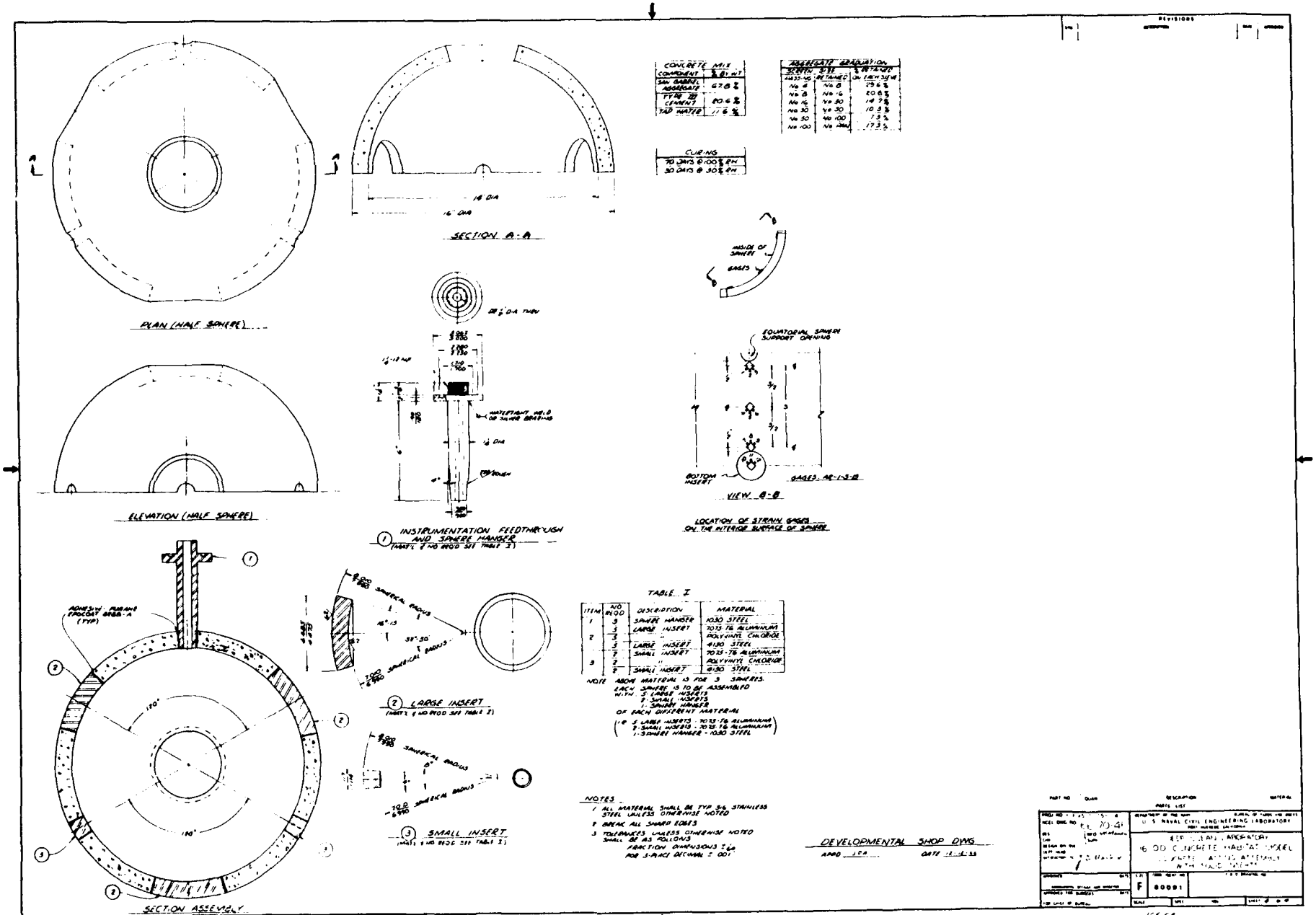

Figure A-4. Solid insert details of model of an ocean-bottom concrete habitat.

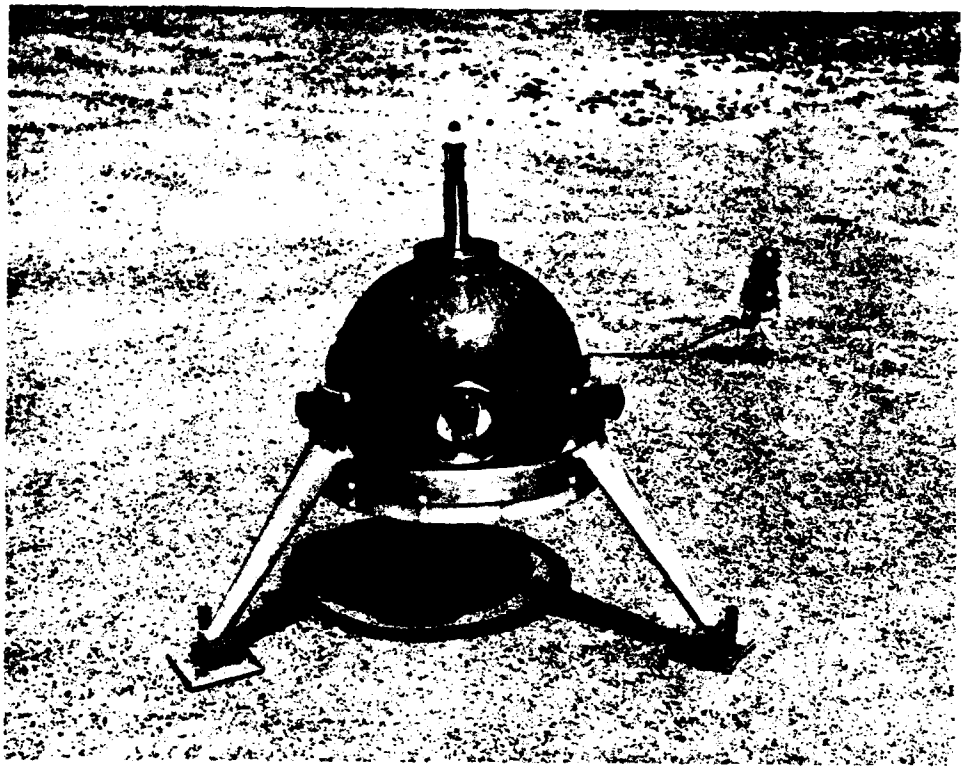

Figure A-5. Model of an ocean-bottom concrete habitat equipped with oceanographic instrument tower for data collection.

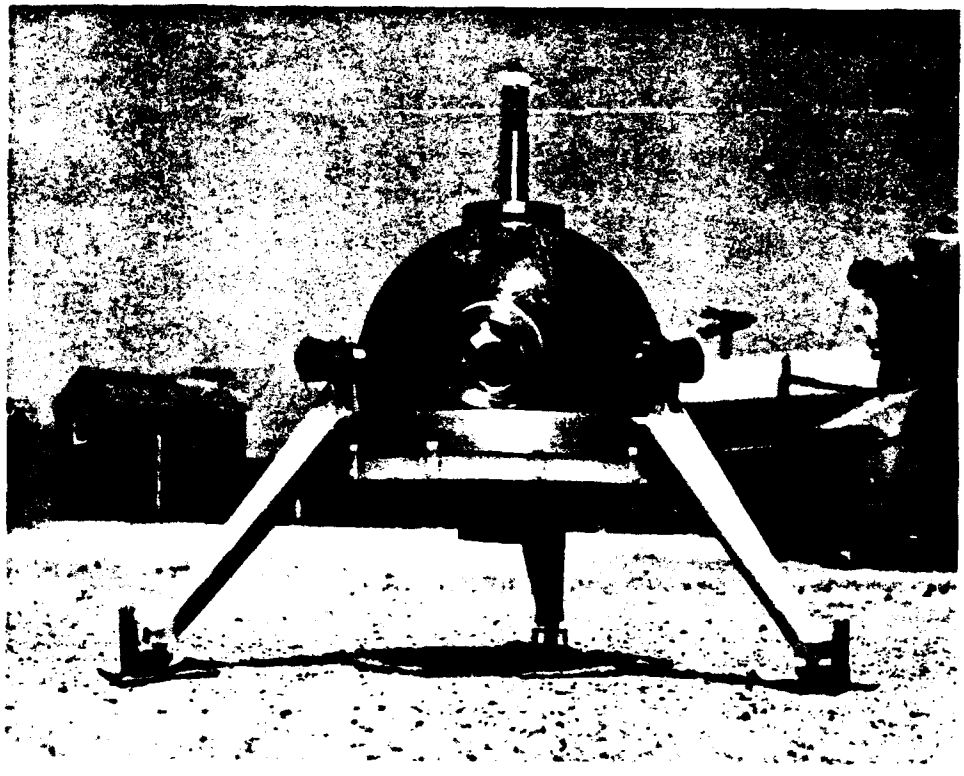

Figure A-6. Model of an ocean-bottom concrete habitat showing bottom configuration.

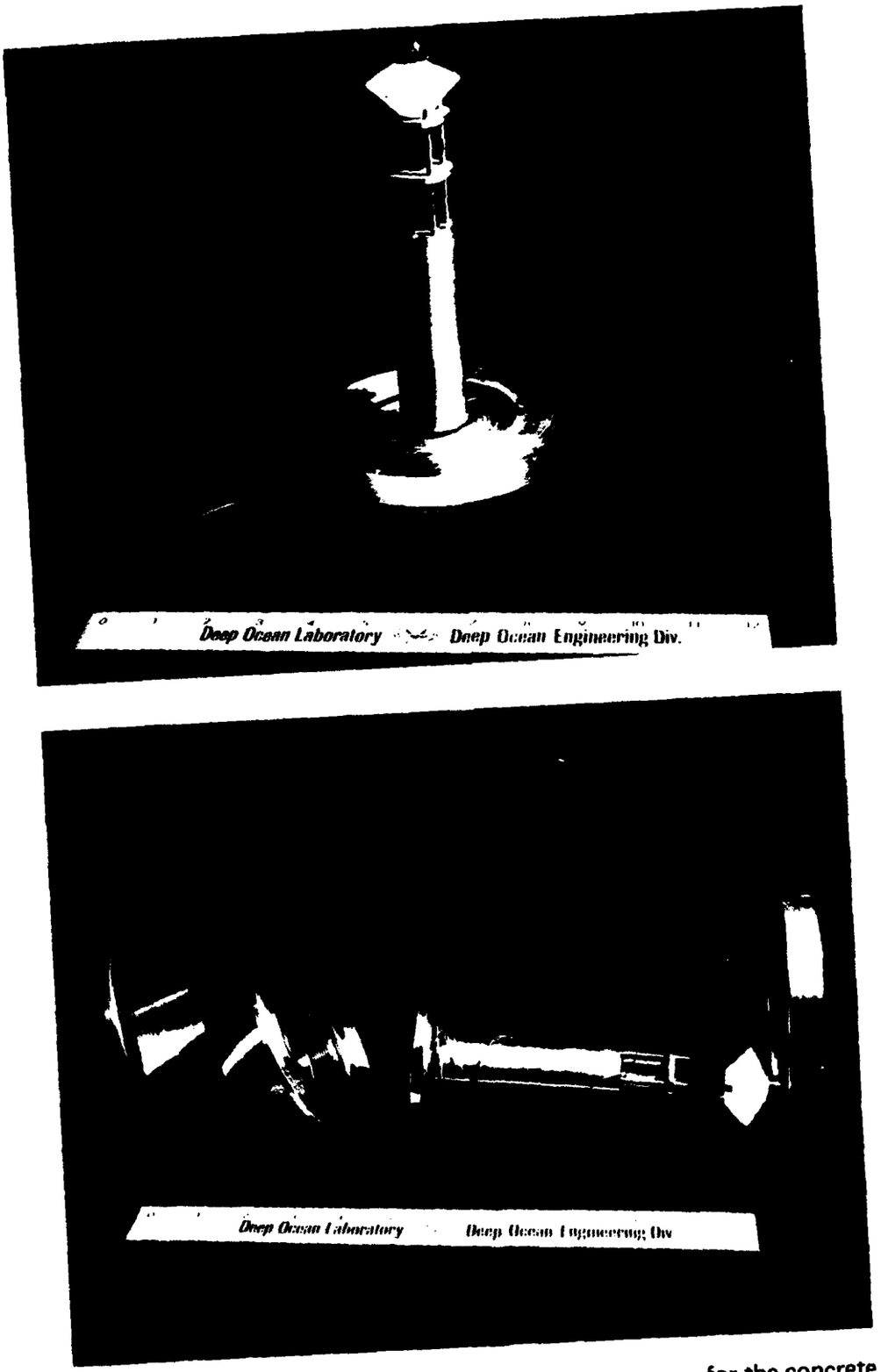

Figure A-7. Model of the oceanographic instrument tower for the concrete habitat model: (a) assembled; (b) disassembled.

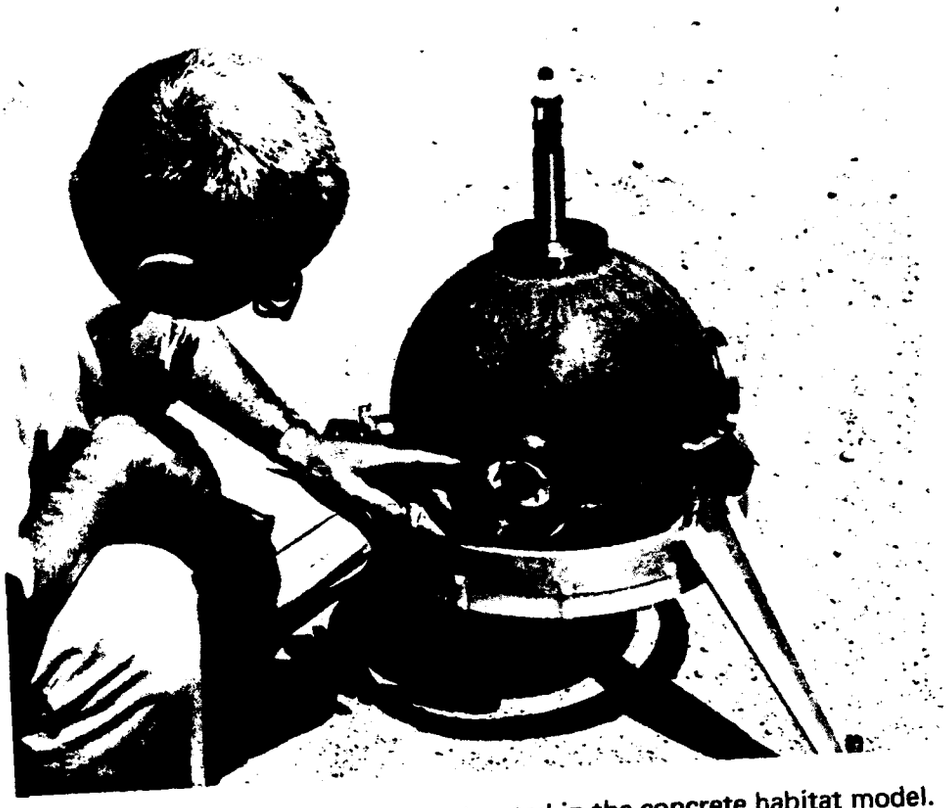

Figure A-8. One of four windows located in the concrete habitat model.

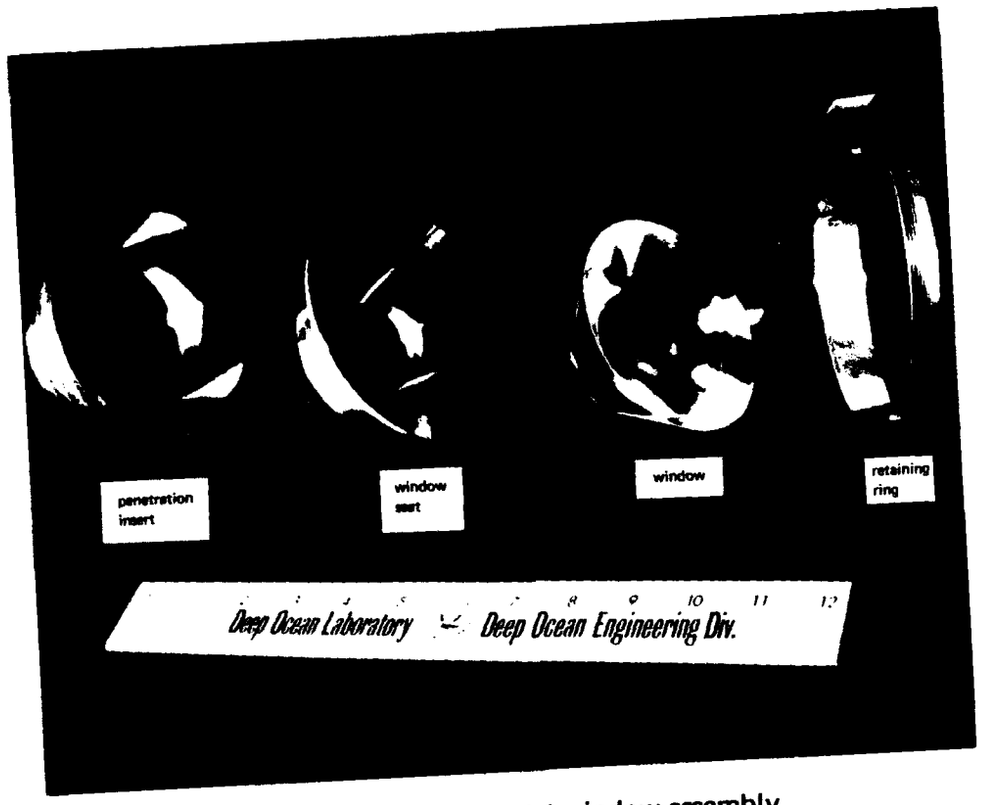

Figure A-9. Habitat model window assembly.

Figure A-10. Lights for the illumination of the ocean bottom are located on each of the tripod legs, as well as in the plastic ring just below the tripod ring.

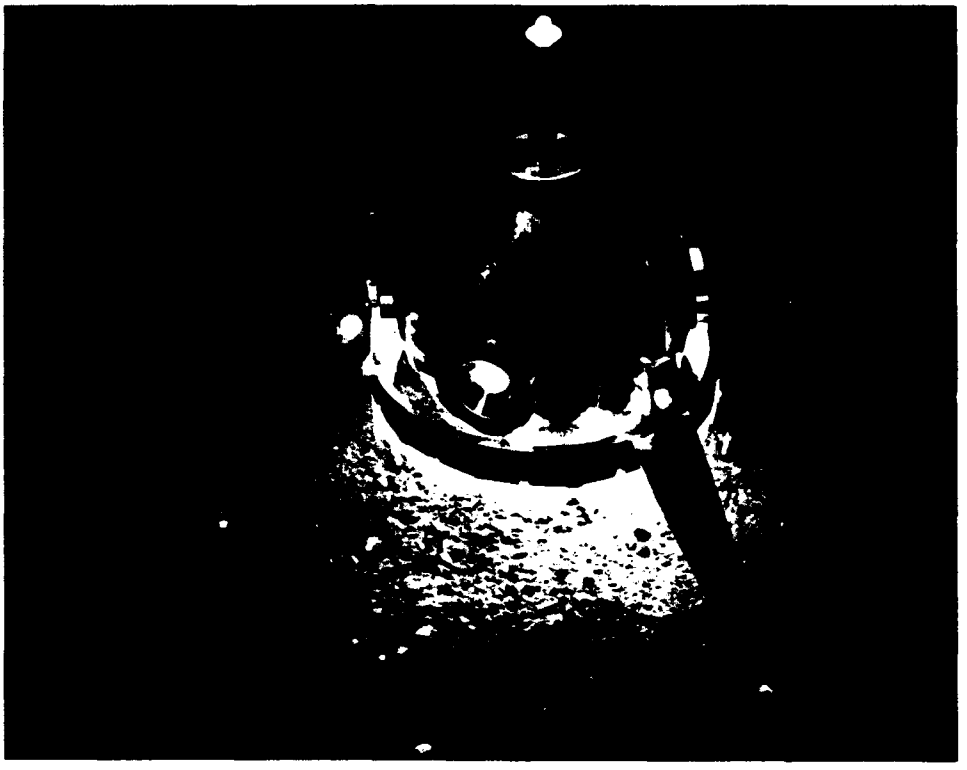

Figure A-11. Concrete habitat model with all the lights operational in simulated hydrospace.

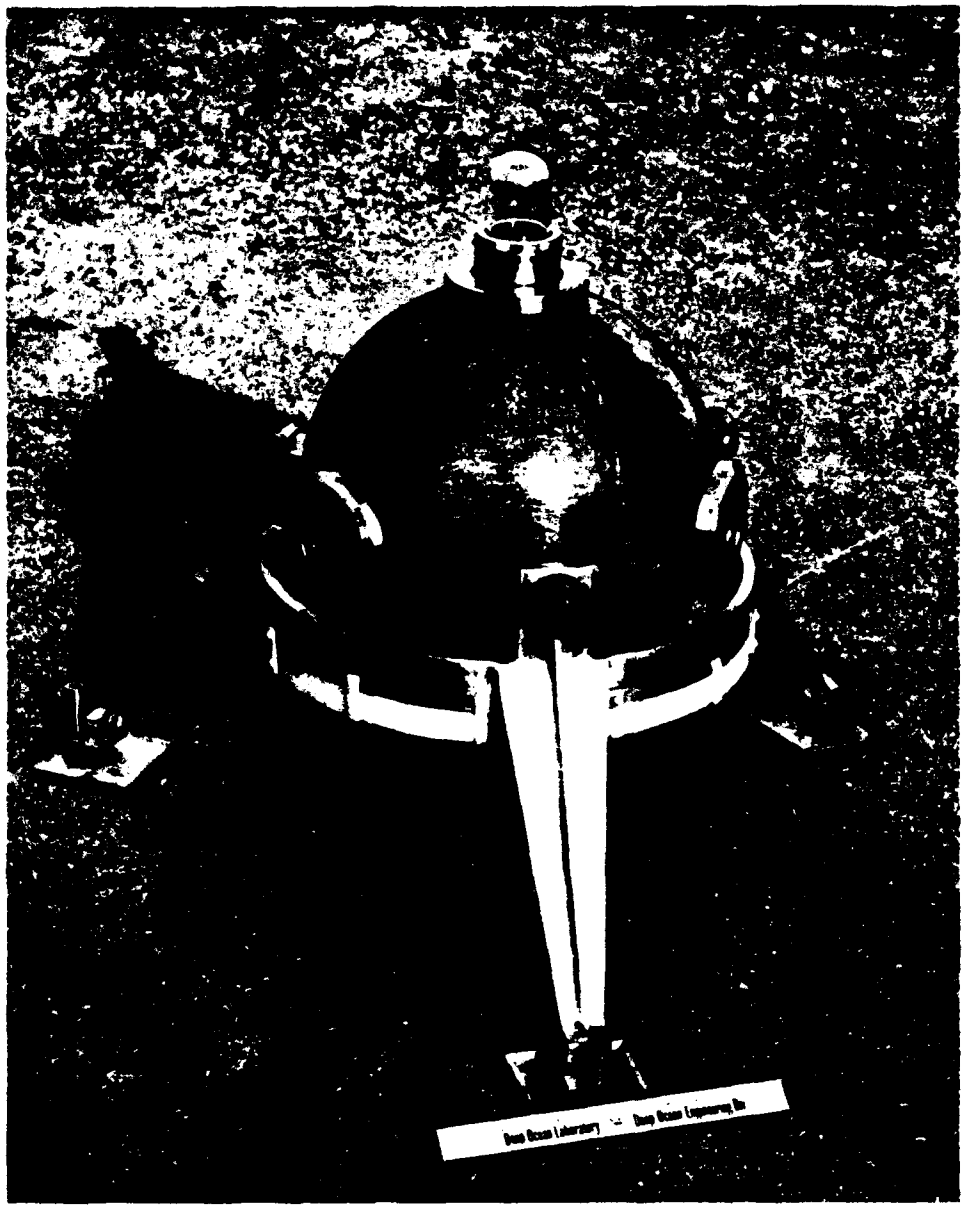

Figure A-12. Concrete habitat model equipped with a glass observation cupola instead of an instrumentation tower.

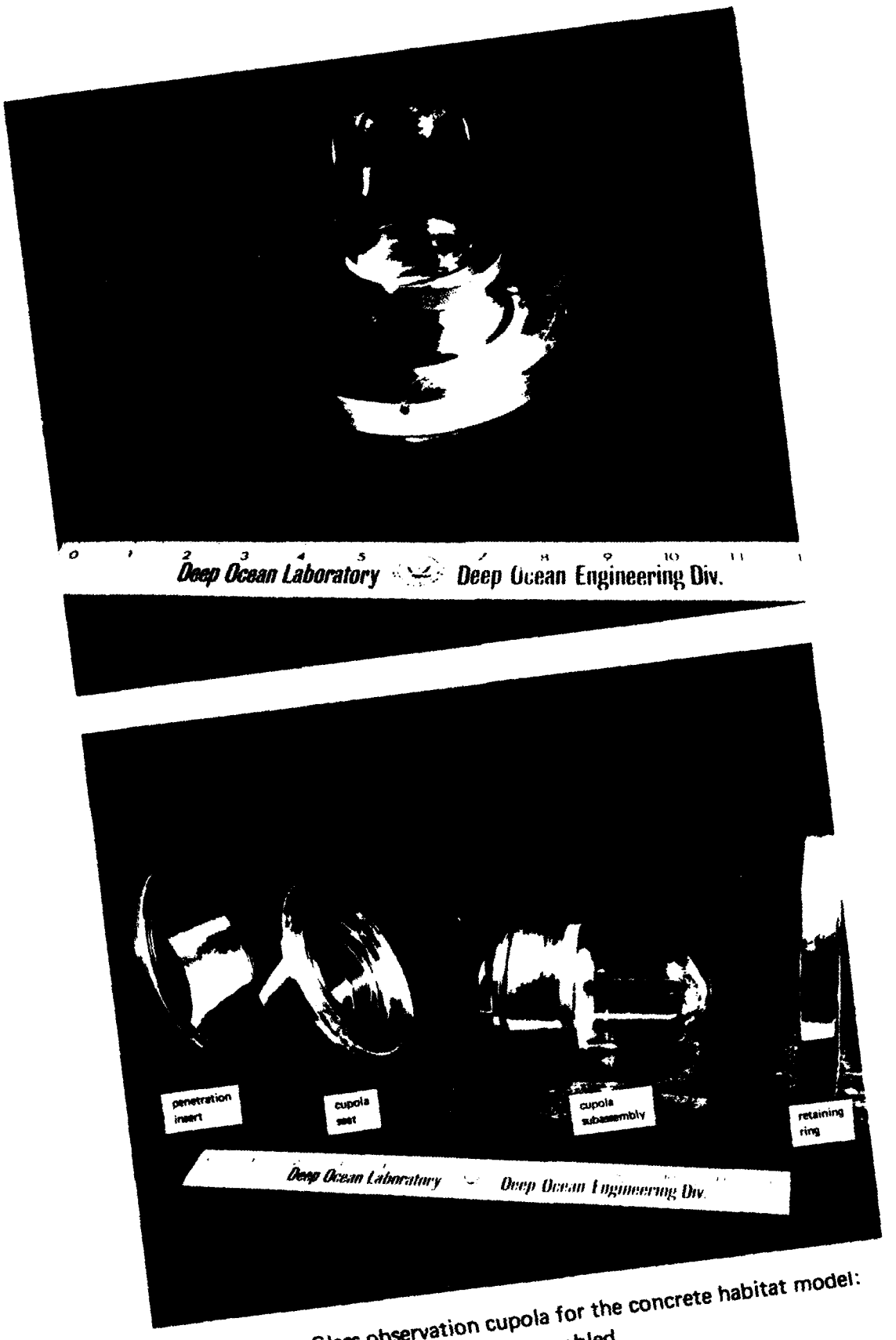

Figure A-13. Glass observation cupola for the concrete habitat model: (a) assembled; (b) disassembled.

Figure A-14. Concrete habitat model support frame.

Appendix B

CALCULATION OF ELASTOPLASTIC STABILITY OF SPHERICAL CONCRETE HULLS

A literature search indicates that only NCEL[1] has tested concrete spheres to destruction under hydrostatic pressure. Since a reference could not be found describing the calculation of elastoplastic stability of spherical concrete hulls, an approximate calculation of the stability was used for the hull models in this study.

The classical formula for the calculation of elastic buckling in perfectly spherical shells has been summarized by Timoshenko[2] as:

$$p_{cr} = \frac{KE\left(\frac{h}{R}\right)^2}{\sqrt{1 - \gamma^2}} \qquad (1)$$

where p_{cr} = critical pressure, lb/in.^{2} *

K = buckling coefficient

E = Young's modulus, lb/in.^{2}

h = hull thickness, in.

R = radius to the midsurface of hull wall, in.

γ = Poisson's ratio

For initially perfect spheres, a small-deflection buckling coefficient K of 1.15 has been derived,[2] which has not been found to agree well with tests done on metallic test models.[3,4,5] The experimentally obtained critical pressures have been found to be 10% to 75% less than calculated values. Many explanations have been given by investigators for these discrepancies, the major ones being inaccuracies in sphericity or wall thickness, as well as presence of residual stresses in the test models. To compensate for this discrepancy the David Taylor Model Basin (DTMB) empirically derived a new value for K of 0.8. This value has been used by DTMB with marked success and therefore has been widely accepted in ocean engineering. However, because the residual stresses of the glass and metallic hulls tested by DTMB

* Pressure at which collapse of sphere occurs due to buckling.

are not comparable to those of the concrete hulls (due to differences in the thickness-to-diameter ratios) and because the maximum eccentricity of NCEL's concrete hulls is less than 3% there is no reason for using the empirical K value of 0.8. However, the DTMB modified classical formula for the calculation of elastic buckling in spheres was originally used for the calculation of possible elastic buckling in concrete test spheres at NCEL.[1] The formula was used without modification, on the assumption that the behavior of concrete was elastic until fracture of the material took place. Tests conducted since that time have shown that this is not a good assumption, and that considerable plastic flow of concrete takes place prior to failure of the material at stress levels above 5,000 psi in compression. The plastic flow of concrete is evidenced primarily by the decrease of Young's modulus with increasing stress, and by the 1- to 2-second duration of hull implosion under hydrostatic pressure.

To accommodate the plastic behavior of concrete under the short-term loading used in this study, the author suggests several modifications to the DTMB formula for calculation of critical pressure of spherical concrete hulls under short-term hydrostatic loading, where short-term loading is defined as pressurization of the test model to destruction at a selected steady pressurization rate.

The modification to the classical buckling formula, which uses the DTMB coefficient of 0.8, consists of substituting the tangent modulus E_t for Young's modulus E in the equation. Such substitution has been used successfully before with acrylic plastic that also exhibits plastic behavior at higher stress levels prior to plastic buckling of the acrylic hull.[7,8] Substitution of the tangent modulus for Young's modulus complicates the calculation of the critical pressure, as different values of E_t must be substituted into the equation corresponding to the increase of compressive stress in the hull with increased pressure. The level of the compressive stress is calculated by the aid of the standard equation for stress distribution in a sphere under external hydrostatic pressure, as shown below:

$$\sigma = -p \frac{3 R_o^3}{2\left(R_o^3 - R_i^3\right)} \qquad (2)$$

where σ = compressive stress on the inner surface of the hull

p = given pressure

R_o = external radius of the spherical hull

R_i = internal radius of the spherical hull

The critical pressure at which elastoplastic instability occurs may be calculated by assuming a certain pressure p, calculating the stress level σ on the interior of the hull at that pressure by Equation 2, finding the corresponding tangent modulus (E_t) of concrete at that stress level from the E_t versus σ curve, substituting that E_t value together with the assumed value for p into the stability Equation 1, and comparing the left- and right-hand parts of the stability equation. If p is larger than the right-hand side of the equation, then the assumed p value is too large, and the hull will buckle before that pressure will be reached. A smaller p value must be now chosen and the whole process repeated. This iteration process is repeated until the chosen p becomes equal to the right-hand side of the stability equation (Equation 1). This iteration process obviously cannot be conducted past the ultimate compressive strength of the material, because the hull would fail by fracture of the material rather than by instability.

Before the buckling of hulls can be successfully calculated, it is necessary to have at hand a series of E_t versus σ curves for concrete mixes of different ages. One such curve of exploratory nature has been experimentally derived for this study by testing a series of solid concrete test cylinders under uniaxial compression and measuring their strains at different stress levels. This curve terminates at the 10,000-psi stress level and thus must be extrapolated to cover the stress levels at which failure of spheres occurred (Figure 45). Curves extending to the stress levels encountered inside spheres at implosion can be experimentally generated only by testing solid test specimens under biaxial stress, since under biaxial stress the concrete can withstand stresses of approximately the same magnitude as those inside the sphere under hydrostatic loading. The magnitude of the tangent modulus of concrete under biaxial stress will probably also be close to that found on the interior of the concrete sphere. Until such sophisticated curves are generated, those obtained by testing cylinders under uniaxial compression will have to suffice, although it is realized that the tangential modulus of elasticity obtained from uniaxial compression tests is invariably lower than the tangential modulus of elasticity of concrete under the same stress level under biaxial, or triaxial loading. Since this would make the calculated critical pressure for elastoplastic failure lower than the pressure at which it actually occurs, the calculation will be on the safe side, although by an unknown margin of safety.

REFERENCES

1. Naval Civil Engineering Laboratory. Technical Report R-517: Behavior of spherical concrete hulls under hydrostatic loading. Part I – Exploratory investigation, by J. D. Stachiw and K. O. Gray. Port Hueneme, Calif., Mar. 1967.

2. S. Timoshenko. Theory of elastic stability. New York, McGraw-Hill, 1936.

3. David Taylor Model Basin. Report 1741: Tests of stiffened and unstiffened machined spherical shells under external hydrostatic pressure, by M. A. Krenzke and T. J. Kiernan. Washington, D. C., Aug. 1963. (AD 422297)

4. ———. Report 1601: Tests of machined deep spherical shells under external hydrostatic pressure, by M. A. Krenzke. Washington, D. C., May 1962.

5. ———. Report 1713: The elastic buckling strength of near-perfect deep spherical shells with ideal boundaries, by M. A. Krenzke. Washington, D. C., July 1963. (AD 416057)

6. ———. Report 1759: The elastic buckling strength of spherical glass shells, by M. A. Krenzke and R. M. Charles. Washington, D. C., Sept. 1963. (AD 423588)

7. J. D. Stachiw. General instability of circumferentially stiffened sandwich shells subjected to uniform external pressure, MS thesis, College of Engineering and Architecture, Pennsylvania State University. University Park, Pa., 1961. (Also published as: Pennsylvania State University, Ordnance Research Laboratory, Serial no. NOrd 16597-91. University Park, Pa., Dec. 1962.) (Contract no. NORD-16597)

8. R. J. Roark. Formulas for stress and strain, 4th ed. New York, McGraw-Hill, 1965.

U. S. Naval Civil Engineering Laboratory
BEHAVIOR OF SPHERICAL CONCRETE HULLS UNDER HYDROSTATIC LOADING — PART I. EXPLORATORY INVESTIGATION
by J. D. Stachiw and K. O. Gray
R-517 69 p. illus March 1967 Unclassified

1. Undersea structures — Spherical concrete hulls I. Y-F015-01-07-001

Hollow concrete spheres 16 inches in outside diameter have been tested to destruction by exposure to external hydrostatic pressure in seawater to determine the compressive strength and permeability of concrete under such loading. The testing has shown that for the particular mix used, the compressive strength of dry concrete in a spherical hull of 16-inch outside diameter and 1-inch wall thickness under biaxial loading (short-term hydrostatic pressurization to failure at a constant rate) is approximately 48% higher than for identical dry concrete in 3-inch-diameter by 6-inch-long solid test cylinders under uniaxial loading conditions. Concrete spheres in which the wall was thoroughly permeated by seawater failed at stress levels approximately 18% higher than 3-inch-diameter by 6-inch-long solid test cylinders. The permeability of uncoated spheres to seawater at simulated ocean pressure of 1,500 psi was approximately 6×10^{-3} milliliters per hour per square inch of area per 1 inch of thickness.

U. S. Naval Civil Engineering Laboratory
BEHAVIOR OF SPHERICAL CONCRETE HULLS UNDER HYDROSTATIC LOADING — PART I. EXPLORATORY INVESTIGATION
by J. D. Stachiw and K. O. Gray
R-517 69 p. illus March 1967 Unclassified

1. Undersea structures — Spherical concrete hulls I. Y-F015-01-07-001

Hollow concrete spheres 16 inches in outside diameter have been tested to destruction by exposure to external hydrostatic pressure in seawater to determine the compressive strength and permeability of concrete under such loading. The testing has shown that for the particular mix used, the compressive strength of dry concrete in a spherical hull of 16-inch outside diameter and 1-inch wall thickness under biaxial loading (short-term hydrostatic pressurization to failure at a constant rate) is approximately 48% higher than for identical dry concrete in 3-inch-diameter by 6-inch-long solid test cylinders under uniaxial loading conditions. Concrete spheres in which the wall was thoroughly permeated by seawater failed at stress levels approximately 18% higher than 3-inch-diameter by 6-inch-long solid test cylinders. The permeability of uncoated spheres to seawater at simulated ocean pressure of 1,500 psi was approximately 6×10^{-3} milliliters per hour per square inch of area per 1 inch of thickness.

U. S. Naval Civil Engineering Laboratory
BEHAVIOR OF SPHERICAL CONCRETE HULLS UNDER HYDROSTATIC LOADING — PART I. EXPLORATORY INVESTIGATION
by J. D. Stachiw and K. O. Gray
R-517 69 p. illus March 1967 Unclassified

1. Undersea structures — Spherical concrete hulls I. Y-F015-01-07-001

Hollow concrete spheres 16 inches in outside diameter have been tested to destruction by exposure to external hydrostatic pressure in seawater to determine the compressive strength and permeability of concrete under such loading. The testing has shown that for the particular mix used, the compressive strength of dry concrete in a spherical hull of 16-inch outside diameter and 1-inch wall thickness under biaxial loading (short-term hydrostatic pressurization to failure at a constant rate) is approximately 48% higher than for identical dry concrete in 3-inch-diameter by 6-inch-long solid test cylinders under uniaxial loading conditions. Concrete spheres in which the wall was thoroughly permeated by seawater failed at stress levels approximately 18% higher than 3-inch-diameter by 6-inch-long solid test cylinders. The permeability of uncoated spheres to seawater at simulated ocean pressure of 1,500 psi was approximately 6×10^{-3} milliliters per hour per square inch of area per 1 inch of thickness.

U. S. Naval Civil Engineering Laboratory
BEHAVIOR OF SPHERICAL CONCRETE HULLS UNDER HYDROSTATIC LOADING — PART I. EXPLORATORY INVESTIGATION
by J. D. Stachiw and K. O. Gray
R-517 69 p. illus March 1967 Unclassified

1. Undersea structures — Spherical concrete hulls I. Y-F015-01-07-001

Hollow concrete spheres 16 inches in outside diameter have been tested to destruction by exposure to external hydrostatic pressure in seawater to determine the compressive strength and permeability of concrete under such loading. The testing has shown that for the particular mix used, the compressive strength of dry concrete in a spherical hull of 16-inch outside diameter and 1-inch wall thickness under biaxial loading (short-term hydrostatic pressurization to failure at a constant rate) is approximately 48% higher than for identical dry concrete in 3-inch-diameter by 6-inch-long solid test cylinders under uniaxial loading conditions. Concrete spheres in which the wall was thoroughly permeated by seawater failed at stress levels approximately 18% higher than 3-inch-diameter by 6-inch-long solid test cylinders. The permeability of uncoated spheres to seawater at simulated ocean pressure of 1,500 psi was approximately 6×10^{-3} milliliters per hour per square inch of area per 1 inch of thickness.

Unclassified

Security Classification

DOCUMENT CONTROL DATA - R & D

(Security classification of title, body of abstract and indexing annotation must be entered when the overall report is classified)

1. ORIGINATING ACTIVITY *(Corporate author)*

Naval Civil Engineering Laboratory
Port Hueneme, California 93041

2a. REPORT SECURITY CLASSIFICATION

Unclassified

2b. GROUP

3. REPORT TITLE

BEHAVIOR OF SPHERICAL CONCRETE HULLS UNDER HYDROSTATIC LOADING – PART II. Effect of Penetrations

4. DESCRIPTIVE NOTES *(Type of report and inclusive dates)*

Not Final; July 1966 - January 1967

5. AUTHOR(S) *(First name, middle initial, last name)*

J. D. Stachiw

6. REPORT DATE	7a. TOTAL NO. OF PAGES	7b. NO. OF REFS
October 1967	58	8

8a. CONTRACT OR GRANT NO.	9a. ORIGINATOR'S REPORT NUMBER(S)
b. PROJECT NO. Y-F015-01-07-001	TR-547
c.	9b. OTHER REPORT NO(S) *(Any other numbers that may be assigned this report)*
d.	

10. DISTRIBUTION STATEMENT

This document has been approved for public release and sale; its distribution is unlimited. Copies available at the Clearinghouse for Federal Scientific & Technical Information (CFSTI), Sills Bldg., 5285 Port Royal Road, Springfield, Va. 22151 Price-$3.00

11. SUPPLEMENTARY NOTES	12. SPONSORING MILITARY ACTIVITY
	Naval Facilities Engineering Command Washington, D. C.

13. ABSTRACT

The objective of the study was (1) to show that concrete hulls with window and hatch penetrations for ocean bottom habitats can be built, and (2) to determine if the collapse pressure of such hulls is degraded by the incorporation of properly designed penetrations. All of the experimental work was performed on six concrete spheres (16-inch outside diameter and 14-inch inside diameter) cast from concrete with a uniaxial compressive strength of 10,000 psi. The concrete sphere models failed under hydrostatic pressures ranging from 2,675 psi to 3,400 psi, depending on the type of penetration insert. It was found that the collapse pressure of a concrete hull equipped with properly designed operational windows and hatches was the same as that of a similar concrete hull without penetrations.

DD FORM 1 NOV 65 1473 (PAGE 1)

S/N 0101-807-6801

Unclassified

Security Classification

14 KEY WORDS	LINK A		LINK B		LINK C	
	ROLE	WT	ROLE	WT	ROLE	WT
Concrete hulls						
Spherical hulls						
Window apertures						
Hatch apertures						
Collapse pressures						
Ocean-bottom habitats						

R 588

Technical Report

BEHAVIOR OF SPHERICAL CONCRETE HULLS UNDER HYDROSTATIC LOADING—PART III

Relationship Between Thickness-To-Diameter Ratio and Critical Pressures, Strains, and Water Permeation Rates

June 1968

NAVAL FACILITIES ENGINEERING COMMAND

NAVAL CIVIL ENGINEERING LABORATORY

Port Hueneme, California

BEHAVIOR OF SPHERICAL CONCRETE HULLS UNDER HYDROSTATIC LOADING—PART III

Relationship Between Thickness-To-Diameter Ratio and Critical Pressures, Strains, and Water Permeation Rates

Technical Report R-588

Y-F015-01-07-001

by

J. D. Stachiw and K. Mack

ABSTRACT

Sixteen hollow concrete spheres of 16-inch outside diameter were subjected to external hydrostatic pressure to investigate the relationship between the sphere's shell thickness and (1) its critical pressure, (2) permeability, and (3) strain magnitude. The shell thickness of the spheres varied from 1 inch to 4 inches in 1-inch steps. All spheres were cast from the same concrete mix, cured under identical temperature and moisture conditions, and tested in the same manner. The strength of concrete in the spheres at the time of testing, as established by uniaxial compression tests on 3 x 6-inch cylinders, was in the 9,000-to-11,000-psi range. The critical pressure of waterproofed hollow concrete spheres was found to be approximately a linear function of the sphere's thickness; the spheres imploded at pressures from 3,240 to 13,900 psi, depending on their thickness. Concrete spheres permeated by seawater failed at hydrostatic pressures 30% to 15% lower than identical waterproofed spheres. In all cases the stress in the spheres at the time of implosion was considerably higher than in concrete test cylinders prepared of the same mix and of the same curing history subjected to uniaxial compression. The resistance of concrete to permeation by seawater into the interior of nonwaterproofed spheres at 2,000-psi hydrostatic pressure was found to be an exponential function of shell thickness. The rate of flow into the sphere's interior ranged from 6.1 to 0.197 ml/day/ ft^2 of exterior surface, depending on the thickness of shell.

CONTENTS

STATEMENT OF THE PROBLEM

Permanent ocean bottom habitats require different hull thicknesses corresponding to the depth at which they will be located during their operational life. For this reason it is necessary to know what relationship exists between the thickness of a monocoque concrete hull and its critical pressure* under hydrostatic loading. Since the magnitude and distribution of strains in an elastic monocoque hull varies nonlinearly with its thickness, it is reasonable to assume that such will be the case for a plastic monocoque hull, such as one made of concrete. Since it is not known for certain, however, how the strains will be distributed in a thick concrete hull, and how the concrete itself will react to such a distribution of strains, design of concrete hulls for different depths is at the present time very much a matter of engineering judgment. It is therefore of great importance to generate experimental data on which empirical relationships between the thickness of concrete hulls and their critical pressure can be derived. Once such relationships have been empirically derived, analytical relationships can be postulated and verified for conformance to experimental data.

In addition to the relationship between critical pressure and wall thickness, it is of great value to know also the relationship between the rate of water permeation and wall thickness. If the rate of permeation is quite independent of wall thickness, then no advantages accrue from the use of thicker walls than those required to withstand the hydrostatic pressure for a certain depth. On the other hand, if the rate of permeation is sensitive to wall thickness, additional waterproofing benefits may be derived from utilizing a greater wall thickness than that required by the structure to resist external pressure.

OBJECTIVE OF STUDY

The objective of the study was to explore experimentally the relationship between the wall thickness of spherical concrete hulls and (1) critical pressure, (2) distribution of strains, and (3) rate of permeation.

* External hydrostatic pressure at which failure occurs.

The experimental data generated in this exploratory study will serve two purposes. It will permit the design of spherical concrete hydrospace hulls with a higher degree of confidence, and it will serve as basis for future analytical studies attempting to correlate the critical pressure, strain magnitude, and rate of permeation of concrete spherical hulls with their wall thickness.

BACKGROUND INFORMATION

It is only very recently that serious thought has been given to utilizing concrete as the main load-carrying material in hulls enclosing ocean-floor-mounted habitats maintained at atmospheric pressure. These exploratory studies[1,2] sponsored by the Naval Facilities Engineering Command utilized spherical concrete hull models of 16-inch outside diameter (OD) and 14-inch inside diameter (ID). These hulls were externally pressurized until implosion occurred. Results show that not only is the concrete in the hull stronger under hydrostatic loading than under uniaxial compression, but also that permeability of concrete hulls under hydrostatic loading of 1,500 psi is negligible from an engineering viewpoint. It was found that the strength of dry concrete in the spherical hull under biaxial compression was 46% higher, while wet concrete was 18% higher than corresponding dry 3 x 6-inch test cylinders under uniaxial compression, which failed in the 10,000-to-11,000-psi stress range. When working models of spherical ocean bottom concrete habitats were built with window and hatch penetrations, the critical pressure of these models was found to be the same as that of identical spherical hulls without penetrations. The critical pressure of the former models tested under short-term pressure loading* was in the 6,500-to-8,000-foot depth range, while their weight to displacement ratio varied from 0.75 to 1.1, depending on the number of steel inserts in the hull penetrations. On the basis of these studies, it was concluded that even with very limited knowledge of the behavior of submerged concrete hulls, it is possible with reasonable assurance to perform conceptual designs of full-sized spherical hulls with window and hatch penetrations for ocean bottom service in the 0-to-3,500-foot depth range. No data is, however, available that would permit the conceptual design of a concrete spherical hull for depths greater than 3,500 feet. The present study sponsored by the Naval Facilities Engineering Command is intended to provide data on the relationship between the hull's thickness, its critical pressure, magnitude of strains, and rate of permeation.

* Short-term pressure loading consists of subjecting the concrete spheres to hydrostatic pressure continuously increasing at a rate of 100 psi/min until implosion takes place.

SCOPE OF INVESTIGATION

The present study was limited to three areas of experimental investigation in spherical concrete hull shape: the critical pressures of dry and wet concrete, distribution of strains, and rate of permeation. Sixteen spherical hull models with 16-inch outside diameter and four different wall thicknesses were investigated. The experimental data was limited to recording of critical pressures, magnitude of strains on the model's exterior and interior surfaces, and the rate of seawater permeation into the interior of the hull. Only one kind of concrete mix was used for casting the hull models, and only one method was employed for curing. Both the concrete mix and the curing method utilized were the same as used in previous studies[1,2] for casting of 16-inch-OD concrete hull models.

EXPERIMENT DESIGN

Experimental models and tests conducted are summarized in Table 1 for ready reference of the reader. Since three different kinds of hull response to hydrostatic pressure were to be investigated, three distinctly different types of hull models were to be utilized. Thus, in experiments whose prime objective was the determination of hull's critical pressure, the spherical models (type I) were built without any penetrations, and their exterior was waterproofed with a 1/32-inch layer of epoxy (Figure 1). For experiments in which the magnitude and distribution of strains on a spherical hull were investigated, the waterproofed spherical concrete models (type II) were equipped with penetrations for feedthrough of electric instrumentation cables (Figure 2). Experiments conducted to determine rates of water permeation into concrete, as well as critical pressures of seawater-permeated spheres, were conducted with type III spherical concrete hull models. These were identical to those used for the determination of strains except that the waterproof coating was omitted (Figure 3).

Since all of the spherical concrete hull models used in the three different types of experiments were cast from the same concrete mix in identical molds, the experimental results generated by these experiments could be correlated. In this manner, one can postulate that a spherical concrete hull model of a given outside diameter and wall thickness has a known critical pressure, magnitude of strains, and rate of seawater permeation even though each one of these parameters is determined on separate test specimens.

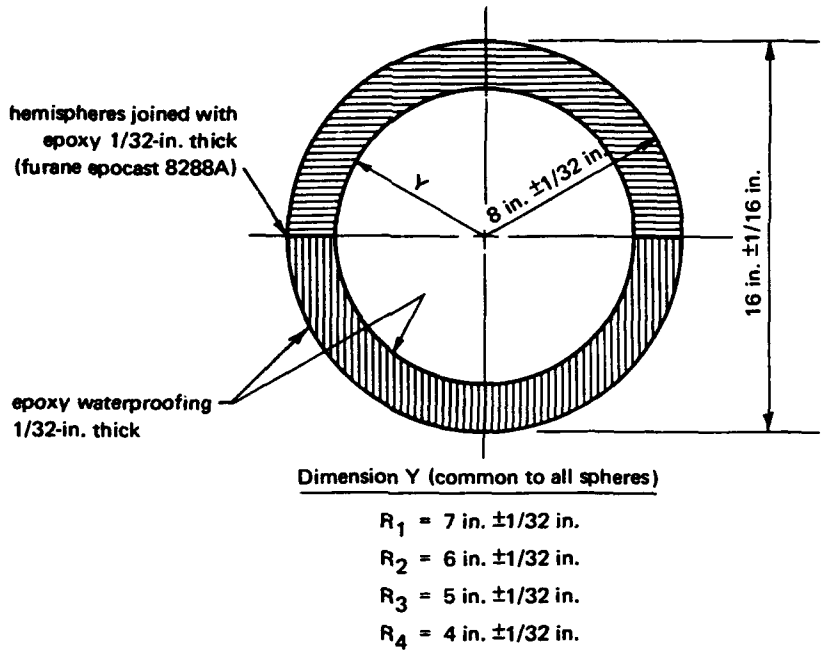

Figure 1. Type I concrete sphere used for critical pressure determination of dry concrete spheres.

The study required a minimum of three variations in the model hull-thickness parameter to establish whether the critical pressure, magnitude of strain, or rate of permeation are linear or nonlinear functions of hull thickness. Since additional variations of the hull-thickness parameter would permit a better definition of the three above-mentioned functions, a total of four hull-thickness parameter variations were selected. The wall thicknesses selected were such that the tests covered the whole range of hull types from thin walled to thick walled.

FABRICATION OF CONCRETE SPHERES

The 16 concrete spheres were cast from a specially designed concrete mix[1] in a hemispherical aluminum mold used in casting spheres in previous NCEL concrete hull studies. In this study, interchangeable male mold inserts of different diameters (Figure 4) were used, thereby making it possible to cast in the same female mold (Figure 5) spheres with different wall thickness (Figure 6).

The design of the concrete mix included aggregate, portland cement, and water in the proportions shown in Table 2. Six 3 x 6-inch control cylinders subjected to the same curing cycle as the hemispheres were cast from the same mix as each hemisphere.

Table 1. Spherical Concrete Hull Models and Test Configurations Used in the Study

Sphere No.	Configuration Type	Penetrations	Wall Thickness (in.)	Waterproof Coating	Instrumentation	Illustration of Model	Type of Test
19	I	none	1	epoxy	none	Figure 1	Short-term implosion testing, pressurized at 100 psi/min
20	I	none	1	epoxy	none	Figure 1	Short-term implosion testing, pressurized at 100 psi/min
21	II	pipe feedthrough	1	epoxy	16 electric resistance strain gages	Figure 2	Short-term implosion testing, pressurized at 100 psi/min
22	III	pipe feedthrough	1	none	pneumatic water level detector	Figure 3	Pressure held at 2,000 psi until water permeates wall, then pressurized at 100 psi/min to failure
23	I	none	2	epoxy	none	Figure 1	Short-term implosion testing, pressurized at 100 psi/min
24	I	none	2	epoxy	none	Figure 1	Short-term implosion testing, pressurized at 100 psi/min
25	II	pipe feedthrough	2	epoxy	16 electric resistance strain gages	Figure 2	Short-term implosion testing, pressurized at 100 psi/min
26	III	pipe feedthrough	2	none	pneumatic water level detector	Figure 3	Pressure held at 2,000 psi until water permeates wall, then pressurized at 100 psi/min to failure
27	I	none	3	epoxy	none	Figure 1	Short-term implosion testing, pressurized at 100 psi/min
28	I	none	3	epoxy	none	Figure 1	Short-term implosion testing, pressurized at 100 psi/min
29	II	pipe feedthrough	3	epoxy	16 electric resistance strain gages	Figure 2	Short-term implosion testing, pressurized at 100 psi/min
30	III	pipe feedthrough	3	none	pneumatic water level detector	Figure 3	Pressure held at 2,000 psi until water permeates wall, then pressurized at 100 psi/min to failure
31	I	none	4	epoxy	none	Figure 1	Short-term implosion testing, pressurized at 100 psi/min
32	I	none	4	epoxy	none	Figure 1	Short-term implosion testing, pressurized at 100 psi/min
33	II	pipe feedthrough	4	epoxy	16 electric resistance strain gages	Figure 2	Short-term implosion testing, pressurized at 100 psi/min
34	III	pipe feedthrough	4	none	pneumatic water level detector	Figure 3	Pressure held at 2,000 psi until water permeates wall, then pressurized at 100 psi/min to failure

Notes
1. All models are assembled from two hemispheres with 16-inch external diameter.
2. Seawater at room temperature was used in all cases as the pressurizing medium.
3. Spheres are numbered in a series originating with the first NCEL study.

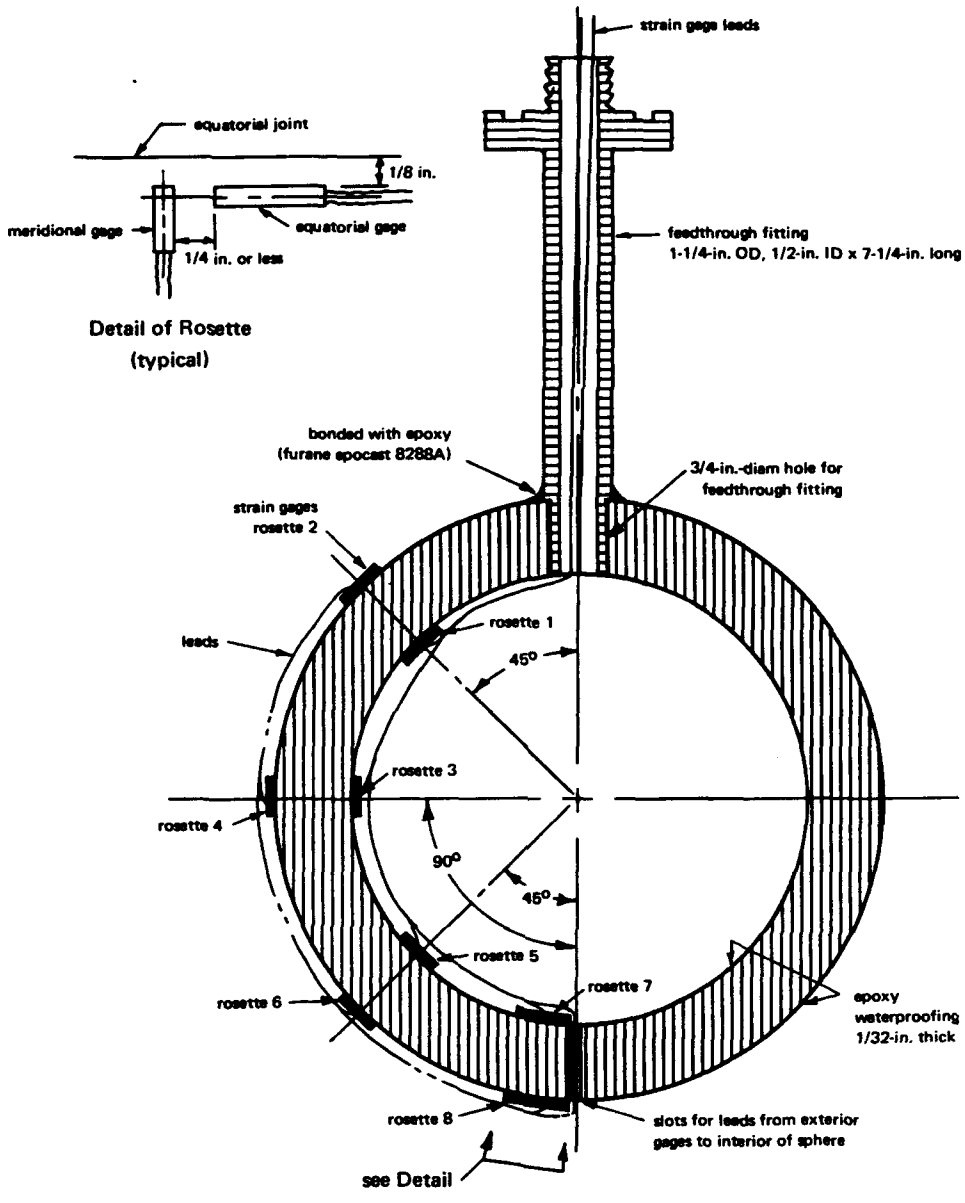

Rosette No.	Exterior Gages		Rosette No.	Interior Gages	
	Meridional	Equatorial		Meridional	Equatorial
2	02	03	1	00	01
4	06	07	3	04	05
6	10	11	5	08	09
8	14	15	7	12	13

Figure 2. Type II concrete sphere used for determination of strains in dry concrete spheres.

Table 2. Composition of Concrete Mix

Constituent	Screen Size		Percent by Weight
	Passing	Retained	
San Gabriel Aggregate	No. 4	No. 8	20.1
	No. 8	No. 16	14.1
	No. 16	No. 30	10.0
	No. 30	No. 50	7.0
	No. 50	No. 100	4.9
	No. 100	on pan	11.7
Type III portland cement			20.6
Tap water			11.6

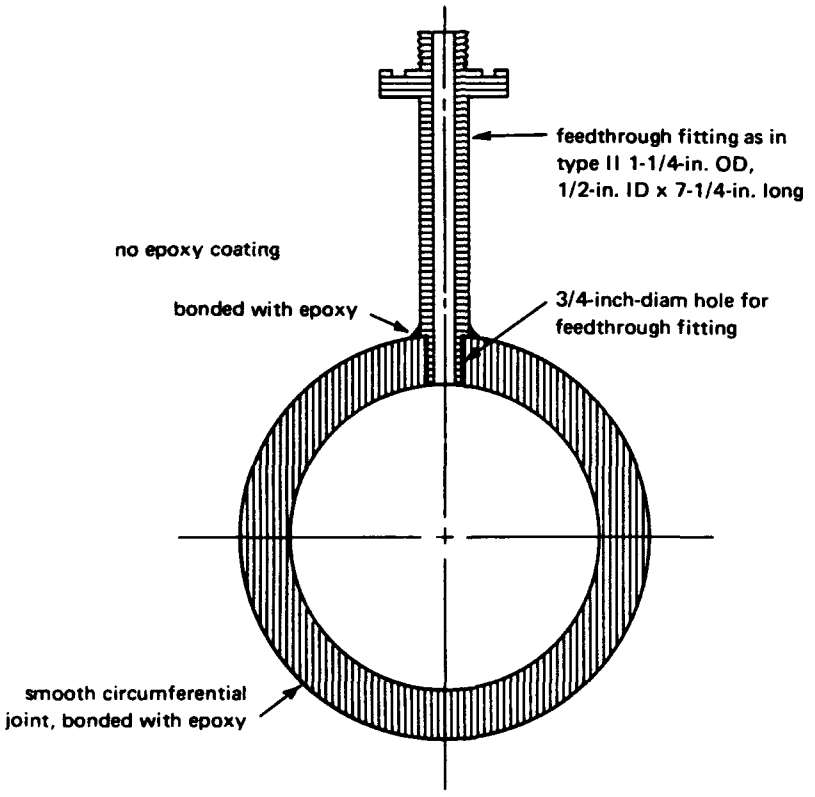

Figure 3. Type III concrete sphere used in the determination of permeability and critical pressure of wet concrete spheres.

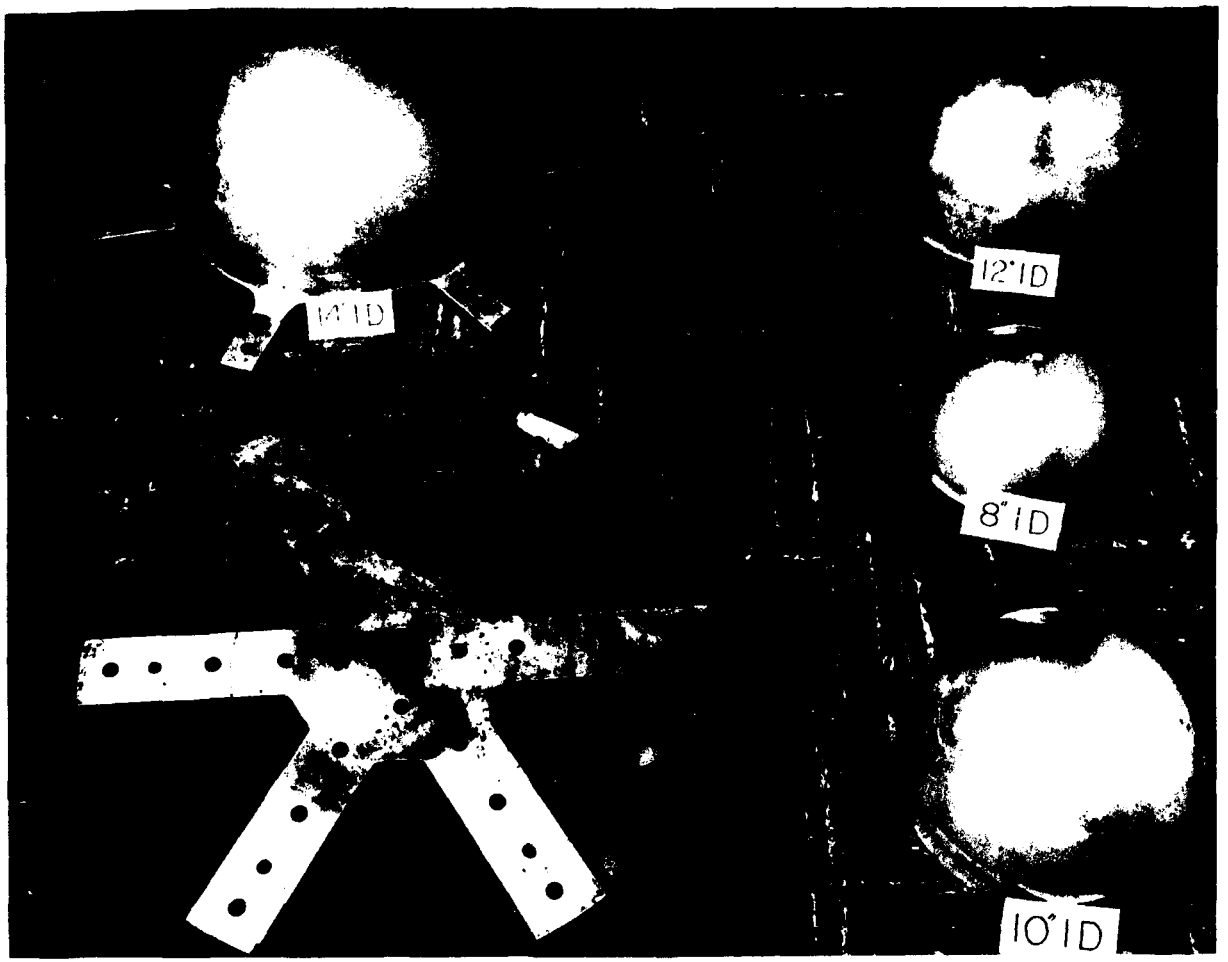

Figure 4. Male mold inserts used in conjunction with 16-inch-diameter female mold for casting concrete hemispheres.

Figure 5. Male and female mold assembly prior to placing of concrete mix for an 8-inch-ID sphere.

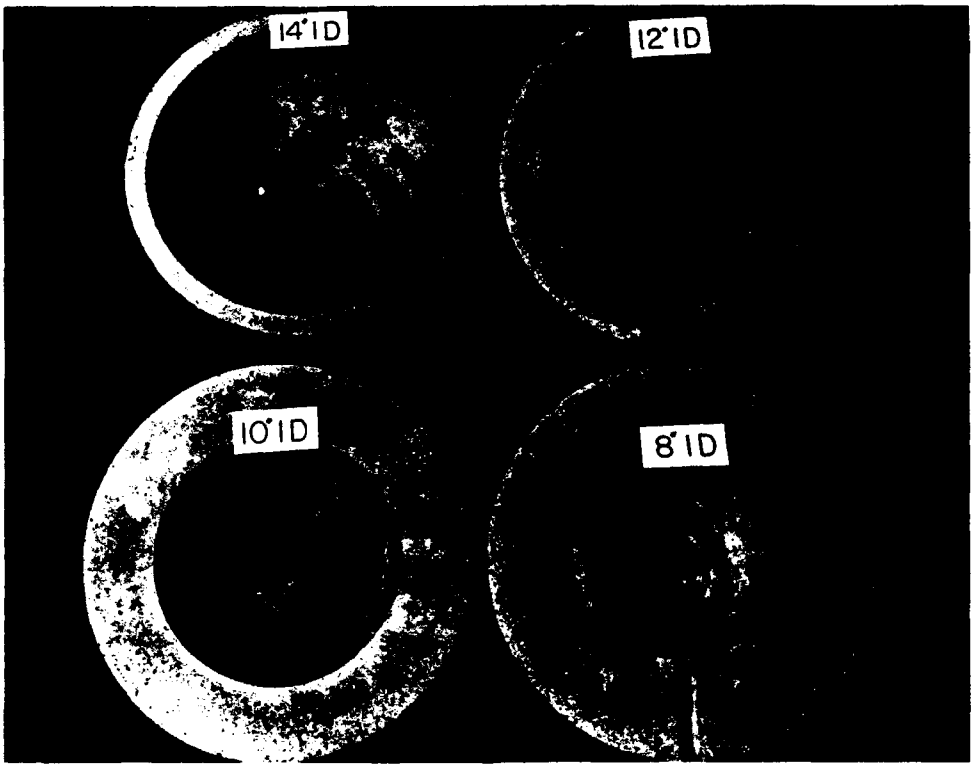

Figure 6. Cast hemispheres of different thickness. Note the deep penetration for pipe feedthrough on the 8-inch-ID hemisphere.

The methods outlined in previous studies[1] were used in casting the specimens. The mold surfaces were coated with a form film and allowed to dry. A thin layer of vaseline was then applied to the form surfaces, and the form was assembled and filled with fresh concrete. A form vibrator was attached to the flange on the underside of the female mold. A nylon string was used as a bleeder line to release the form by breaking the vacuum.

After being placed in the 100% relative humidity room for 24 hours, the specimen was removed from the mold. As shown in previous studies,[1] the exterior surface of a hemisphere as cast was always smooth, whereas the interior surface always had holes caused by trapped air bubbles. All surfaces were rubbed down with steel wool and the interior surface of the hemisphere was patched with a mix consisting of 50% type III cement, 50% aggregate passing the no. 100 sieve, and enough water to make the mix plastic. This application gave the interior surface a smooth finish.

The hemisphere and cylinders were appropriately given a specimen number and placed in the 100% relative humidity room for 28 days at 70° to 75°F. Upon their removal, the circumferential edge of the hemisphere was ground flat to within ±1/64 of an inch (Figure 7). The exterior and interior surfaces of the hemisphere were sanded and then washed with a 10% hydrochloric acid solution. The hemispheres were then placed in the 25% relative humidity room for a minimum of 28 days at 70° to 75°F for drying prior to instrumentation with electric strain gages (Figure 8).

When the hemispheres were dry, the necessary strain gages were attached to the concrete, the hemispheres were bonded together, and a waterproofing coat applied when specified. Subsequently the assembled spheres remained in the 25% relative humidity room until test date.

INSTRUMENTATION

Since there were three different parameters being investigated in the study, there were also three different test configurations. Type I spheres were built solely for determination of their critical pressure and therefore had no internal instrumentation (Figure 1).

Type II spheres were built for the determination of both critical pressure and strains on the exterior and interior of the spheres. These spheres were instrumented with BLH-A-5 electric resistance strain gages, which were arranged in a 90-degree rosette fashion, thereby making eight rosettes (Figure 2). The gages on the inside of the sphere were cemented directly opposite the gages on the outside of the sphere (Figures 9 and 10). Each of the gages was wired independently. The leads from the external

gages passed through a notch cut in the hemisphere edge to the sphere's interior and from there through the feedthrough-tube fitting to the exterior of the pressure vessel. The interior and exterior were also coated with waterproofing compound, and the wire passage in the circumferential joint was potted with the same epoxy compound used for bonding the hemispheres.

Type III spheres (Figure 3), used primarily for permeability studies, were equipped with a pneumatic water-influx detecting device. The apparatus for measuring water inflow (Figure 11) consisted of two tubes: one to pressurize the interior of the sphere with air and the other to siphon out at prescribed intervals any water that permeated to the interior of the sphere. Both tubes penetrated the concrete sphere by means of a simple feedthrough pipe.

Several of the test cylinders were also instrumented with strain gages. The BLH-A-12 gages were situated in a 90-degree rosette fashion midway between cylinder ends. There were four such cylinders instrumented for each group of spheres of same t/D_o ratio.* Each cylinder was instrumented with one rosette.

Figure 7. Manual grinding of sphere edge to obtain desired flatness. Glass plate serving as the table surface is covered with No. 60 wet silicon grinding compound.

* Here, t refers to wall thickness and D_o to external diameter.

Figure 8. Drying of hemispheres and test cylinders in the 25% humidity room.

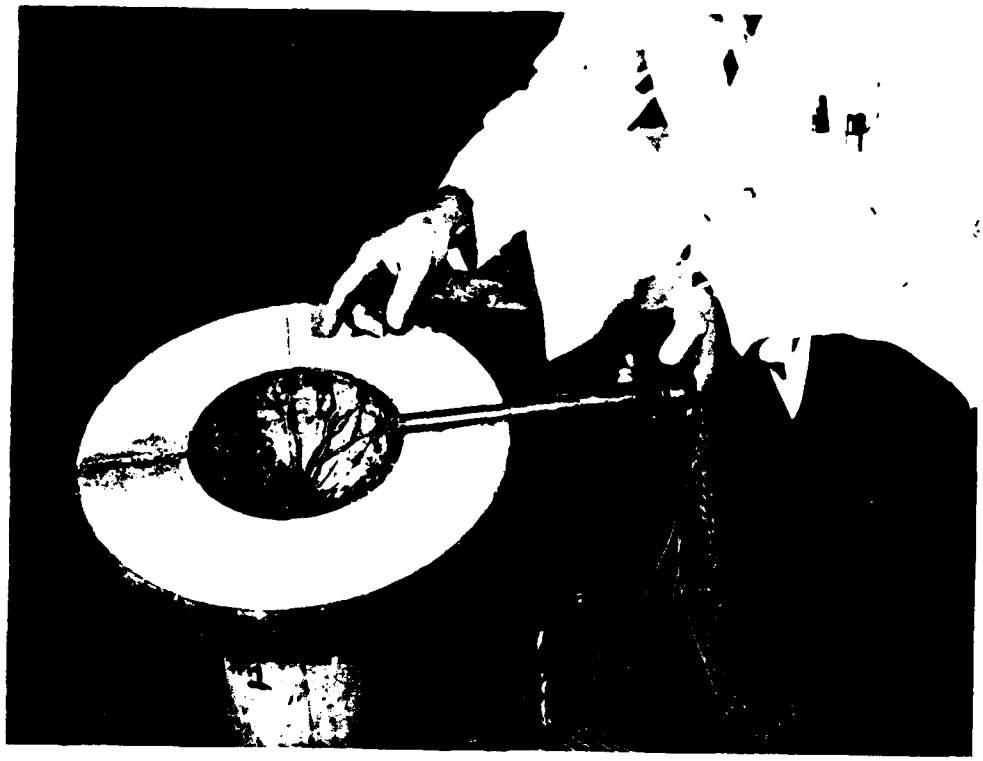

Figure 9. Typical location of strain gages on sphere's interior.

Figure 10. Typical location of strain gages on sphere's exterior.

TESTING

The concrete spheres were tested under short-term hydrostatic pressure in the 18-inch-ID pressure vessel of the Deep Ocean Laboratory as in previous studies.[1,2]

Since the type I spheres had no attachments for holding them rigidly in the vessel, a retaining cage was used to prevent any movement (Figure 12). Each sphere was pressurized at a 100-psi/min rate until failure occurred. After each of the spheres was imploded, the corresponding test cylinders were capped and tested to failure at the standard ASTM(C-469) rate of 2,000 psi/min by uniaxial compression.

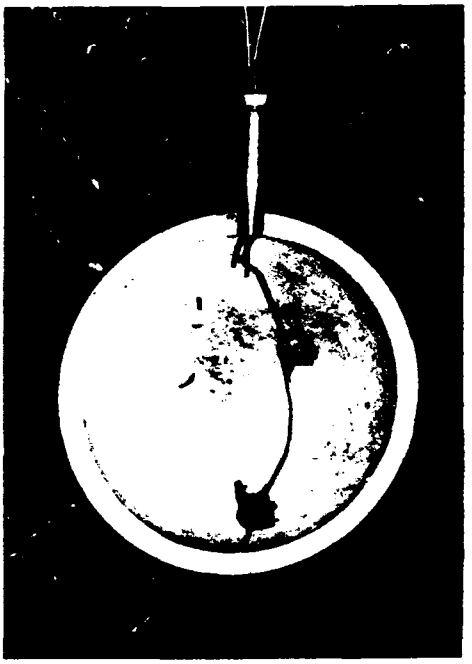

Figure 11. Typical hemisphere with internal piping for purging the sphere interior of accumulated seawater.

Type II spheres were also pressurized at a 100-psi/min rate until failure took place. During the tests strain readings were taken at 500-psi intervals. Type II spheres were equipped with pipe feedthroughs; these were used to attach the spheres to the pressure vessel end closure to hold them in a fixed position with respect to the pressure vessel walls (Figure 13).

Type III concrete spheres under long-term hydrostatic pressure were tested in the same 18-inch pressure vessel as used in the previous short-term investigations. In the vessel, the sphere was connected to the pressure vessel head with the same type of feedthrough pipe fitting as used in type II spheres. The two tubes previously mentioned to detect leakage were brought through the pipe fitting to the outside of the pressure vessel. The sphere was pressurized to 2,000 psi at a rate of 100 psi/min and held constant. When water was detected on the inside of the sphere (anywhere from 2 to 14 days after pressurization, depending on wall thickness) readings were taken of the water flow rate. After the flow readings were taken for 5 days, the sphere was pressurized to failure at a rate of 100 psi/min and the corresponding cylinders crushed under uniaxial compression.

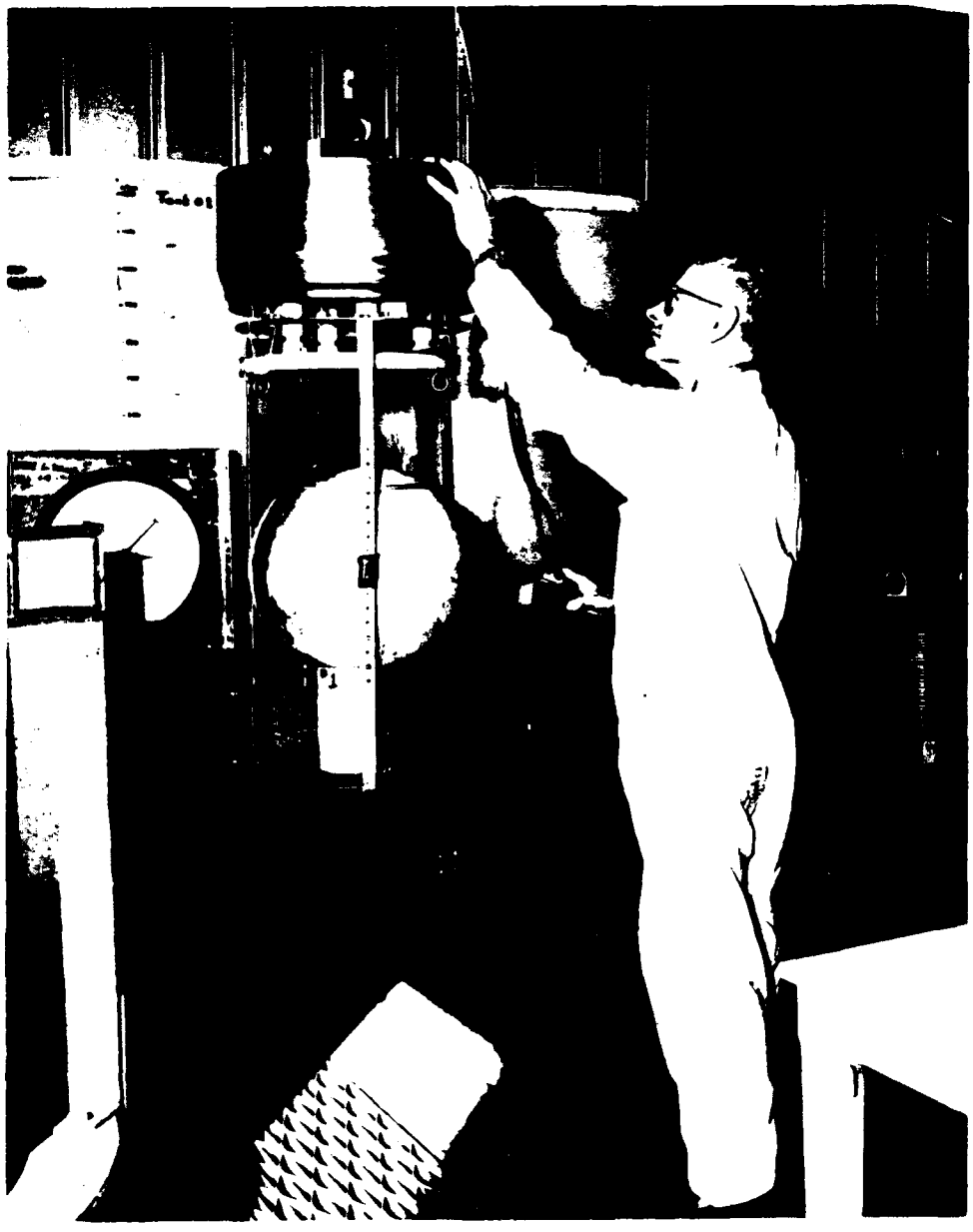

Figure 12. Retaining cage used to restrain type I spheres during implosion testing inside pressure vessel.

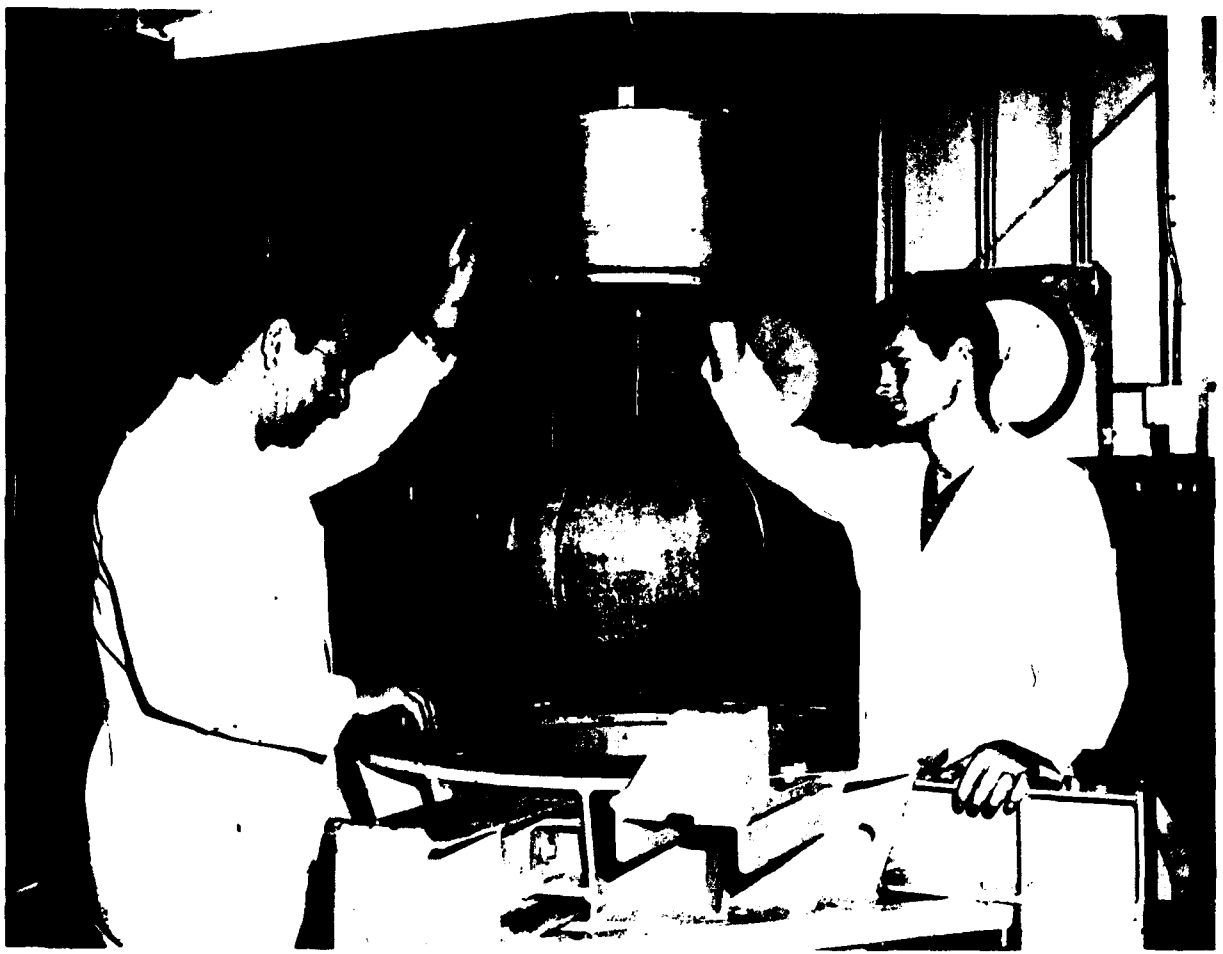

Figure 13. Typical type II sphere attached to pressure vessel end closure by means of pipe feedthrough fitting.

DISCUSSION OF TESTS

Mechanical Properties of Concrete

The physical properties of concrete used in spheres, determined by crushing the test cylinders under standard ASTM conditions while the strains on their exterior were monitored (Figure 14), showed that the concrete had an average dry compressive strength of 11,090 psi (Table A-1 of Appendix A), an average modulus of elasticity* of 3.83×10^6 psi, and an average Poisson's ratio of 0.2. The tangent** and secant*** moduli of elasticity were approximately constant in the 0-to-4,500-psi compression stress range and then began to decrease as the stress increased (Figures 14 and 15). Poisson's ratio (Figure 16) as determined by dividing the transverse strain by the axial strain (Figure 17) on the 3 x 6-inch test cylinders under uniaxial compression varied from approximately 0.16 to 0.30, but averaged very close to the commonly accepted value of 0.2 for concrete.

Short-Term Critical Pressure

Dry Concrete. Short-term critical pressure of dry concrete spheres, as defined by testing waterproofed hollow concrete spheres to implosion under a steady hydrostatic pressurization rate of 100 psi/min, was performed on type I (Figure 1) and type II (Figure 2) spherical test specimens. The test results are shown in Table 3. The relationship of the average critical pressure to shell thickness when plotted appears to be almost linear for all spheres tested (Figure 18). When the calculated average stress was calculated

---

* Modulus of Elasticity, **E**: the physical property of concrete represented by the slope of the initial straight portion of the stress-strain curve developed from the the test cylinders. It is constant for a given test specimen.

** Tangent Modulus of Elasticity, E_t: the physical property of concrete represented by the slope of the tangent line at a particular stress level on the stress-strain curve developed from uniaxial compression testing of test cylinders at 2,000-psi/min stressing rate. It is a function of stress for a given test specimen.

*** Secant Modulus of Elasticity, E_s: the physical property of concrete represented by the slope of the line from the origin to a particular stress level on the stress-strain curve developed from uniaxial compression testing of test cylinders at 2,000-psi/min stressing rate. It is a function of stress for a given test specimen.

Table 3. Critical Pressure of Dry[1] Spheres

Sphere No.	Type[2]	Thickness/Outside Diameter Ratio (t/D_o)	Age (days)	Critical Pressure[3] (psi)	Concrete Strength[4] (psi)
19	I	0.0625	73	3,450	11,270
20	I	0.0625	74	3,420	11,530
21	II	0.0625	72	3,240	11,240
Average				3,370	11,340
23	I	0.125	73	5,720	11,190
24	I	0.125	74	6,330	11,040
25	II	0.125	72	6,590	10,920
Average				6,210	11,050
27	I	0.1875	72	9,250	10,370
28	I	0.1875	73	9,170	10,830
29	II	0.1875	76	9,500	11,530
Average				9,310	10,910
31	I	0.250	72	13,900	10,990
32	I	0.250	74	13,570	11,180
33	II	0.250	90	13,550	10,920
Average				13,680	11,030

[1] Inside and outside sphere surfaces waterproofed with epoxy 0.032-inch thick.

[2] Type I spheres had waterproof coatings, but no penetrations. Type II spheres had waterproof coatings and penetrations.

[3] Short-term implosion testing, pressurized at 100-psi/min rate to implosion.

[4] Test cylinders (3 x 6 inches) were tested at 2,000-psi/min rate in uniaxial compression; dry concrete.

by dividing the force exerted on a plane passing through the center of the sphere by the cross-sectional area of the sphere wall, it was found to be:

t/D_o Ratio	Average Stress (psi)
0.0625	14,400
0.125	14,230
0.1875	15,300
0.250	18,200

(See Figure 19.) This indicates an exponential rise of average compressive strength of concrete depending on the t/D_o ratio of sphere tested.

Wet Concrete. The short-term critical pressures of wet concrete spheres* were lower than the critical pressures of identical dry concrete spheres. The critical pressures for concrete spheres permeated by seawater are shown in Table 4. The decrease in the critical pressure of seawater-permeated spheres was 30% to 15% in comparison to the critical pressures of comparable waterproofed spheres (same t/D_o ratios) in which the concrete was dry at the time of fracture. When the critical pressures of nonwaterproofed spheres of different t/D_o ratios were plotted with respect to their t/D_o ratios (Figure 20), it appeared that the critical pressure of seawater-permeated spheres varied in approximately a linear manner with the shell's t/D_o ratio.

Table 4. Critical Pressure of Wet[1] Spheres

Sphere No.	Age (days)	Thickness/Outside Diameter Ratio (t/D_o)	Duration of Long-Term Pretest Pressurization at 2,000 psi (days)	Critical Pressure[2] (psi)	Concrete Strength[3] (psi)
22	105	0.0625	12	2,810	10,620
26	124	0.125	14	4,970	10,980
30	126	0.1875	18	8,080	11,230
34	155	0.250	34	9,700	9,100

[1] Permeated with seawater at pressure of 2,000 psi.

[2] Long-term pretest at 2,000 psi, then pressurized to failure at a rate of 100 psi/min.

[3] Dry concrete test cylinders (3 x 6 inches) were tested at 2,000-psi/min rate in uniaxial compression.

* These values were determined by the pressurization at a 100-psi/min rate to implosion of type III (Figure 3) spherical shells which had been previously completely permeated by seawater under 2,000 psi of external pressure.

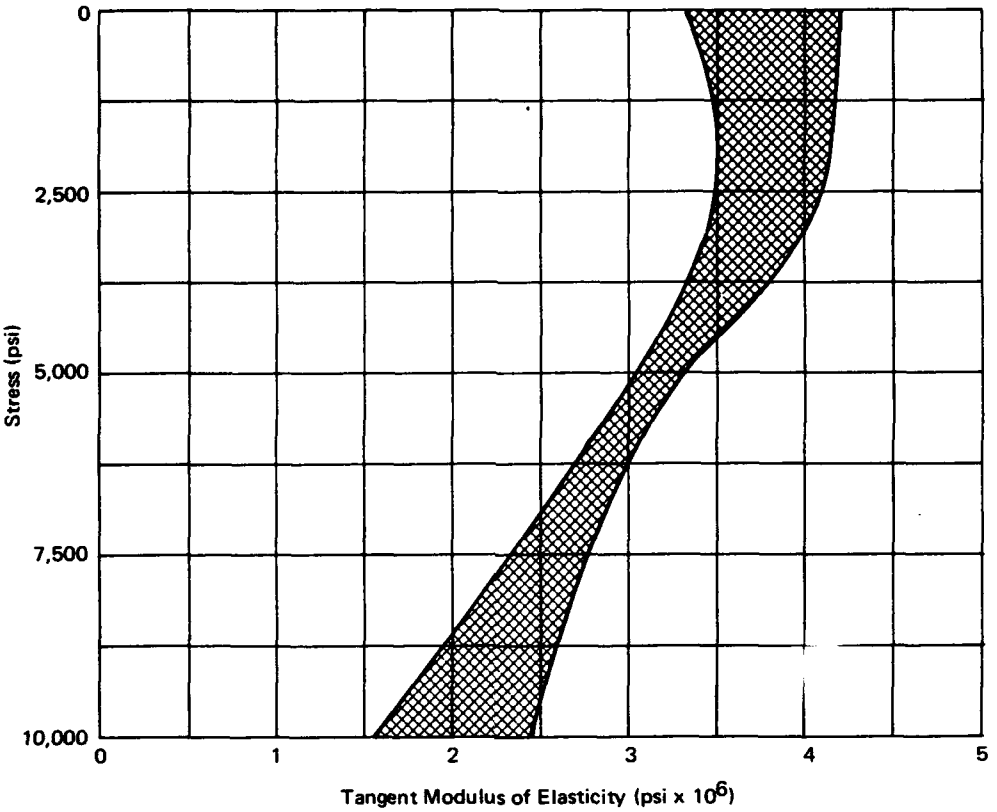

Figure 14. Typical range of values for tangent modulus of elasticity of 3x6-inch test cylinders uniaxially compressed at 2,000-psi/min rate.

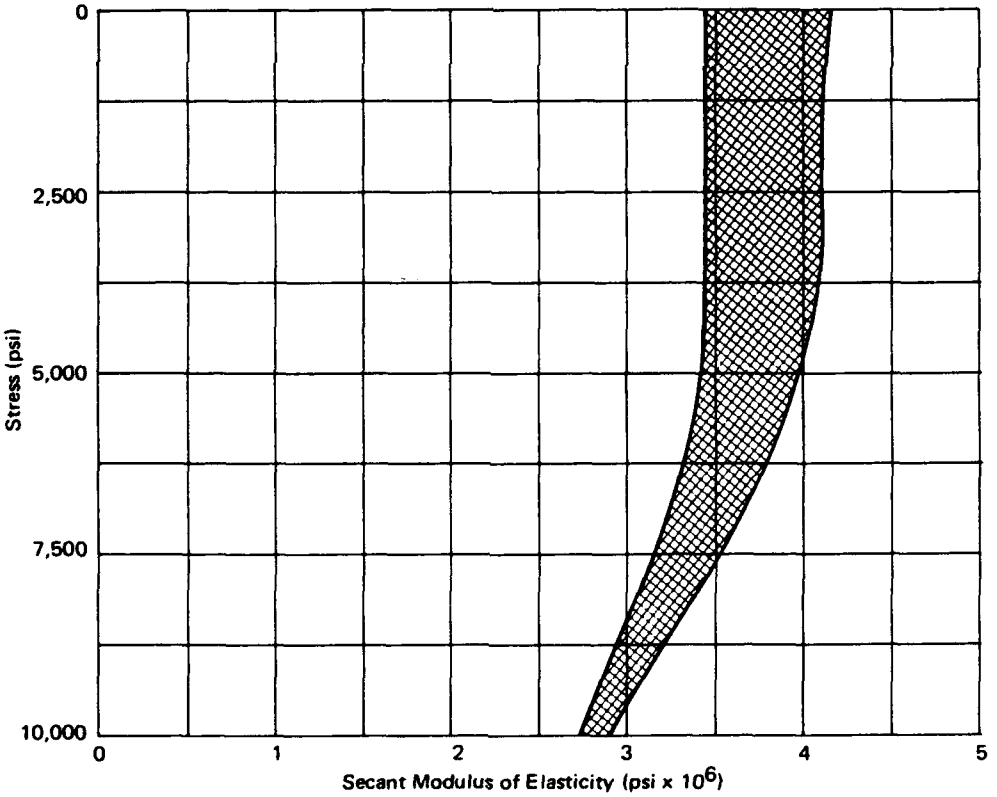

Figure 15. Typical range of values for secant modulus of elasticity of 3x6-inch test cylinders uniaxially compressed at 2,000-psi/min rate.

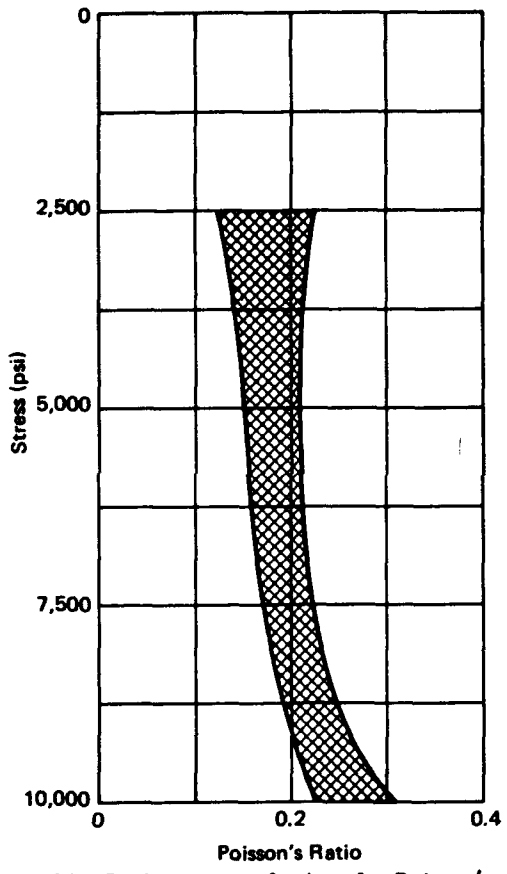

Figure 16. Typical range of values for Poisson's ratio of 3x6-inch test cylinders uniaxially compressed at 2,000-psi/min rate.

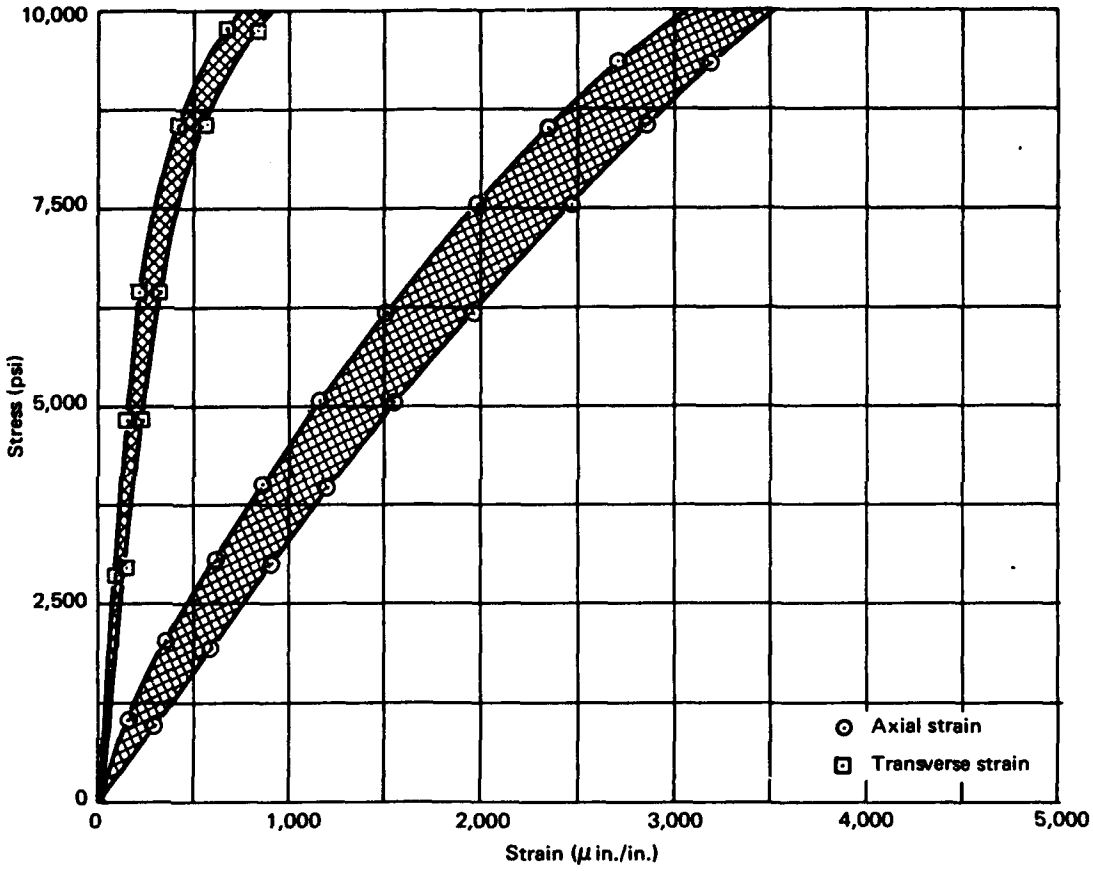

Figure 17. Typical range of values for strains of 3x6-inch test cylinders uniaxially compressed at 2,000-psi/min rate.

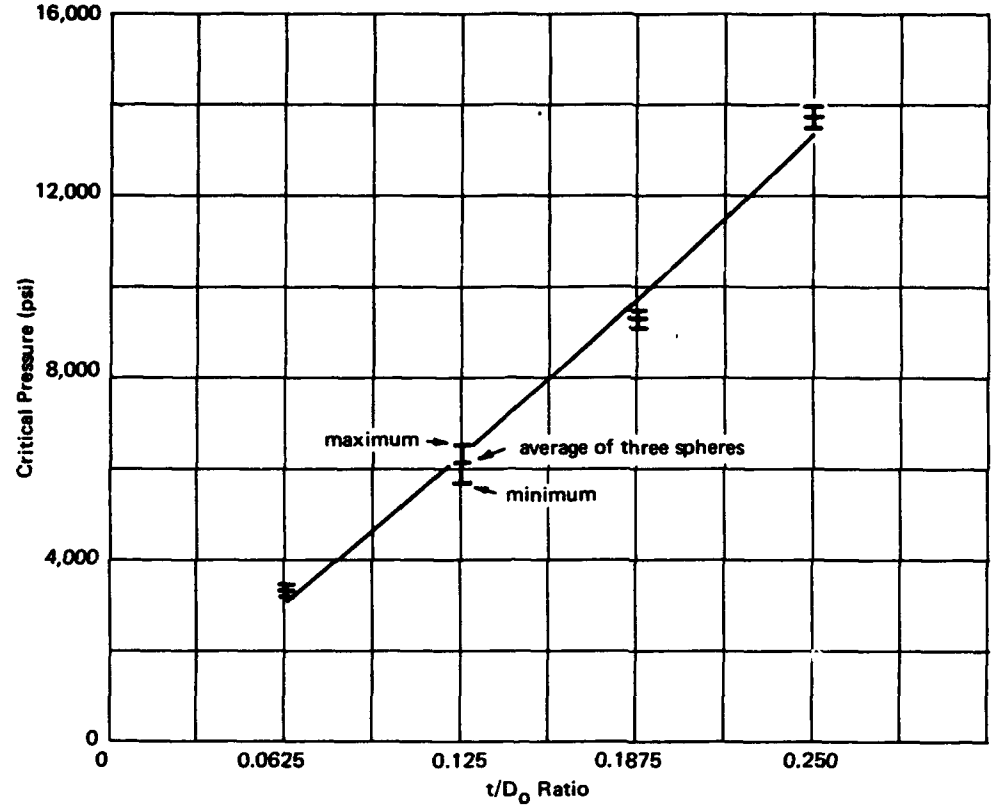

Figure 18. Critical pressure of dry concrete spheres pressurized at 100-psi/min rate.

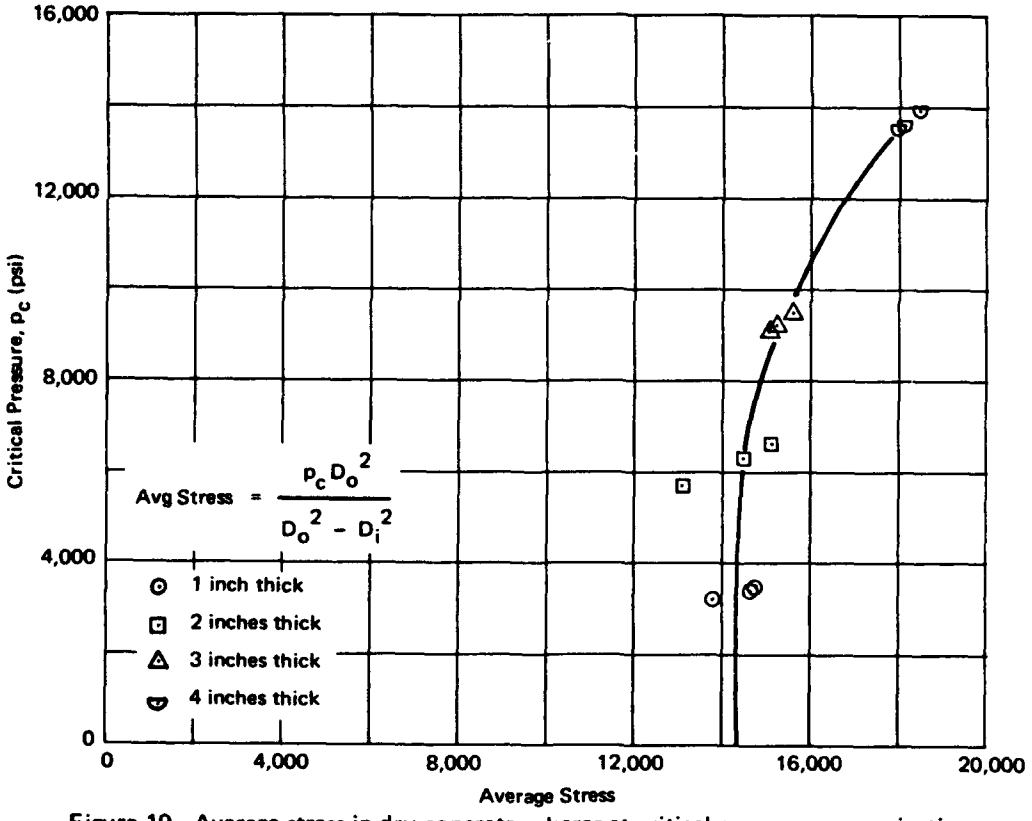

Figure 19. Average stress in dry concrete spheres at critical pressure; pressurization rate 100 psi/min.

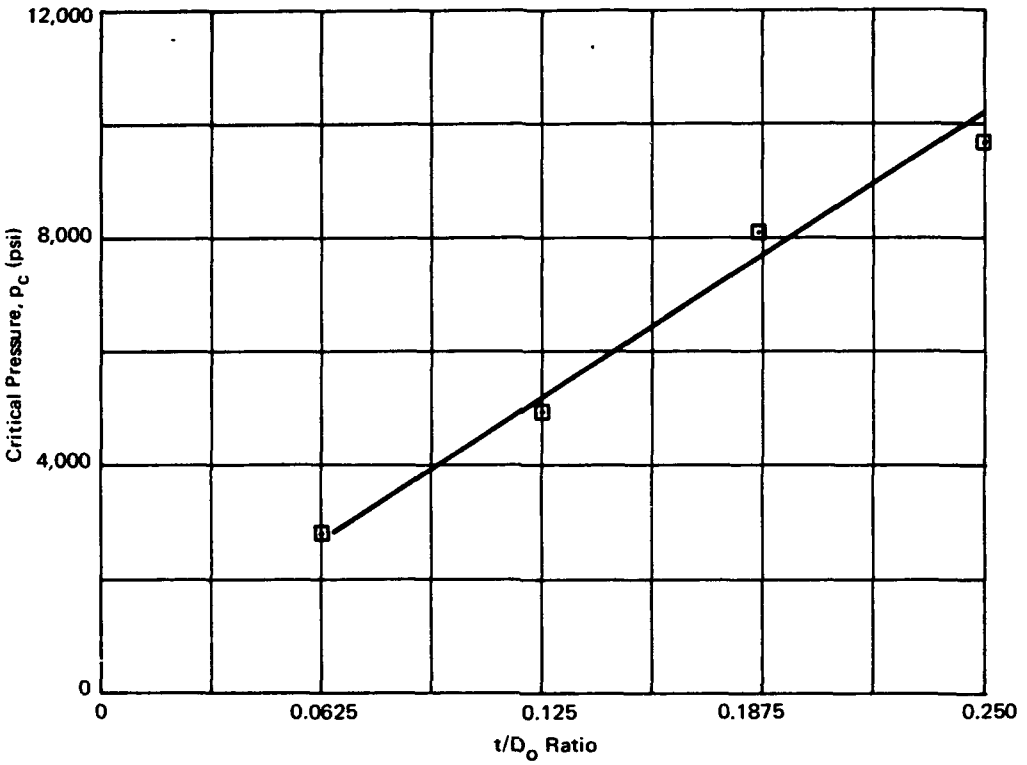

Figure 20. Critical pressure of seawater-permeated concrete spheres pressurized at rate of 100 psi/min. Previous to implosion testing, the spheres were subjected to 2,000-psi hydrostatic pressure for 400 hours.

Fragmentation of Imploded Spheres

The fragments of the spheres which failed were examined, and two visual findings were made. First, a peculiarity was observed in the behavior of the epoxy surface coatings upon failure. The interior and exterior epoxy surface coats of spheres with a 0.0625 t/D_o ratio were still adhering to the concrete fragments after failure. Examination of fragments from the spheres with 0.125, 0.1875, and 0.250 t/D_o ratios, however, revealed that the epoxy coat and some of the concrete on the interior surface had completely spalled off, whereas the epoxy coat on the exterior surface remained intact. Second, a peculiarity was observed in the size and number of fragments from imploded spheres. The number of fragments in the spheres, with the exception of the 0.250 t/D_o spheres, increased as the thickness of the sphere tested increased. The 0.0625 t/D_o (Figure 21), 0.125 t/D_o (Figure 22), and 0.1875 t/D_o (Figure 23) ratio spheres broke up completely upon implosion, forming many fragments. The 0.250 t/D_o (Figure 24) ratio spheres remained in a roughly

spherical shape after failure even though large cracks were randomly distributed over the entire surface. It appears that the 8-inch-diameter cavity inside the 0.250 t/D_o ratio spheres was so small in relation to the thickness of the wall fragments that only one or two fragments of the wall could separate themselves completely from the wall before the cavity was filled. Once the cavity was filled, no more fragmentation of the sphere could take place. Also, a detailed examination of the fracture area on the 0.250 t/D_o ratio sphere revealed a well-defined spherical failure plane 2 inches in from the exterior surface (Figure 25), suggesting a lamination type failure. The spherical failure plane was parallel to the exterior surface and appeared to run continuously around the sphere giving the fractured sphere the appearance of being made up of 2-inch-thick laminations. The 0.250 t/D_o ratio sphere was later broken apart and the originally hollow space in the sphere was found to be filled with fine concrete fragments.

Figure 21. Fragments of imploded 0.0625 t/D_o ratio concrete sphere.

Figure 22. Fragments of imploded 0.125 t/D_o ratio concrete sphere.

Figure 23. Fragments of imploded 0.1875 t/D_o ratio concrete sphere.

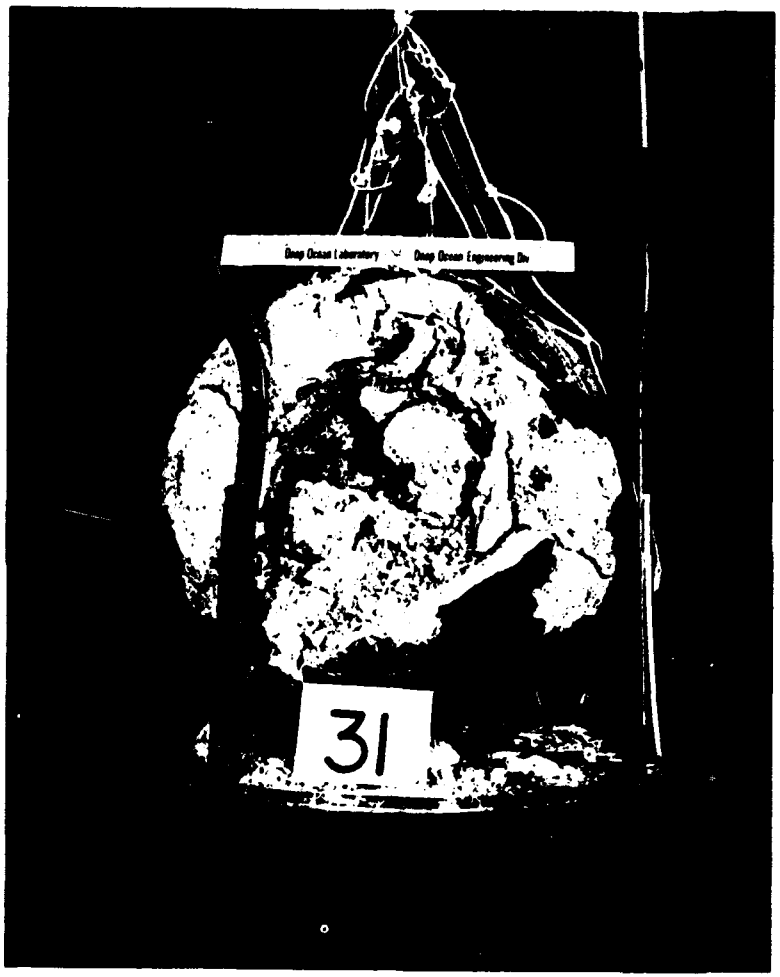

Figure 24. Imploded 0.250 t/D_o ratio concrete sphere.

Figure 25. Detail of imploded 0.250 t/D_o ratio sphere. Note the failure plane 2 inches below the sphere's surface.

Permeability

The nonwaterproofed spheres when pressurized with seawater at 2,000-psi hydrostatic pressure permitted the seawater to seep through to their interior after a period of time. The rate of water seepage varied from sphere to sphere depending on the shell's thickness. The average measured rates of seepage for 5 days of flow after the first water was detected in the sphere are shown in Table 5.

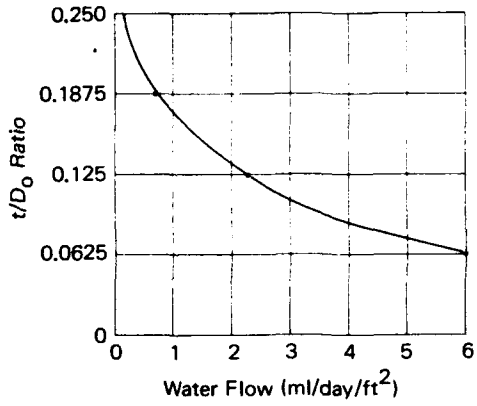

Figure 26. Rate of seawater seepage into sphere's interior 200 hours after first signs of water inside the sphere.

When the rates of seepage for different spheres were compared to each other (Figure 26), it appeared that an exponential relationship existed between the spherical shell thickness and the resistance to seepage through the shell of a 16-inch-OD sphere.

Absorption is a physical process by which concrete draws water into its pores and capillaries. As expected, the rate of absorption at the beginning of each permeability test was high and caused a noticeably high rate of operation by the hydraulic pump which maintained a hydrostatic pressure of 2,000 psi. When the concrete reached saturation, however, the rate of absorption decreased considerably and eventually a stabilized point was reached at which the amount of fluid being pumped to maintain the hydrostatic pressure approximated the amount of fluid extracted from the interior of the sphere.

Table 5. Permeability of Concrete Spheres Under 2,000-psi External Hydrostatic Pressure

Sphere No.	Thickness/Outside Diameter Ratio (t/D_o)	Thickness, t (in.)	Flow Rate[1] (ml/hr)	Permeability[2] (ml/day/ft^2)
22	0.0625	1	1.4	6.0
26	0.125	2	0.535	2.3
30	0.1875	3	0.156	0.67
34	0.250	4	0.038	0.197

[1] Rate of flow measured 5 days after the water has permeated to the interior of the sphere; this takes place from 4 to 24 days after pressurization, depending on shell thickness.

[2] The exterior surface area of the sphere was used to determine the permeability coefficient.

Permeability is probably a more complex property of concrete than strength. The measure of permeability has been defined as the unit rate at which a fluid is discharged from a material under unit hydraulic gradient. Previous research[3,4,5] has shown that the leakage can be determined from D'Arcy's law for viscous flow:

$$\frac{Q}{A} = K_c \frac{H}{L}$$

where Q = rate of flow, ft^3/sec

A = area of cross section under pressure, ft^2

H/L = ratio of head of fluid to percolation length

K_c = permeability coefficient for concrete

The several factors known to influence the permeability of concrete fall into two basic categories: (1) the influence of the constituent materials, and (2) the influence of the testing environment. The spheres tested for permeability in this study were unique in these two areas. The material used in the spheres was essentially a concrete mortar mix (i.e., the aggregate was mostly smaller than the No. 4 sieve size), and the testing environment was seawater used to apply a constant hydrostatic pressure of 2,000 psi to the sphere.

A literature search was conducted with the objective of finding comparable test data and results which would support or reject this report's findings. The latest and most extensive investigation on permeability of concrete was completed by the American Concrete Institute in 1935 with particular reference to Hoover Dam.[3] An experimental program was set up to measure the effects on permeability of pressure variation, specimen length, end conditions, size of aggregate, curing, and the direction of flow. The report does state that even though a hundred or so experiments were made, most of the conclusions are tentative and strictly apply only to the data presented. The primary points of interest deal with the two categories mentioned earlier. Even though testing was conducted on mortar mixes similar to those in the NCEL study, the testing environment was distinctly different from that of the spheres in this study. The specimens were tested by using ordinary tap water to apply hydrostatic pressures from 150 to 500 psi. The permeability coefficient established by ACI for mortar was approximately 100 times as large as the coefficient determined for the spheres using D'Arcy's Equation. The ACI data cannot be compared to those for the concrete spheres in this study because of the dissimilar testing environment. Review of research indicates there are no results available to date from a testing program similar to that of the concrete spheres in this study.

Although there are many variables which affect the permeability of concrete, little research on this property has been done, even with respect to the permeation of water through concrete on land. A few characteristics have been cited,[6] however, which relate to this property's behavior. It appears from previous findings that as the water-cement ratio increases, so does the permeability. Permeability is also reduced as the size of the maximum aggregate used is decreased. The effect of age also varies inversely with permeability. Tests on hand-packed and vibrated concrete show that permeability is reduced greatly if the concrete is vibrated. Care should be taken, however, to prevent excessive water and laitance from accumulating on the surface. Air-entrainment and cement-dispersing agents have been found by others to have a useful effect in lowering permeability.

Strains

The strains on the exterior of each waterproofed sphere, regardless of its t/D_o ratio, were observed to vary nonlinearly with external hydrostatic pressure applied at 100-psi/min rate (Figure 27 and Appendix A). The external strains at failure for the spheres measured by electric resistance strain gages were approximately of the following magnitude:

t/D_o Ratio	Strains (μin./in.)
0.0625	3,000-3,500
0.125	5,000-6,000
0.1875	6,000-7,000
0.250	7,000-8,000

When the strains on the exterior of spheres with different t/D_o ratios were compared to each other at any given hydrostatic loading (Figure 28), it could be clearly seen that the relationship between the magnitude of strain and the t/D_o ratio was also nonlinear.

The strains on the interior of each waterproofed sphere did not vary linearly with external hydrostatic pressure (Figures 29 and 30 and Appendix A). The maximum recorded strains recorded prior to implosion for spheres were in the range of

t/D_o Ratio	Strains (μin./in.)
0.0625	3,500-4,000
0.125	4,000-6,000
0.1875	3,500-5,500
0.250	4,000-8,000

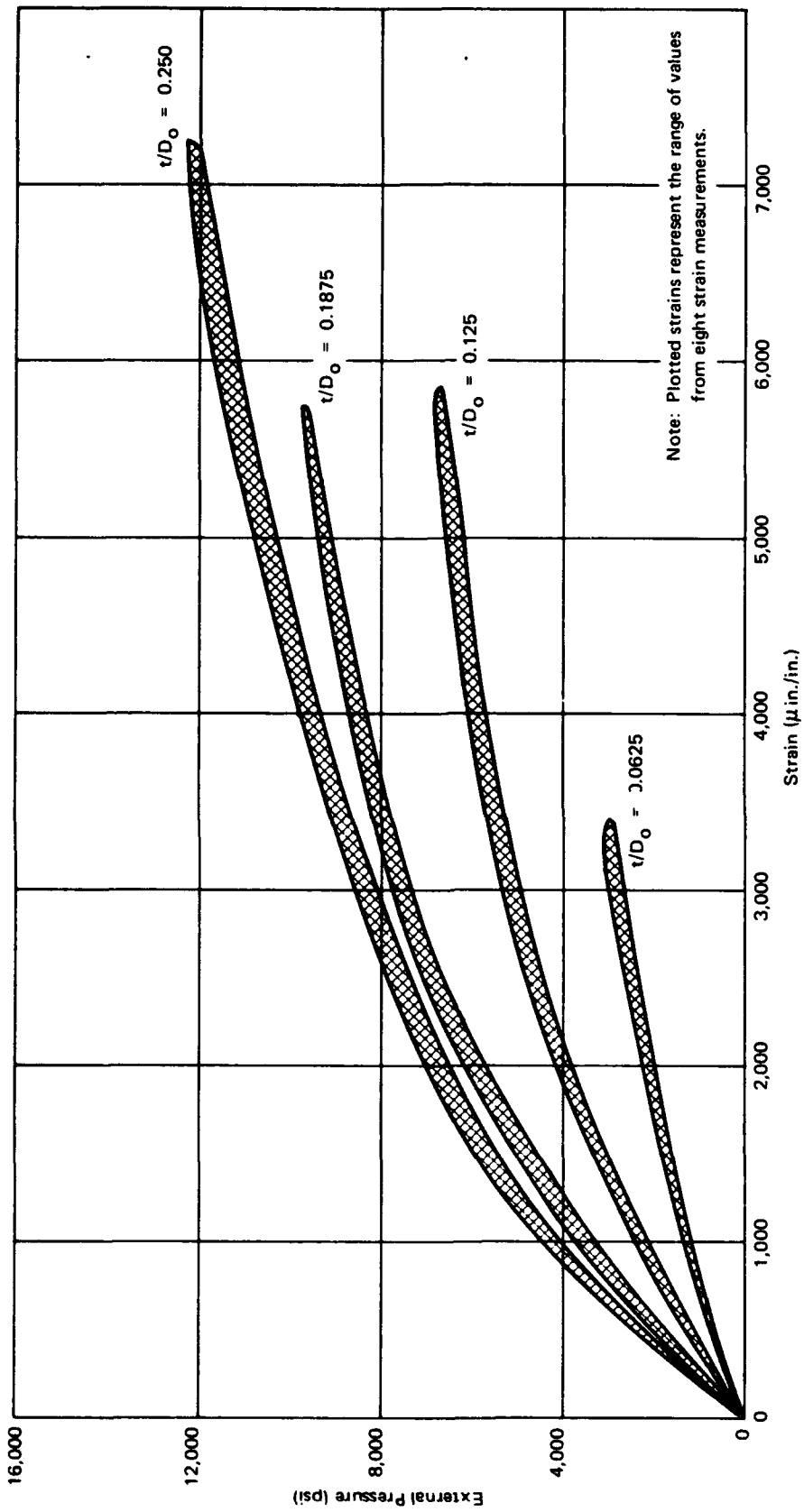

Figure 27. Strains on the exterior of dry concrete spheres as a function of hydrostatic pressurization rate of 100 psi/min.

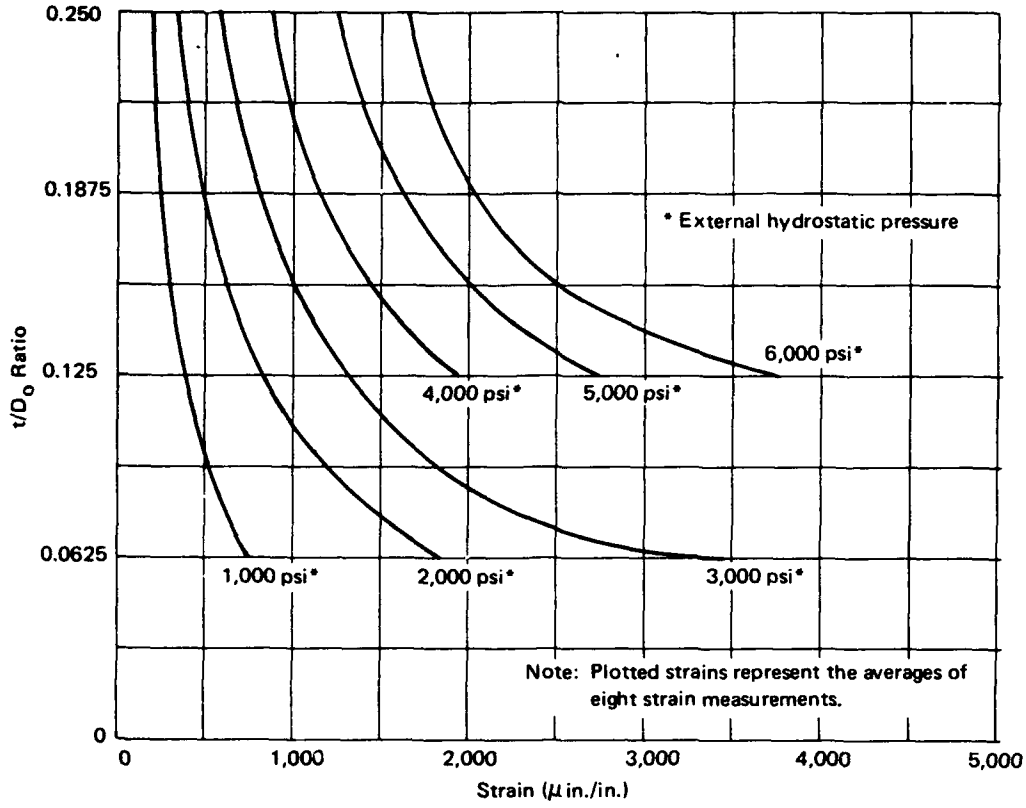

Figure 28. Strains on the exterior of dry concrete spheres as a function of t/D_o ratio at a pressurization rate of 100 psi/min.

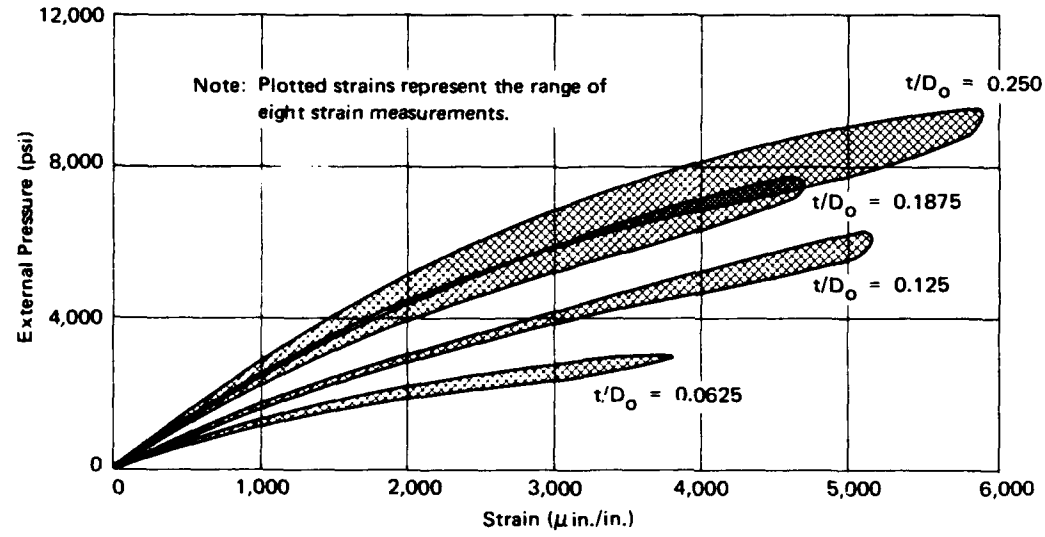

Figure 29. Strains on the interior of dry concrete spheres as a function of hydrostatic pressurization rate of 100 psi/min.

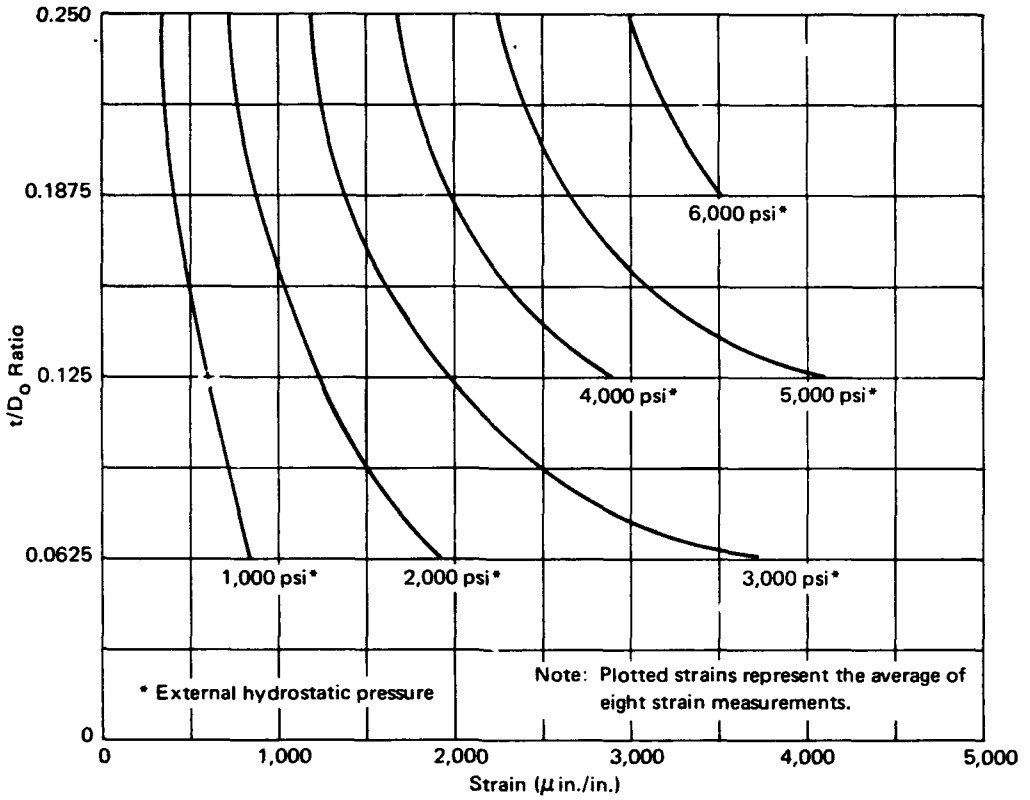

Figure 30. Strains on the interior of dry concrete spheres as a function of t/D_o ratio at a pressurization rate of 100 psi/min.

An interesting phenomenon was observed while some of the spheres were being pressurized to failure. While the external and internal strains on a typical 0.0625 t/D_o ratio sphere (Figure 31) progressively increased with hydrostatic loading, a sudden decrease in the magnitude of internal strains was noted in spheres with 0.125, 0.1875, and 0.250 t/D_o ratios at some hydrostatic pressure less than critical (Figures 32, 33, and 34). It was not likely that the strain gages or adhesive attaching the gages to concrete failed. The gages were capable of measuring strains up to 20,000 μ in./in. and the adhesive had a strain limit of 100,000 μ in./in., both of which were sufficiently higher than the experimental strains being measured to insure against failure. The reversal in interior strains occurred in the 0.125, 0.1875, and 0.250 t/D_o spheres when approximately 87%, 74%, and 71%, respectively, of their critical pressures had been reached—probably indicating delamination of the spheres' wall. As already observed, the fragments of the failed 0.125, 0.1875, and 0.250 t/D_o ratio spheres had no epoxy coating left on their interior surfaces, giving further support to the delamination hypothesis. This hypothesis postulates that a layer of concrete on the inside surface becomes

detached from the main part of the sphere wall still carrying the load. This layer did not separate in a haphazard manner, but spalled off the sphere's wall when the stress level on the sphere's interior surface reached the ultimate strain capability of the particular concrete mix. Thus it would appear that failure of concrete spheres started on the sphere's interior and continued to the exterior as hydrostatic loading was increased, until total failure occurred at critical pressure.

When the strains on the interior of spheres with different t/D_o ratios were compared to each other at any given hydrostatic loading (Figure 30), it could be seen that the relationship between the magnitude of strain and the t/D_o ratio was nonlinear. There was also a considerable difference between the magnitude of the smaller strains measured on the exterior (Figure 27), and the larger strains on the interior (Figure 29) of the water-proofed spheres at any given hydrostatic loading.

Prediction of Strains

Attempts of exploratory nature were made to predict the magnitude of strains on the basis of analytical expressions. The calculations were based on the standard analytical expression for stresses[7] in thick-wall elastic spheres

$$S_1 = S_2 = -p \frac{R_o^3(R_i^3 + 2r^3)}{2r^3(R_o^3 - R_i^3)} \qquad (1a)$$

$$S_3 = -p \frac{R_o^3(r^3 - R_i^3)}{r^3(R_o^3 - R_i^3)} \qquad (1b)$$

where S_1 = meridional wall stress, psi

S_2 = hoop wall stress, psi

S_3 = radial wall stress, psi

p = external hydrostatic pressure, psi

R_o = external radius of sphere, inches

R_i = internal radius of sphere, inches

r = radius from center of sphere to point where stress is to be found, inches

and on the expression for conversion of calculated triaxial stresses[8] to strains that could be experimentally measured on the spheres under short-term loading

$$\epsilon_1 = \frac{1}{E}[S_1 - \mu(S_2 + S_3)] \qquad (2)$$

where ϵ_1 = meridional strain, μ in./in.

μ = Poisson's ratio

E = modulus of elasticity, psi

Since values for Poisson's ratio and the moduli of elasticity in triaxial stress fields are not available for concrete in general, and the mix used in the NCEL tests in particular, these values were only approximated by uniaxial testing of 3 x 6-inch cylinders cast from the same mix as the spheres and cured in the same manner (Figures 14, 15, and 16). These test cylinders were not tested at the same stress rate as the spheres, but at the standard ASTM rate of 2,000 psi/min. However, as shown in Appendix B, the mechanical properties of cylinders which were tested at the same stress rate as the spheres were not significantly different from those determined by the standard ASTM stress rate. Therefore, the difference between the stress rate of the cylinders and spheres is assumed to introduce no changes in mechanical properties. Strains were computed by substituting either E, E_t or E_s into Equation 2. When the calculated strains were compared to the average value of strains measured on the exterior or interior of 16-inch-OD hollow concrete spheres, several relationships between calculated and measured values became apparent (Figures 35-42). The major observations were that up to a strain magnitude of 1,000 μin./in. the agreement between measured and calculated strains is very good regardless of whether E, E_t or E_s (measured on test cylinders uniaxially compressed at 2,000 psi/min) is used. Beyond this strain range the divergence between measured strains and strains calculated utilizing E or E_t in Equation 2 increases rapidly with strain magnitude. Still, the range of strain for which a good correlation between experimental and calculated values may be obtained can be extended to 3,000 μin./in. by using E_s modulus instead of E in Equation 2.

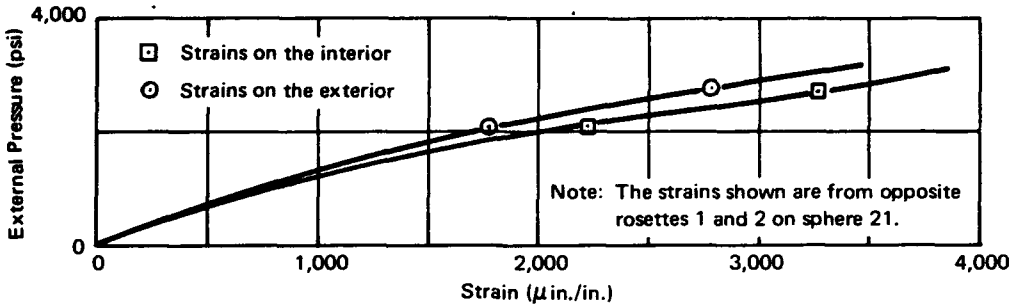

Figure 31. Comparison of typical external and internal strains on 0.0625 t/D_o ratio dry concrete spheres under 100-psi/min pressurization rate.

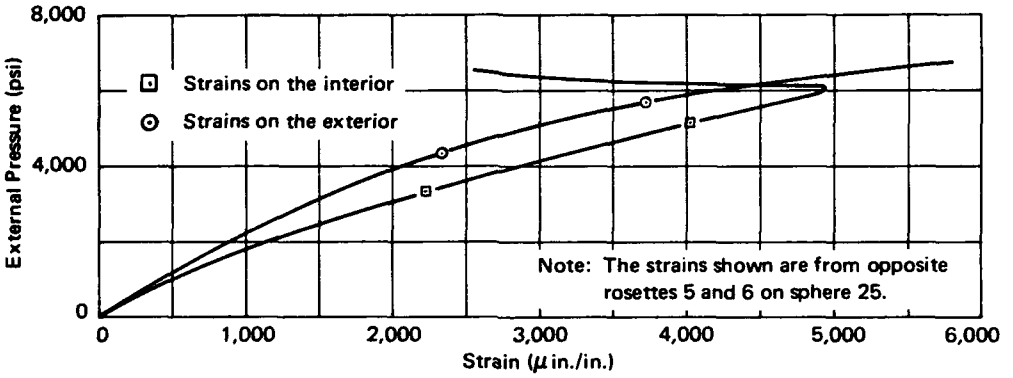

Figure 32. Comparison of typical external and internal strains on 0.125 t/D_o ratio dry concrete spheres under 100-psi/min pressurization rate.

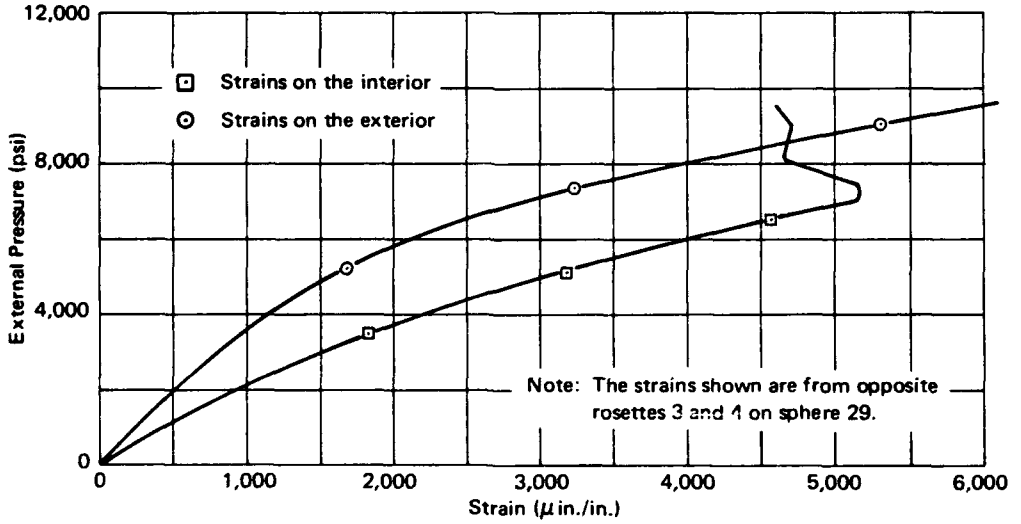

Figure 33. Comparison of typical external and internal strains on 0.1875 t/D_o ratio dry concrete spheres under 100-psi/min pressurization rate.

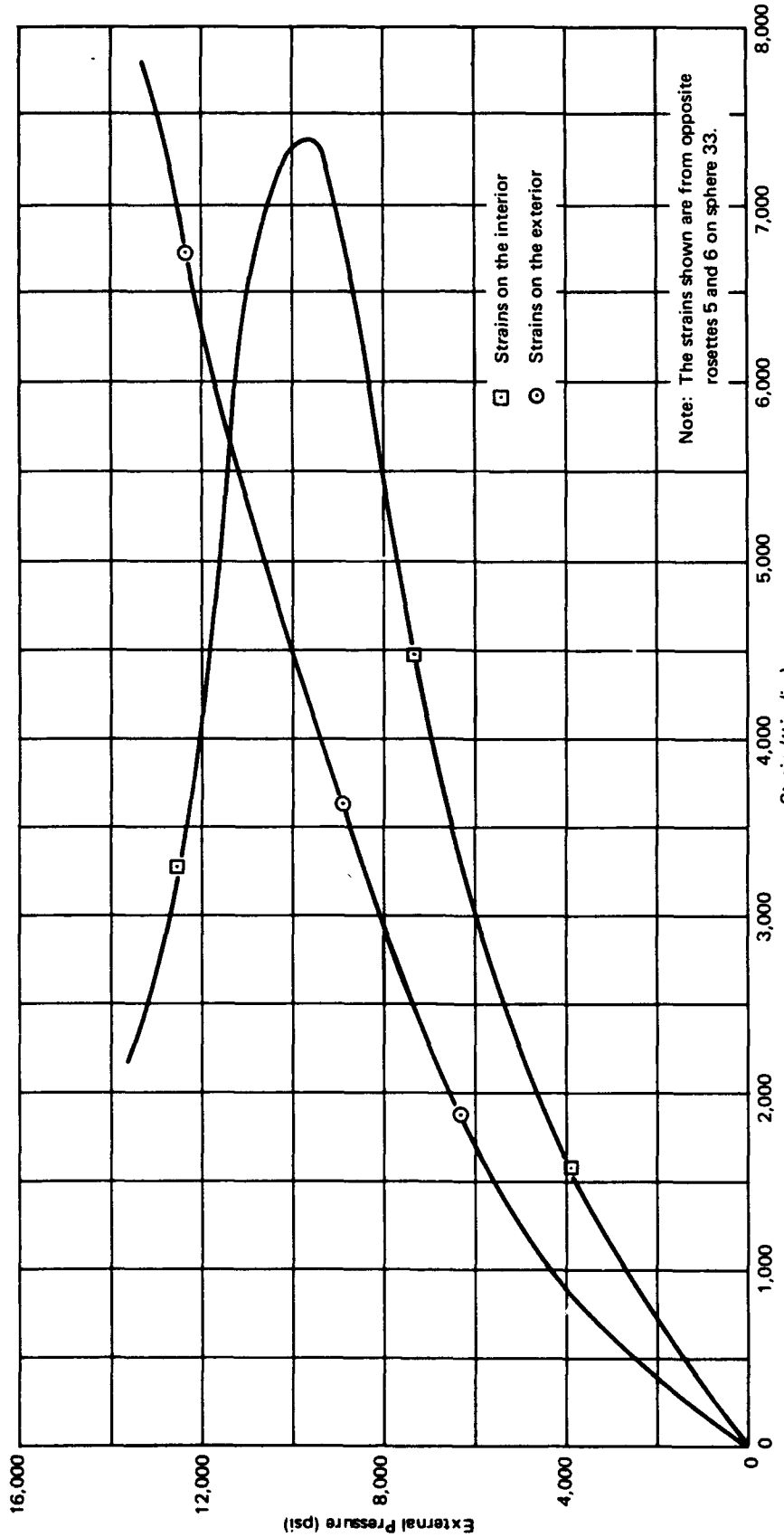

Figure 34. Comparison of typical external and internal strains on 0.250 t/D_o ratio dry concrete spheres under 100-psi/min pressurization rate.

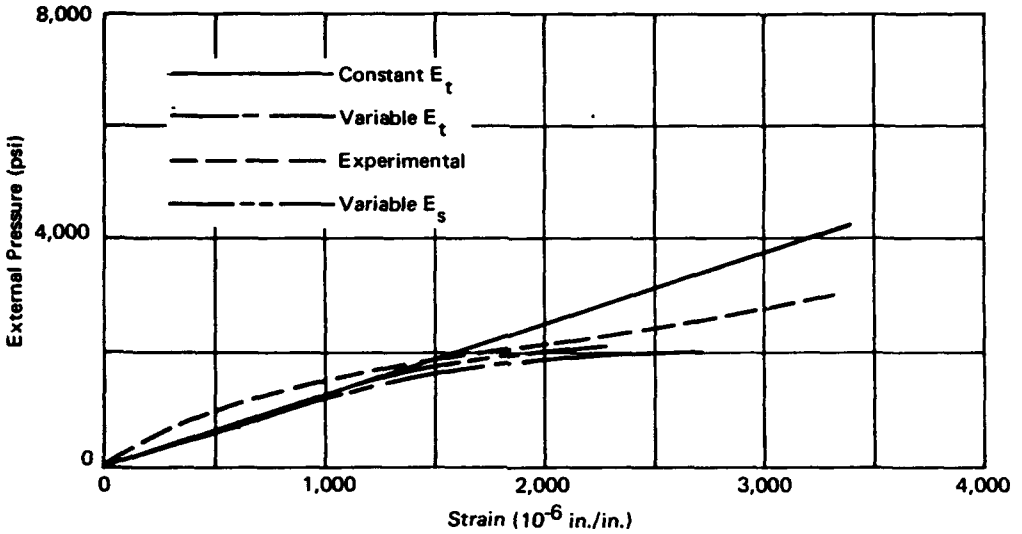

Figure 35. Comparison of calculated and experimental strains for sphere exterior; t/D_o ratio = 0.0625.

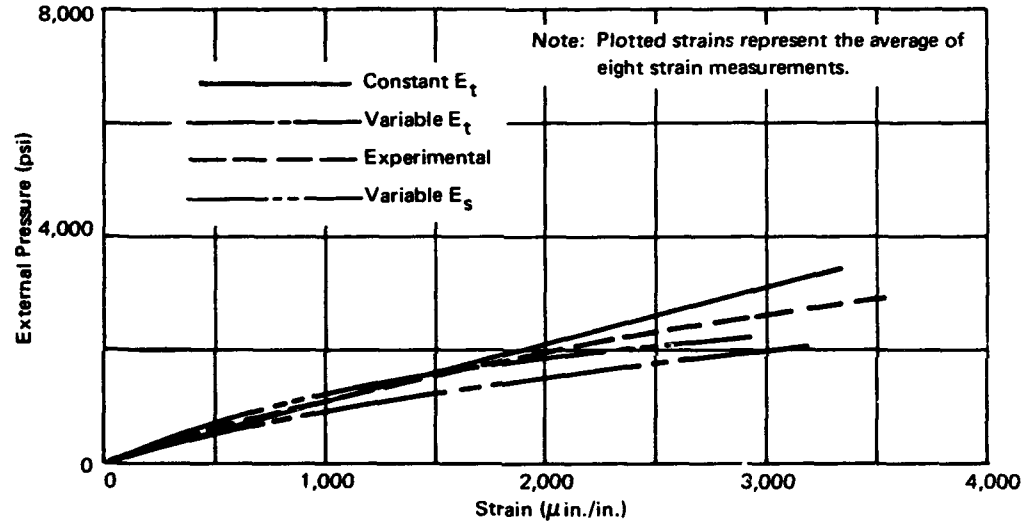

Figure 36. Comparison of calculated and experimental strains for sphere interior; t/D_o ratio = 0.0625.

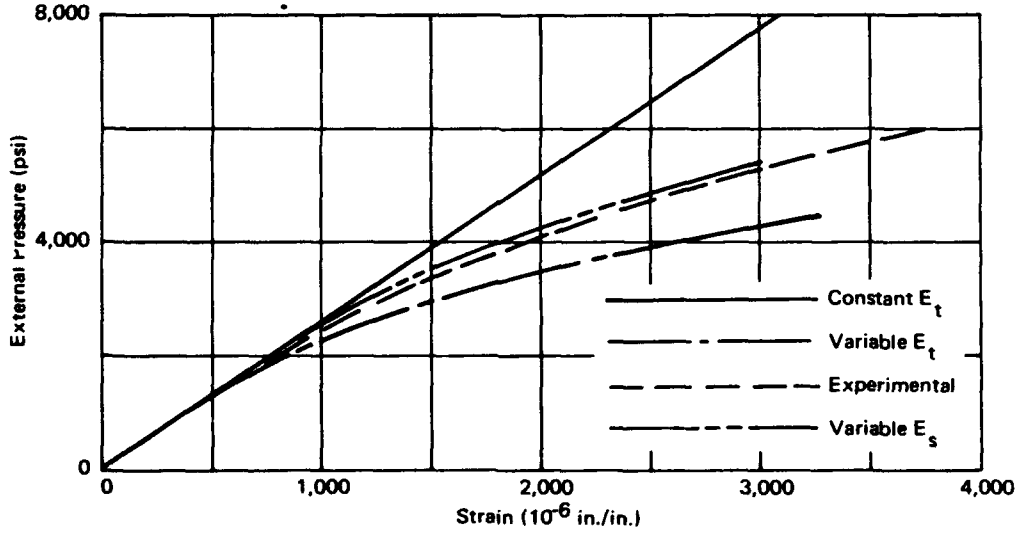

Figure 37. Comparison of calculated and experimental strains for sphere exterior; t/D_o ratio = 0.125.

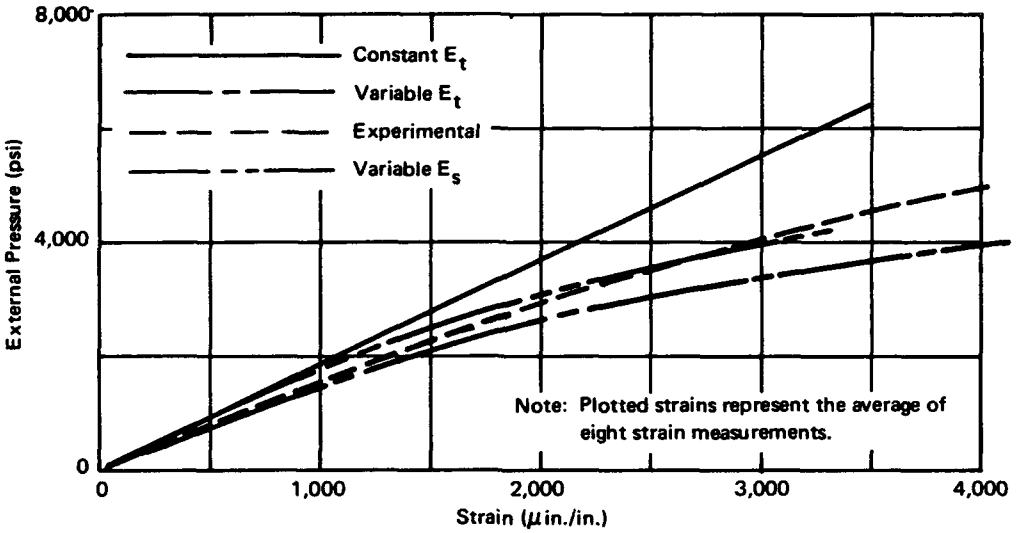

Figure 38. Comparison of calculated and experimental strains for sphere interior; t/D_o ratio = 0.125.

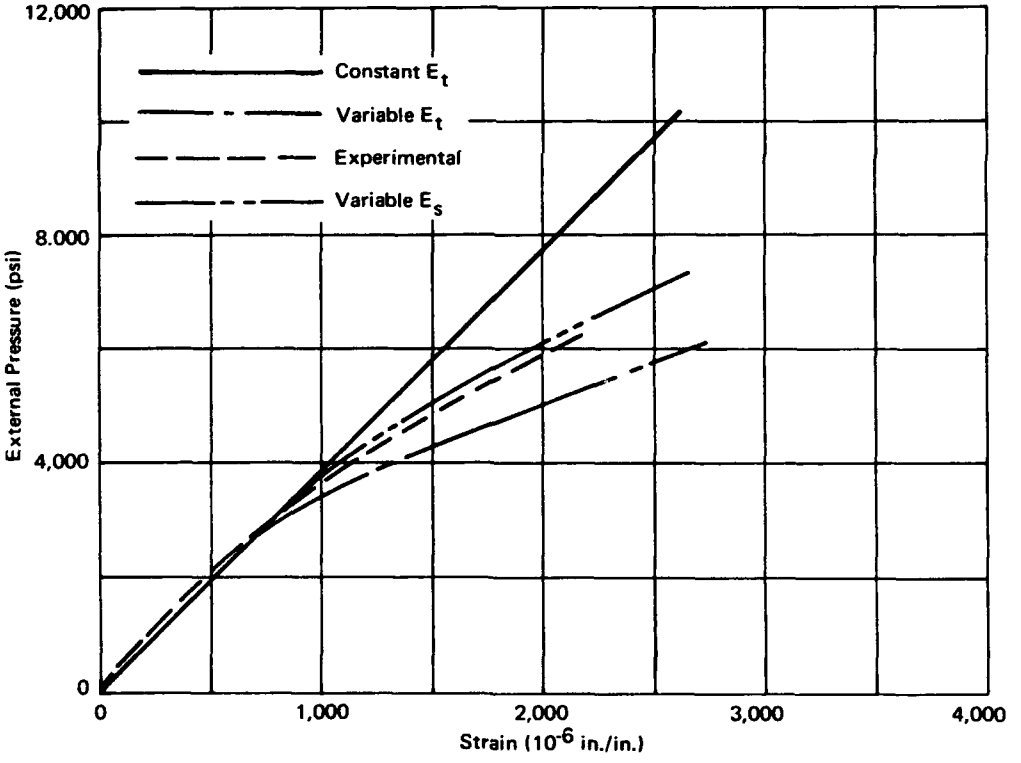

Figure 39. Comparison of calculated and experimental strains for sphere exterior; t/D_o ratio = 0.1875.

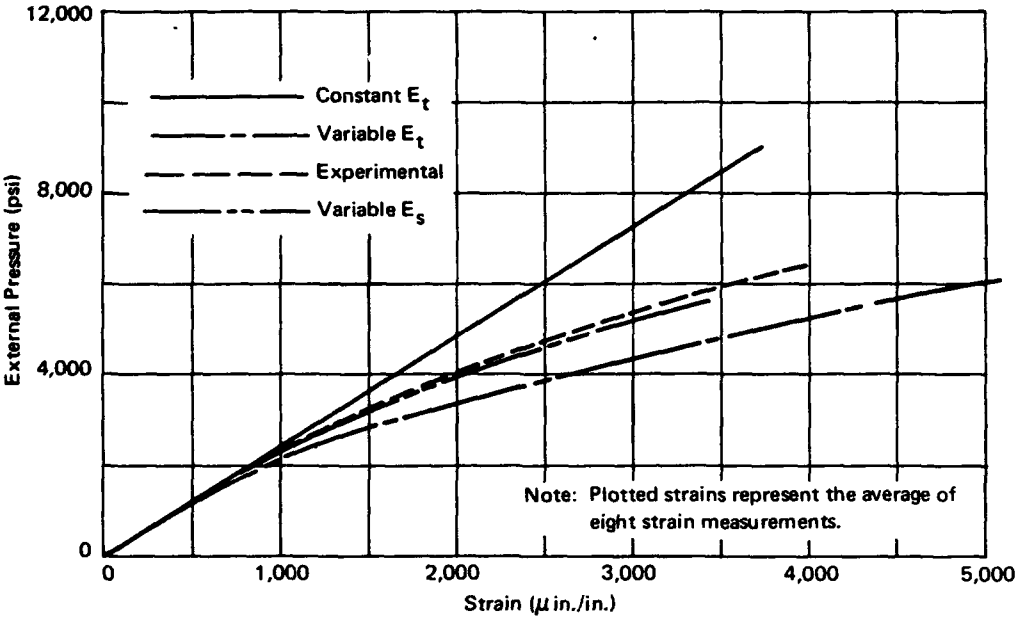

Figure 40. Comparison of calculated and experimental strains for sphere interior; t/D_o ratio = 0.1875.

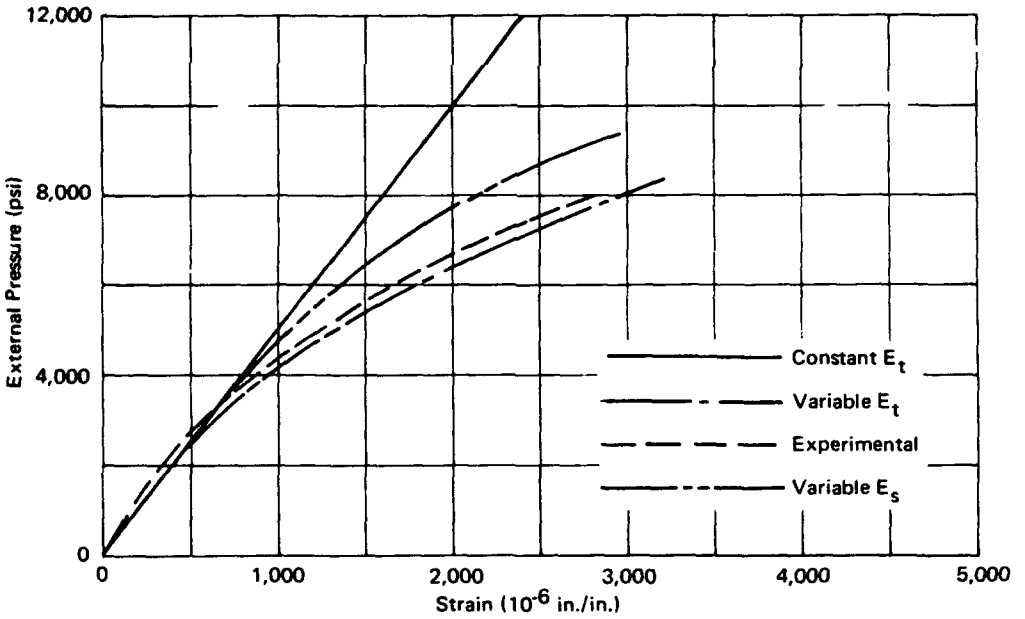

Figure 41. Comparison of calculated and experimental strains for sphere exterior; t/D_o ratio = 0.250.

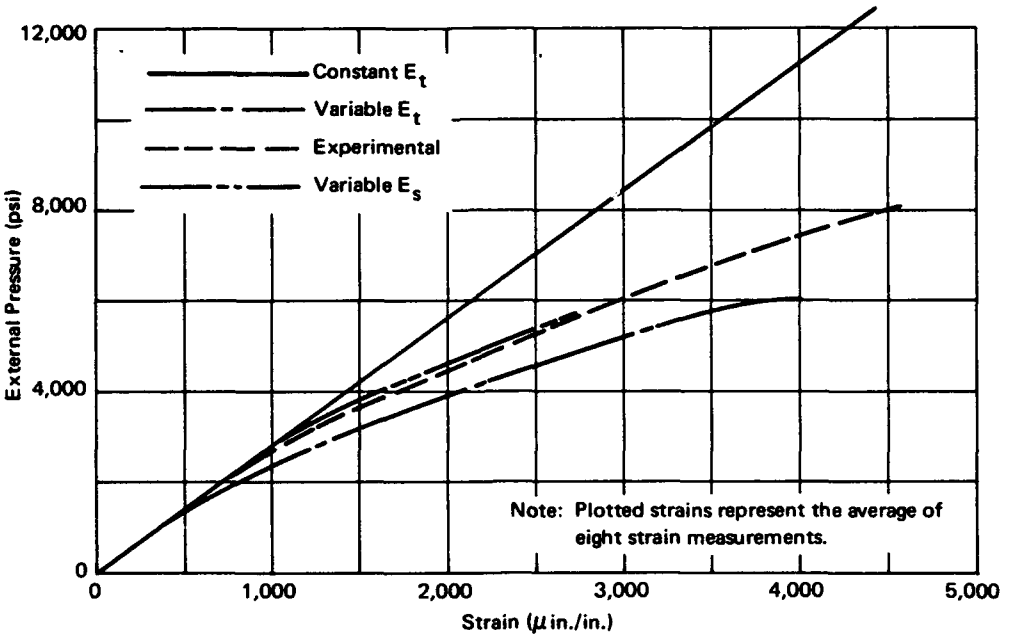

Figure 42. Comparison of calculated and experimental strains for sphere interior; t/D_o ratio = 0.250.

Poor correlation between measured and experimental strains was found for strains larger than 3,000 μ in./in., even when E_s was used in Equation 2. In the range of strains beyond 3,000 μ in./in., the only value in calculating strains lies in the fact that the calculated strains bracket the experimental ones, and thus give the engineer the ability to predict the possible range of actual strain values. For long-term pressure loading conditions a new approach for predicting the strains on the spheres will have to be developed that takes into account the duration of sustained pressure application.

FINDINGS

1. Hollow waterproofed concrete spheres with t/D_o ratios in the $0.0625 \leq t/D_o \leq 0.250$ range and cast from identical mix and cured in a manner identical to that used for 3 x 6-inch test cylinders were found to implode under 100-psi/min hydrostatic loading at compressive stresses 35% to 65% higher than the stresses for test cylinders under uniaxial compression.

2. The critical pressures of waterproofed concrete spheres, cast from identical mix, cured in an identical manner, and tested under a hydrostatic pressurization rate of 100 psi/min, appear to vary almost linearly with the t/D_o ratio of the spheres in the $0.0625 \leqslant t/D_o \leqslant 0.250$ range.

3. Spalling on the interior surface of the spheres appears to take place at hydrostatic pressures lower than the critical pressure inside all of the waterproofed spheres with t/D_o ratios greater than 0.0625. The pressures at which spalling began are 13% to 29% below the critical pressures. The ratio of the pressure at which spalling occurs to the critical pressure appears to decrease as the t/D_o ratio of the spheres increases.

4. No spalling took place on the exterior surface of any of the waterproofed spheres, regardless of their t/D_o ratio.

5. The critical pressures of concrete spheres permeated by seawater under external hydrostatic pressure of 2,000 psi are approximately 15% to 25% lower than those of waterproofed spheres of same t/D_o ratio and concrete mix when both series of spheres are tested under 100-psi/min pressurization rate.

6. The critical pressures of seawater-permeated concrete spheres appear to vary directly and linearly with the t/D_o ratio of spheres.

7. Under constant hydrostatic pressure of 2,000 psi, the resistance to seawater permeation into the interior of nonwaterproofed concrete spheres of different t/D_o ratios, when measured 120 hours after the first drops of water penetrated to the interior of the sphere, appears to vary exponentially with the shell thickness.

8. The analytical expressions (Equations 1 and 2) for calculation of strains on the interior and exterior of perfectly elastic spherical hulls under external hydrostatic pressure have been found to agree closely in the 0-to-3,000-μ in./in. range with experimentally measured strains on concrete spheres hydrostatically pressurized at a constant 100-psi/min rate—providing the secant modulus of elasticity, E_s corresponding to the surface stress on the sphere at that hydrostatic loading was used in Equation 2.

9. The secant modulus of elasticity, E_s, that performed satisfactorily for the calculation of strains on concrete spheres under a 100-psi/min hydrostatic pressure rise was experimentally obtained by recording the stress-strain relationships of uniaxially compressed 3 x 6-inch test cylinders at a 2,000-psi/min loading rate.

CONCLUSION

Implosion of hollow concrete spheres with a 0.250-shell-thickness-to-diameter ratio at a simulated depth of 30,000 feet under short-term submersion seems to indicate that it is feasible to consider concrete hulls cast from 10,000-psi concrete for use as fixed, ocean-bottom habitats at depths as great as 10,000 feet.

Appendix A

DETAILED STRAIN DATA FROM IMPLOSION TESTING OF SPHERES

Table A-1. Strength of Concrete Mix Used in the Spherical Shells*

Sphere No.	Days Cured at 100% RH	Days Cured at 25% RH	Age at Test (days)	Ultimate Uniaxial Compressive Strength (psi)			
				Hemisphere A		Hemisphere B	
				Average	Standard Deviation	Average	Standard Deviation
19	29	47	76	11,480	180	11,220	240
20	29	45	74	11,560	150	11,510	200
21	29	43	72	11,190	280	11,290	130
22	28	77	105	10,670	460	10,560	280
23	29	44	73	11,050	150	11,340	230
24	29	45	74	11,050	150	11,040	200
25	29	43	72	10,990	130	10,760	320
26	30	94	124	11,190	240	10,780	80
27	29	43	72	10,370	260	10,370	280
28	29	44	73	10,370	120	11,290	110
29	30	46	76	11,520	170	11,540	240
30	28	98	126	10,770	170	11,690	350
31	30	42	72	11,070	140	10,910	70
32	29	45	74	10,900	130	11,360	220
33	29	62	91	10,790	565	11,050	145
34	29	126	155	9,300	120	8,900	150

* Strength based on tests of six 3 x 6-inch standard cylinders, except: hemisphere B of sphere 22 and hemisphere B of sphere 32, for which five specimens were tested.

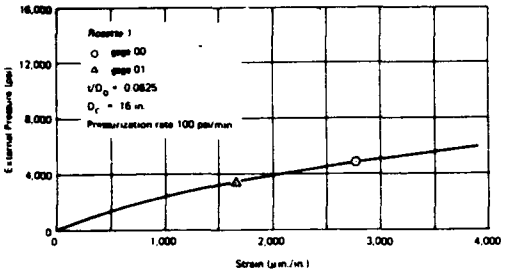

Figure A-1. Strains on the interior of sphere No. 21 under external hydrostatic pressure; rosette 1.

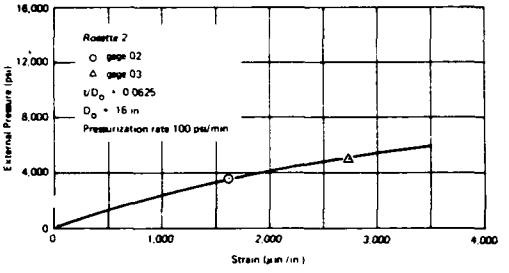

Figure A-2. Strains on the exterior of sphere No. 21 under external pressure; rosette 2.

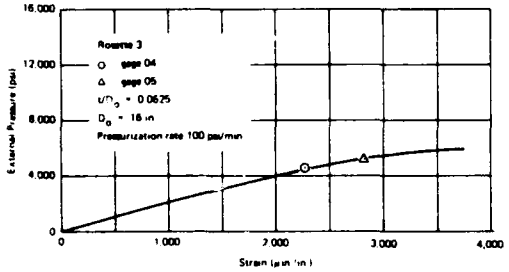

Figure A-3. Strains on the interior of sphere No. 21 under external pressure; rosette 3.

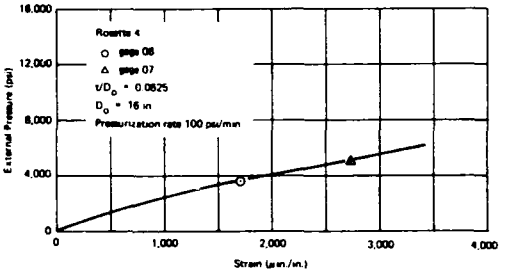

Figure A-4. Strains on the exterior of sphere No. 21 under external pressure; rosette 4.

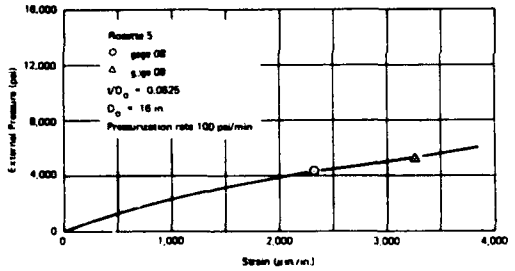

Figure A-5. Strains on the interior of sphere No. 21 under external pressure; rosette 5.

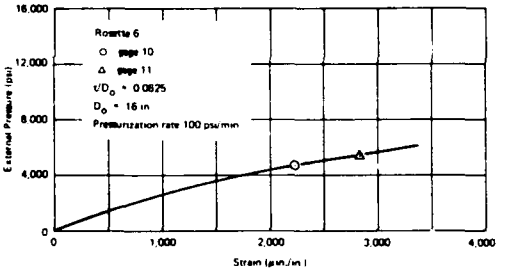

Figure A-6. Strains on the exterior of sphere No. 21 under external pressure; rosette 6.

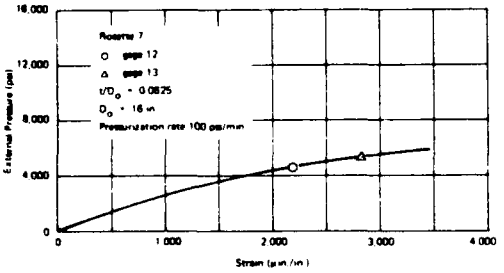

Figure A-7. Strains on the interior of sphere No. 21 under external pressure; rosette 7.

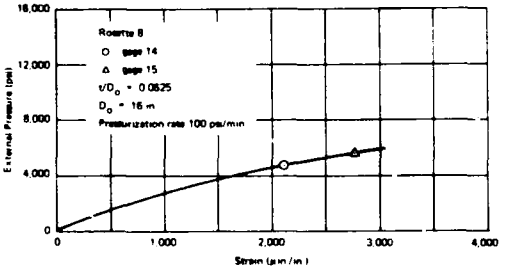

Figure A-8. Strains on the exterior of sphere No. 21 under external pressure; rosette 8.

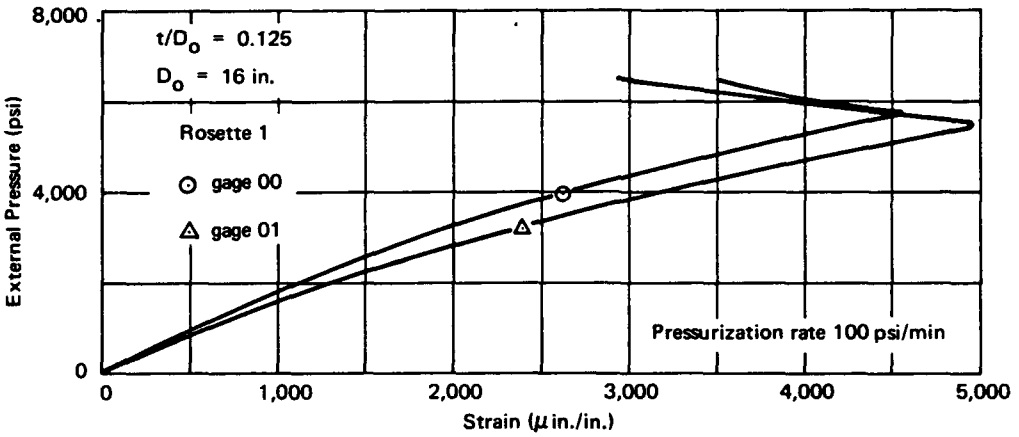

Figure A-9. Strains on the interior of sphere No. 25 under external pressure; rosette 1.

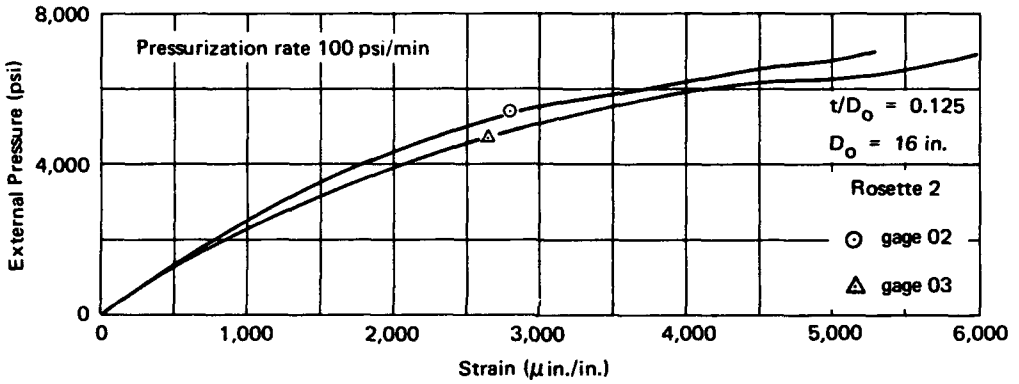

Figure A-10. Strains on the exterior of sphere No. 25 under external pressure; rosette 2.

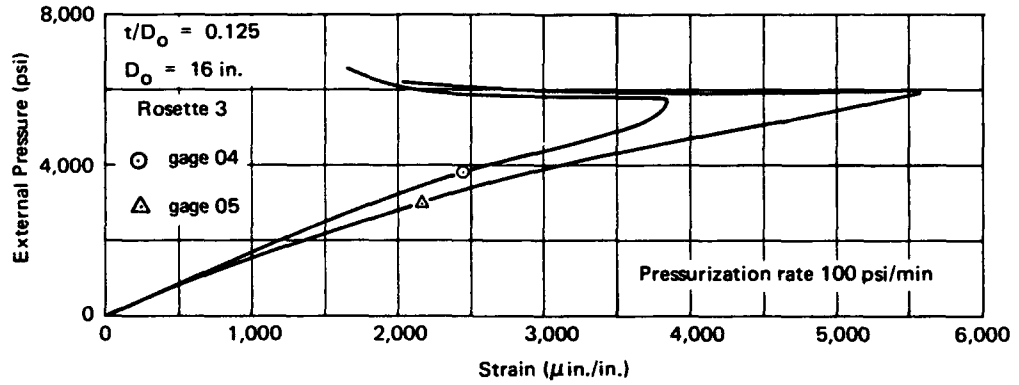

Figure A-11. Strains on the interior of sphere No. 25 under external pressure; rosette 3.

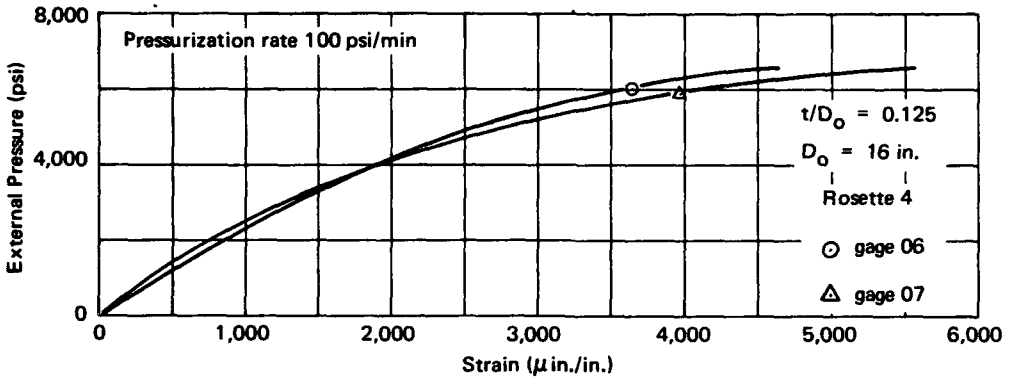

Figure A-12. Strains on the exterior of sphere No. 25 under external pressure; rosette 4.

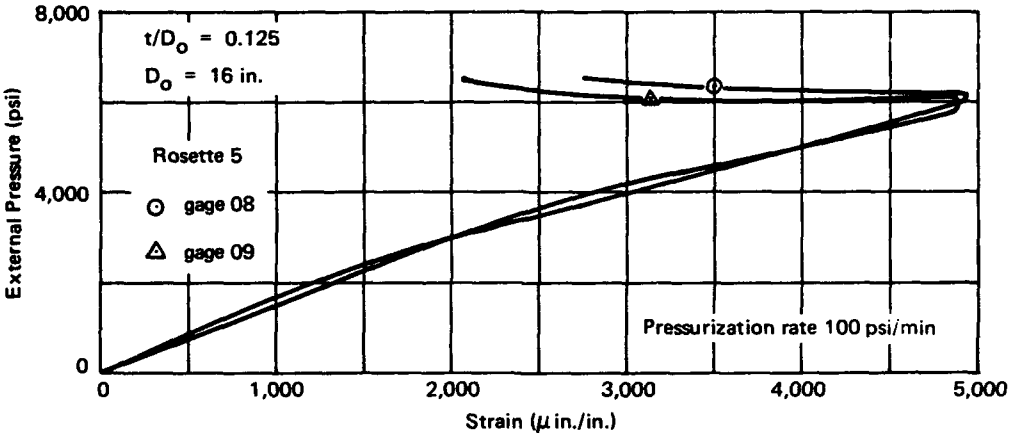

Figure A-13. Strains on the interior of sphere No. 25 under external pressure; rosette 5.

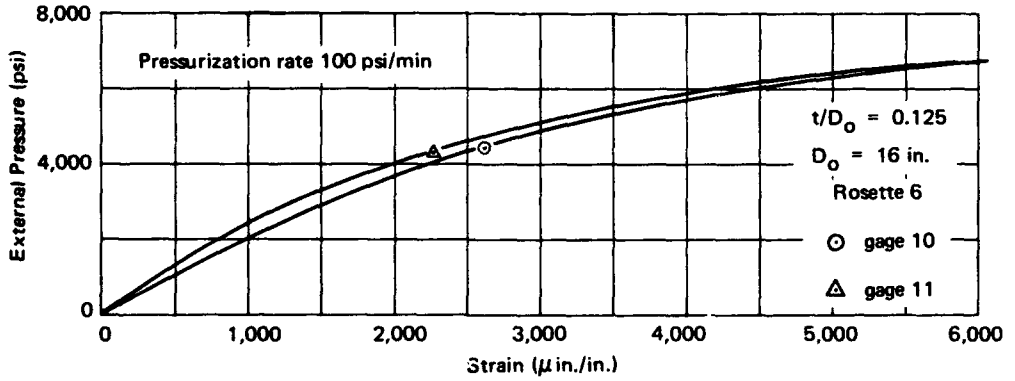

Figure A-14. Strains on the exterior of sphere No. 25 under external pressure; rosette 6.

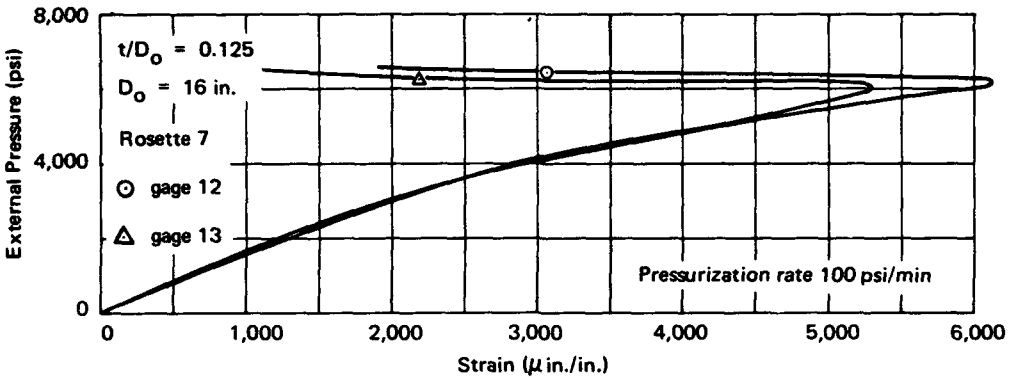

Figure A-15. Strains on the interior of sphere No. 25 under external pressure; rosette 7.

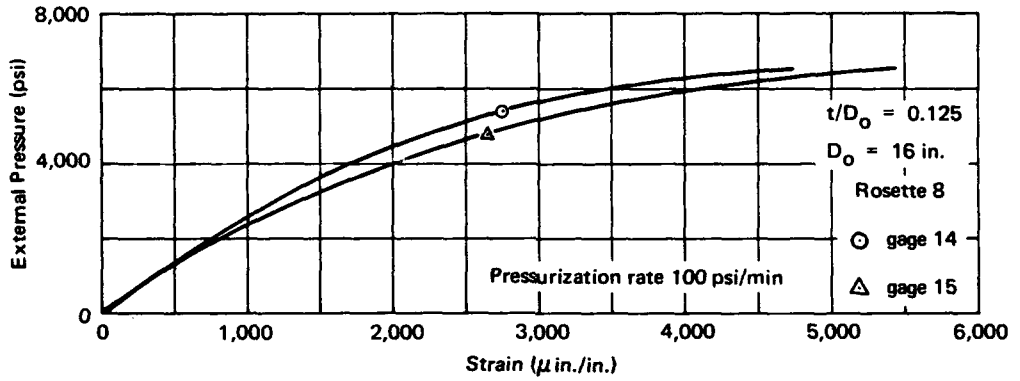

Figure A-16. Strains on the exterior of sphere No. 25 under external pressure; rosette 8.

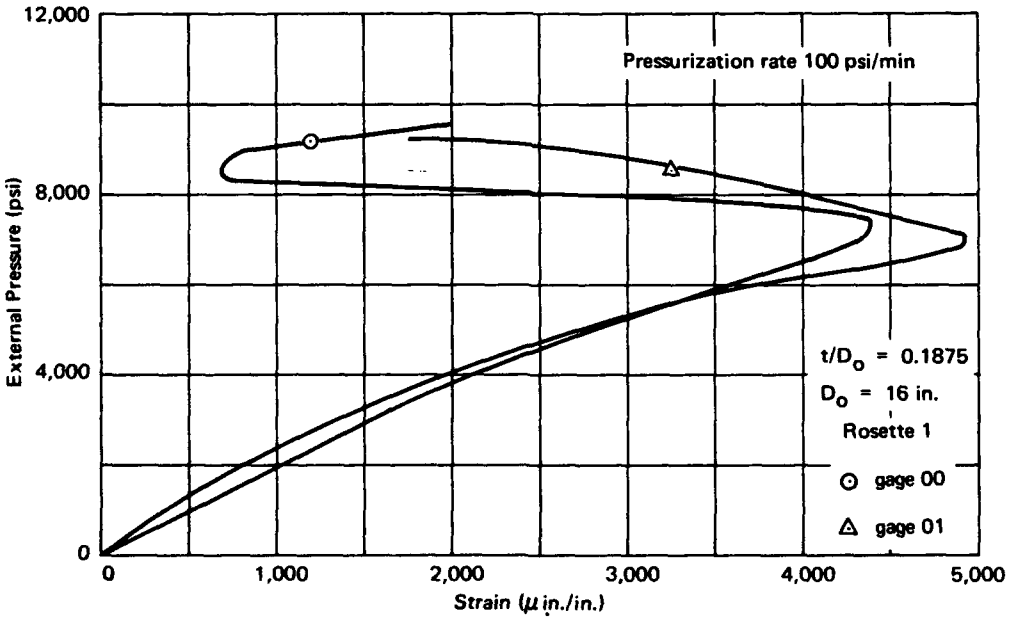

Figure A-17. Strains on the interior of sphere No. 29 under external pressure; rosette 1.

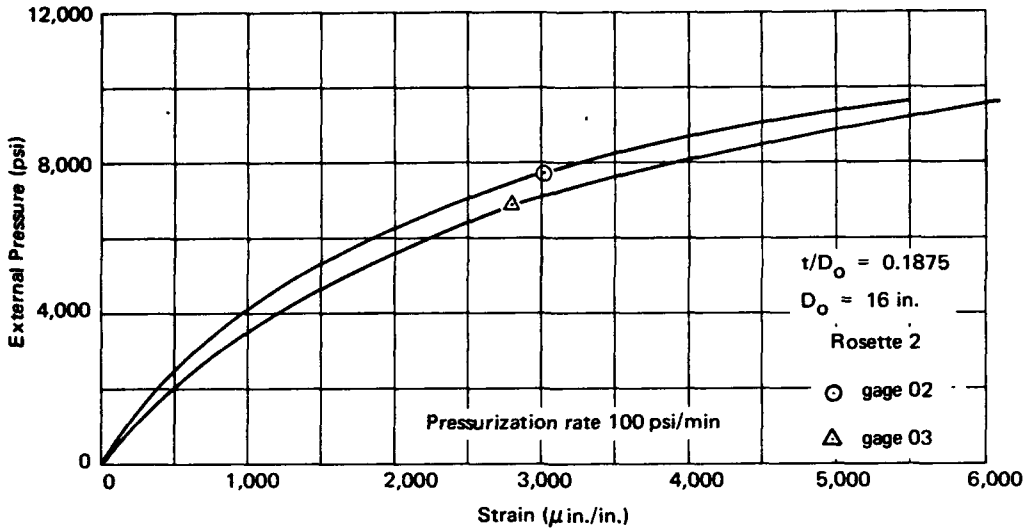

Figure A-18. Strains on the exterior of sphere No. 29 under external pressure; rosette 2.

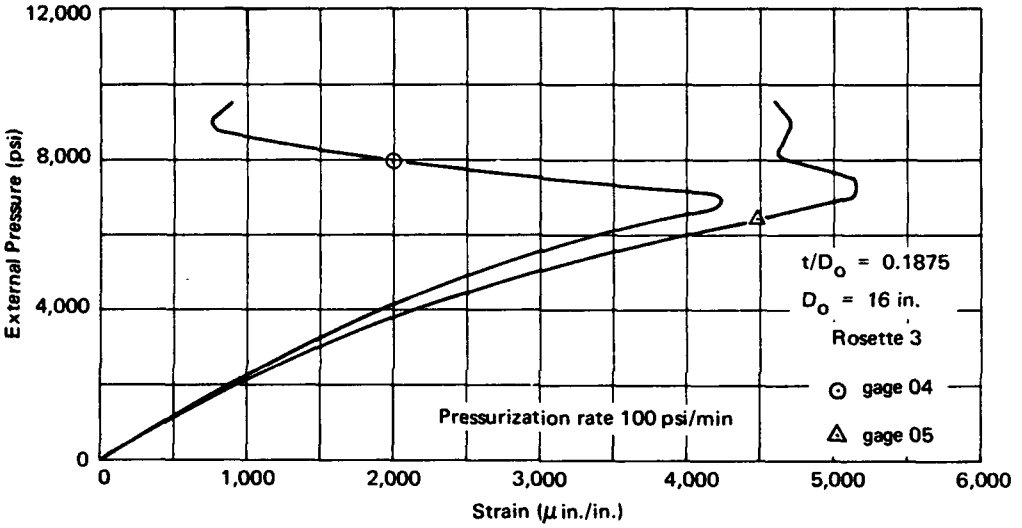

Figure A-19. Strains on the interior of sphere No. 29 under external pressure; rosette 3.

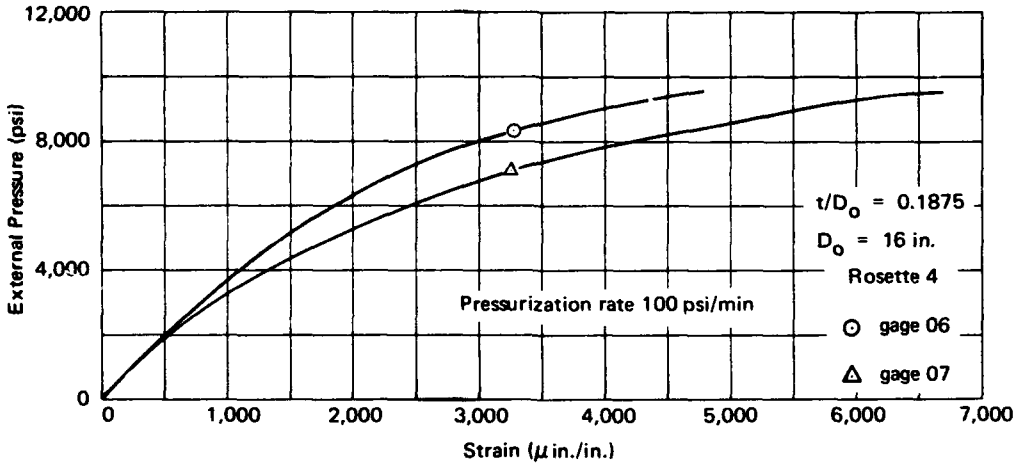

Figure A-20. Strains on the exterior of sphere No. 29 under external pressure; rosette 4.

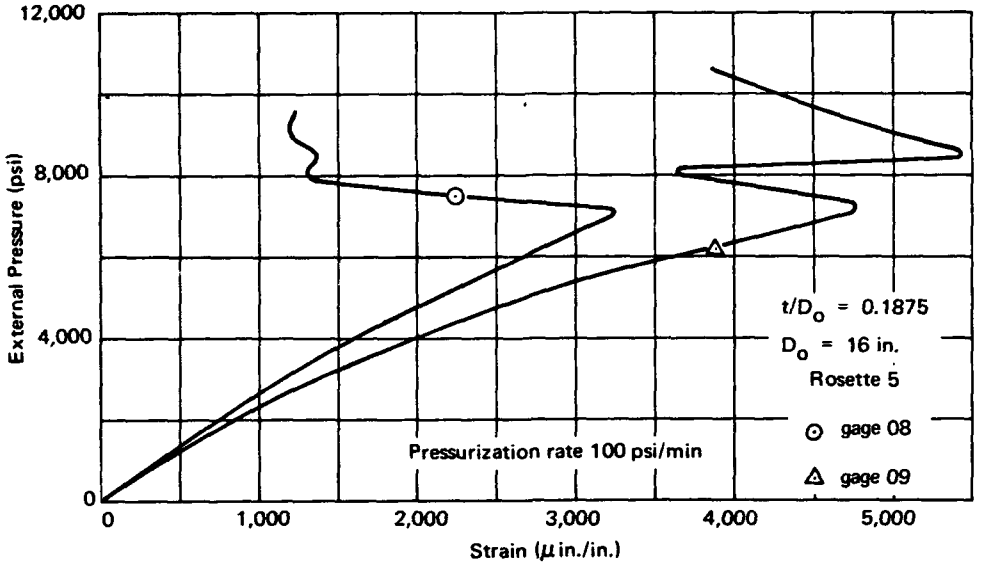

Figure A-21. Strains on the interior of sphere No. 29 under external pressure; rosette 5.

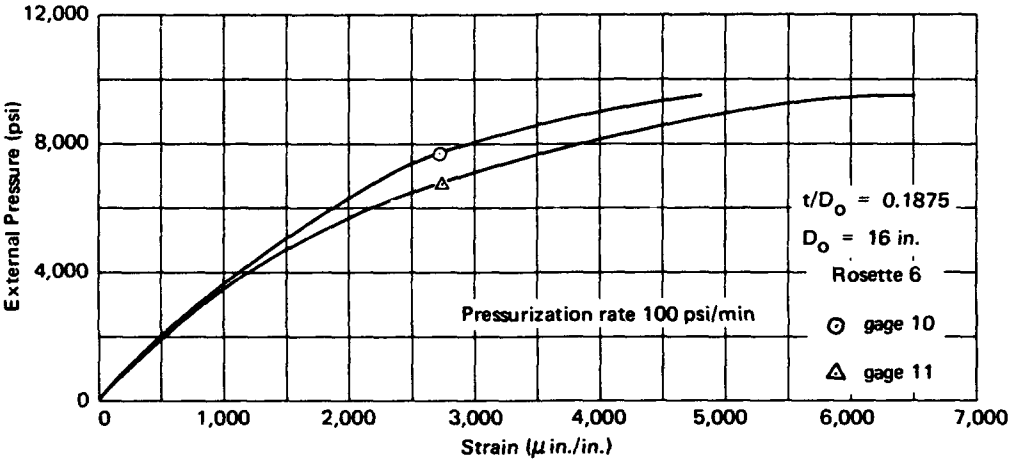

Figure A-22. Strains on the exterior of sphere No. 29 under external pressure; rosette 6.

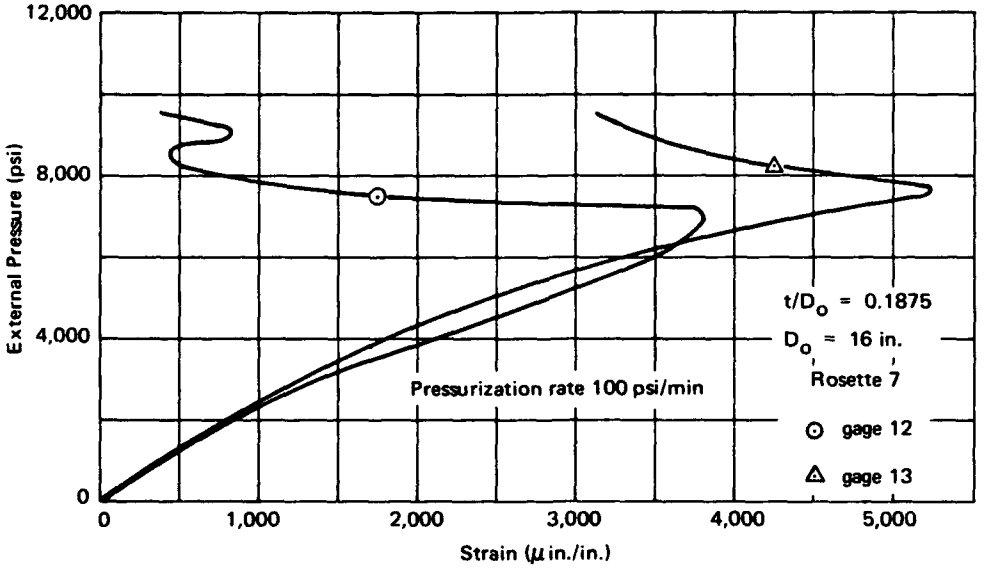

Figure A-23. Strains on the interior of sphere No. 29 under external pressure; rosette 7.

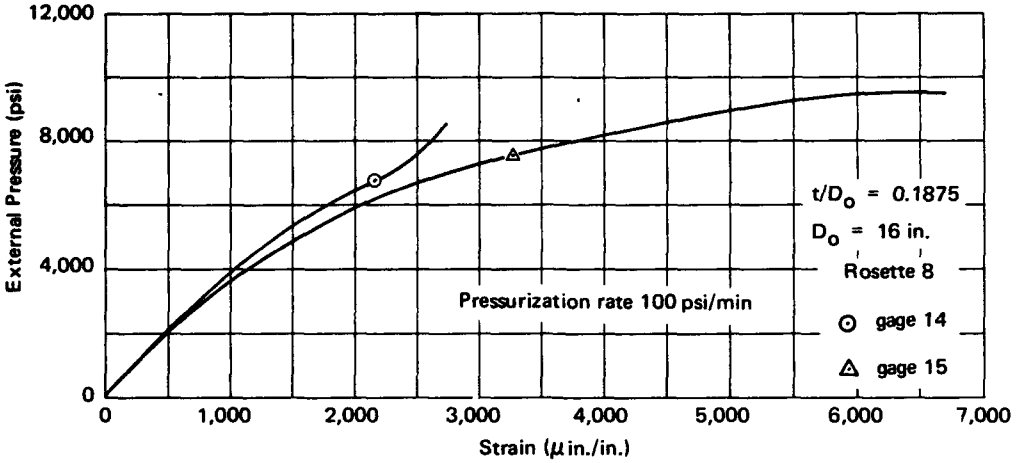

Figure A-24. Strains on the exterior of sphere No. 29 under external pressure; rosette 8.

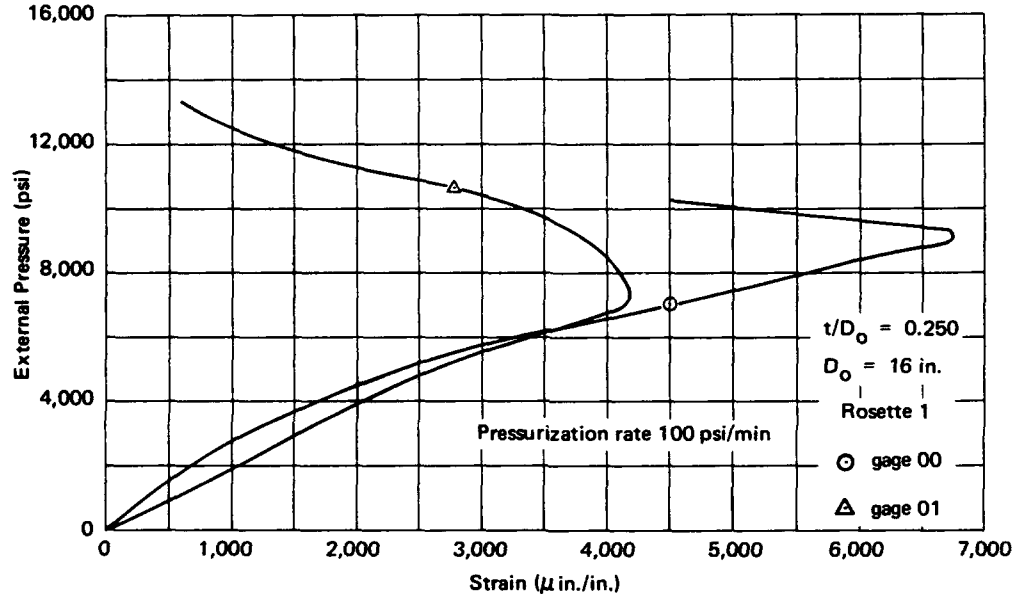

Figure A-25. Strains on the interior of sphere No. 33 under external pressure; rosette 1.

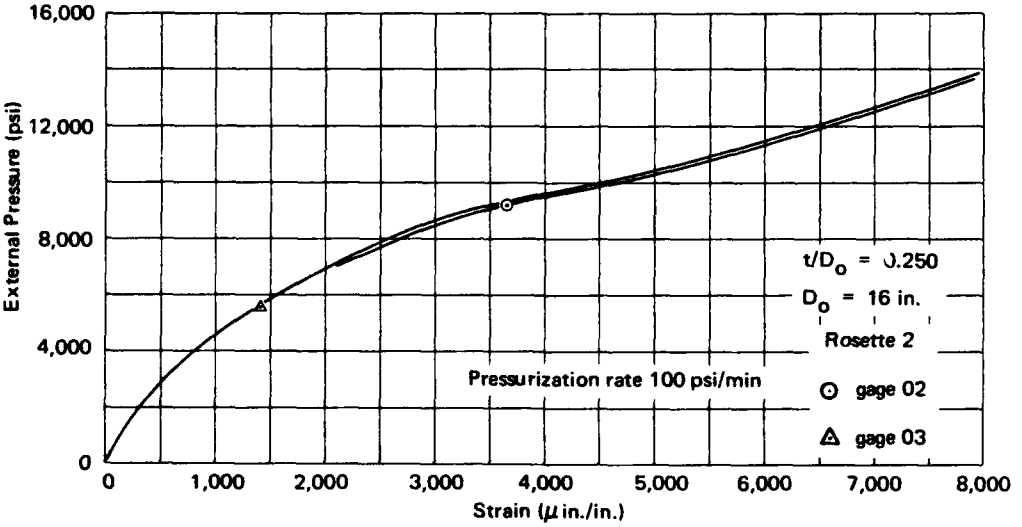

Figure A-26. Strains on the exterior of sphere No. 33 under external pressure; rosette 2.

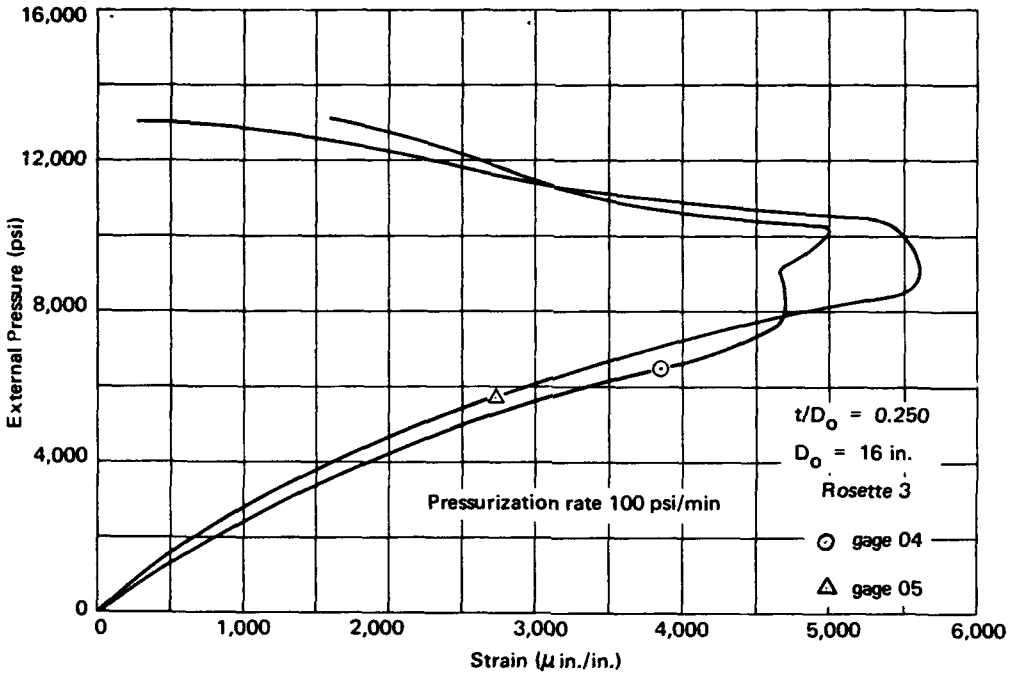

Figure A-27. Strains on the interior of sphere No. 33 under external pressure; rosette 3.

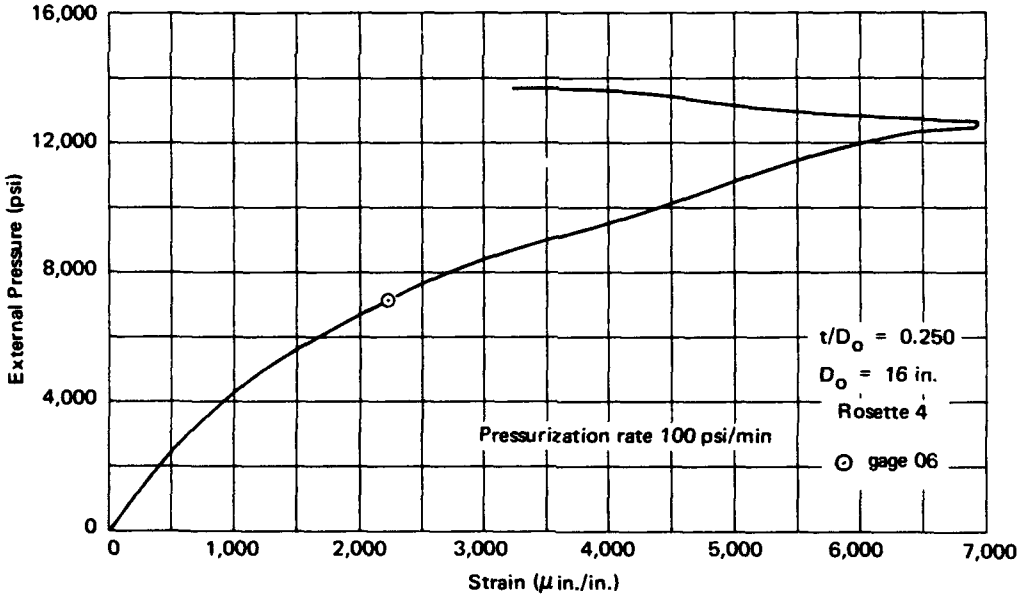

Figure A-28. Strains on the exterior of sphere No. 33 under external pressure; rosette 4.

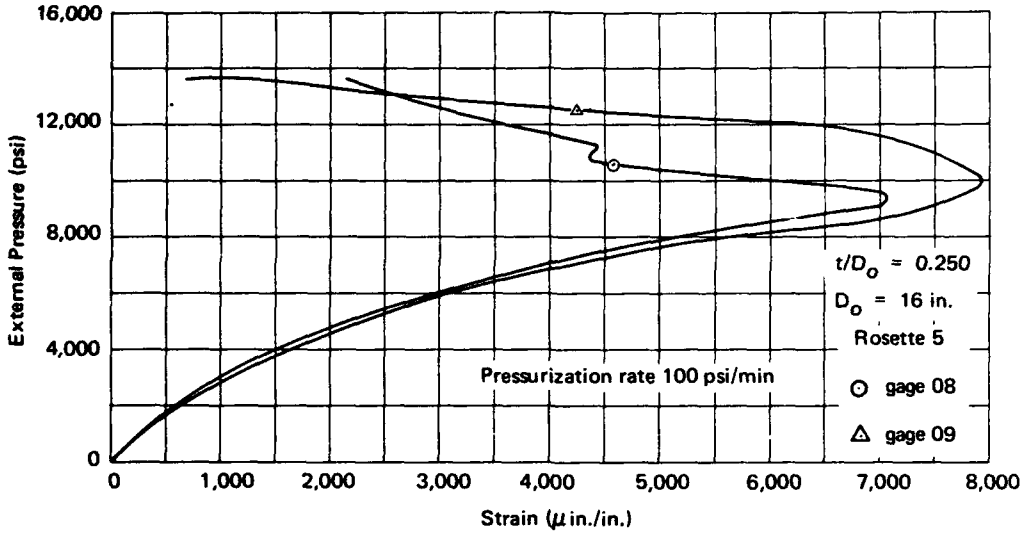

Figure A-29. Strains on the interior of sphere No. 33 under external pressure; rosette 5.

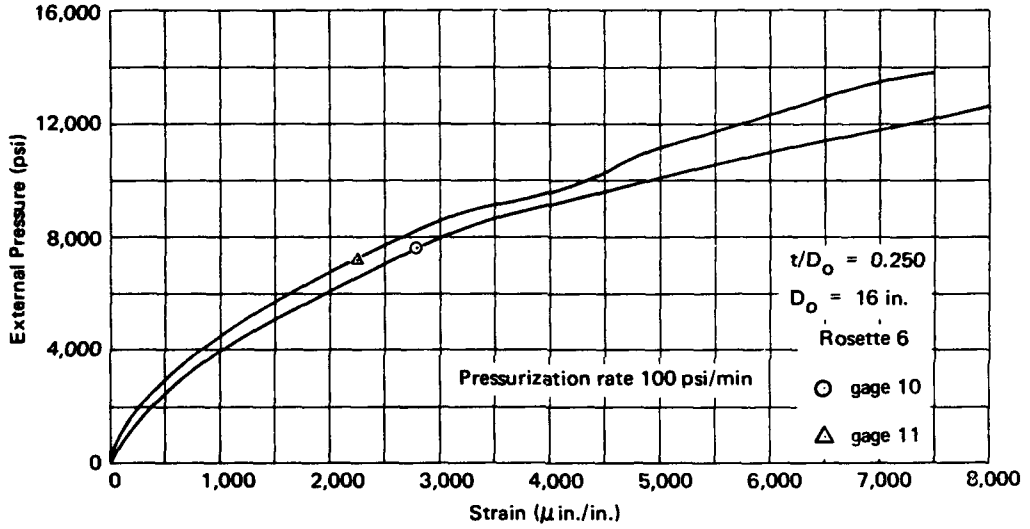

Figure A-30. Strains on the exterior of sphere No. 33 under external pressure; rosette 6.

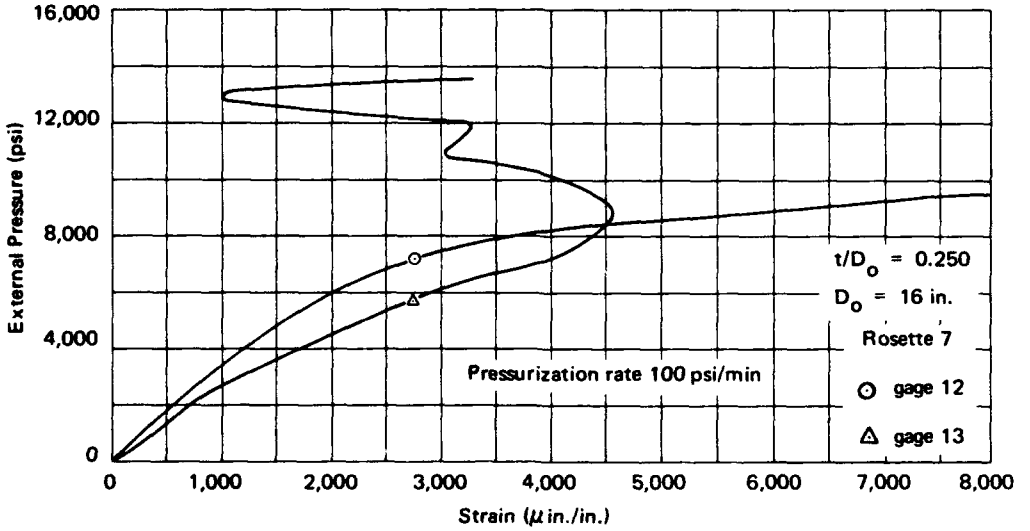

Figure A-31. Strains on the interior of sphere No. 33 under external pressure; rosette 7.

Appendix B

INVESTIGATION OF THE RELATIONSHIP BETWEEN LOADING RATE AND STRAIN RATE ON CONCRETE

The concrete spheres tested in this study were pressurized at a rate of 100 psi/min; however, the resultant stress rates varied with the thickness of sphere tested. The minimum average stress rate for the spherical specimens was in the order of 130 psi/min for the 4-inch-thick spheres, while the maximum average stress rate was approximately 430 psi/min for the 1-inch-thick spheres. Since the maximum stressing rate is approximately three times larger than the minimum stress rate, it was conceivable that the response to the stresses of the concrete mix used in spheres differed between these stress rates.

To find what effect the stress application rate had on the strength, magnitude of strain rate, moduli of elasticity, or Poisson's ratio of concrete mix used in the spheres, cylindrical specimens (measuring 3 inches in diameter and 6 inches in height) of the same concrete mix and age as the spheres were tested in uniaxial compression at different loading rates. Assuming that the critical pressures of the spheres are directly proportional to the mechanical properties of the cylindrical specimens, the information obtained from the cylindrical specimens would show to what extent the strength of spheres is affected by the varying of stress rate, and that some of the variation in experimental data from one sphere to another was not due to difference in shell thickness, but to difference in stressing rates.

The effect of varying the stress rate on mechanical properties of concrete could also have been determined by the testing of spheres at different pressurization rates, but the testing of cylindrical specimens would give approximately the same results. The limited number of expensive sphere specimens could then be used for determination of more important properties of the sphere.

Eight cylindrical test specimens were tested at four different loading rates in order to analyze the relationship between stress application rate and mechanical properties of concrete. Two specimens were tested at each of the four stress application rates: 130 psi/min, 165 psi/min, 230 psi/min, and 430 psi/min. The selected stress application rates for the cylindrical specimens were to simulate the average stress application rates generated in the 4-inch, 3-inch, 2-inch and 1-inch-thick spheres by the uniform hydrostatic loading rate of 100 psi/min. This was accomplished by matching the rate at which the test cylinders were stressed uniaxially to the rate at which

average stress increased in each sphere prior to failure. The average stress in the spheres was determined by dividing the hydrostatic force exerted on a plane passing through the center of a sphere by the cross-sectional area of that sphere.

The dimensional requirements of the cylindrical specimens were chosen to conform to ASTM Specification D695-63T. Cylinders were cast from the same concrete mix as used for the spheres (Figure B-1) and were cured for 100 days prior to compression testing.

The cylindrical specimens were tested at room temperature ($75^{o} \pm 5^{o}F$) in a 400,000-pound-capacity Baldwin-Tate-Emery, Universal Testing Machine. The load was applied axially on the lower face of the cylinder by a pump-driven hydraulic ram, which compressed the specimen against a stationary flat plate (Figure B-2). The deformation during testing of each specimen was measured in both the axial and transverse directions by BLH-A-12 strain gages (Figure B-1). Readings were taken at 1,000-pound intervals up to 10,000 pounds and then every 5,000 pounds until failure occurred.

The measured strains based on the original cross-sectional area of test cylinders showed that varying the stress-application rates in the 130-to-430-psi/min range had little effect upon the strains (Figure B-3), moduli of elasticity (Figures B-4 and 5), and Poisson's ratios (Figure B-6). Certainly, if there was any variation in these mechanical properties due to the difference in stress application rates, it was obscured by the spread of experimental values caused by minute differences in mix composition, casting procedures, curing, instrumentation, capping of specimen ends, and compression testing. When an additional comparison was made between the mechanical properties of the 8 cylinders tested in the 130-to-430-psi/min range and 192 cylinders tested previously at a 2,000-psi/min rate, the only significant difference observed was in ultimate compressive strength (Table B-1), which for the cylinders tested at 2,000 psi/min was approximately 5% higher than for those tested in the 130-to-430-psi/min range. Thus it appears that no significant difference in mechanical properties, as exemplified by comparison of strain rates (Figure B-7), moduli of elasticity (Figures B-8 and 9), and Poisson's ratios (Figure B-10), exists for identical concrete test cylinders tested at stress application rates that vary from 130 to 2,000 psi/min. Since the 130-to-430-psi/min range of stress application rates in the spheres under discussion was smaller than the 130-to-2,000-psi/min stress application range for which very little variation in mechanical properties of concrete was found, it can be concluded that the different stress application rates that took place in concrete spheres tested at uniform 100-psi/min hydrostatic pressurization rate had very little influence on the test results reported in the main body of the report.

Table B-1. Test Cylinder Data

Cylinder	Stress Application Rate (psi/min)	Critical Load (lb)	Compressive Strength (psi)
A	130	69,400	9,820
B	130	70,200	9,930
C	165	70,800	10,020
D	165	71,500	10,110
E	230	66,900	9,460
F	230	67,900	9,600
G	430	72,900	10,310
H	430	69,700	9,860
Average of A through H			9,890
J*	2,000	Average	11,060

* Represents the average of 192 test cylinders tested at the standard rate with a maximum compressive strength value of 11,880 psi and a minimum value of 9,780 psi.

A review of literature disclosed that several studies[9,10,11] have been made previously on the relationship between stress rate and mechanical properties of concrete test cylinders under uniaxial compression. Unfortunately, only one of them dealt with stress rates applicable to this study,[9] while the others[10,11] addressed themselves to stress rates 10 to 10^5 times larger than those in this study. The applicability of published data to the present study was further decreased by the differences in strength and ages of concrete used in the NCEL spheres and those properties of concrete used in other studies.

However, by extrapolation of stress rates, concrete strengths, and ages wherever applicable in published studies, several findings can be postulated. These findings can be summarized by stating that ultimate strength and secant and tangent moduli of elasticity of concrete test cylinders under uniaxial compression increase with the increase in stress rate, while axial strains decrease. In the stress rate range applicable to this study of 1 to 35 psi/sec, the average change of mechanical properties in 10,000-psi concrete at the age of approximately 75 days is extrapolated to be approximately 2% of standard test speed for each factor of 10 in stress rate change.

The range of stress rates under discussion in Appendix B is less than the standard ASTM stress rate of 33 psi/sec by a factor of 10, and because of it the mechanical properties of concrete should be approximately 2% different in magnitude from those determined by standard ASTM testing procedures. Since the variation in mechanical properties between individual cylinders tested in this study at standard stress rates (Appendix A) is on the order of 10%, it would obscure the smaller (2%) variation between average mechanical properties of concrete tested at 33 psi/sec and concrete tested in the stress-rate range between 2-to-7-psi/sec. The experimental data described in Appendix B bears this out, as variations in mechanical properties between individual test cylinders obscure to a large extent the difference between mechanical properties caused by the small difference in stress rates.

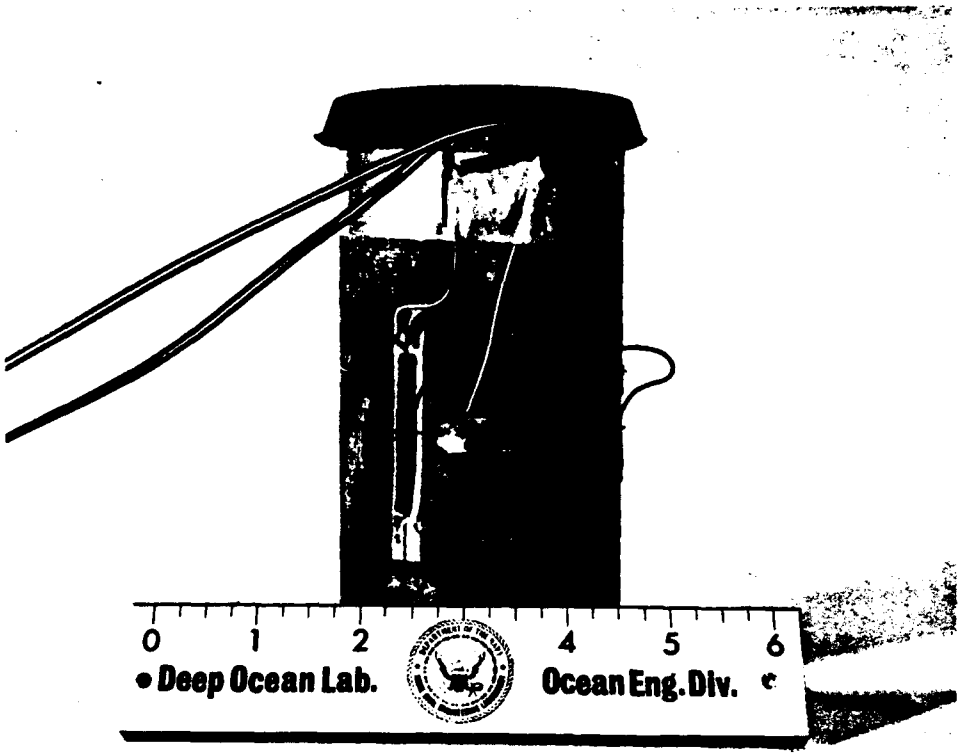

Figure B-1. Typical 3x6-inch test cylinder for uniaxial compression testing.

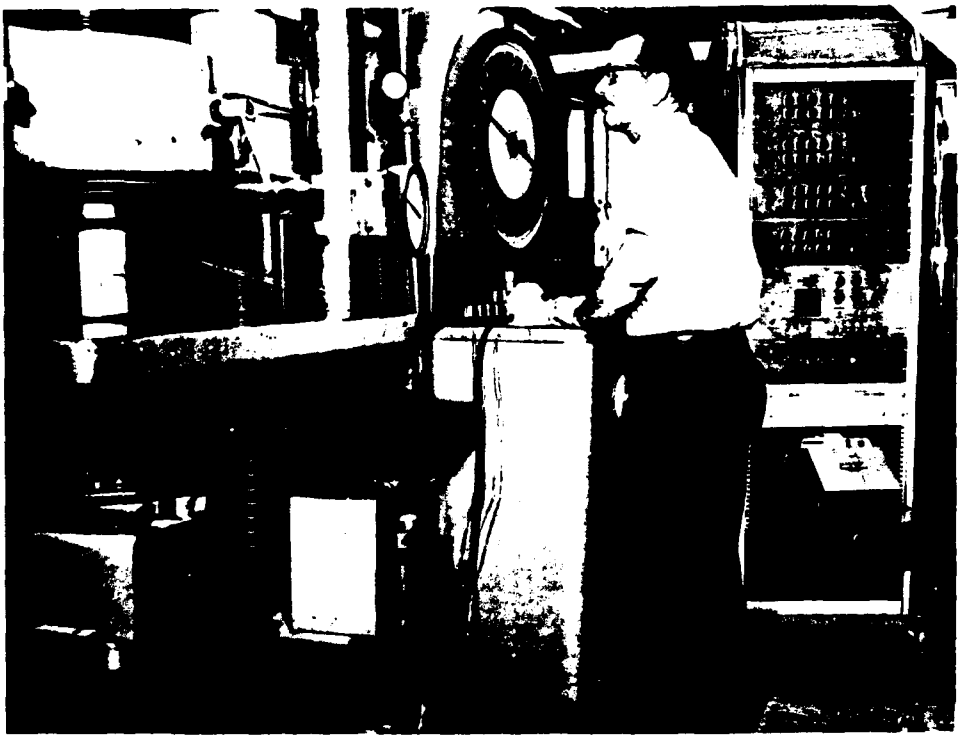

Figure B-2. Testing apparatus used to subject the cylinders to a uniaxial load.

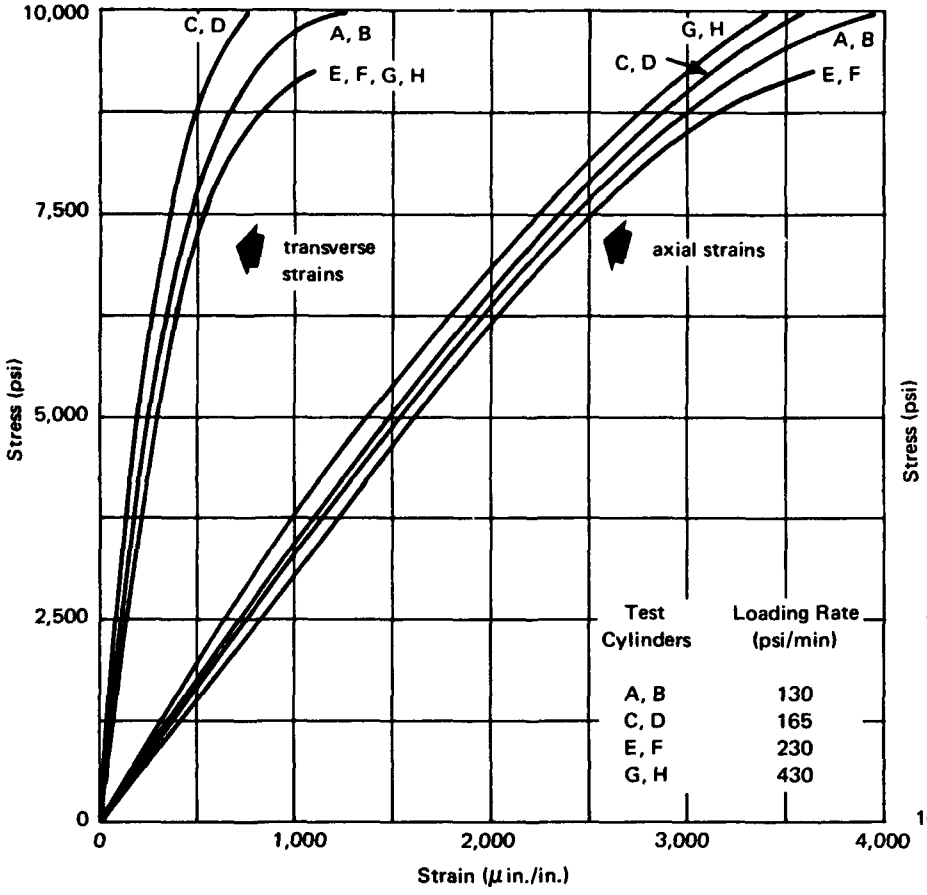

Figure B-3. Strains on the exterior of 3x6-inch test cylinders under uniaxial compression.

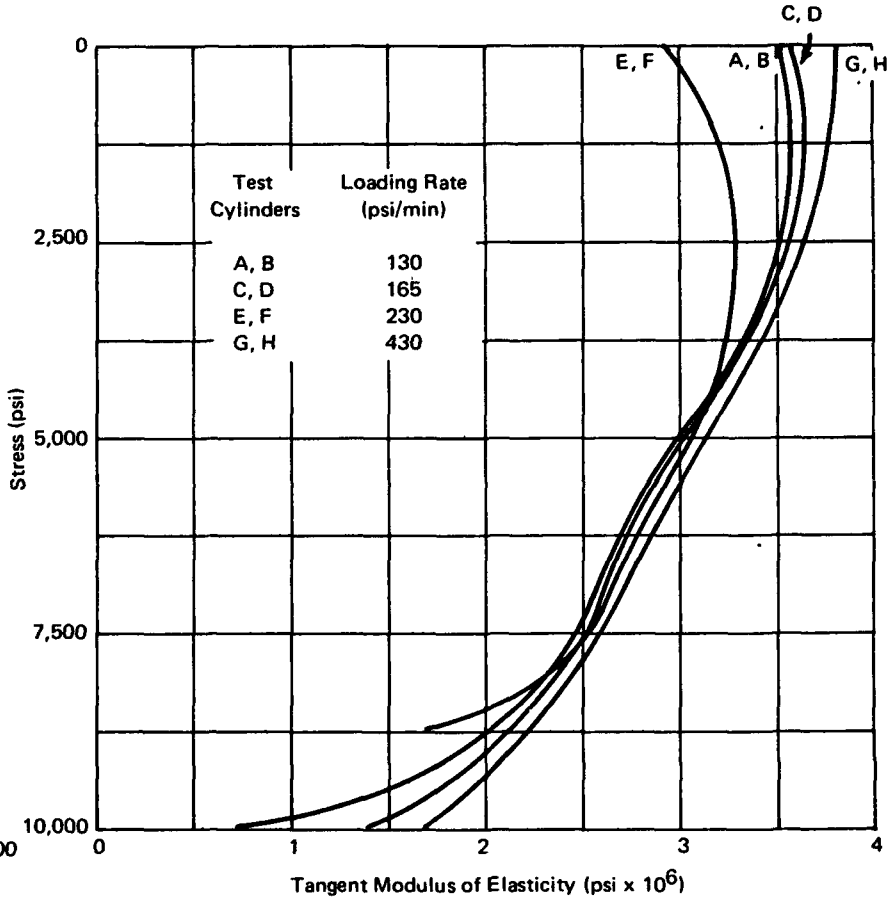

Figure B-4. Tangent modulus of elasticity of 3x6-inch test cylinders under axial compression.

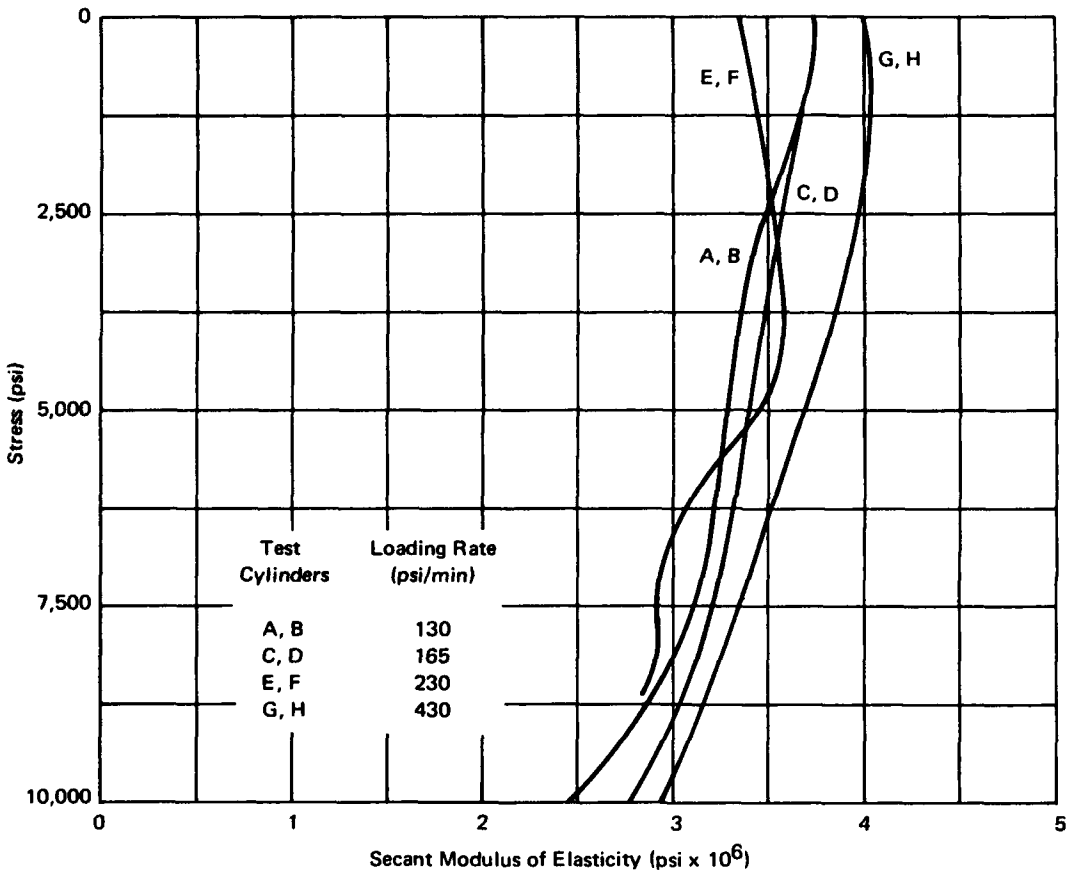

Figure B-5. Secant modulus of elasticity of 3x6-inch test cylinders under uniaxial compression.

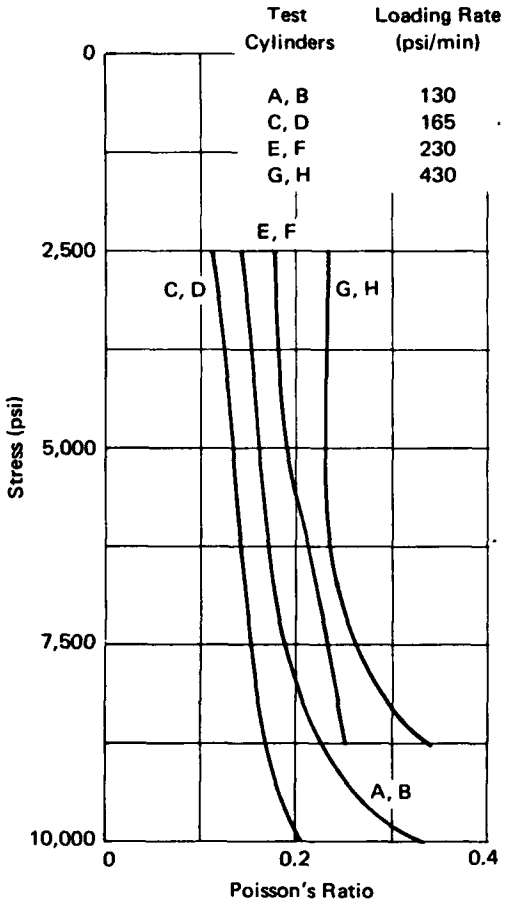

Figure B-6. Poisson's ratio of 3x6-inch test cylinders under axial compression.

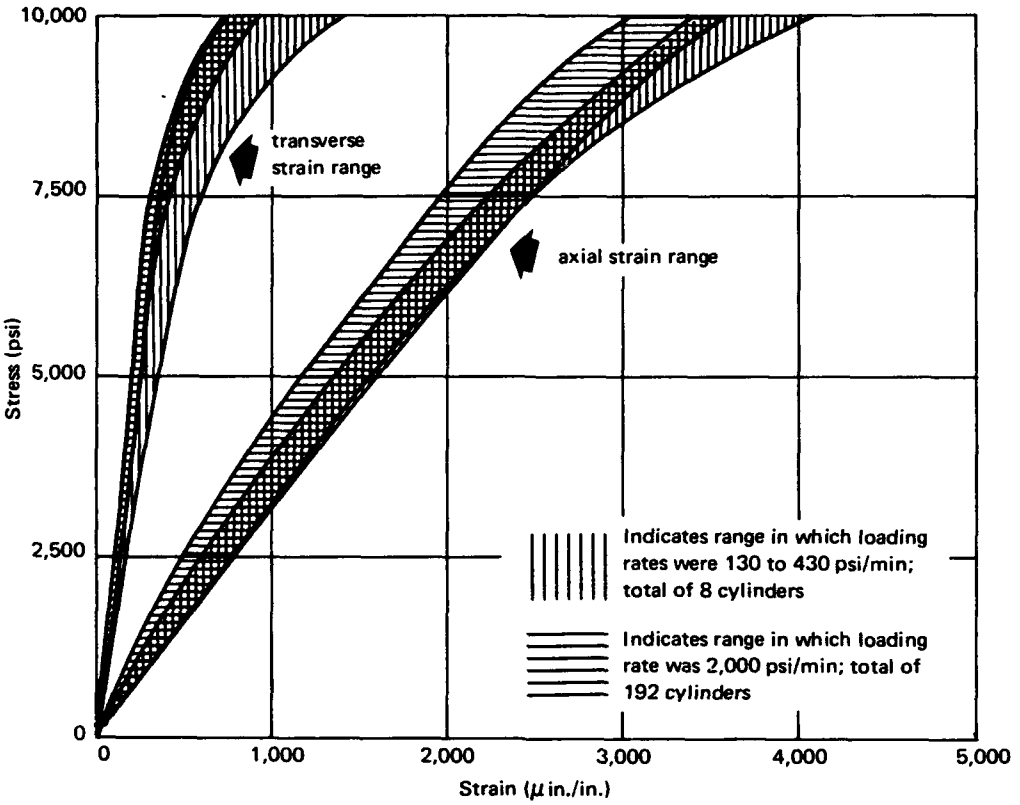

Figure B-7. Comparison of strains on 3x6-inch test cylinders under uniaxial compression.

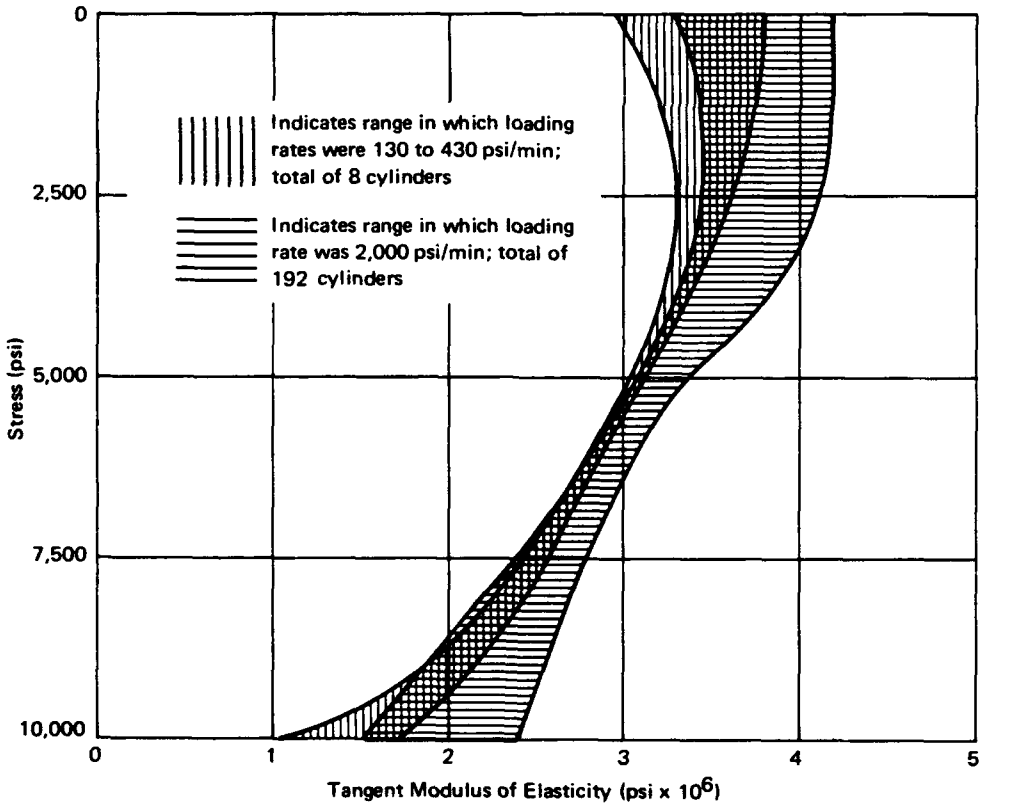

Figure B-8. Comparison of tangent modulus of elasticity of 3x6-inch test cylinders under uniaxial compression.

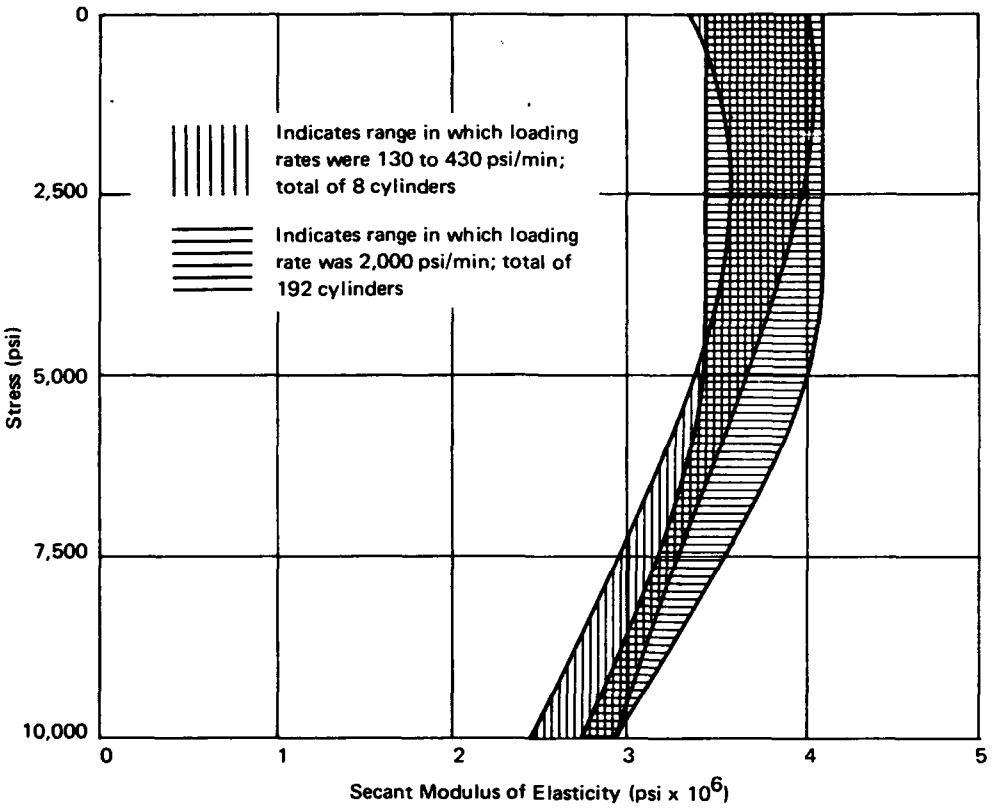

Figure B-9. Comparison of secant modulus of elasticity of 3x6-inch test cylinders under uniaxial compression.

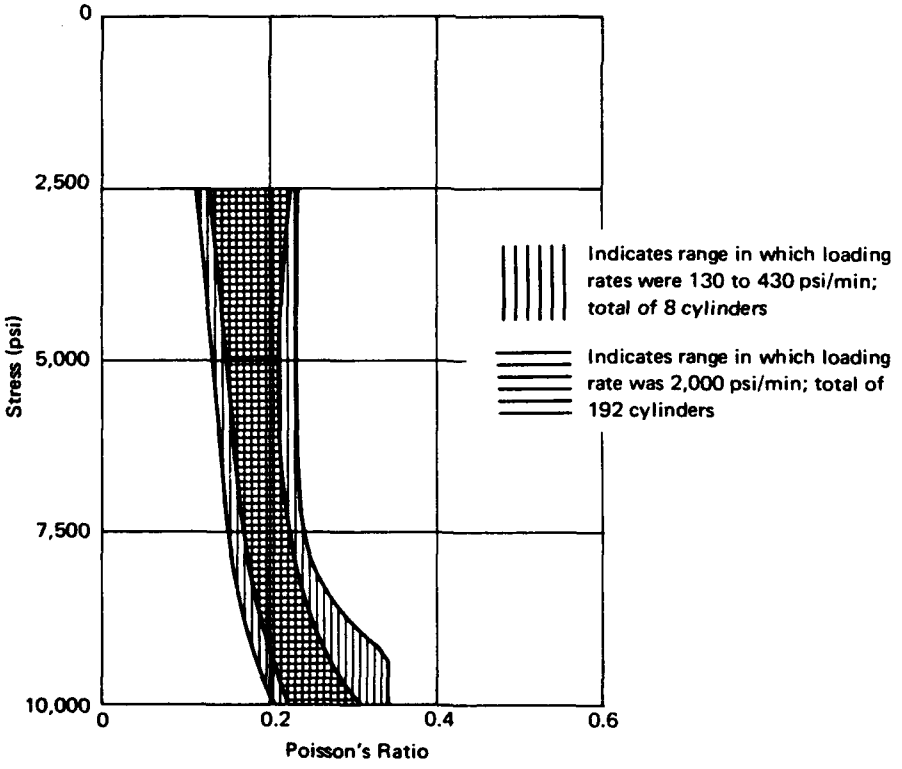

Figure B-10. Comparison of Poisson's ratios on 3x6-inch test cylinders under uniaxial compression.

REFERENCES

1. Naval Civil Engineering Laboratory. Technical Report R-517: Behavior of spherical concrete hulls under hydrostatic loading, Part I. Exploratory investigation, by J. D. Stachiw and K. O. Gray. Port Hueneme, Calif., Mar 1967.

2. ———. Technical Report R-547: Behavior of spherical concrete hulls under hydrostatic loading, Part II. Effect of penetrations, by J. D. Stachiw. Port Hueneme, Calif., Oct 1967.

3. A. Ruettgers, E. N. Vidal, and S. P. Wing. "An investigation of the permeability of mass concrete with particular reference to Boulder Dam," American Concrete Institute, Proceedings, vol. 31, Mar-Apr 1935, pp. 382-416.

4. W. H. Taylor. Concrete technology and practice. New York, American Elsevier, 1965, pp. 222-224.

5. G. E. Troxell and H. E. Davis. Composition and properties of concrete. New York, McGraw-Hill, 1956, chap. 11.

6. Bureau of Reclamation. Concrete manual, 7th ed. rev. Denver, Colo., 1966, pp. 15, 40, 55.

7. R. H. Roark. Formulas for stress and strain, 4th ed. New York, McGraw-Hill, 1965, p. 308.

8. C. C. Perry and H. R. Lissner. The strain gage primer. New York, McGraw-Hill, 1955, p. 131.

9. P. G. Jones and F. E. Richart. "The effect of testing speed on strength and elastic properties of concrete," American Society for Testing Materials, Proceedings, vol. 36, pt. 2, 1936, pp. 380-392.

10. National Bureau of Standards. Report 1523: The effect of loading rate on the compressive strength and elastic properties of plain concrete, by P. Watstein and A. P. Boresi. Washington, D. C., Mar 1952.

11. Naval Civil Engineering Laboratory. Technical Report R-447: Dynamic properties of plain portland cement concrete, by W. L. Cowell. Port Hueneme, Calif., June 1966.

LIST OF SYMBOLS

A	Area of cross section under pressure, sq ft
D_i	Inside diameter of concrete sphere
D_o	Outside diameter of concrete sphere
E	Modulus of elasticity
E_t	Tangent modulus of elasticity
E_s	Secant modulus of elasticity
K_c	Permeability coefficient for concrete
H/L	Ratio of head of fluid to percolation length
p	External hydrostatic pressure, psi
p_c	Critical pressure, psi
R_i	Internal radius of sphere, in.
R_o	External radius of sphere, in.
r	Radius from center of sphere to point where stress is to be found, in.
S_1	Meridional wall stress, psi
S_2	Hoop wall stress, psi
S_3	Radial wall stress, psi
Q	Rate of flow, cu ft/sec
ϵ_1	Meridional strain, μin./in.
μ	Poisson's ratio

DEPARTMENT OF THE NAVY
HEADQUARTERS NAVAL MATERIAL COMMAND
WASHINGTON, D. C. 20360

IN REPLY REFER TO
MAT 09D
CNM Control: #12

20 August 1968

Commanding Officer
Naval Civil Engineering Laboratory
Port Hueneme, California 93041
ATTN: Code L30

Report R-568 entitled "Behavior of Spherical Concrete Hulls Under Hydrostatic Loading - Part III," return of

The above described material submitted by you for security review is returned. It has been:

XXXXXXX Cleared, without amendment and may be released at your discretion.

_____ Cleared, with amendments noted. It may be released, as amended, at your discretion.

_____ Classified _____ and may not be released in its present form. Recommendations regarding declassification are indicated / / in text / / on attached sheet.

_____ Recommended for revision for the following reasons.

_____ Other:

R. W. Seagraves

R.W.A. SEAGRAVES
LIEUTENANT, USNR
ADMINISTRATIVE ASS'T

Naval Civil Engineering Laboratory
BEHAVIOR OF SPHERICAL CONCRETE HULLS UNDER HYDROSTATIC LOADING–PART III, by J. D. Stachiw and K. Mack
TR-588 65 p. illus June 1968 Unclassified

1. Underwater habitats 2. Hydrostatic loading I. Y-F015-01-07-001

Sixteen hollow concrete spheres of 16-inch outside diameter were subjected to external hydrostatic pressure to investigate the relationship between the sphere's shell thickness and (1) its critical pressure, (2) permeability, and (3) strain magnitude. The critical pressure of waterproofed hollow concrete spheres was found to be approximately a linear function of the sphere's thickness; the spheres imploded at pressures from 3,240 to 13,900 psi, depending on their thickness. Concrete spheres permeated by seawater failed at hydrostatic pressures 30% to 15% lower than identical waterproofed spheres. In all cases the stress in the spheres at the time of implosion was considerably higher than in concrete test cylinders prepared of the same mix and of the same curing history subjected to uniaxial compression. The resistance of concrete to permeation by seawater into the interior of nonwaterproofed spheres at 2,000-psi hydrostatic pressure was found to be an exponential function of shell thickness. The rate of flow into the sphere's interior ranged from 6.1 to 0.197 ml/day/ft^2 of exterior surface, depending on the thickness of shell.

Naval Civil Engineering Laboratory
BEHAVIOR OF SPHERICAL CONCRETE HULLS UNDER HYDROSTATIC LOADING–PART III, by J. D. Stachiw and K. Mack
TR-588 65 p. illus June 1968 Unclassified

1. Underwater habitats 2. Hydrostatic loading I. Y-F015-01-07-001

Sixteen hollow concrete spheres of 16-inch outside diameter were subjected to external hydrostatic pressure to investigate the relationship between the sphere's shell thickness and (1) its critical pressure, (2) permeability, and (3) strain magnitude. The critical pressure of waterproofed hollow concrete spheres was found to be approximately a linear function of the sphere's thickness; the spheres imploded at pressures from 3,240 to 13,900 psi, depending on their thickness. Concrete spheres permeated by seawater failed at hydrostatic pressures 30% to 15% lower than identical waterproofed spheres. In all cases the stress in the spheres at the time of implosion was considerably higher than in concrete test cylinders prepared of the same mix and of the same curing history subjected to uniaxial compression. The resistance of concrete to permeation by seawater into the interior of nonwaterproofed spheres at 2,000-psi hydrostatic pressure was found to be an exponential function of shell thickness. The rate of flow into the sphere's interior ranged from 6.1 to 0.197 ml/day/ft^2 of exterior surface, depending on the thickness of shell.

Naval Civil Engineering Laboratory
BEHAVIOR OF SPHERICAL CONCRETE HULLS UNDER HYDROSTATIC LOADING–PART III, by J. D. Stachiw and K. Mack
TR-588 65 p. illus June 1968 Unclassified

1. Underwater habitats 2. Hydrostatic loading I. Y-F015-01-07-001

Sixteen hollow concrete spheres of 16-inch outside diameter were subjected to external hydrostatic pressure to investigate the relationship between the sphere's shell thickness and (1) its critical pressure, (2) permeability, and (3) strain magnitude. The critical pressure of waterproofed hollow concrete spheres was found to be approximately a linear function of the sphere's thickness; the spheres imploded at pressures from 3,240 to 13,900 psi, depending on their thickness. Concrete spheres permeated by seawater failed at hydrostatic pressures 30% to 15% lower than identical waterproofed spheres. In all cases the stress in the spheres at the time of implosion was considerably higher than in concrete test cylinders prepared of the same mix and of the same curing history subjected to uniaxial compression. The resistance of concrete to permeation by seawater into the interior of nonwaterproofed spheres at 2,000-psi hydrostatic pressure was found to be an exponential function of shell thickness. The rate of flow into the sphere's interior ranged from 6.1 to 0.197 ml/day/ft^2 of exterior surface, depending on the thickness of shell.

Naval Civil Engineering Laboratory
BEHAVIOR OF SPHERICAL CONCRETE HULLS UNDER HYDROSTATIC LOADING–PART III, by J. D. Stachiw and K. Mack
TR-588 65 p. illus June 1968 Unclassified

1. Underwater habitats 2. Hydrostatic loading I. Y-F015-01-07-001

Sixteen hollow concrete spheres of 16-inch outside diameter were subjected to external hydrostatic pressure to investigate the relationship between the sphere's shell thickness and (1) its critical pressure, (2) permeability, and (3) strain magnitude. The critical pressure of waterproofed hollow concrete spheres was found to be approximately a linear function of the sphere's thickness; the spheres imploded at pressures from 3,240 to 13,900 psi, depending on their thickness. Concrete spheres permeated by seawater failed at hydrostatic pressures 30% to 15% lower than identical waterproofed spheres. In all cases the stress in the spheres at the time of implosion was considerably higher than in concrete test cylinders prepared of the same mix and of the same curing history subjected to uniaxial compression. The resistance of concrete to permeation by seawater into the interior of nonwaterproofed spheres at 2,000-psi hydrostatic pressure was found to be an exponential function of shell thickness. The rate of flow into the sphere's interior ranged from 6.1 to 0.197 ml/day/ft^2 of exterior surface, depending on the thickness of shell.

Naval Civil Engineering Laboratory
BEHAVIOR OF SPHERICAL CONCRETE HULLS UNDER HYDROSTATIC LOADING–PART III, by J. D. Stachiw and K. Mack
TR-588 65 p. illus June 1968 Unclassified

1. Underwater habitats 2. Hydrostatic loading I. Y-F015-01-07-001

Sixteen hollow concrete spheres of 16-inch outside diameter were subjected to external hydrostatic pressure to investigate the relationship between the sphere's shell thickness and (1) its critical pressure, (2) permeability, and (3) strain magnitude. The critical pressure of waterproofed hollow concrete spheres was found to be approximately a linear function of the sphere's thickness; the spheres imploded at pressures from 3,240 to 13,900 psi, depending on their thickness. Concrete spheres permeated by seawater failed at hydrostatic pressures 30% to 15% lower than identical waterproofed spheres. In all cases the stress in the spheres at the time of implosion was considerably higher than in concrete test cylinders prepared of the same mix and of the same curing history subjected to uniaxial compression. The resistance of concrete to permeation by seawater into the interior of nonwaterproofed spheres at 2,000-psi hydrostatic pressure was found to be an exponential function of shell thickness. The rate of flow into the sphere's interior ranged from 6.1 to 0.197 ml/day/ft^2 of exterior surface, depending on the thickness of shell.

Naval Civil Engineering Laboratory
BEHAVIOR OF SPHERICAL CONCRETE HULLS UNDER HYDROSTATIC LOADING–PART III, by J. D. Stachiw and K. Mack
TR-588 65 p. illus June 1968 Unclassified

1. Underwater habitats 2. Hydrostatic loading I. Y-F015-01-07-001

Sixteen hollow concrete spheres of 16-inch outside diameter were subjected to external hydrostatic pressure to investigate the relationship between the sphere's shell thickness and (1) its critical pressure, (2) permeability, and (3) strain magnitude. The critical pressure of waterproofed hollow concrete spheres was found to be approximately a linear function of the sphere's thickness; the spheres imploded at pressures from 3,240 to 13,900 psi, depending on their thickness. Concrete spheres permeated by seawater failed at hydrostatic pressures 30% to 15% lower than identical waterproofed spheres. In all cases the stress in the spheres at the time of implosion was considerably higher than in concrete test cylinders prepared of the same mix and of the same curing history subjected to uniaxial compression. The resistance of concrete to permeation by seawater into the interior of nonwaterproofed spheres at 2,000-psi hydrostatic pressure was found to be an exponential function of shell thickness. The rate of flow into the sphere's interior ranged from 6.1 to 0.197 ml/day/ft^2 of exterior surface, depending on the thickness of shell.

Naval Civil Engineering Laboratory
BEHAVIOR OF SPHERICAL CONCRETE HULLS UNDER HYDROSTATIC LOADING–PART III, by J. D. Stachiw and K. Mack
TR-588 65 p. illus June 1968 Unclassified

1. Underwater habitats 2. Hydrostatic loading I. Y-F015-01-07-001

Sixteen hollow concrete spheres of 16-inch outside diameter were subjected to external hydrostatic pressure to investigate the relationship between the sphere's shell thickness and (1) its critical pressure, (2) permeability, and (3) strain magnitude. The critical pressure of waterproofed hollow concrete spheres was found to be approximately a linear function of the sphere's thickness; the spheres imploded at pressures from 3,240 to 13,900 psi, depending on their thickness. Concrete spheres permeated by seawater failed at hydrostatic pressures 30% to 15% lower than identical waterproofed spheres. In all cases the stress in the spheres at the time of implosion was considerably higher than in concrete test cylinders prepared of the same mix and of the same curing history subjected to uniaxial compression. The resistance of concrete to permeation by seawater into the interior of nonwaterproofed spheres at 2,000-psi hydrostatic pressure was found to be an exponential function of shell thickness. The rate of flow into the sphere's interior ranged from 6.1 to 0.197 ml/day/ft^2 of exterior surface, depending on the thickness of shell.

Unclassified
Security Classification

DOCUMENT CONTROL DATA - R & D

(Security classification of title, body of abstract and indexing annotation must be entered when the overall report is classified)

1. ORIGINATING ACTIVITY (Corporate author)
Naval Civil Engineering Laboratory
Port Hueneme, Calif. 93041

2a. REPORT SECURITY CLASSIFICATION
Unclassified

2b. GROUP

3. REPORT TITLE
BEHAVIOR OF SPHERICAL CONCRETE HULLS UNDER HYDROSTATIC LOADING—PART III. Relationship Between Thickness-To-Diameter Ratio and Critical Pressures, Strains, and Water Permeation Rates

4. DESCRIPTIVE NOTES (Type of report and inclusive dates)
Not final; July 1, 1967—August 1, 1967

5. AUTHOR(S) (First name, middle initial, last name)
J. D. Stachiw and K. Mack

6. REPORT DATE	7a. TOTAL NO. OF PAGES	7b. NO. OF REFS
June 1968	65	11

8a. CONTRACT OR GRANT NO	9a. ORIGINATOR'S REPORT NUMBER(S)
b. PROJECT NO Y-F015-01-07-001	TR-588
c.	9b. OTHER REPORT NO(S) (Any other numbers that may be assigned this report)
d.	

10. DISTRIBUTION STATEMENT
Each transmittal of this document outside the agencies of the U. S. Government must have prior approval of the Naval Civil Engineering Laboratory.

11. SUPPLEMENTARY NOTES	12. SPONSORING MILITARY ACTIVITY
	Naval Facilities Engineering Command Washington, D. C.

13. ABSTRACT

Sixteen hollow concrete spheres of 16-inch outside diameter were subjected to external hydrostatic pressure to investigate the relationship between the sphere's shell thickness and (1) its critical pressure, (2) permeability, and (3) strain magnitude. The shell thickness of the spheres varied from 1 inch to 4 inches in 1-inch steps. All spheres were cast from the same concrete mix, cured under identical temperature and moisture conditions, and tested in the same manner. The strength of concrete in the spheres at the time of testing, as established by uniaxial compression tests on 3 x 6-inch cylinders, was in the 9,000-to-11,000-psi range. The critical pressure of waterproofed hollow concrete spheres was found to be approximately a linear function of the sphere's thickness; the spheres imploded at pressures from 3,240 to 13,900 psi, depending on their thickness. Concrete spheres permeated by seawater failed at hydrostatic pressures 30% to 15% lower than identical waterproofed spheres. In all cases the stress in the spheres at the time of implosion was considerably higher than in concrete test cylinders prepared of the same mix and of the same curing history subjected to uniaxial compression. The resistance of concrete to permeation by seawater into the interior of non-waterproofed spheres at 2,000-psi hydrostatic pressure was found to be an exponential function of shell thickness. The rate of flow into the sphere's interior ranged from 6.1 to 0.197 ml/day/ft^2 of exterior surface, depending on the thickness of shell.

DD FORM 1 NOV 65 1473 (PAGE 1)
S/N 0101-807-6801

Unclassified
Security Classification

14 KEY WORDS	LINK A		LINK B		LINK C	
	ROLE	WT	ROLE	WT	ROLE	WT
Concrete hulls						
Spherical hulls						
Ocean bottom habitations						
Critical pressure						
Water permeation rates						
Hydrostatic loading						

R 753

Technical Report

POLYMER-IMPREGNATED CONCRETE SPHERICAL HULLS UNDER HYDROSTATIC LOADING

December 1971

Sponsored by

NAVAL FACILITIES ENGINEERING COMMAND

NAVAL CIVIL ENGINEERING LABORATORY

Port Hueneme, California 93043

POLYMER-IMPREGNATED CONCRETE SPHERICAL HULLS UNDER HYDROSTATIC LOADING

Technical Report R-753

3.1610-1

by

H. H. Haynes and N. D. Albertsen

ABSTRACT

Eight spherical models with outside diameters of 16 inches and wall thicknesses of 1 or 2 inches were fabricated of polymer-impregnated concrete (PIC) having a uniaxial compressive strength of 21,000 psi. The spherical specimens were tested under hydrostatic loading conditions of short-term, long-term, and cyclic pressure. The test results show that the PIC spheres respond to hydrostatic loading with linearly elastic behavior and that the implosion pressures are greater by approximately 40% than those for similar regular-concrete spheres. Under short-term loading the specimens having a wall-thickness-to-outside-diameter ratio of 0.063 and 0.125 (1- or 2-inch walls to 16-inch OD) implode at average hydrostatic pressures of 4,810 and 8,475 psi, respectively. Classical elastic theory predicts the strain behavior and implosion pressures of the PIC sphere within engineering accuracy.

CONTENTS

INTRODUCTION

The United States Navy and the United States Atomic Energy Commission (AEC) cosponsored this experimental program to investigate polymer-impregnated concrete (PIC) as a construction material for deep-ocean pressure-resistant structures. Polymer-impregnated concrete warranted investigation because its compressive strength, impermeability, and durability are greater than those of regular concrete. The Naval Civil Engineering Laboratory (NCEL) has been studying for the past 5 years the behavior of regular-concrete structures subjected to hydrostatic loading;[1-5] a natural extension to NCEL's research was to study PIC structures for underwater applications. The Division of Isotopes Development, AEC, has been promoting the development of PIC materials since the original concept was presented to them in 1965; their contribution to this research effort was to support the Brookhaven National Laboratory (BNL) in performing the impregnation and polymerization of the concrete test specimens.

The primary objective of the program was to experimentally investigate the structural behavior of PIC spheres subjected to various hydrostatic loadings and to determine tentatively the maximum operational depth for buoyant PIC spheres. A secondary objective was to compare PIC and regular-concrete materials when used in underwater structures.

Polymer-Impregnated Concrete (PIC)

Polymer-impregnated concrete (PIC) is precast portland cement concrete impregnated with a monomer system (plastic in a liquid or gaseous state) which is subsequently polymerized in situ. The resulting polymer system (plastic in a solid state) fills much of the voids in the concrete and, in so doing, acts both as a filler and a binder between cement paste and aggregate to improve the properties of the concrete. In general, the procedure employed to produce PIC materials is: precast, mature concrete is dried to constant weight; then the specimen is evacuated to remove air from the voids and soaked in a low viscosity liquid monomer until constant weight is attained. The specimen is wrapped in a vapor barrier to reduce evaporation

and finally placed in a chamber to polymerize the monomer. The two methods used most extensively to polymerize the monomer are gamma radiation from a cobalt 60 source and thermal catalytic processes.

Numerous monomer systems and their effect on the mechanical and physical properties of concrete have been investigated.[6-8] Compressive strengths greater than 20,000 psi and tensile strengths of 1,600 psi were obtained along with significant improvements in the durability properties; for example:

- Freeze–thaw durability increases of greater than 400%
- Chemical attack by sulfate brines reduced to negligible values
- Water permeability reduced to negligible values

Development work on PIC materials is in the early stages. Advances in PIC technology can be expected to improve further the properties of the material and to simplify the manufacturing techniques.

Pressure-Resistant Concrete Structures

Research at NCEL on the behavior of pressure-resistant concrete structures has been directed toward studying the response of the structure and the concrete material under hydrostatic pressure. The main objective of the research has been to develop the technology and design criteria necessary to accurately and safely utilize concrete as an underwater construction material for pressure-resistant structures.

Spherical and cylindrical model specimens have been tested; the major effort to date has been investigating spherical hulls having a 16-inch outside diameter and wall thicknesses of 1, 2, 3, or 4 inches. Test results have shown two stages of failure for the concrete spheres—development of cracks in the plane of the wall parallel to the major principal stresses, followed by implosion failure. Figure 1 compares graphically the pressures at in-plane cracking and implosion failure.[4]

TEST PROGRAM

Scope of Investigation

Eight 16-inch-OD spheres were tested under hydrostatic loading—six specimens had a 1-inch wall thickness and two specimens had a 2-inch wall thickness. Two types of monomers were used to make the polymer-impregnated

concrete: diallyl phthalate (DAP) which was polymerized by using a thermal catalytic process, and methyl-methacrylate (MMA) which was polymerized by using gamma radiation from a cobalt 60 source.

One of the 1-inch-thick specimens had an aluminum joint located at the equator which allowed the sphere to be separated into halves. The other specimens had a thin epoxy joint, approximately 1/32-inch thick, which bonded the two hemispheres together.

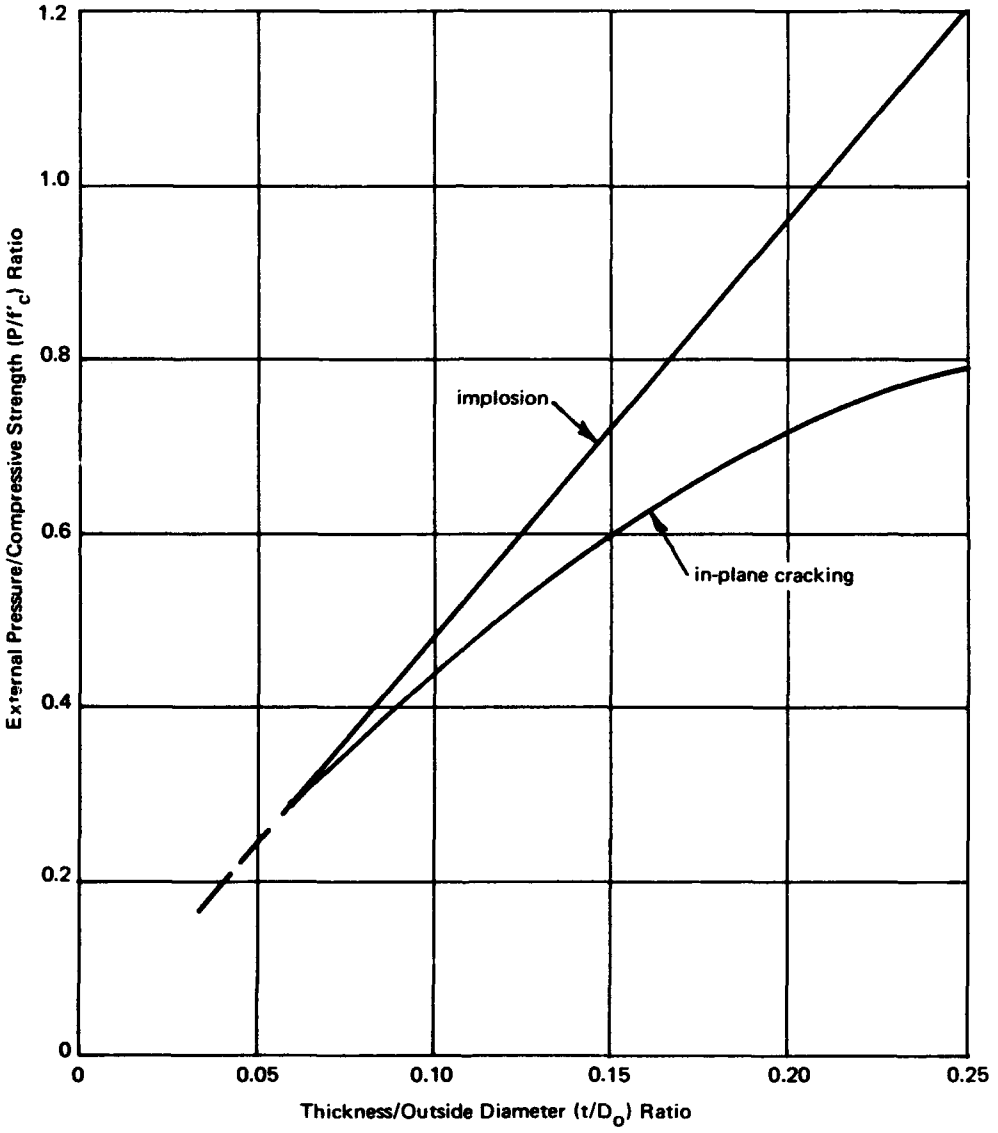

Figure 1. Comparison of failure modes for regular-concrete spheres subjected to hydrostatic loading.

Short-term, long-term, and cyclic hydrostatic loading conditions were imposed on different specimens in an effort to obtain data on the response of the PIC material to loading conditions which a real structure might undergo. Emphasis was placed on short-term tests so that comparisons in behavior could be made with existing data for regular-concrete spheres. The testing program is outlined in Table 1.

Table 1. Test Program

(Outside diameter of sphere was 16 inches.)

Sphere Description	Wall Thickness (in.)	Type of Monomer[a]	Monomer Load[b] (% by wt)	Type of Joint	Loading Condition
A	1	DAP	8.4	epoxy	short-term
B	1	DAP	7.9	epoxy	short-term
I	1	MMA	6.4	epoxy	short-term
C	2	DAP	9.0	epoxy	short-term
D	2	DAP	8.8	epoxy	short-term
F	1	DAP	8.0	aluminum	short-term
G	1	DAP	8.6	epoxy	long-term
H	1	DAP	8.0	epoxy	cyclic

[a] DAP = diallyl phthalate; 16.5-centipoise viscosity
MMA = methyl-methacrylate; 0.5-centipoise viscosity

[b] Average of two hemispheres.

Fabrication of Specimens

Fabrication of the specimens consisted of casting concrete hemispheres, curing the concrete, impregnating the concrete with a monomer to create polymer-impregnated concrete, and then joining together two hemispheres to form a sphere.

The concrete mix design given in Table 2 was the same as used in past studies on regular-concrete spheres. The concrete was moist-cured for the first 28 days and then stored at room conditions (for approximately 2 years) before it was impregnated with a monomer.

Six 3 x 6-inch control cylinders were cast with each hemisphere and cured under the same conditions as the hemisphere. Three control cylinders were used to obtain regular-concrete properties, and the other three cylinders were impregnated along with the hemisphere to obtain the PIC properties.

Even though the monomer impregnation and polymerization procedures (Table 3) were different for the DAP and MMA specimens, few problems were encountered in completely impregnating the concrete with either monomer. One problem encountered with the MMA impregnation procedure was that the monomer evaporated from the surface prior to polymerization. This resulted in a nonuniform monomer load in the wall of the hemispheres—the middle of the wall was completely impregnated, but the inner and outer wall surfaces had an 1/8-inch-thick layer that was lightly impregnated. Hemispheres 855B and 874B (sphere I) were re-impregnated in an attempt to raise the monomer load at the surfaces; the implosion results indicate the re-impregnation was successful. Subsequent to this experience, the monomer type was changed to DAP which is a less volatile monomer. Figure 2 shows a hemisphere section after impregnation with DAP.

Sphere F, which had a 1/4-inch-thick aluminum joint at the equator, is shown in Figure 3; Figure 4 is a cross-sectional view of the joint. The surface of the aluminum joint that mates with the concrete was beveled toward the center of the sphere at an included angle of $1^{\circ}50'$. The mating surfaces of the PIC hemispheres were machined to match the angle of the joint.

Each specimen, except for sphere I which had only two interior gages, was instrumented with at least 12 electrical resistance strain gages which were applied to the exterior and interior surfaces of one hemisphere. Figure 5 shows the typical gage layout.

Table 2. Concrete Mix Design

Water/cement ratio = 0.55 by weight

Aggregate/cement ratio = 3.30 by weight

San Gabriel River wash aggregate

Type III portland cement

Screen No.		Percent Retained
Passing	Retained	
4	8	29.6
8	16	20.8
16	30	14.7
30	50	10.3
50	100	7.3
100	pan	17.3

Table 3. Monomer Impregnation and Polymerization Procedure

Step in Process	Method Used for—	
	DAP Monomer	MMA Monomer
Drying of concrete	Oven dried to constant weight at 150°C	Oven dried to constant weight at 90°C
Evacuation of concrete	2 hr at a vacuum of 29 inches mercury	2 hr at a vacuum of 29 inches mercury
Monomer soak	16 hr at 20 psig	2 hr at 10 psig
Polymerization	Thermal-catalytic; 5% (by wt) of *t*-butyl perbenzoate catalyst; 110°C for 24 hr, plus 150°C for 150 hr	Gamma radiation from a 60 cobalt source; 250,000 rad/hr for 22 hr; total dose of 5.5×10^6 rad

Figure 2. Appearance of concrete hemisphere after impregnation with DAP monomer.

Figure 3. Assembly of sphere F with an aluminum joint.

Test Procedure

The specimens were tested under hydrostatic loading using freshwater as the pressure medium in NCEL's 18-inch-ID pressure vessel. Figure 6 shows a specimen attached to the pressure vessel head with a tubular steel penetrator vented outside the vessel. All the strain gage lead wires passed through this penetrator for hookup to data recording instruments.

Regardless of the type of test, pressure was applied to or removed from the specimen at a constant rate of 100 psi/min. Implosion of the specimen was easily noted by a sharp noise and instantaneous pressure drop.

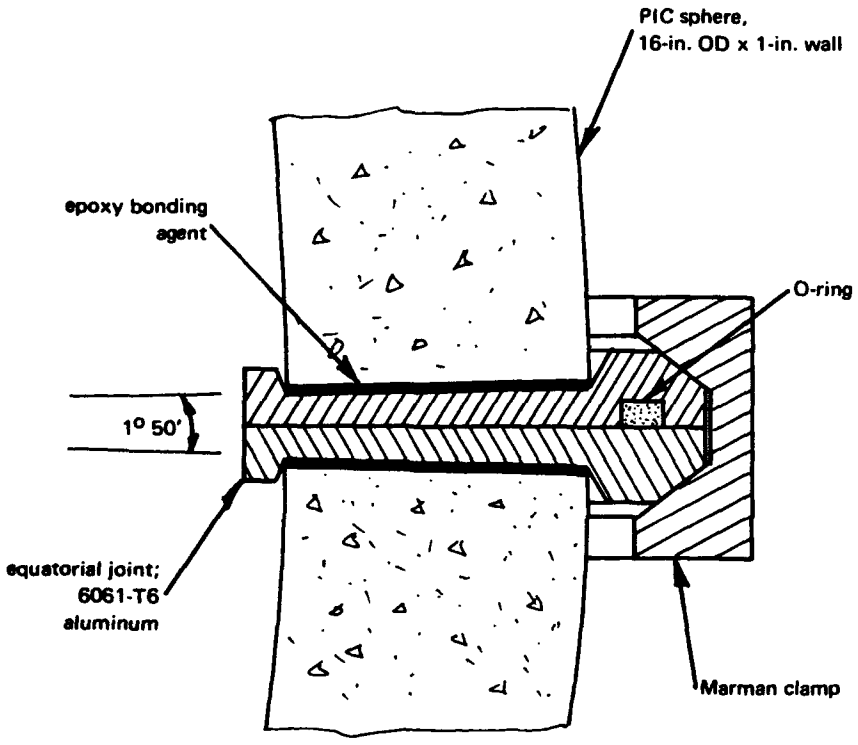

Figure 4. Cross-sectional view of aluminum joint.

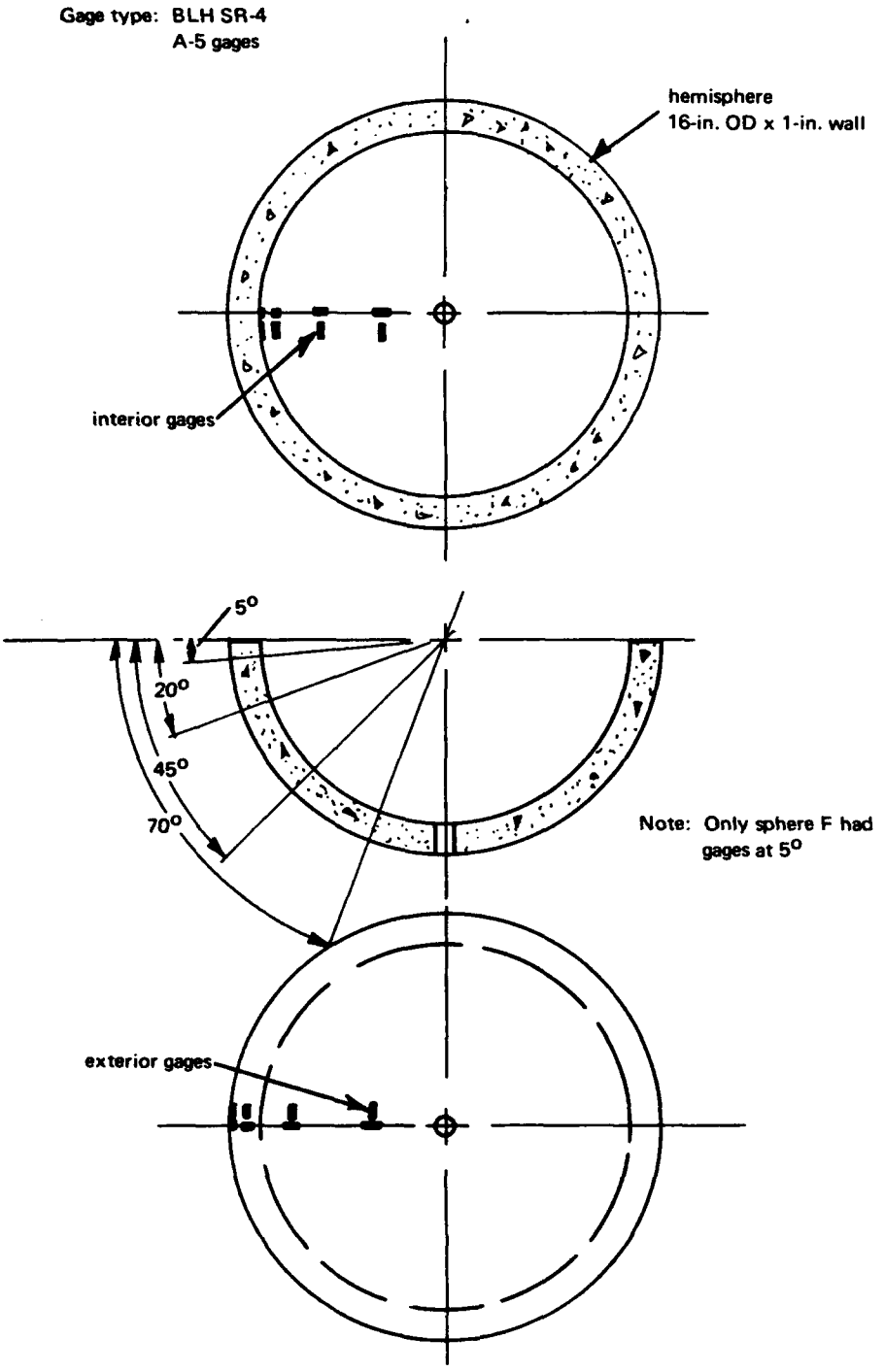

Figure 5. Typical strain gage layout for spheres.

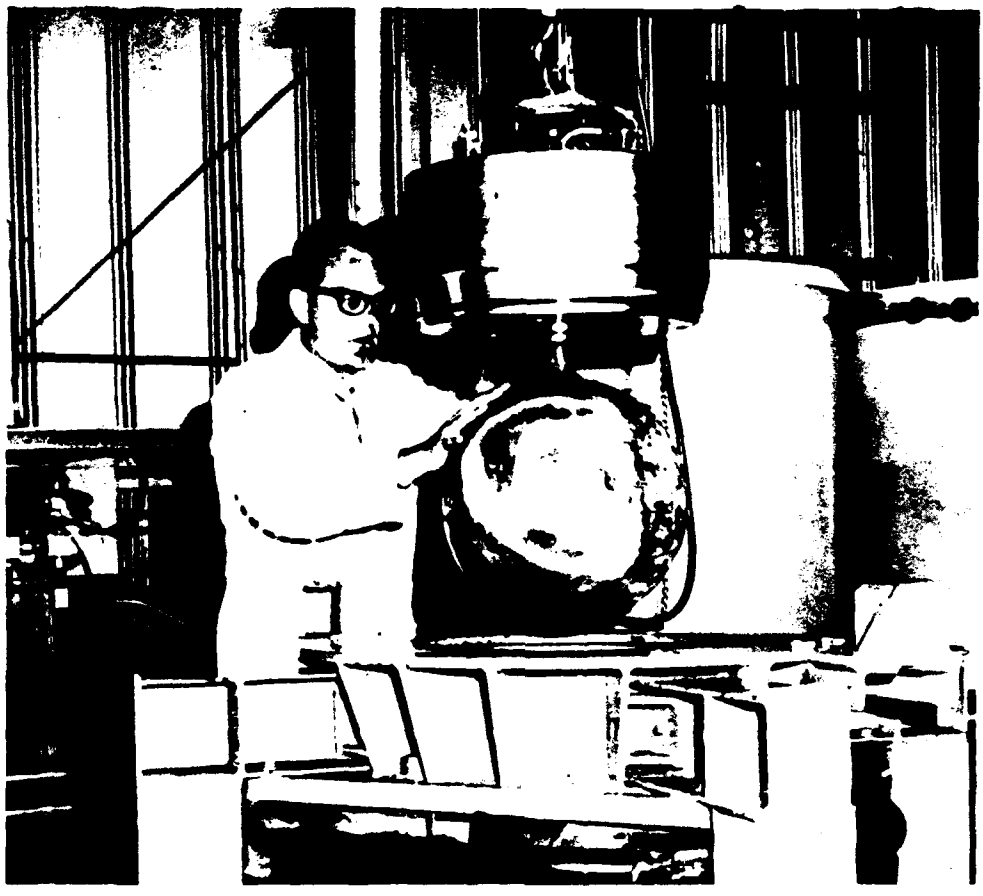

Figure 6. Specimen prepared for test in pressure vessel.

TEST RESULTS

Control Cylinder Tests

PIC and regular-concrete control cylinders were tested under uniaxial compression to determine compressive strength, modulus of elasticity and Poisson's ratio. Table 4 summarizes the results obtained from the 3 x 6-inch control cylinders. On the average, the PIC specimens contained 8.4% by weight DAP monomer, and exhibited an average compressive strength of 20,970 psi and a modulus of elasticity of 5.34×10^6 psi; these values were increases of 121 and 52%, respectively, over those of the regular-concrete control specimens. Poisson's ratio was found to be approximately the same, 0.17, for the PIC and regular-concrete specimens.

A typical stress–strain relationship for PIC and regular concrete is shown in Figure 7. These curves show the nearly linear behavior of PIC in comparison to the nonlinear behavior of regular concrete. The PIC material consistently showed elastic, brittle behavior under uniaxial compression.

Table 4. Test Data for 3 x 6-Inch Control Cylinder

Sphere Designation	Hemisphere No.	Type of Monomer	Monomer Load (% by wt)	Polymer-Impregnated Concrete			Regular Concrete			Increase in Compressive Strength (%)	Increase in Modulus of Elasticity (%)
				Compressive[a] Strength, f'_{PIC} (psi)	Modulus of[b] Elasticity, E (psi x 10^6)	Poisson's[b] Ratio, ν	Compressive[a] Strength, f'_c (psi)	Modulus of[b] Elasticity, E (psi x 10^6)	Poisson's[b] Ratio, ν		
A	724C	DAP	8.2	21,550	5.16	0.16	9,750	–	–	121	–
	730C		8.7	20,960	4.76	0.23	9,940	–	–	111	–
B	725C	DAP	8.4	22,350	5.10	0.19	10,000	–	–	123	–
	731C		7.5	23,070	6.70	0.20	11,220	–	–	106	–
I	855B	MMA	6.7	20,060	7.50	0.27	8,740	3.80	0.17	130	97
	874B		6.1	21,300	7.10	0.23	8,740	3.80	0.17	144	87
C	963B	DAP	9.0	21,200	4.82	0.13	8,110	3.00	0.17	161	61
	966B		9.1	21,000	5.19	0.21	8,720	3.35	0.24	141	55
D	435C	DAP	9.0	19,950	5.00	0.16	9,200	3.62	0.14	117	38
	967B		8.7	20,000	4.53	0.14	8,070	2.79	0.12	148	62
F	721C	DAP	7.8	20,800	5.36	0.14	10,050	–	–	107	–
	735C		8.2	20,500	5.72	0.19	10,050	–	–	104	–
G	850B	DAP	8.5	20,900	5.24	0.13	8,600	3.80	0.15	143	38
	890B		8.7	22,900	6.00	0.19	8,920	3.95	0.20	157	52
H	738C	DAP	8.0	20,900	5.44	–	10,350	4.05	–	102	34
	751C		8.1	17,500	5.35	0.23	9,740	–	–	80	–

[a] Average of three specimens.

[b] One specimen.

Short-Term Tests

Spheres A, B, I, C, and D were tested under short-term hydrostatic loading by applying pressure at a constant rate until implosion occurred; the implosion pressures for these spheres are given in Table 5.

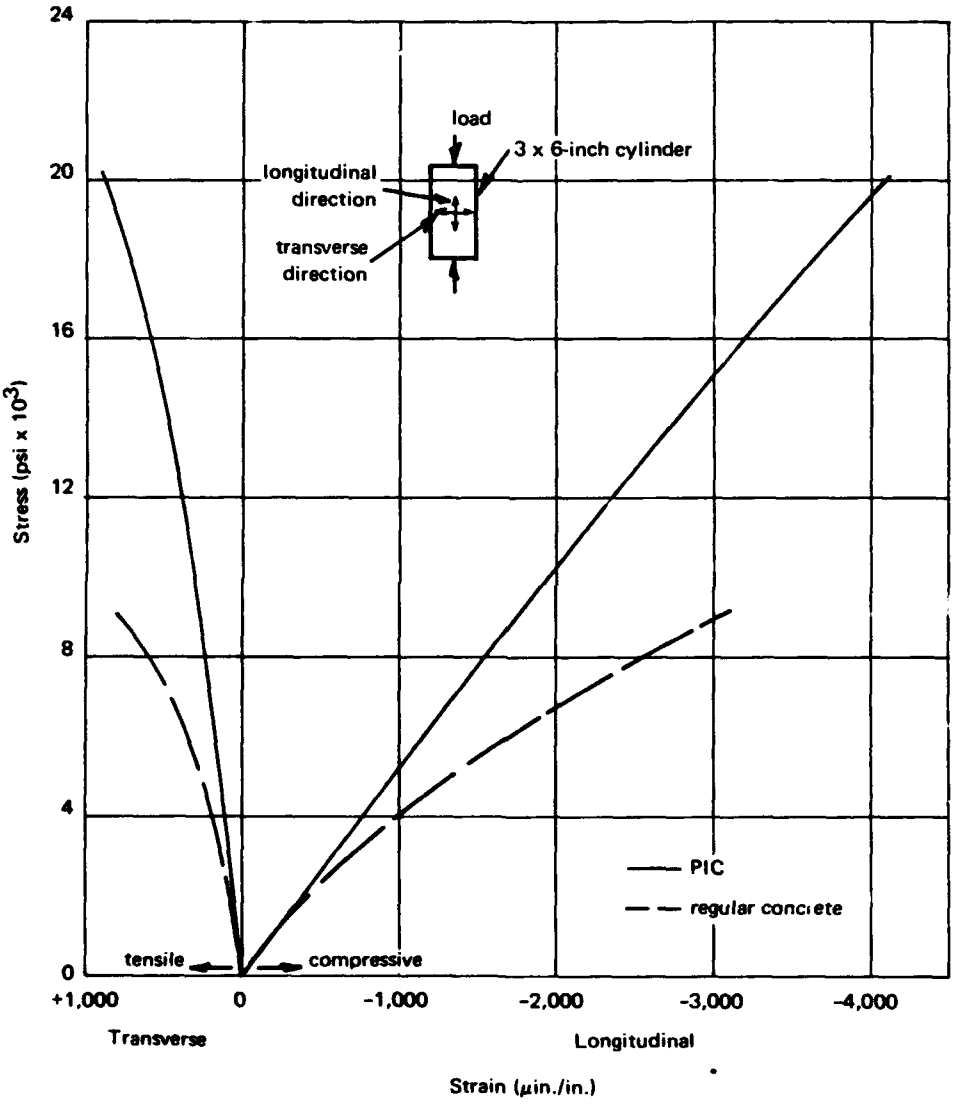

Figure 7. Typical stress–strain relationship for PIC and regular-concrete control cylinders under uniaxial compression.

Table 5. Implosion Results

Sphere Designation	Loading Condition	Wall Thickness (in.)	Uniaxial Compressive Strength, f'_{PIC} (psi)	Implosion Pressure, P_{im} (psi)	P_{im}/f'_{PIC}
A	short-term	1	20,960	4,670	0.222
B	short-term	1	22,350	5,065	0.226
I	short-term	1	20,060	4,700	0.234
C	short-term	2	21,000	8,750	0.417
D	short-term	2	19,950	8,200	0.411
F	short-term	1	20,500	4,130	0.202
G	long-term	1	20,900	4,000	0.191
H	cyclic	1	17,500	4,000	0.228

The average strain performance of the 1-inch-thick specimens, spheres A, B, and I, is shown in Figure 8 along with the performance of a previously tested regular-concrete sphere.[1] These curves show the striking differences in behavior between the PIC and regular-concrete spheres. One significant difference was the linear response of the PIC spheres to increasing hydrostatic pressure as opposed to the typical nonlinear behavior of regular concrete. Another difference was the pressure at which PIC spheres imploded—an average pressure of 4,810 psi. This was 43% higher than regular-concrete spheres, whose implosion pressure was predicted from an empirical equation developed in Reference 4.

The 2-inch-thick PIC specimens, spheres C and D, imploded at an average pressure of 8,475 psi, which was an increase of 36.5% over regular concrete. The strain performance of these spheres is shown in Figure 9; again the linear pressure–strain behavior was prevalent.

Sphere C unintentionally underwent two load cycles. The first cycle reached 84% of the actual implosion pressure before the pressure accidently decreased to zero at a rate of approximately 5,000 psi/min because of mechanical difficulties with the pressure vessel equipment. After a 10-minute delay, the second cycle was commenced and progressed to the implosion level. The slope of the pressure–strain curve for the second cycle increased approximately 7% over that of the first cycle. Also, during the second cycle the slope of the curve increased slightly with load up to implosion; in other words, the sphere became slightly stiffer with increased load.

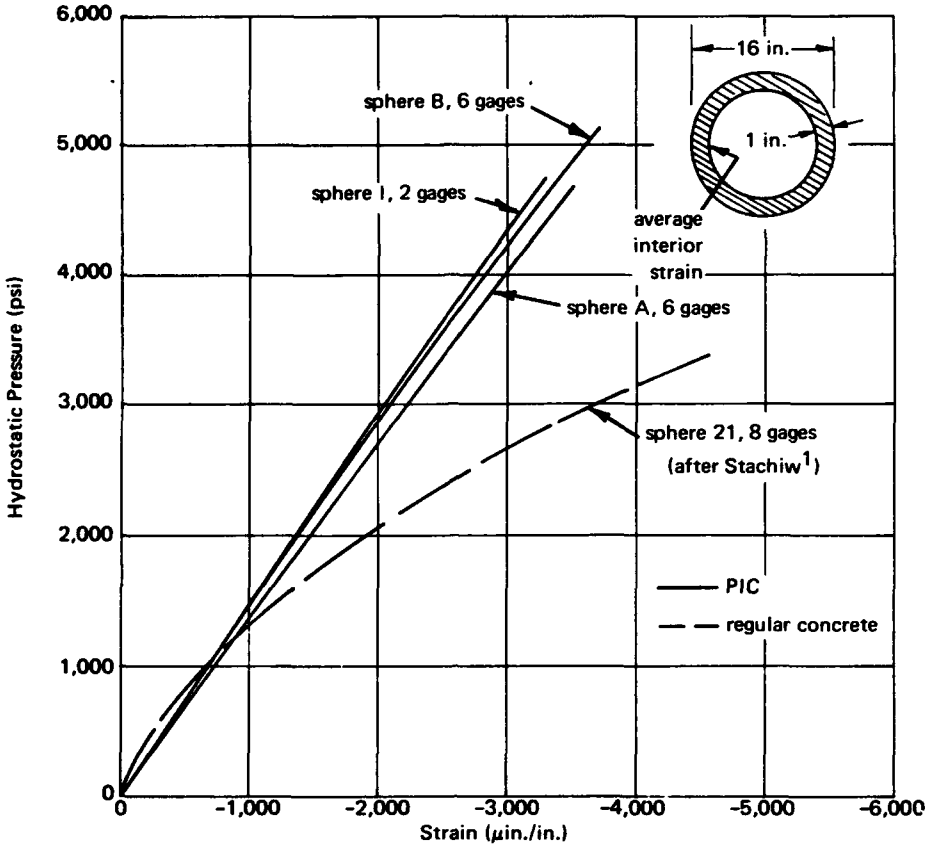

(a) Interior.

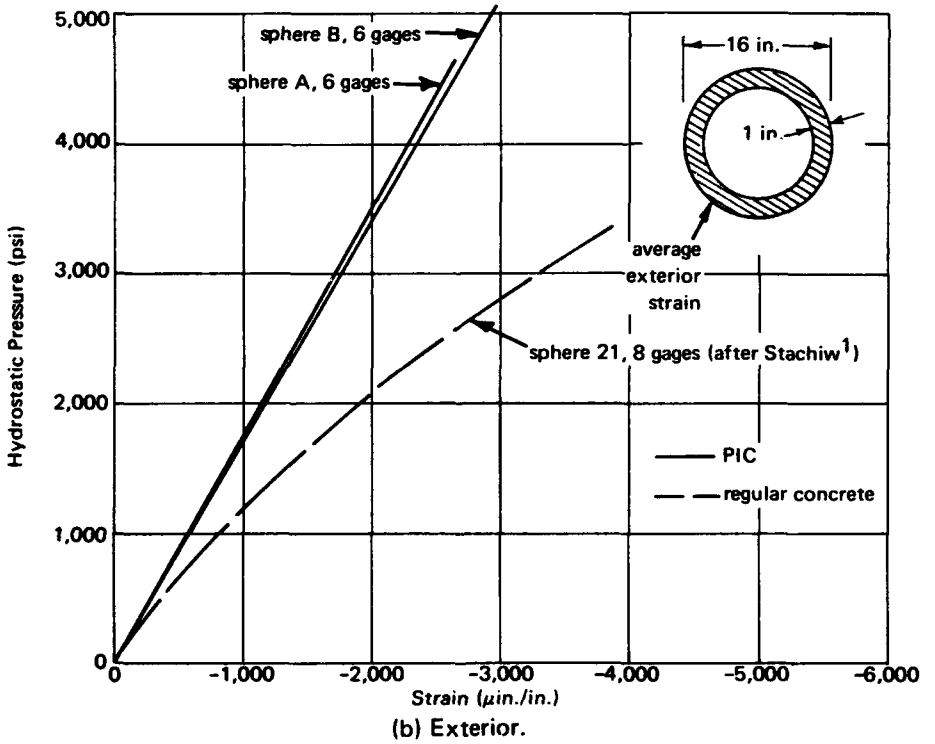

(b) Exterior.

Figure 8. Strain behavior of spheres subjected to short-term loading; $t/D_o = 0.063$.

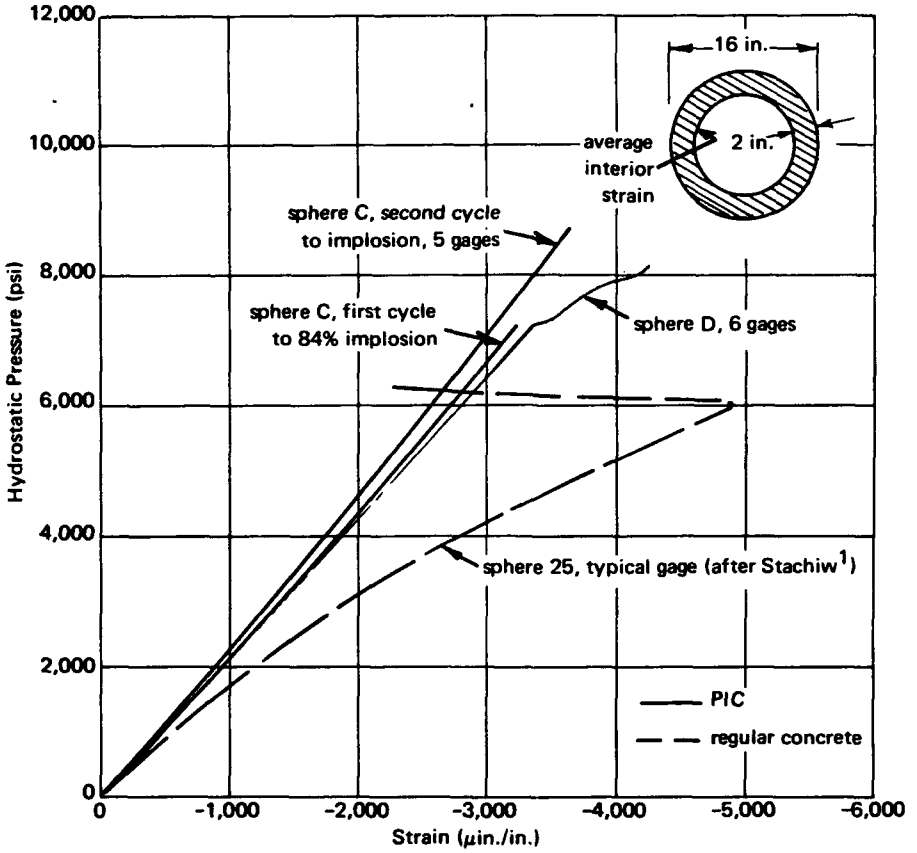

(a) Interior.

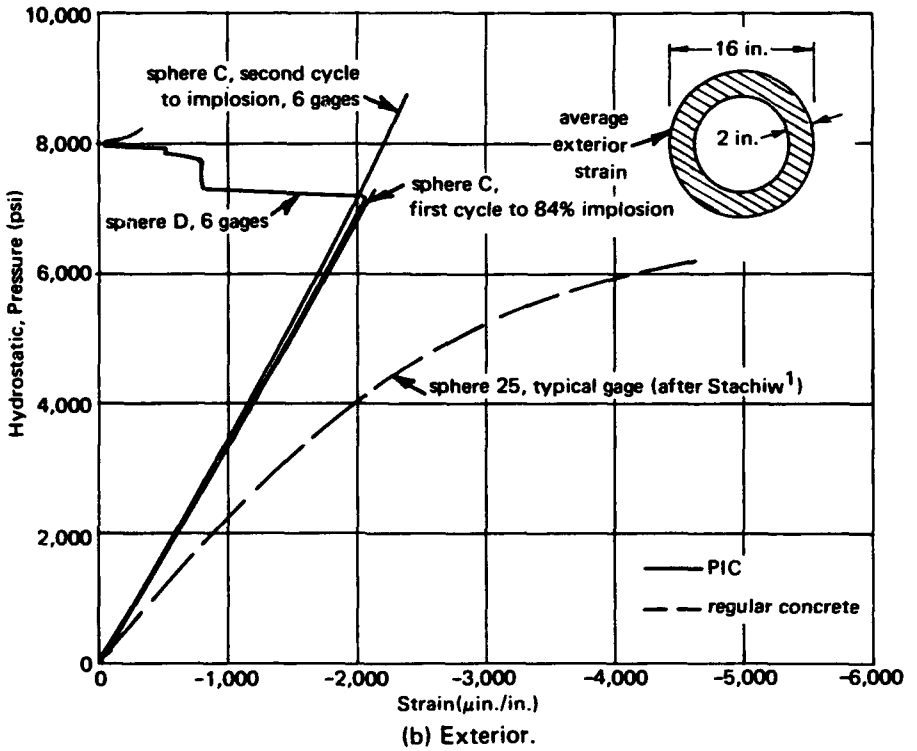

(b) Exterior.

Figure 9. Strain behavior of spheres subjected to short-term loading; $t/D_o = 0.125$.

Sphere D exhibited in-plane cracking* similar to regular-concrete spheres,[4] except cracking began at or near the exterior surface whereas the regular-concrete spheres cracked near the interior surface. The pressure at initiation of in-plane cracking, P_{pl}, was taken at the pressure where the strains (interior or exterior) were maximum before decreasing in value; for sphere D, P_{pl} was 7,200 psi. Figure 10 shows a fragment of sphere D after implosion which portrays these cracks. It was apparent from studying the individual gage data, Figure 11, that the in-plane cracks developed near the epoxy joint and propagated away from the joint. A plausible explanation for in-plane cracking is that the epoxy material at the joint is under a compressive stress of approximately 19,000 psi; at such high compressive stresses the tangent modulus of elasticity for epoxies is known to be quite low. The epoxy would

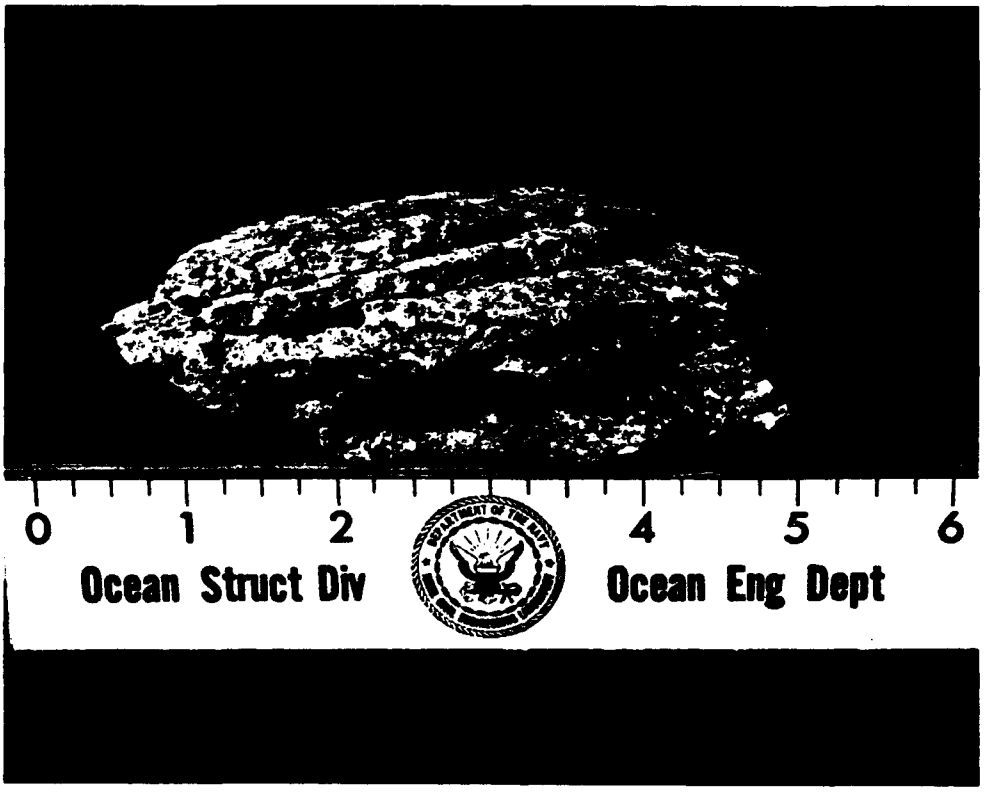

Figure 10. Fragment of sphere D showing in-plane cracks.

* In-plane cracking is the development of cracks in the concrete wall parallel to the major principal stresses, hence, cracking "in-the-plane" of the wall.

tend to extrude from the joint and, in so doing, would create tensile radial strains; these would add to the "normal" tensile strains already existing in the wall (300 μin./in. at 7,200 psi according to elastic theory). Thus, in-plane cracks could begin at the joint near the exterior wall as found in sphere D or near the interior wall as found in regular-concrete spheres.

Table 6 compares the uniaxial compressive strength, f'_{PIC}, of PIC control cylinders with the calculated interior wall stress at implosion, σ_{im}, for the PIC spheres. The interior surface of the spheres was under biaxial loading conditions where the tangential stresses were equal and the radial stress was zero. The tangential wall stress at implosion increased approximately 4% over the uniaxial compressive strength; this was a small increase compared to that of regular concrete which increased approximately 35%.[4] Hence, the PIC material did not show the improved strength under biaxial loading that was characteristic of regular concrete.

Table 6. Tangential Wall Stress at Implosion

Sphere Designation	Wall Thickness (in.)	Uniaxial[a] Compressive Strength, f'_{PIC} (psi)	Stress at Implosion, σ_{im} (psi)	σ_{im}/f'_{PIC}
A	1	20,960	21,250[b]	1.01
B	1	22,350	23,045[b]	1.03
I	1	20,060	21,385[b]	1.07
C	2	21,000	22,750[b]	1.08
D	2	19,950	18,720[c]	0.94

[a] For 3 x 6-inch control cylinders corresponding to the weaker hemisphere in the sphere.

[b] On interior wall of sphere; calculated using elastic theory, Equation 2.

[c] At in-plane cracking; calculated using Equation 2.

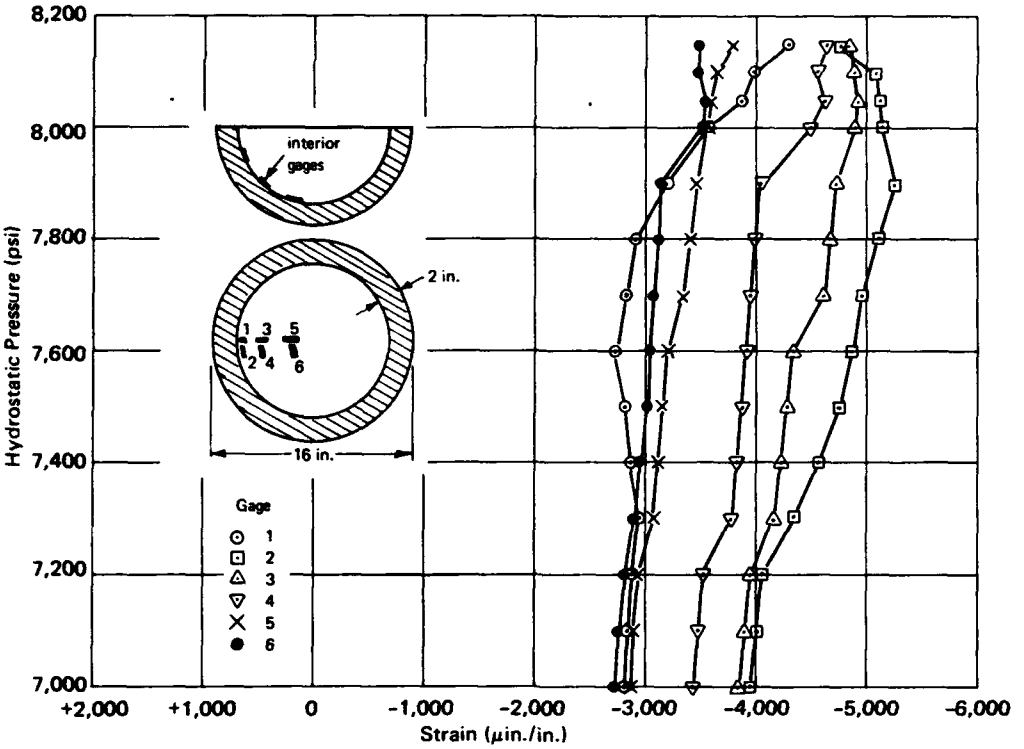

(a) Interior gages.

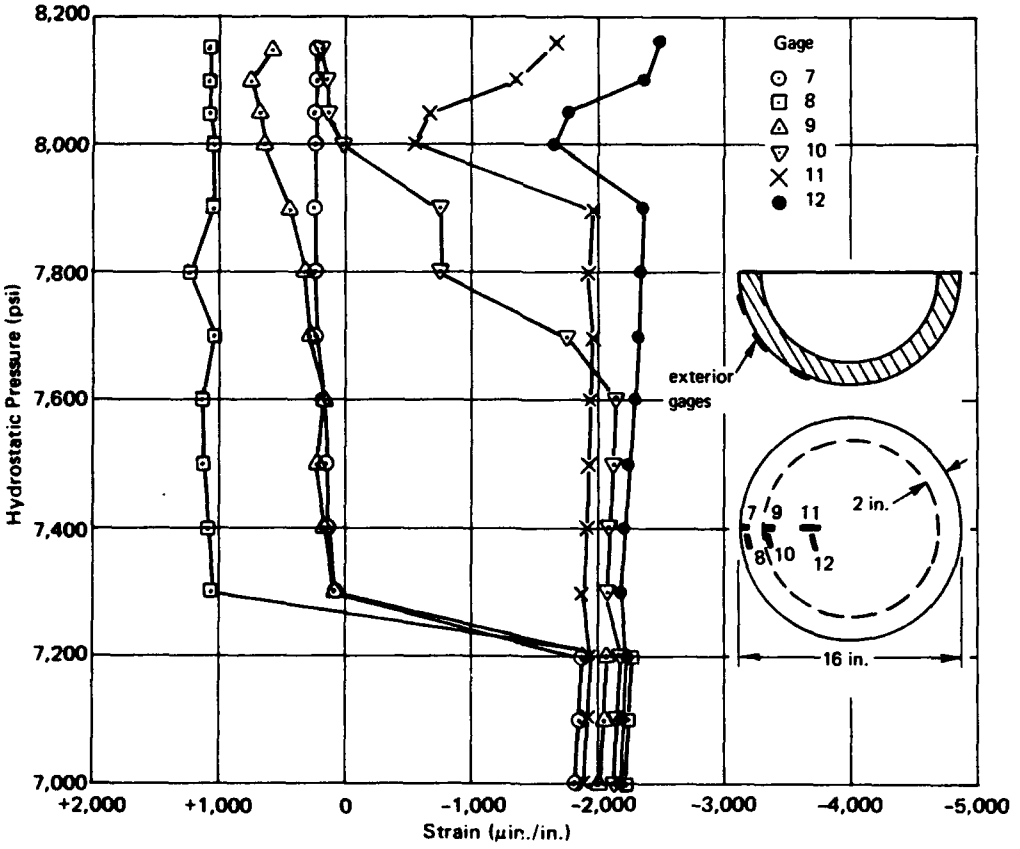

(b) Exterior gages.

Figure 11. Behavior of individual gages at in-plane cracking of sphere D.

Long-Term Test

Sphere G was tested under long-term loading where the pressure load was held constant for 100-hour periods at successively increasing 1,000-psi increments. Implosion occurred 3 minutes after reaching the 4,000-psi level; this pressure was 82% of the average implosion pressure for PIC spheres tested under short-term loading.

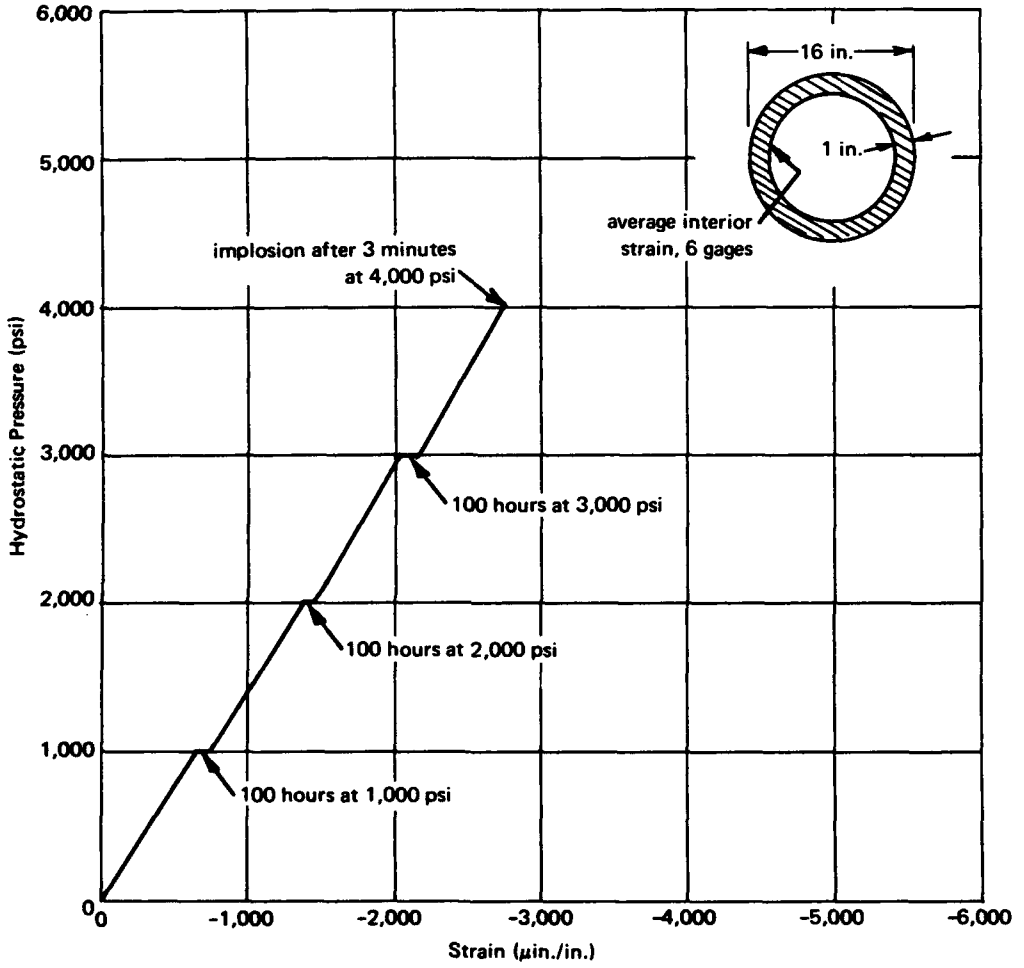

Figure 12. Interior strain versus hydrostatic pressure for sphere G under long-term loading; $t/D_o = 0.063$.

Figure 12 shows the strain performance of the specimen under the long-term loading sequence as a function of hydrostatic pressure. The specimen exhibited linear strain behavior between the constant pressure levels, and the secant slope to failure of the pressure–strain curve was almost identical to that exhibited by the PIC specimens under short-term loading. In addition,

the slope of the pressure—strain curve between sustained pressure levels became slightly steeper with higher pressure, indicating that the polymer-impregnated concrete became stiffer with time under load.

Figure 13 shows the strain performance of the specimen under long-term loading as a function of time. At 3,000 psi the specimen showed an increase in creep strain of approximately 100 μin./in. for the 100-hour duration of the load. Previous studies on similar regular-concrete spheres[1] indicated that sustained pressure loads of 1,500 psi produced several times this amount of creep strain for the same time interval.

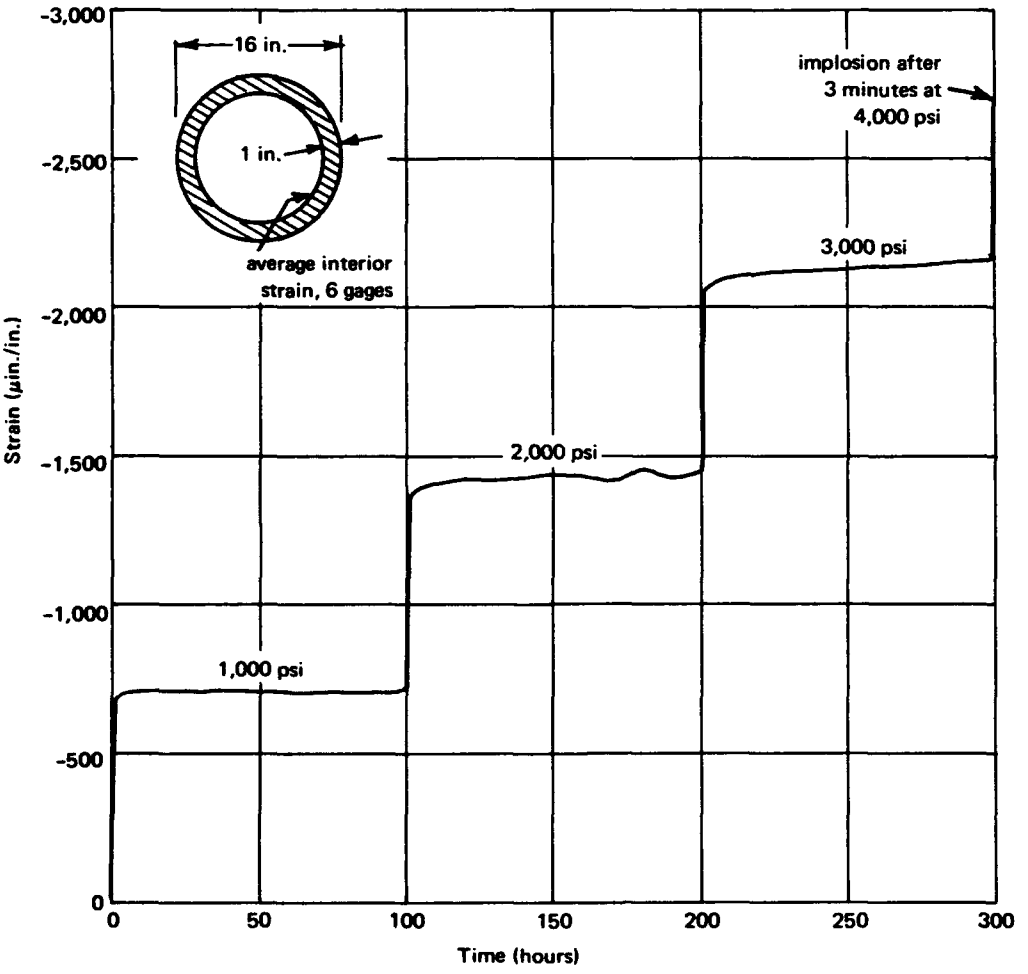

Figure 13. Interior strain versus time for sphere G under long-term loading; $t/D_o = 0.063$.

Cyclic Test

Sphere H was tested under cyclic loading where the pressure load was held constant for 50 hours followed by zero pressure for 50 hours at successively increasing 1,000-psi increments. The test simulated a set of placement–retrieval cycles that a structure might undergo during actual operating conditions.

Figure 14 shows the average interior and exterior strain performance of the specimen under cyclic loading as a function of hydrostatic pressure. These figures again illustrate the linear strain behavior of PIC spheres and the small amount of creep strain at each load level. Also, when the load was decreased at the rate of 100 psi/min, the sphere responded with linearly diminishing strain until, at zero load, the strain values were near zero. This behavior indicates that PIC is an elastic material which recovers from sustained loading with only small residual effects. In contrast, Figures 15 and 16 show that a regular-concrete sphere responded to one cycle of 67 hours at 3,000 psi with approximately 600 μin./in. of residual compressive strain.

Figure 17 illustrates the average interior and exterior strain performance of sphere H as a function of time. These figures show that during the no-load portion of each cycle the sphere displayed strain recovery into the positive strain range. This phenomenon, which has been observed by other investigators studying PIC materials, is not fully understood, but a proposed hypothesis is that an applied stress may induce a monomer phase change which results in an increased unit volume.[6]

Implosion of sphere H occurred after 15 minutes at 4,000 psi, which was the same implosion pressure and nearly the same time to implosion as that experienced in the long-term test, sphere G. This indicates that differences in extended loading conditions may have little effect on the implosion strength of the specimens—a quality which will be important to structures in actual use because of the implied predictability of the PIC material.

Although no direct measurements of the hull's watertightness were taken, a reliable indicator of watertightness is the degree to which the external pressure remains constant during a sustained load period. For both spheres G and H the indications were that the hulls were highly watertight.

Test of Sphere With Aluminum Joint

Sphere F with a mechanical aluminum joint located at the equator was tested under short-term loading to determine the effect of the joint on the behavior of the sphere.

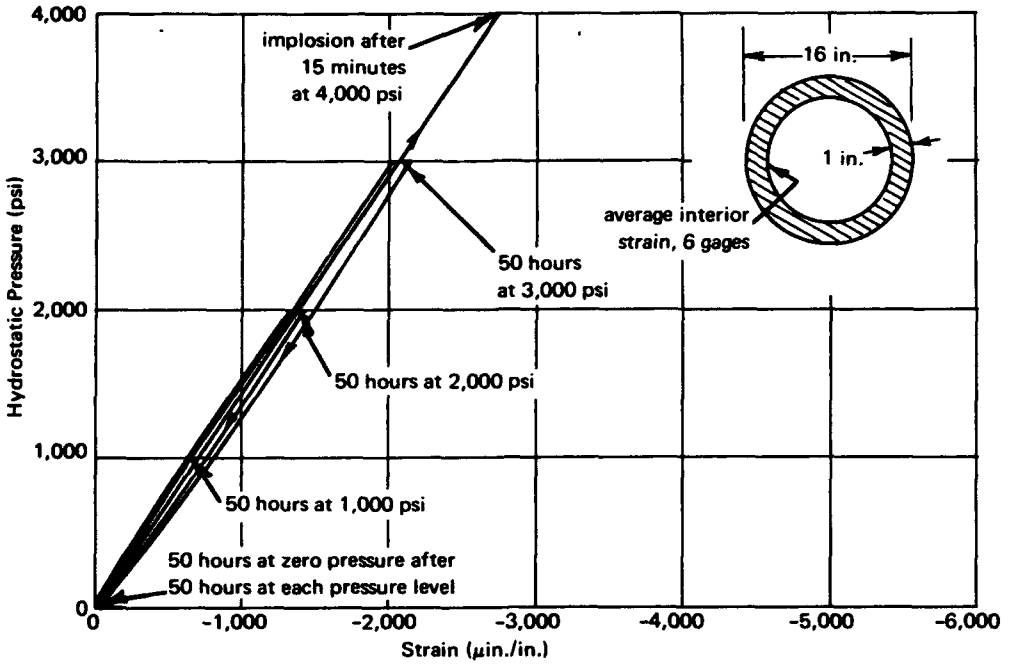

(a) Interior.

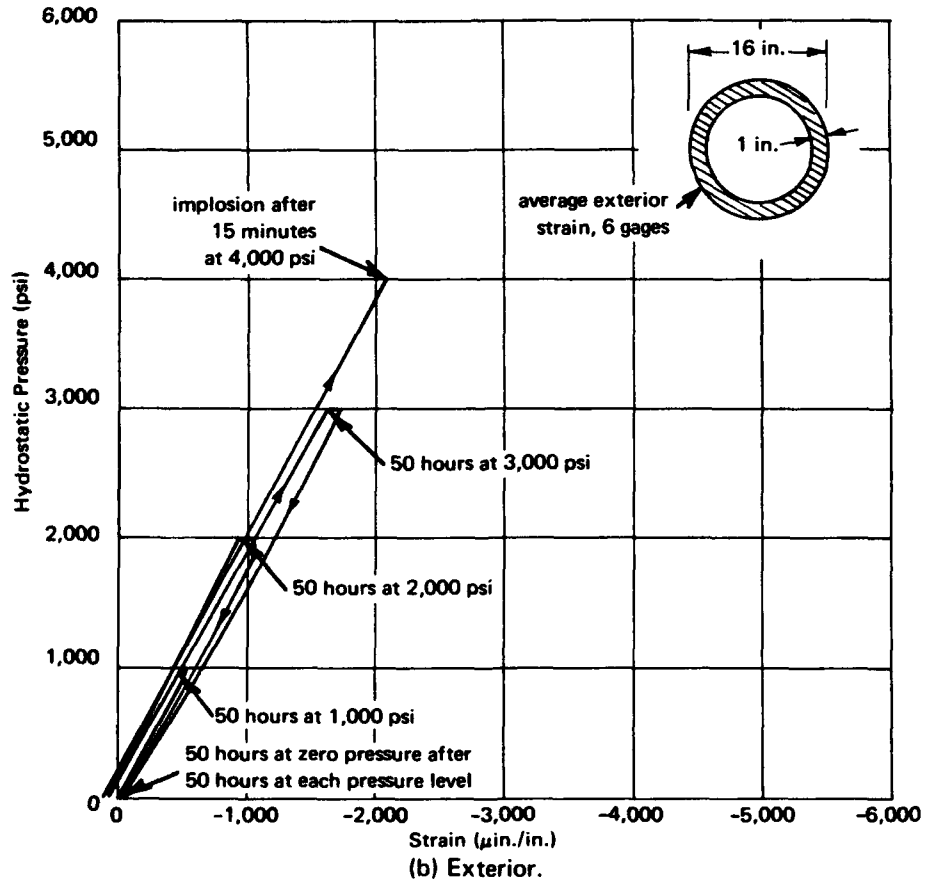

(b) Exterior.

Figure 14. Strain behavior of sphere H under cyclic loading; $t/D_o = 0.063$.

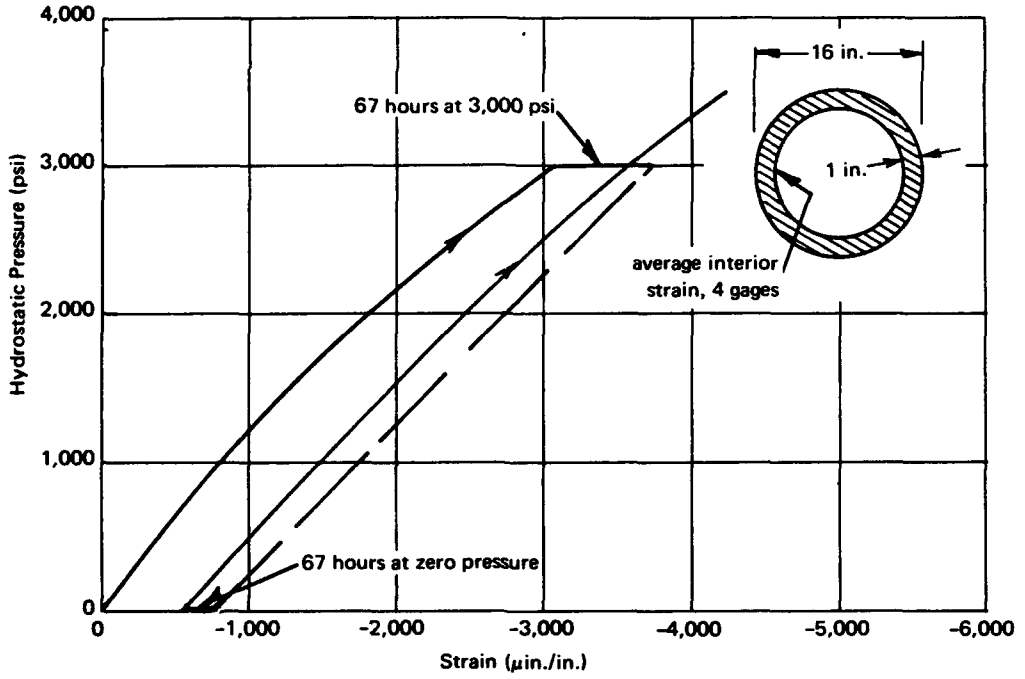

Figure 15. Interior strain versus hydrostatic pressure for a regular-concrete sphere[1] under cyclic loading; $t/D_o = 0.063$.

The implosion pressure for sphere F was 4,130 psi; this pressure was 86% of the average implosion pressure for the PIC spheres (A, B, and I) with a thin epoxy joint. Figure 18 shows that the decrease in implosion pressure due to the presence of the joint compared reasonably well to that of regular-concrete spheres with joints of similar relative stiffnesses.[9] Relative stiffness of a joint was defined as:

$$R = \frac{E_r A_r}{E_c A_c}$$

where R = relative stiffness

E_r = modulus of elasticity of ring joint material (psi)

A_r = cross-sectional area of ring joint (in.^{2})

E_c = secant modulus of elasticity of concrete (or PIC) to $\frac{1}{2} f'_c$ (psi)

A_c = area of concrete replaced by the ring joint (in.^{2})

The aluminum joint used on sphere F had a relative stiffness of 3.80.

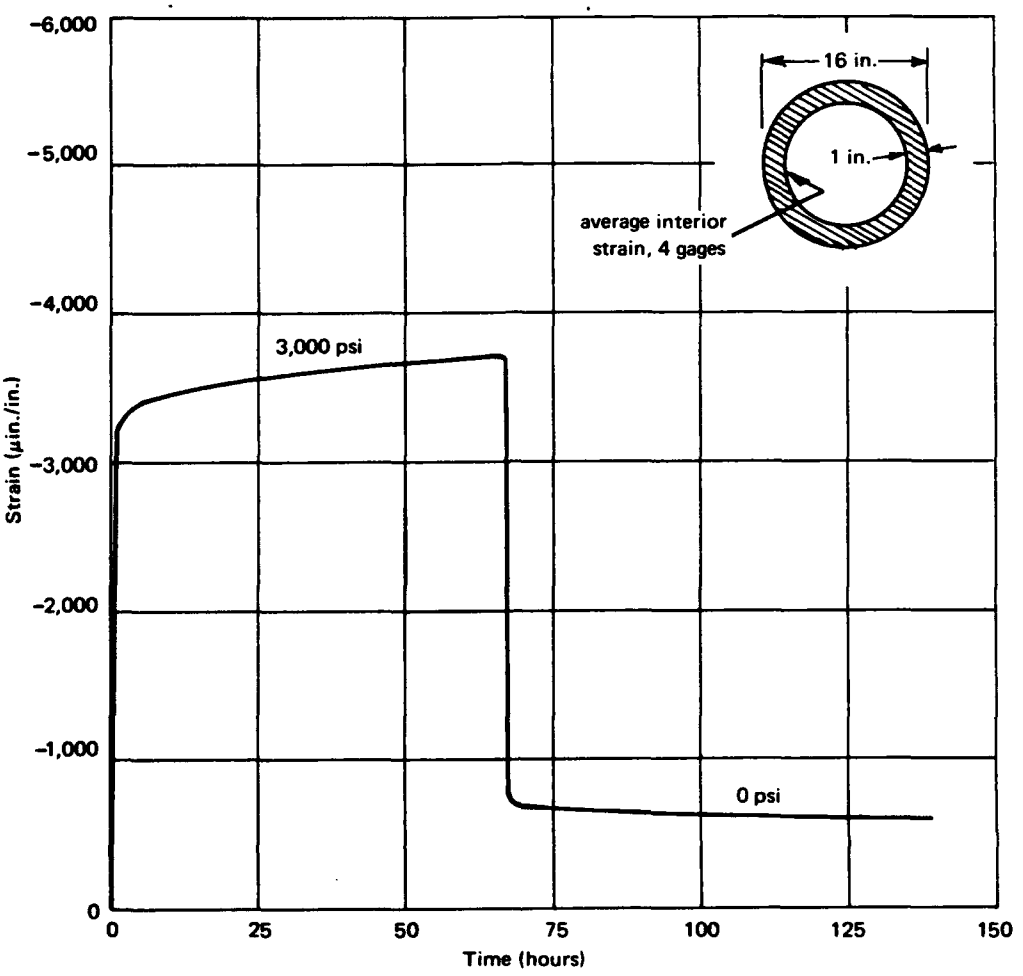

Figure 16. Interior strain versus time for a regular-concrete sphere[1] under cyclic loading; $t/D_o = 0.063$.

The strain behavior for sphere F is shown in Figures 19 and 20 along with the behavior for the PIC spheres with a thin epoxy joint. The aluminum joint changed the deformation pattern of the hemisphere sections from that of a sphere with a thin epoxy joint. However, the aluminum joint did not affect the strain behavior of the PIC sphere as significantly or severely as aluminum joints affected regular-concrete spheres. Actually, the strain behavior of sphere F compared quite well with that of a regular-concrete sphere having a fiber glass joint.[9] The fiber glass joint (Figure 18) had a relative stiffness of approximately 1.0, which was equivalent to the stiffness of the concrete hull.

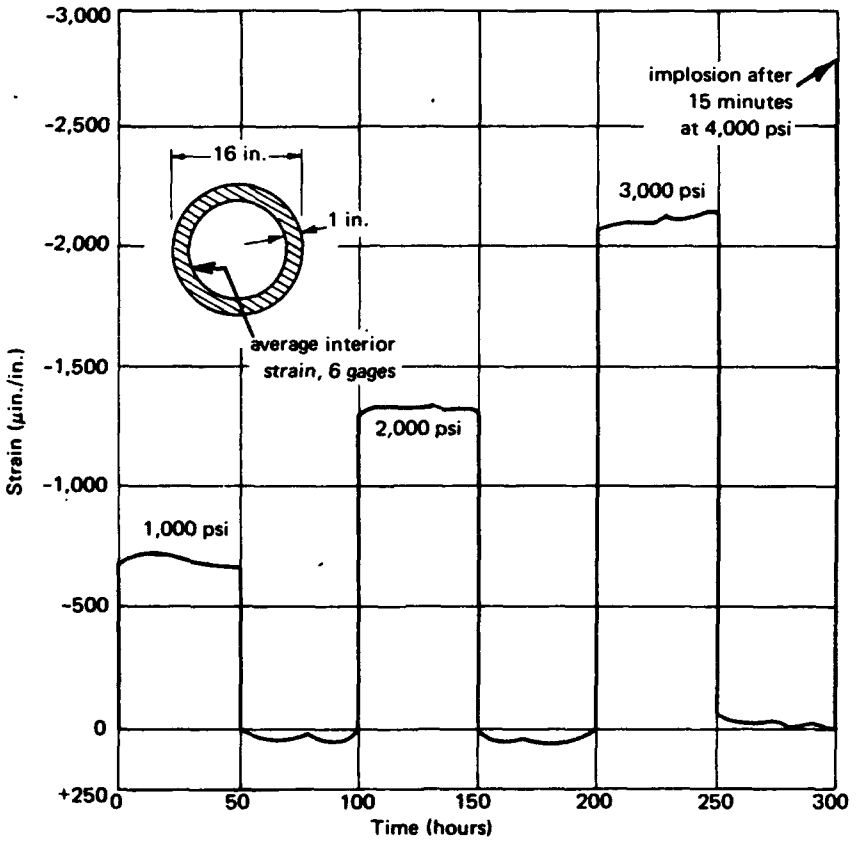

(a) Interior.

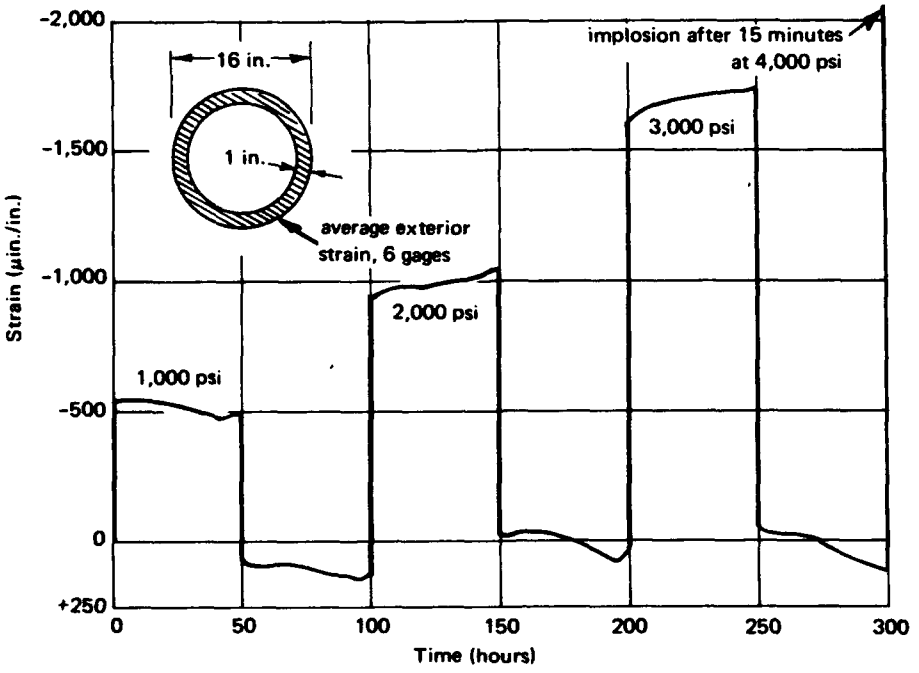

(b) Exterior.

Figure 17. Strain behavior of sphere H under cyclic loading; $t/D_o = 0.063$.

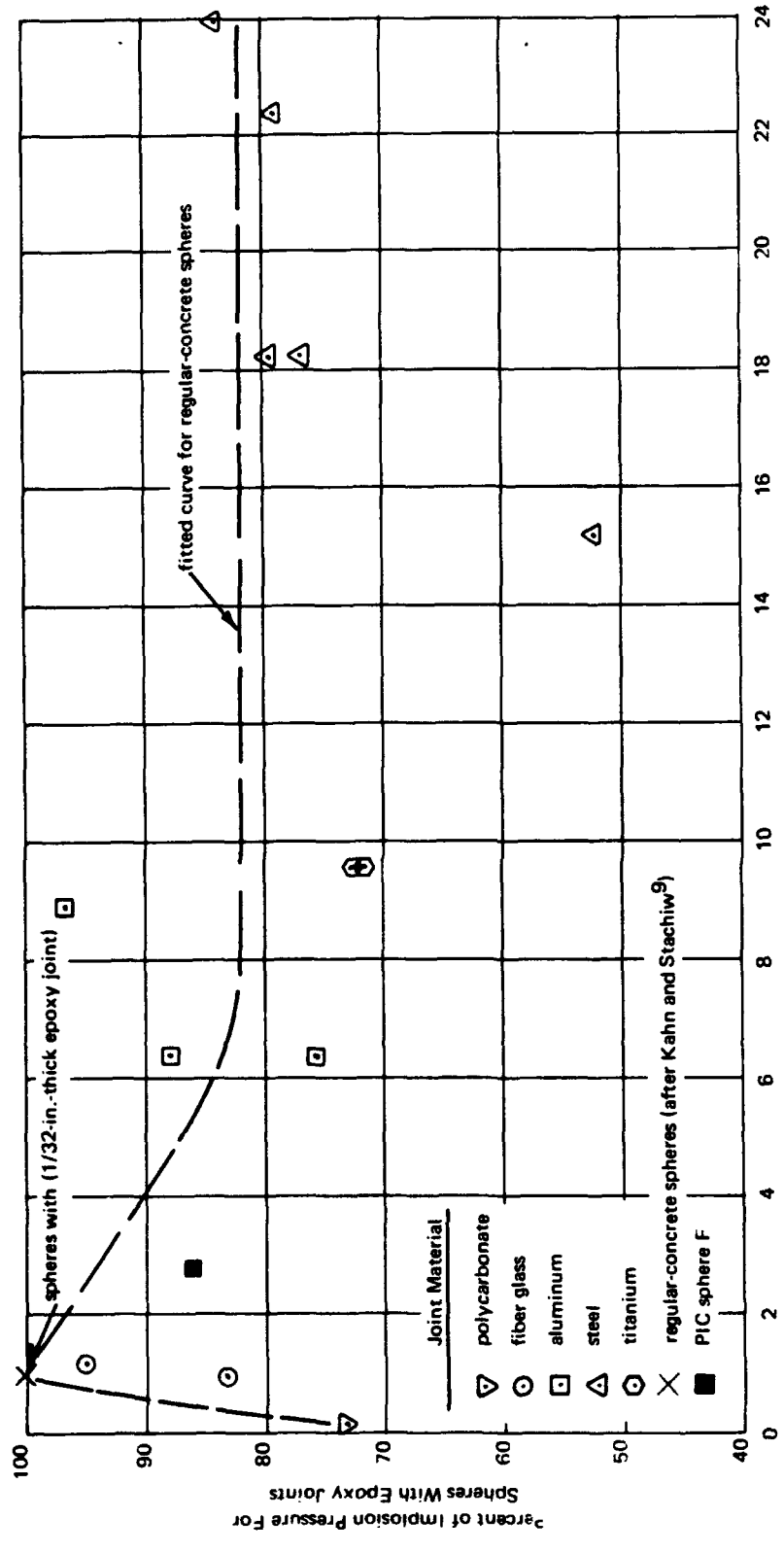

Figure 18. Comparison of implosion behavior of sphere F with regular-concrete spheres having mechanical joints.

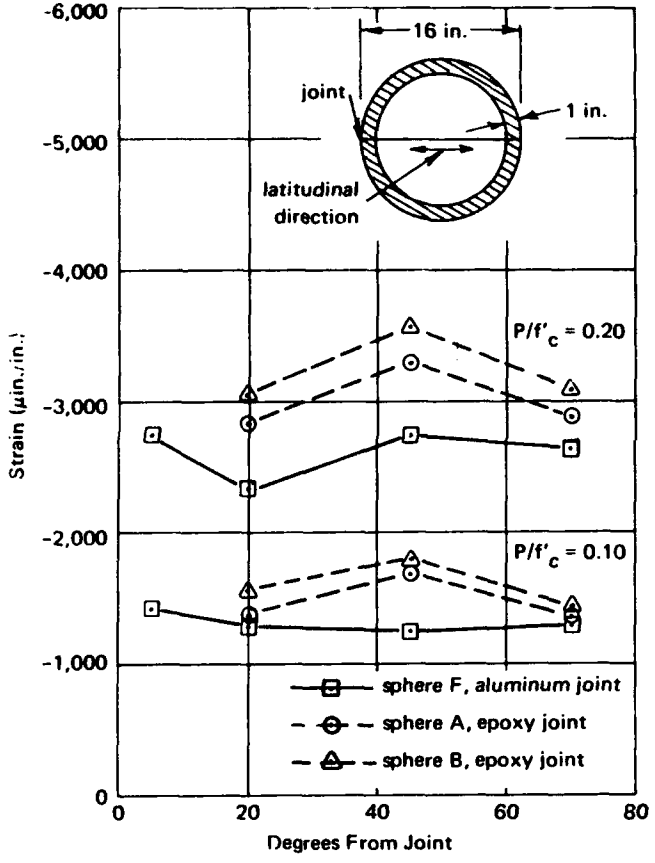

(a) Latitudinal direction.

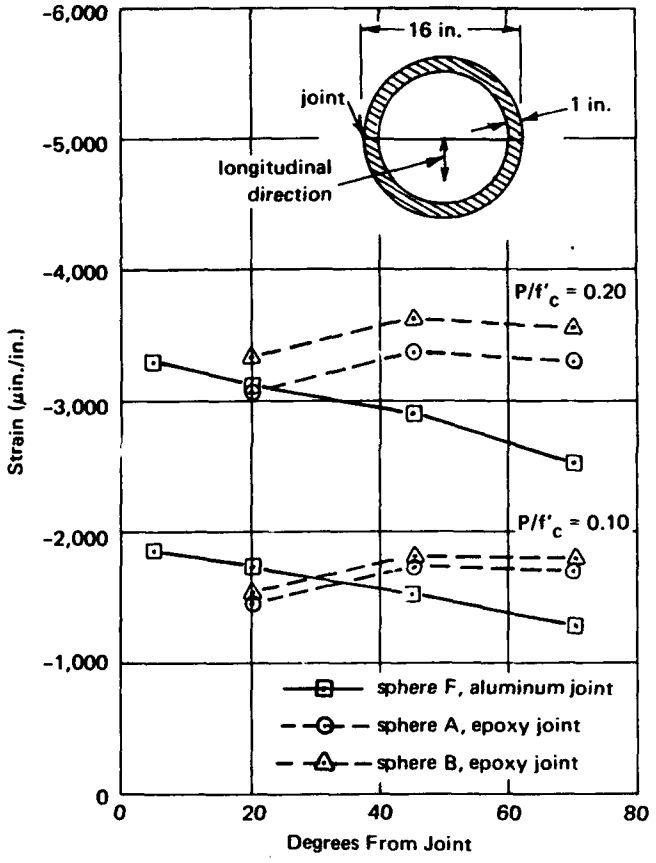

(b) Longitudinal direction.

Figure 19. Interior strains of sphere F.

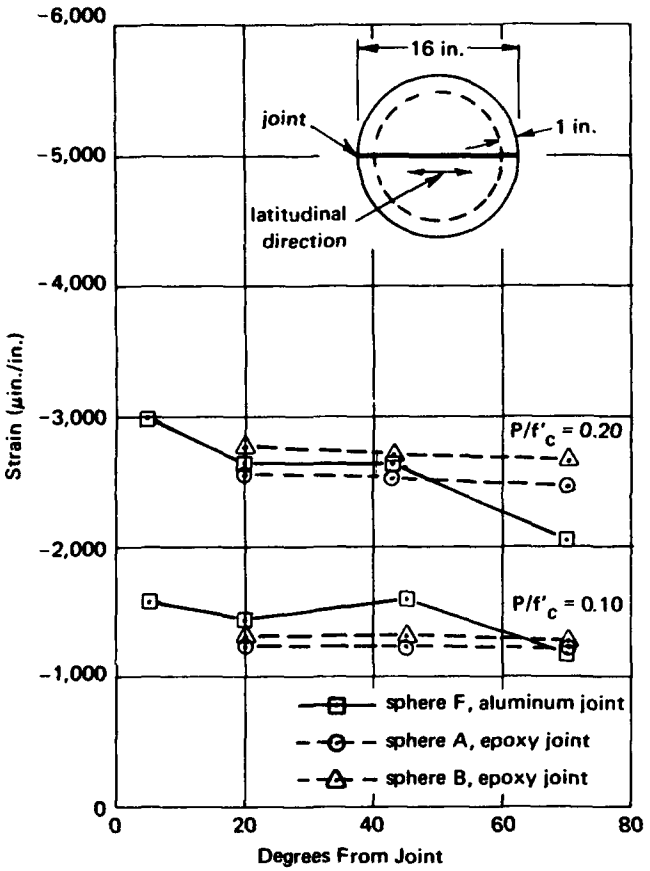

(a) Latitudinal direction.

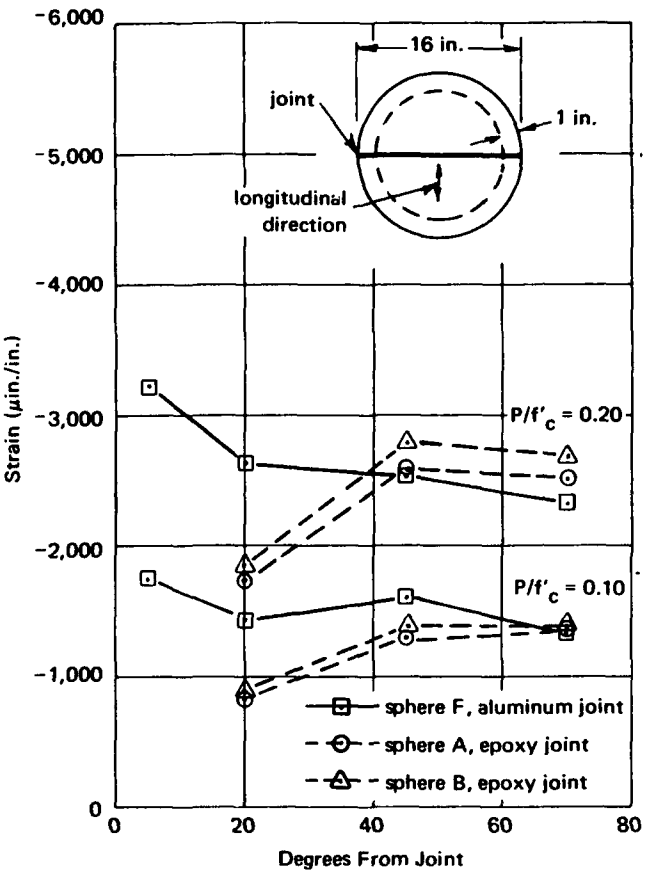

(b) Longitudinal direction.

Figure 20. Exterior strains of sphere F.

. The aluminum joint on the PIC sphere had a mating surface with the hull that was beveled; this was unlike the joints on the regular-concrete spheres which had flat mating surfaces. From the strain data it is evident that the beveled mating surface helped the joint appear less stiff to the PIC sphere by reducing the high bearing stresses on the interior edge. The flat mating surface produced high bearing stresses in the regular-concrete spheres. Hence, the beveled joint design was found to be an improvement over the joint design used by Kahn and Stachiw.[9]

DISCUSSION

Strain

The observed strain behavior of the PIC spheres tested under short-term loading was compared to theoretical strain behavior as shown in Figure 21. Theoretical strains were computed using the following elastic theory expression[10]

$$\epsilon_x = \frac{\sigma_x}{E} - \frac{\nu}{E}(\sigma_y + \sigma_z) \qquad (1)$$

where ϵ_x = strain in tangential direction (in./in.)

σ_x, σ_y = stresses in tangential direction normal to each other (psi)

σ_z = stress in radial direction (psi)

E = modulus of elasticity (psi)

ν = Poisson's ratio

The stresses were computed from Lame's equations for spheres:

$$\sigma_x = \sigma_y = P_o \frac{r_o^3}{2r^3}\left(\frac{r_i^3 - 2r^3}{r_o^3 - r_i^3}\right) \qquad (2)$$

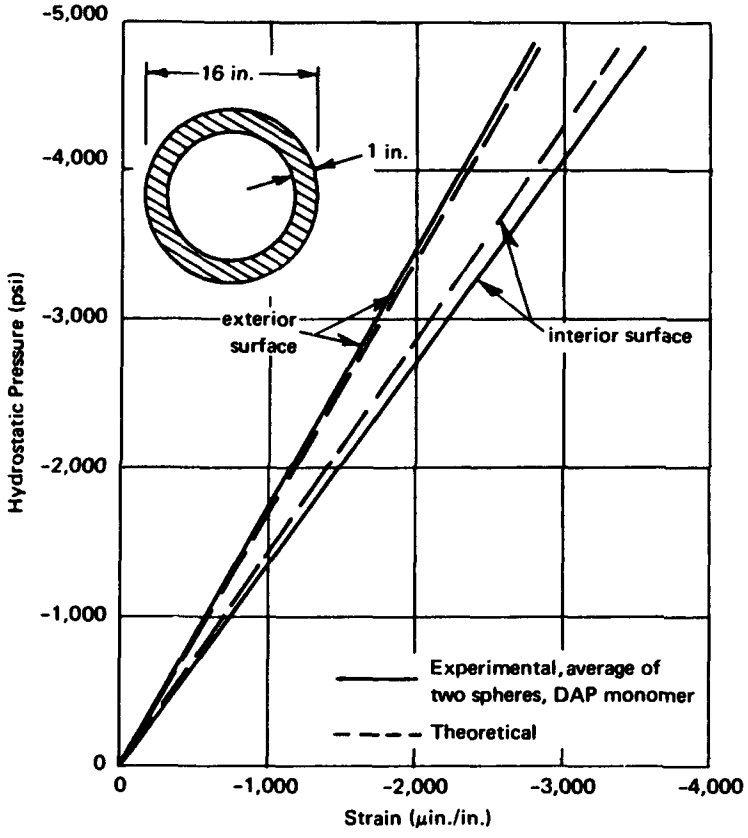

(a) $t/D_o = 0.063$.

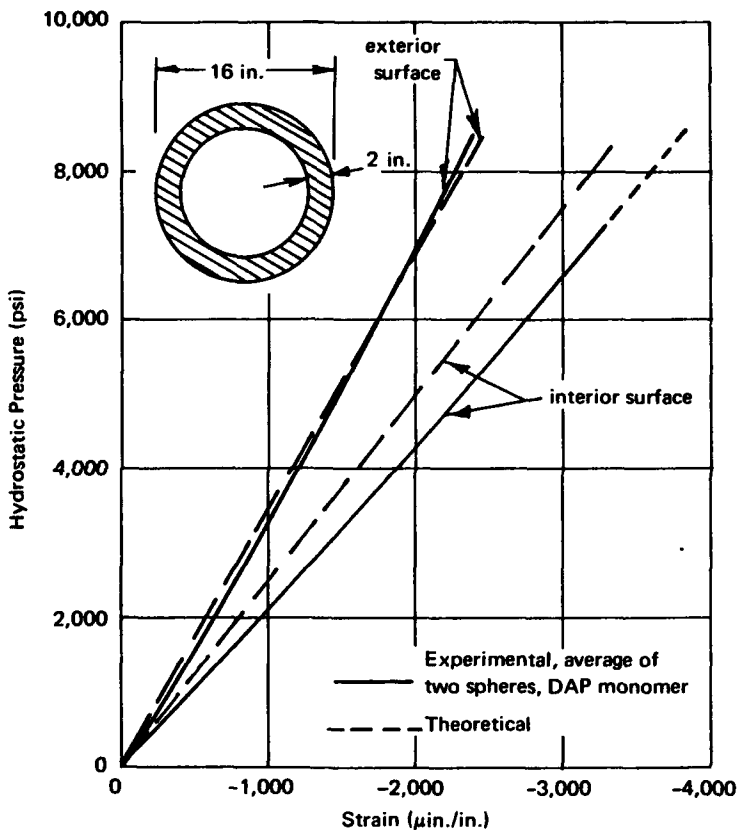

(b) $t/D_o = 0.125$.

Figure 21. Comparison of experimental to theoretical strain behavior for PIC spheres.

and

$$\sigma_z = -P_o \frac{r_o^3}{r^3}\left(\frac{r^3 - r_i^3}{r_o^3 - r_i^3}\right) \quad (3)$$

where P_o = external pressure (psi)

r_o = external radius (in.)

r_i = internal radius (in.)

r = radius under consideration (in.)

At the exterior surface of the 1- and 2-inch-thick PIC spheres, observed and theoretical strain behavior compared exceptionally well. However, at the interior surface the experimental strain was greater than the theoretical by approximately 5 and 14% for the 1- and 2-inch-thick spheres, respectively.

Implosion Behavior

The implosion behavior for the spheres under short-term loading is shown in Figure 22 in terms of two ratios—implosion pressure to uniaxial compressive strength, P_{im}/f'_{PIC}, and wall thickness to outside diameter, t/D_o. Lame's elastic theory for spheres compared quite well with the experimental behavior. Equation 2 was used to predict the implosion pressures of PIC spheres by substituting r_i for r (because the interior wall was the location of the highest stresses), P_{im} for P_o, and f'_{PIC} for σ_x. Rearranging the equation yielded:

$$P_{im} = \frac{2}{3} f'_{PIC}\left[1 - \left(\frac{r_i}{r_o}\right)^3\right] \quad (4)$$

where $r_i/r_o = 1 - 2(t/D_o)$

P_{im} = implosion pressure (psi)

f'_{PIC} = uniaxial compressive strength of 3x6-inch control cylinders (psi)

t = wall thickness (in.)

D_o = outside diameter (in.)

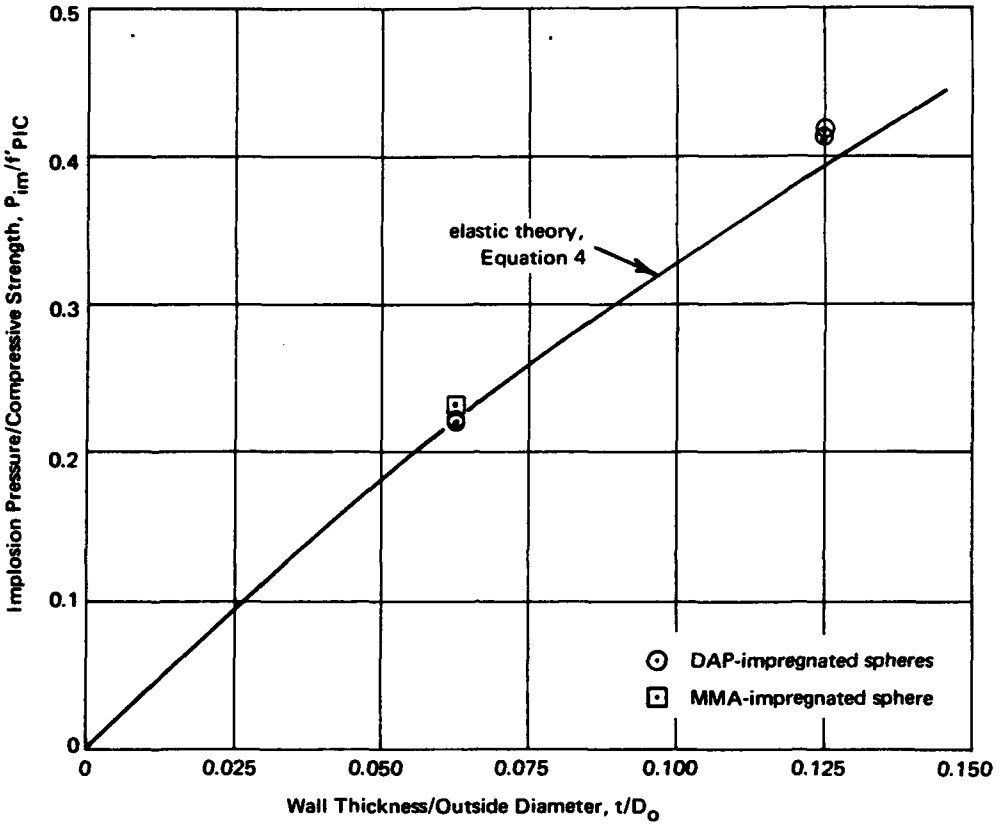

Figure 22. Comparison of implosion pressure for PIC spheres with elastic theory.

Applying Equation 4 to large spheres, say outside diameters of 20 feet or more, which have the same t/D_o ratios as the test specimens, design curves can be drawn to predict the operational depth in the ocean for PIC spheres. Figure 23 shows a family of operational depth curves; the reader may apply his own safety factor to the hull by relating allowable stress to the ultimate stress of 20,000 psi. For example, a neutrally buoyant sphere, $t/D_o = 0.082$, with a safety factor of 2 (allowable wall stress of 10,000 psi) would have a maximum operational depth of approximately 6,200 feet; if the safety factor was increased to 3, the maximum operational depth would be reduced to 4,100 feet. The reader must understand that the design curves are based on short-term test data, so the safety factor should compensate for the effect of long-term loading.

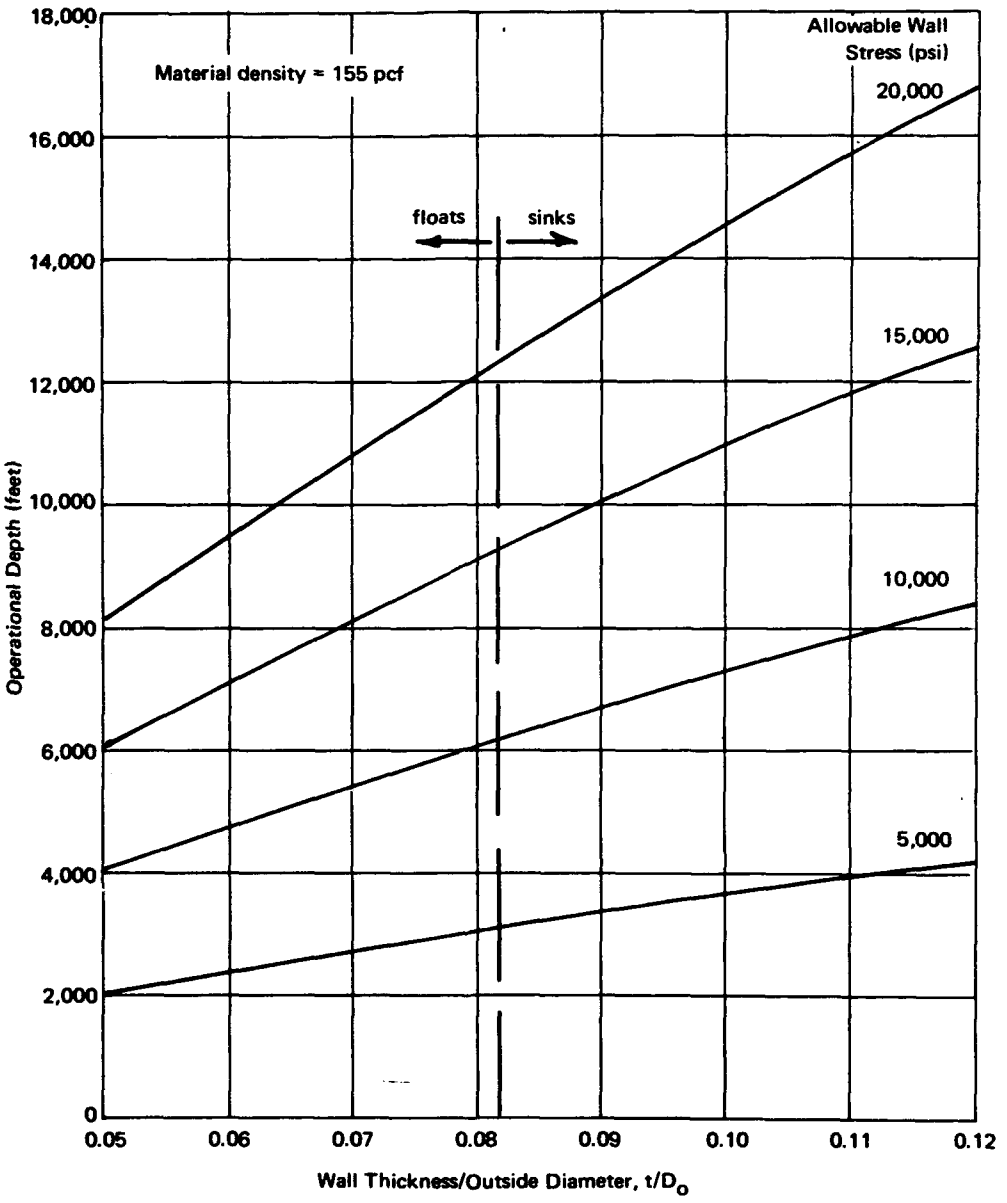

Figure 23. Operational depths for PIC spheres based on elastic theory.

Applications

Polymer-impregnated concrete appears to have a good future as a construction material for underwater structures. The behavior of PIC spheres in terms of high implosion pressures and linearly elastic response to various

hydrostatic loads demonstrated substantial improvements over regular-concrete sphere behavior; however, these improvements must be weighed against cost. The unit cost of PIC materials in a finished product is given in Reference 6 as being twice the unit cost of regular concrete. Using this information, Figure 24 was developed which compares the cost and depth of operation for buoyant spheres fabricated of PIC, concrete, and steel. The cost parameter is in terms of dollars per cubic foot of interior volume, making it a constant regardless of the actual size of the structure. (However, the comparison is estimated to be valid only for spheres with an outside diameter greater than 20 feet.) Regular-concrete spheres were found to be the most economical to a depth of approximately 3,000 feet, then PIC materials were cost effective to 4,100 feet, and for greater depths steel was the favored material, mainly because of strength, not cost. Other materials, such as aluminum or glass, were not considered in the comparison, because the cost of these materials is greater than steel.

The desirable features of PIC materials, such as watertightness and durability, can be incorporated into a regular-concrete structure without a major increase in cost by impregnating with a monomer a small portion of the outer wall of the structure. Only if increases in strength are required is it necessary to completely impregnate the wall with a monomer. Actually what is achieved by completely impregnating a sphere is an extended operational depth range—from 3,000 feet for regular-concrete spheres to 4,100 feet for PIC spheres.

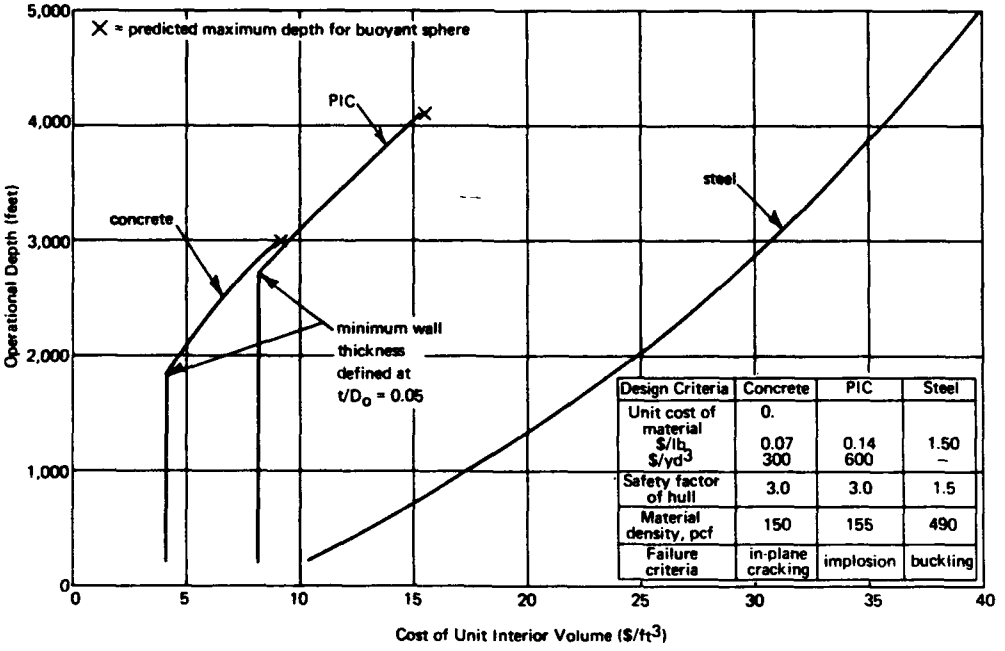

Figure 24. Cost comparison of buoyant spherical hulls with outside diameters greater than 20 feet.

PIC structures have the potential for a wide range of underwater applications, such as containment vessels for nuclear reactors or military structures to store materiel. Similar structures are feasible using regular concrete; however, by utilizing PIC materials, the structures could operate at deeper levels, would be less permeable to seawater, and could possess better durability characteristics than regular concrete.

FINDINGS

1. Polymer-impregnated concrete (PIC) control cylinders, 3 x 6 inches, containing an average 8.4% by weight DAP monomer had an average compressive strength of 20,970 psi and a modulus of elasticity of 5.34×10^6 psi; these properties were an increase of 121 and 52%, respectively, over those of regular-concrete control specimens.

2. PIC spheres with an outside diameter of 16 inches and wall thicknesses of 1 or 2 inches (t/D_o ratios of 0.063 or 0.125, respectively) imploded at average pressures of 4,810 and 8,475 psi or simulated depths of 10,700 and 18,800 feet, respectively.

3. The 1-inch-thick PIC sphere with an operational aluminum joint at the equator imploded at 86% of the pressure for similar spheres with thin epoxy joints.

4. The PIC spheres consistently showed linearly elastic behavior under hydrostatic loading conditions of short-term, long-term, and cyclic pressure.

5. Predictions of strain behavior and implosion pressures for PIC spheres having t/D_o ratios between 0.063 and 0.125 can be made using classical elastic theory.

CONCLUSIONS

Polymer-impregnated concrete (PIC) spheres with an outside diameter of 16 inches and t/D_o ratios of 0.063 and 0.125 implode at pressures greater than similar regular-concrete spheres. This implies that spheres fabricated of PIC materials will ultimately operate at deeper levels in the ocean than regular-concrete spheres. It is projected that the maximum depth for buoyant PIC spheres will be approximately 4,000 feet, whereas the maximum depth for regular-concrete spheres appears to be 3,000 feet.

A cost comparison of spherical structures fabricated of PIC, regular concrete, and steel indicates that polymer-impregnated concrete is competitive with regular concrete and is substantially less expensive than steel.

REFERENCES

1. Naval Civil Engineering Laboratory. Technical Report R-517: Behavior of spherical concrete hulls under hydrostatic loading, pt. 1. Exploratory investigation, by J. D. Stachiw and K. O. Gray. Port Hueneme, Calif., Mar. 1967.

2.———. Technical Report R-547: Behavior of spherical concrete hulls under hydrostatic loading, pt. 2. Effect of Penetrations, by J. D. Stachiw. Port Hueneme, Calif., Oct. 1967.

3.———. Technical Report R-588: Behavior of spherical concrete hulls under hydrostatic loading, pt. 3. Relationship between thickness-to-diameter ratio and critical pressures, strains, and water permeation rates, by J. D. Stachiw and K. Mack. Port Hueneme, Calif., June 1968.

4.———. Technical Report R-679: Failure of thick-walled concrete spheres subjected to hydrostatic loading, by H. H. Haynes and R. A. Hoofnagle. Port Hueneme, Calif., May 1970. (AD 708011)

5.———. Technical Report R-696: Influence of length-to-diameter ratio on the behavior of concrete cylindrical hulls under hydrostatic loading, by H. H. Haynes and R. J. Ross. Port Hueneme, Calif., Sep. 1970. (AD 713088)

6. Brookhaven National Laboratory. Report BNL 50134: Concrete-polymer materials. First topical report, by M. Steinberg, et at. Upton, N. Y., Dec. 1968. (Also Bureau of Reclamation, GEN. REP.-41, Denver, Col.)

7.———. Report BNL 50218: Concrete-polymers materials, 2d topical report, by M. Steinberg, et al. Upton, N. Y., Dec. 1969. (Also Bureau of Reclamation, Rec OCE-70-1, Denver, Col.)

8.———. Report BNL 50275: Concrete-polymer materials, 3d topical report, by J. T. Dikeou, et al. Denver, Col., Jan. 1971. (Also Bureau of Reclamation, Rec ERC-71-6, Denver, Col.)

9. Naval Civil Engineering Laboratory. Technical Report R-735: The influence of stiff equatorial rings on concrete spherical hulls subjected to hydrostatic loading, by L. F. Kahn and J. D. Stachiw. Port Hueneme, Calif., Aug. 1971.

10. R. J. Roark. Formulas for stress and strain, 4th ed. New York, McGraw-Hill, 1965, pp. 432.

DISTRIBUTION LIST

SNDL Code	No. of Activities	Total Copies	
—	1	12	Defense Documentation Center
FKAIC	1	10	Naval Facilities Engineering Command
FKNI	6	6	NAVFAC Engineering Field Divisions
FKN5	9	9	Public Works Centers
FA25	1	1	Public Works Center
—	9	9	RDT&E Liaison Officers at NAVFAC Engineering Field Divisions and Construction Battalion Centers
—	403	403	NCEL Special Distribution List No. 9 for persons and activities interested in reports on Deep Ocean Studies

Naval Civil Engineering Laboratory
POLYMER-IMPREGNATED CONCRETE SPHERICAL HULLS UNDER HYDROSTATIC LOADING (Final), by H. H. Haynes and N. D. Albertsen
TR-753 37 p. illus December 1971 Unclassified

1. *Polymer-impregnated concrete* 2. *Underwater concrete structures* I. 3.1610-1

Eight spherical models with outside diameters of 16 inches and wall thicknesses of 1 or 2 inches were fabricated of polymer-impregnated concrete (PIC) having a uniaxial compressive strength of 21,000 psi. The spherical specimens were tested under hydrostatic loading conditions of short-term, long-term, and cyclic pressure. The test results show that the PIC spheres respond to hydrostatic loading with linearly elastic behavior and that the implosion pressures are greater by approximately 40% than those for similar regular-concrete spheres. Under short-term loading the specimens having a wall-thickness-to-outside-diameter ratio of 0.063 and 0.125 (1- or 2-inch walls to 16-inch OD) implode at average hydrostatic pressures of 4,810 and 8,475 psi, respectively. Classical elastic theory predicts the strain behavior and implosion pressures of the PIC sphere within engineering accuracy.

Naval Civil Engineering Laboratory
POLYMER-IMPREGNATED CONCRETE SPHERICAL HULLS UNDER HYDROSTATIC LOADING (Final), by H. H. Haynes and N. D. Albertsen
TR-753 37 p. illus December 1971 Unclassified

1. *Polymer-impregnated concrete* 2. *Underwater concrete structures* I. 3.1610-1

Eight spherical models with outside diameters of 16 inches and wall thicknesses of 1 or 2 inches were fabricated of polymer-impregnated concrete (PIC) having a uniaxial compressive strength of 21,000 psi. The spherical specimens were tested under hydrostatic loading conditions of short-term, long-term, and cyclic pressure. The test results show that the PIC spheres respond to hydrostatic loading with linearly elastic behavior and that the implosion pressures are greater by approximately 40% than those for similar regular-concrete spheres. Under short-term loading the specimens having a wall-thickness-to-outside-diameter ratio of 0.063 and 0.125 (1- or 2-inch walls to 16-inch OD) implode at average hydrostatic pressures of 4,810 and 8,475 psi, respectively. Classical elastic theory predicts the strain behavior and implosion pressures of the PIC sphere within engineering accuracy.

Naval Civil Engineering Laboratory
POLYMER-IMPREGNATED CONCRETE SPHERICAL HULLS UNDER HYDROSTATIC LOADING (Final), by H. H. Haynes and N. D. Albertsen
TR-753 37 p. illus December 1971 Unclassified

1. Polymer-impregnated concrete 2. Underwater concrete structures I. 3.1610-1

Eight spherical models with outside diameters of 16 inches and wall thicknesses of 1 or 2 inches were fabricated of polymer-impregnated concrete (PIC) having a uniaxial compressive strength of 21,000 psi. The spherical specimens were tested under hydrostatic loading conditions of short-term, long-term, and cyclic pressure. The test results show that the PIC spheres respond to hydrostatic loading with linearly elastic behavior and that the implosion pressures are greater by approximately 40% than those for similar regular-concrete spheres. Under short-term loading the specimens having a wall-thickness-to-outside-diameter ratio of 0.063 and 0.125 (1- or 2-inch walls to 16-inch OD) implode at average hydrostatic pressures of 4,810 and 8,475 psi, respectively. Classical elastic theory predicts the strain behavior and implosion pressures of the PIC sphere within engineering accuracy.

Naval Civil Engineering Laboratory
POLYMER-IMPREGNATED CONCRETE SPHERICAL HULLS UNDER HYDROSTATIC LOADING (Final), by H. H. Haynes and N. D. Albertsen
TR-753 37 p. illus December 1971 Unclassified

1. Polymer-impregnated concrete 2. Underwater concrete structures I. 3.1610-1

Eight spherical models with outside diameters of 16 inches and wall thicknesses of 1 or 2 inches were fabricated of polymer-impregnated concrete (PIC) having a uniaxial compressive strength of 21,000 psi. The spherical specimens were tested under hydrostatic loading conditions of short-term, long-term, and cyclic pressure. The test results show that the PIC spheres respond to hydrostatic loading with linearly elastic behavior and that the implosion pressures are greater by approximately 40% than those for similar regular-concrete spheres. Under short-term loading the specimens having a wall-thickness-to-outside-diameter ratio of 0.063 and 0.125 (1- or 2-inch walls to 16-inch OD) implode at average hydrostatic pressures of 4,810 and 8,475 psi, respectively. Classical elastic theory predicts the strain behavior and implosion pressures of the PIC sphere within engineering accuracy.

Naval Civil Engineering Laboratory
POLYMER-IMPREGNATED CONCRETE SPHERICAL HULLS UNDER HYDROSTATIC LOADING (Final), by H. H. Haynes and N. D. Albertsen
TR-753 37 p. illus December 1971 Unclassified

1. Polymer-impregnated concrete 2. Underwater concrete structures I. 3.1610-1

Eight spherical models with outside diameters of 16 inches and wall thicknesses of 1 or 2 inches were fabricated of polymer-impregnated concrete (PIC) having a uniaxial compressive strength of 21,000 psi. The spherical specimens were tested under hydrostatic loading conditions of short-term, long-term, and cyclic pressure. The test results show that the PIC spheres respond to hydrostatic loading with linearly elastic behavior and that the implosion pressures are greater by approximately 40% than those for similar regular-concrete spheres. Under short-term loading the specimens having a wall-thickness-to-outside-diameter ratio of 0.063 and 0.125 (1- or 2-inch walls to 16-inch OD) implode at average hydrostatic pressures of 4,810 and 8,475 psi, respectively. Classical elastic theory predicts the strain behavior and implosion pressures of the PIC sphere within engineering accuracy.

Naval Civil Engineering Laboratory
POLYMER-IMPREGNATED CONCRETE SPHERICAL HULLS UNDER HYDROSTATIC LOADING (Final), by H. H. Haynes and N. D. Albertsen
TR-753 37 p. illus December 1971 Unclassified

1. Polymer-impregnated concrete 2. Underwater concrete structures I. 3.1610-1

Eight spherical models with outside diameters of 16 inches and wall thicknesses of 1 or 2 inches were fabricated of polymer-impregnated concrete (PIC) having a uniaxial compressive strength of 21,000 psi. The spherical specimens were tested under hydrostatic loading conditions of short-term, long-term, and cyclic pressure. The test results show that the PIC spheres respond to hydrostatic loading with linearly elastic behavior and that the implosion pressures are greater by approximately 40% than those for similar regular-concrete spheres. Under short-term loading the specimens having a wall-thickness-to-outside-diameter ratio of 0.063 and 0.125 (1- or 2-inch walls to 16-inch OD) implode at average hydrostatic pressures of 4,810 and 8,475 psi, respectively. Classical elastic theory predicts the strain behavior and implosion pressures of the PIC sphere within engineering accuracy.

Naval Civil Engineering Laboratory
POLYMER-IMPREGNATED CONCRETE SPHERICAL HULLS UNDER HYDROSTATIC LOADING (Final), by H. H. Haynes and N. D. Albertsen
TR-753 37 p. illus December 1971 Unclassified

1. Polymer-impregnated concrete 2. Underwater concrete structures I. 3.1610-1

Eight spherical models with outside diameters of 16 inches and wall thicknesses of 1 or 2 inches were fabricated of polymer-impregnated concrete (PIC) having a uniaxial compressive strength of 21,000 psi. The spherical specimens were tested under hydrostatic loading conditions of short-term, long-term, and cyclic pressure. The test results show that the PIC spheres respond to hydrostatic loading with linearly elastic behavior and that the implosion pressures are greater by approximately 40% than those for similar regular-concrete spheres. Under short-term loading the specimens having a wall-thickness-to-outside-diameter ratio of 0.063 and 0.125 (1- or 2-inch walls to 16-inch OD) implode at average hydrostatic pressures of 4,810 and 8,475 psi, respectively. Classical elastic theory predicts the strain behavior and implosion pressures of the PIC sphere within engineering accuracy.

Naval Civil Engineering Laboratory
POLYMER-IMPREGNATED CONCRETE SPHERICAL HULLS UNDER HYDROSTATIC LOADING (Final), by H. H. Haynes and N. D. Albertsen
TR-753 37 p. illus December 1971 Unclassified

1. Polymer-impregnated concrete 2. Underwater concrete structures I. 3.1610-1

Eight spherical models with outside diameters of 16 inches and wall thicknesses of 1 or 2 inches were fabricated of polymer-impregnated concrete (PIC) having a uniaxial compressive strength of 21,000 psi. The spherical specimens were tested under hydrostatic loading conditions of short-term, long-term, and cyclic pressure. The test results show that the PIC spheres respond to hydrostatic loading with linearly elastic behavior and that the implosion pressures are greater by approximately 40% than those for similar regular-concrete spheres. Under short-term loading the specimens having a wall-thickness-to-outside-diameter ratio of 0.063 and 0.125 (1- or 2-inch walls to 16-inch OD) implode at average hydrostatic pressures of 4,810 and 8,475 psi, respectively. Classical elastic theory predicts the strain behavior and implosion pressures of the PIC sphere within engineering accuracy.

Unclassified
Security Classification

DOCUMENT CONTROL DATA - R & D

(Security classification of title, body of abstract and indexing annotation must be entered when the overall report is classified)

1. ORIGINATING ACTIVITY (Corporate author) Naval Civil Engineering Laboratory Port Hueneme, California 93043	2a. REPORT SECURITY CLASSIFICATION Unclassified 2b. GROUP

3. REPORT TITLE
POLYMER-IMPREGNATED CONCRETE SPHERICAL HULLS UNDER HYDROSTATIC LOADING

4. DESCRIPTIVE NOTES (Type of report and inclusive dates)
Final; June 1969 – February 1971

5. AUTHOR(S) (First name, middle initial, last name)
H. H. Haynes and N. D. Albertsen

6. REPORT DATE	7a. TOTAL NO. OF PAGES	7b. NO. OF REFS
December 1971	37	10

8a. CONTRACT OR GRANT NO.	9a. ORIGINATOR'S REPORT NUMBER(S) TR-753
b. PROJECT NO. 3.1610-1	
c.	9b. OTHER REPORT NO(S) (Any other numbers that may be assigned this report)
d.	

10. DISTRIBUTION STATEMENT
Approved for public release; distribution unlimited.

11. SUPPLEMENTARY NOTES	12. SPONSORING MILITARY ACTIVITY
	Naval Facilities Engineering Command Washington, D. C. 20390

13. ABSTRACT

Eight spherical models with outside diameters of 16 inches and wall thicknesses of 1 or 2 inches were fabricated of polymer-impregnated concrete (PIC) having a uniaxial compressive strength of 21,000 psi. The spherical specimens were tested under hydrostatic loading conditions of short-term, long-term, and cyclic pressure. The test results show that the PIC spheres respond to hydrostatic loading with linearly elastic behavior and that the implosion pressures are greater by approximately 40% than those for similar regular-concrete spheres. Under short-term loading the specimens having a wall-thickness-to-outside-diameter ratio of 0.063 and 0.125 (1- or 2-inch walls to 16-inch OD) implode at average hydrostatic pressures of 4,810 and 8,475 psi, respectively. Classical elastic theory predicts the strain behavior and implosion pressures of the PIC sphere within engineering accuracy.

14 KEY WORDS	LINK A		LINK B		LINK C	
	ROLE	WT	ROLE	WT	ROLE	WT
Polymer-impregnated concrete						
Monomers						
Regular concrete						
Concrete spheres						
Deep ocean structures						
Habitats						
Diallyl phthalate (DAP)						
Methyl-methacrylate (MMA)						
Polymerization						
Thermal-catalytic						
60 cobalt source						
Gamma radiation						
Hydrostatic pressure						
Short-term test						
Long-term test						
Cyclic test						
Aluminum joints						
Epoxy joints						
Strains						
Stresses						
Cost data						

Technical Report

R 785

Sponsored by

NAVAL FACILITIES ENGINEERING COMMAND

April 1973

NAVAL CIVIL ENGINEERING LABORATORY

Port Hueneme, California 93043

HYDROSTATIC LOADING OF CONCRETE SPHERICAL HULLS REINFORCED WITH STEEL LINERS

By

H. H. Haynes, G. L. Page, and R. J. Ross

HYDROSTATIC LOADING OF CONCRETE SPHERICAL HULLS REINFORCED WITH STEEL LINERS

Technical Report R-785

3.1610-1D

by

H. H. Haynes, G. L. Page, and R. J. Ross

ABSTRACT

Nine model concrete spheres reinforced with steel liners located on the inside, outside, or both inside and outside were tested to failure under hydrostatic loading. The quantity of reinforcement varied from 1.8 to 23.9% by area; for this range of reinforcement, the spheres showed increases in failure pressure from 0 to 374% over that of unreinforced concrete spheres (2,810 psi). Using a nominal 12% reinforcement, it was found that the best reinforcing method was to place liners on both the inside and outside of the wall.

CONTENTS

INTRODUCTION

The Naval Facilities Engineering Command is sponsoring the development of concrete as a construction material for undersea pressure-resistant structures. Tests on unreinforced concrete spheres[1-6] have demonstrated the feasibility of using concrete structures to 3,000-foot depths. It is likely that concrete structures slated for the ocean will be reinforced to resist, at the least, handling and towing stresses if not more significant stresses. There is also the possibility that reinforced structures could operate at depths greater than similar unreinforced structures. Therefore, it is important to determine what the actual effects of the reinforcement will have on the behavior of the structures.

Several advantages are apparent for using steel liners as the reinforcing system instead of using conventional reinforcing bars. Not only would the liners serve as the reinforcement, but they also could serve as the mold during fabrication and as a permanent watertight barrier for the structure. The combination of steel and concrete creates a sandwich construction material which might enable each material to resist higher loads than they could resist individually. This study was undertaken to determine the actual behavior of concrete spheres reinforced with steel-liners.

EXPERIMENTAL PROGRAM

Specimen Description

Nine reinforced concrete spheres were fabricated as outlined in Table 1. The concrete portion of the structures remained constant—16 inches in outside diameter and 1 inch in wall thickness—while the steel reinforcement liners were placed on either the inside, outside, or inside and outside surfaces of the concrete (Figure 1). The steel liners were either 20, 60 (Figure 2), or 120 mils thick, producing percentages of reinforcement between 1.8 and 23.9 by area (across an equatorial plane).

Table 1. Description of Test Specimens

Specimen Designation	Location of Liner	Thickness of Liner, t (mils)	Percent Reinforcement by Area	Ratio of Single Liner Thickness to Total Wall Thickness, t/T	Concrete Strength[a] (psi)	Water Proofing Agent	Machined Edge[b]	
							Yes	No
I020	inside	20	1.8	0.020	9,530	gage coat and RTV	X	
I060	inside	60	5.5	0.057	9,870	gage coat and RTV	X	
I120-1	inside	120	11.1	0.107	9,420	epoxy		X
I120-2	inside	120	11.1	0.107	9,180	wax		X
ϕ060	outside	60	6.4	0.057	9,610	epoxy	X	
ϕ120-1	outside	120	12.9	0.107	9,410	epoxy		X
ϕ120-2	outside	120	12.9	0.107	9,420	epoxy		X
D060	inside and outside	60	11.9	0.054	10,290	none	X	
D120	inside and outside	120	23.9	0.097	9,530	none	X	

[a] Uniaxial compressive strength of six 3 x 6-inch control cylinders which corresponded to the hemisphere having the weaker strength.

[b] Equatorial edge of hemispheres.

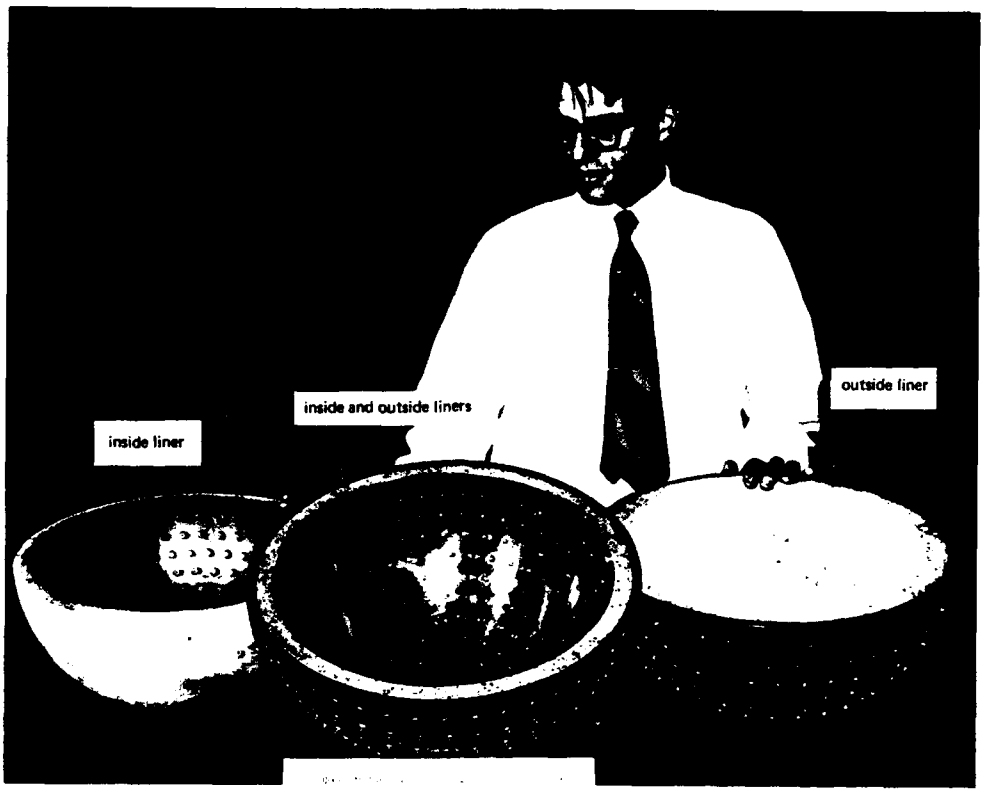

Figure 1. Hemispherical sections of reinforced concrete spheres.

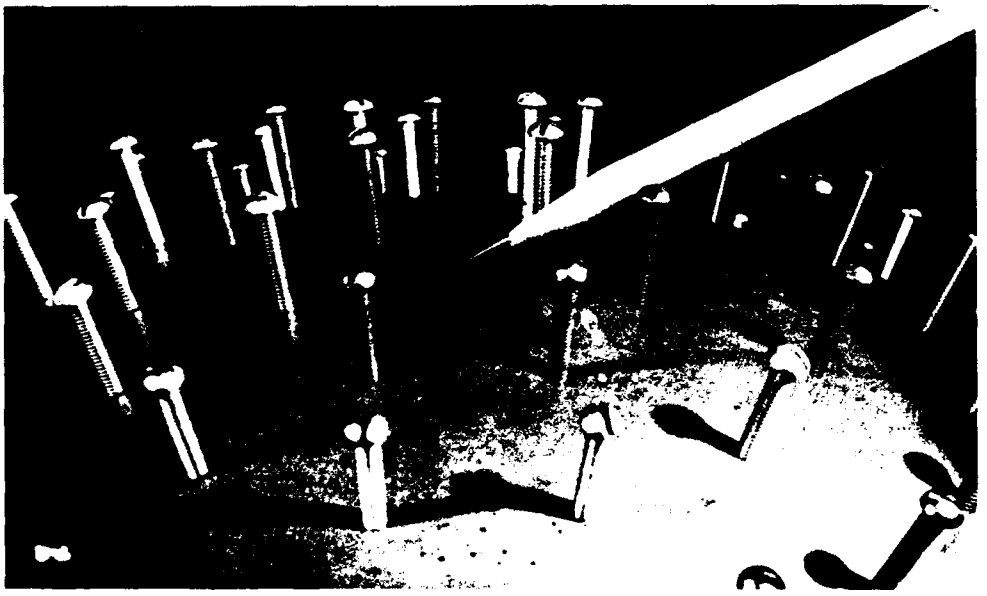

Figure 2. Machine screws act as the radial reinforcement in a 60-mil-thick liner.

The mix design and casting and curing processes for the concrete materials are given in References 1 through 4. The concrete for this study used a maximum size aggregate that passed the No. 4 sieve size and had an average uniaxial compressive strength, f'_c, of 9,580 psi and a secant modulus of elasticity at 1/2 f'_c of 3.50×10^6 psi.

The reinforcement liners were A4130 steel with an approximate yield strength of 200,000 psi as determined by the Rockwell "C" hardness test. Radial reinforcement for the sphere was attained through 572 no. 5 machine screws per sphere; the screws were spaced 1 inch apart to provide positive attachment between the liner and the concrete. The screws had an ultimate tensile strength of 23,800 psi (no yield point was observed).

All specimens were formed from two hemispheres, one of which was instrumented with at least 20 strain gages; half of the gages were on the inside surface and the other half were on the outside surface. The strain gages were electrical-resistance wire gages of 1/2-inch gage length.

Shrinkage cracks in the concrete were observed in the hemispheres having an inside or outside reinforced liner. It was not known whether the double liner hemispheres had shrinkage cracks. In general, four cracks were equally spaced around the circumference. Figure 3 shows a typical shrinkage crack. The reason for these cracks is believed to be the restraint provided by the steel liner as the concrete shrank during a drying-out period at room conditions. Concrete normally exhibits shrinkage as its moisture content decreases.

The equatorial edges of the hemispheres were either ground flat by hand or machined flat on a lathe. The machined edges were superior to ground edges because in the hand grinding process more concrete was removed than steel; thus the steel was slightly higher than the concrete. After edge preparation, two hemispheres were bonded together with a 1/32-inch-thick layer of epoxy.

The fabricated spheres were coated using various types of waterproofing agents (Table 1) in an attempt to keep water from entering the shrinkage cracks during pressure testing. The epoxy and silicone rubber coatings appeared more effective than the wax coating; however, no system was completely successful.

Test Procedure

The specimens were tested under external hydrostatic pressure in an 18-inch-ID pressure vessel having an operational pressure of 20,000 psi (Figure 4). The strain gage wires were passed through the top penetrator on the specimen, up through the pressure vessel head, to the vessel exterior and the recording instrumentation.

The hydrostatic load was applied to the specimen at a constant rate of 100 psi/min to failure. The pressure medium was freshwater.

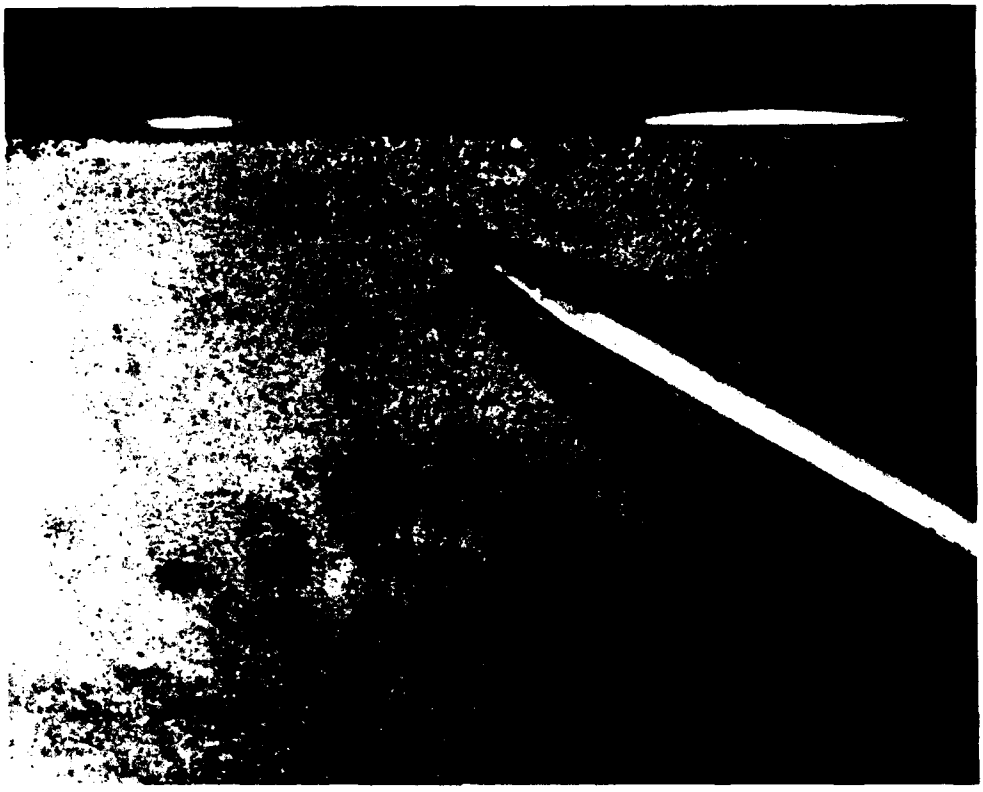

Figure 3. Typical shrinkage crack in the concrete.

TEST RESULTS

Table 2 lists the failure pressures for the reinforced spheres, and Figure 5 shows the relationship between failure pressure and percent reinforcement. The reinforced spheres with double (inside and outside) liners showed substantial increases in failure pressure over spheres with inside or outside liners.

The implosion pressure of unreinforced concrete spheres* was calculated from the empirical relationship[7]

$$\frac{P_{im}}{f'_c} = 0.294 \qquad (1)$$

where P_{im} = implosion pressure (psi)

f'_c = uniaxial compressive strength of 3 x 6-inch control cylinders (psi)

* Equation 1 applies only to unreinforced concrete spheres having a wall-thickness-to-outside-diameter ratio, t/D_o, of 0.0625.

The average concrete compressive strength of the reinforced spheres, f'_c = 9,580 psi, was used in Equation 1 to calculate the implosion pressure, P_{im} = 2,820 psi, for unreinforced spheres.

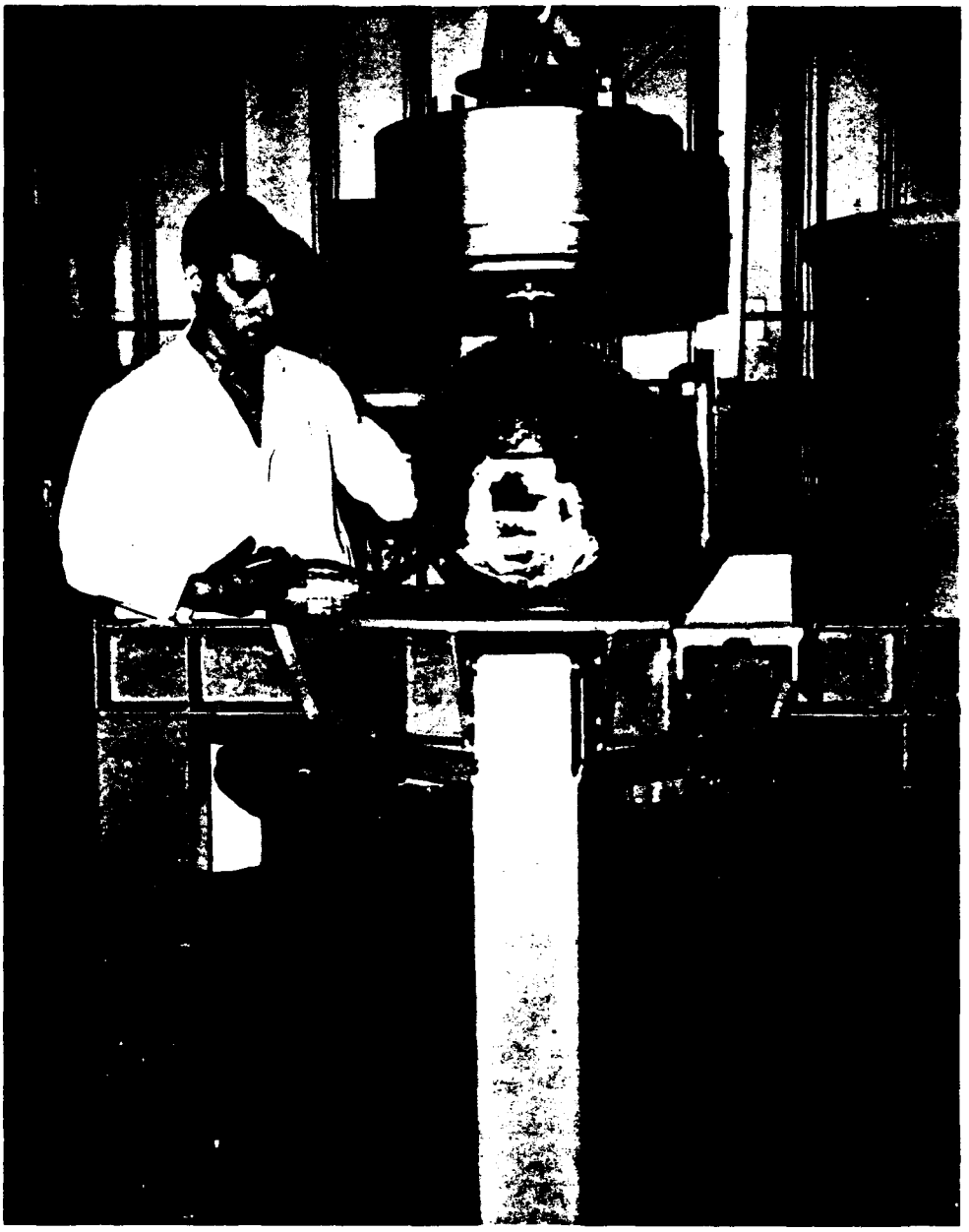

Figure 4. Test setup showing spheres being placed into pressure vessel.

Visual inspection of the specimens after testing indicated three types of failure: failure of the equatorial joint, failure by buckling of the liner, or failure by yielding of the liner. Although the concrete showed, and perhaps influenced, the type of failure, only steel failure modes were classified because these could be identified after the tests. Table 2 summarizes the types of failure which the specimens exhibited; in some cases, a specimen showed two types of failure. Postimplosion views of the specimens are shown in Appendix A.

Table 2. Failure Pressures

Specimen Designation	Failure Pressure (psi)	Type of Failure		
		Joint	Buckling	Yield
I020	2,810		X	
I060	3,480	X		
I120-1	4,630		X	
I120-2	3,450	X		
ϕ060	3,605		X	
ϕ120-1	4,910	X		
ϕ120-2	4,260	X	X	
D060	6,100			X
D120	13,360			X
Unreinforced concrete spheres	2,820[a]			

[a] Calculated using Equation 1.

Of particular interest is specimen D120; this sphere underwent three cycles of load in an attempt to reach failure pressure. The epoxy adhesive at the joint leaked at 9,800 psi for the first cycle and 10,350 psi for the second cycle; after each cycle the joint was completely reconstructed. Prior to the third (and final) cycle, efforts were made to prevent the joint from leaking, even though the epoxy adhesive might fail. The third effort was successful; the sphere failed by yielding of the steel liner at 13,360 psi.

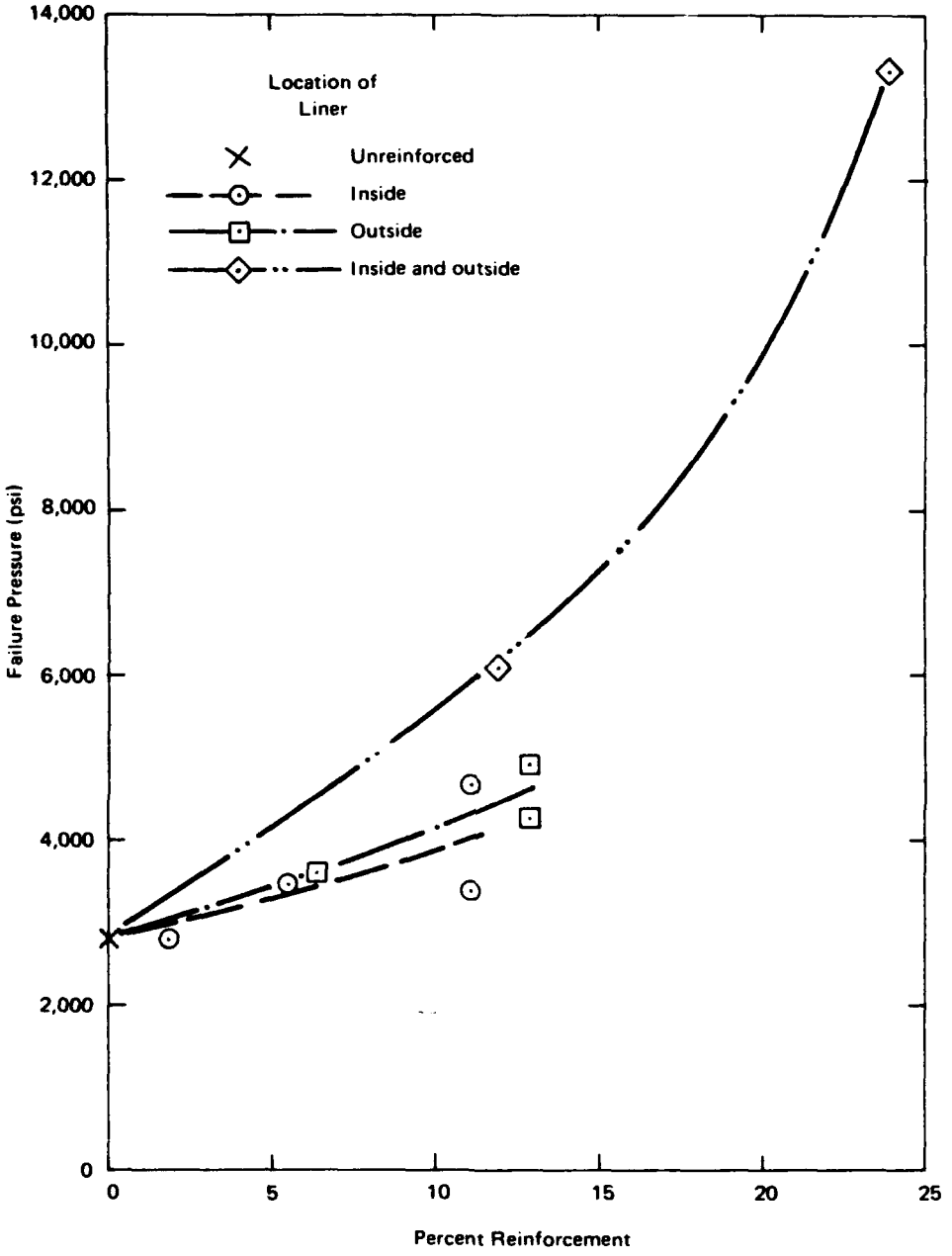

Figure 5. Failure pressures of reinforced concrete spherical hulls.

The effect of steel liner reinforcement on the pressure–strain behavior of the specimens is shown in Figures 6 and 7. In general, stiffness and ultimate strain increased with greater percentages of reinforcement.

Of the three specimens having approximately 12% reinforcement, the best structural behavior was exhibited by the double-lined sphere, D060. It is evident that the optimum placement of steel liner reinforcement is on both sides of the sphere, as opposed to placing all the reinforcement on either the inside or outside of the sphere.

ANALYSIS OF RESULTS

Stresses at Failure

Stresses in the concrete and steel were calculated using Lamé's classical elastic theory developed for multilayered spheres (Appendix B). Table 3 gives the stresses at failure for the concrete and steel materials. The stresses in the concrete are compared to the uniaxial compressive strength of the concrete obtained from 3 x 6-inch control cylinders; the comparison shows that the concrete wall was stressed at failure near its ultimate uniaxial strength. However, the concrete in the sphere should have been capable of resisting higher stresses than the uniaxial strength because of the multiaxial loading condition in the wall. Unreinforced concrete spheres show a 35% increase in material strength under multiaxial loading conditions; hence, in a reinforced sphere, the strength should be capable of increasing even more because of the additional confinement of the concrete.

Calculated stresses in the steel liners did not approach the yield strength of the steel, except for specimen D120 which showed a yield-type of failure (Figure A-3). Specimen D60 was the only other specimen which showed a yield-type failure.

Buckling Pressures of Liners

The pressures that would cause buckling of unrestrained, near perfect steel spheres were calculated using the following modified elastic equation.[8]

$$P_c = \frac{1.4\,E\left(\frac{t}{r_o}\right)^2}{\sqrt{3(1-\nu^2)}} \qquad (2)$$

where P_c = critical buckling pressure

E = modulus of elasticity

ν = Poisson's ratio

t = thickness

r_o = outside radius

Table 3. Stresses at Failure

Specimen Designation	Concrete			Calculated Stress in Steel[a, c] (psi)	
	Calculated Stress at Failure[a] (psi)	Experimental Compressive Strength,[b] f'_c (psi)	Calculated / Experimental	Inside Liner	Outside Liner
I020	9,600	9,530	1.01	154,500	–
I060	8,390	9,870	0.85	121,910	–
I120-1	8,030	9,420	0.85	162,000	–
I120-2	5,820	9,180	0.63	90,000	–
ϕ060	8,705	9,610	0.91	–	122,400
ϕ120-1	8,330	9,410	0.88	–	162,000
ϕ120-2	7,510	9,420	0.80	–	102,000
D060	9,715	10,290	0.95	152,400	134,830
D120	12,550	9,530	1.32	211,240	175,600
Unreinforced concrete spheres	12,700	9,580	1.33	–	–

[a] Using Lamé equations presented in Appendix B.

[b] For six 3 x 6-inch control cylinders tested under uniaxial compression; control cylinders corresponded to weakest hemisphere.

[c] Yield strength of steel was 200,000 psi.

Table 4 compares the calculated buckling pressures to the experimental pressures. The specimens having a 60-mil or less liner thickness were restrained from buckling by the presence of the concrete. The specimens having a 120-mil-thick liner failed at lower pressures than the calculated buckling pressure.

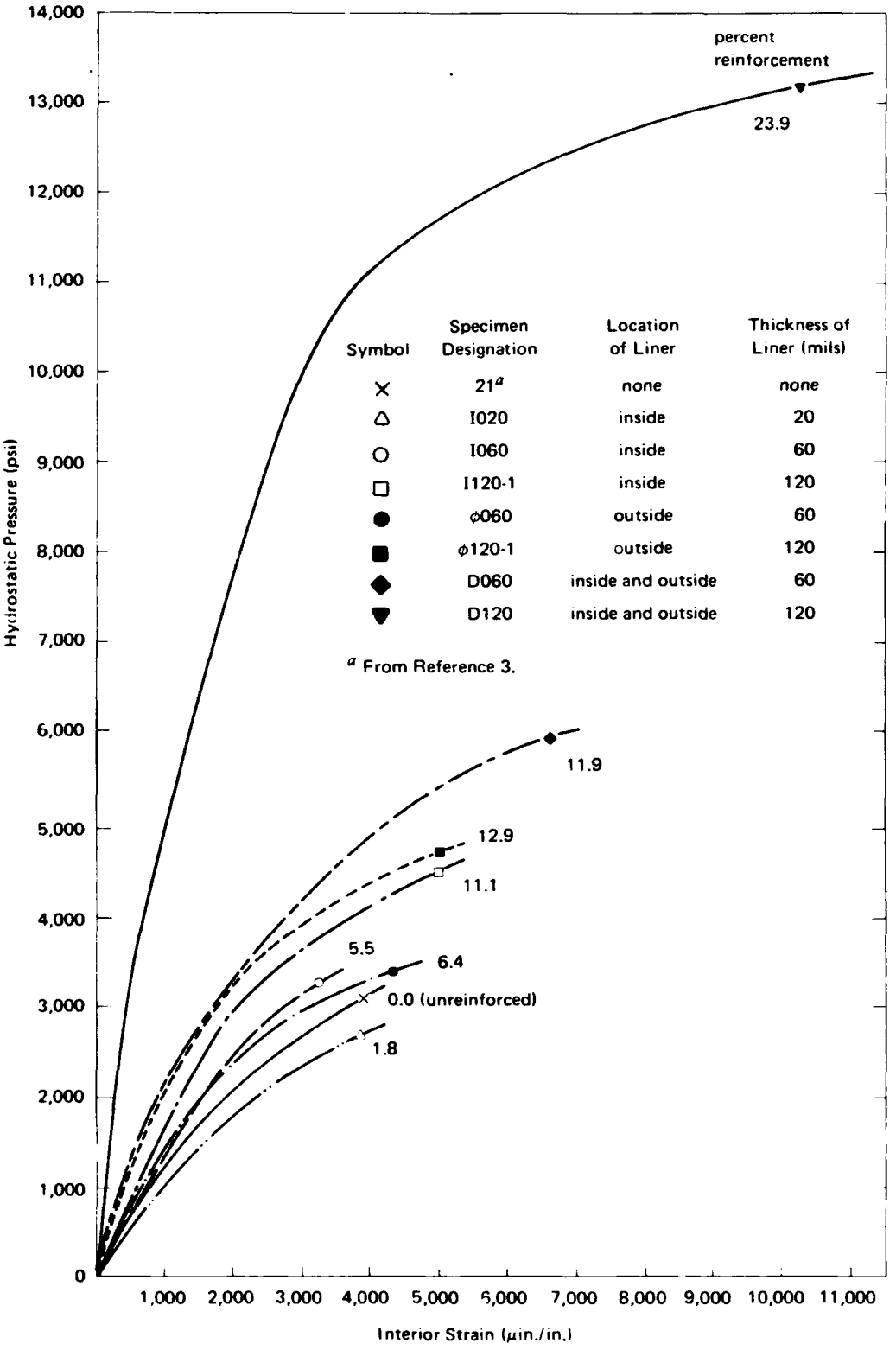

Figure 6. Interior strain behavior for specimens having various percentages of steel reinforcement.

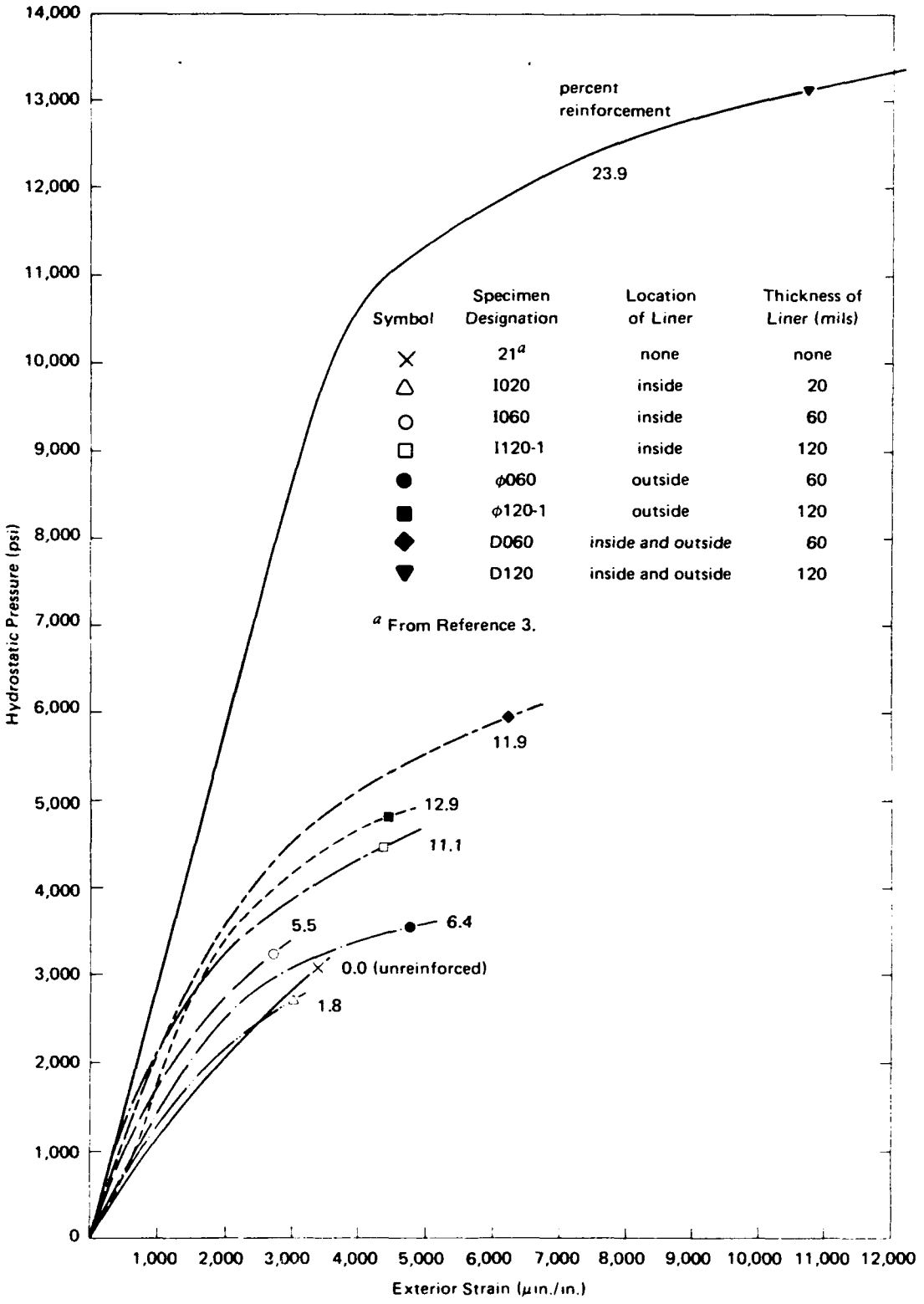

Figure 7. Exterior strain behavior for specimens having various percentages of steel reinforcement.

Table 4. Buckling Pressures for Steel Liners

Specimen Designation	Inside Liner			Outside Liner		
	Calculated Buckling Pressure[a] (psi)	Experimental Pressure[b] (psi)	Experimental / Calculated	Calculated Buckling Pressure[a] (psi)	Experimental Pressure[b] (psi)	Experimental / Calculated
I020	206	980	4.75	–	–	–
I060	1,867	1,950	1.05	–	–	–
I120-1	7,530	3,097	0.41	–	–	–
I120-2	7,530	2,145	0.28	–	–	–
ϕ060	–	–	–	1,400	1,697	1.21
ϕ120-1	–	–	–	5,579	3,092	0.55
ϕ120-2	–	–	–	5,579	2,430	0.44
D060	1,867	2,556	1.37	1,400	1,960	1.40
D120	7,530	6,690	0.89	5,579	5,230	0.94

[a] Using Equation 2.

[b] Differential pressure on liner; calculated using Lamé equations.

To summarize the behavior of the spheres, at pressures lower than 50% of the failure pressure, the reinforced spheres conformed to elastic behavior. At greater pressures, the spheres exhibited inelastic behavior. For the sphere reinforced with a liner 20 mils thick, no improvement in behavior over that of unreinforced spheres was observed. For the spheres reinforced with liners 60 mils thick, the liners resisted loadings beyond their buckling pressures because of the restraint provided by the concrete. For most of the spheres reinforced with liners 120 mils thick, failure was probably premature because of joint problems.

Prediction of Failure

Two methods were used to predict failure pressures of the reinforced spheres. The first method was to sum the individual failure pressures of the concrete and steel spheres; the second method was to use Lamé's equations with a defined failure criteria.

The sum-of-parts method adds the buckling pressures of the steel liners to the concrete sphere implosion pressure to equal a predicted failure pressure. Table 5 shows that the predicted pressures are considerably higher than the experimental pressures, except for specimen D060. More important, the table shows that for spheres with a single 120-mil-thick liner, the steel liner by itself should have been capable of resisting considerably higher pressures than those actually resisted by the reinforced spheres. Therefore, it may not be practical to use steel liners with a liner-thickness-to-total-wall-thickness ratio of approximately 0.10 or greater as reinforcement for concrete spheres. However, it is practical to use single or double liners with a liner-thickness-to-total-wall-thickness ratio greater than 0.02 but less than 0.06, because higher failure pressures are attained than either the concrete or steel spheres could attain individually.

The second method to predict failure pressures used classical Lamé equations for thick-walled spheres in conjunction with the following assumptions: (1) continuity of radial and tangential displacements existed at the interfaces of the concrete and steel layers, (2) failure occurred when the strain reached 3,000 μin./in. in the concrete* or 6,400 μin./in. in the steel,** and (3) a trilinear modulus of elasticity*** for the concrete modeled the stress–strain behavior of the uniaxially loaded control cylinders. Appendix B presents the Lamé Equations and the computer program used to calculate

---

* Ultimate strength design limit for strain in concrete, Building Code Requirements for Reinforced Concrete, ACI Standard 318-71, American Concrete Institute, 1971.

** Strain at 2% off-set yield for A4130 steel.

*** Obtained from 3 x 6-inch control cylinder stress–strain curves using the procedure given in Appendix A of Reference 9. Trilinear modulus of elasticity values were 3.56, 1.93, and 1.50 x 10^6 psi for the following strain ranges of 0 to 1,500, 1,500 to 2,500, and 2,500 μin./in. to ultimate strain, respectively.

the failure pressures. Table 6, which gives the predicted failure pressures, shows that the predicted pressures were an average 6% greater than experimental for the reinforced spheres with inside or outside liners and 38% less than experimental for the reinforced spheres with double liners. In general, Lame's equations predicted failure pressures with fair accuracy.

Table 5. Predicted Failure Pressures By Sum-Of-Parts Method

Specimen	Predicted Failure Pressure (psi)			Experimental Failure Pressure (psi)	Experimental / Predicted
	Steel[a]	Concrete[b]	Total		
I020	206	2,820	3,026	2,810	0.93
I060	1,867	2,820	4,687	3,480	0.74
I120-1	7,530	2,820	10,350	4,630	0.45
I120-2	7,530	2,820	10,350	3,450	0.33
ϕ060	1,400	2,820	4,220	3,605	0.86
ϕ120-1	5,579	2,820	8,399	4,910	0.59
ϕ120-2	5,579	2,820	8,399	4,260	0.50
D060	3,267[c]	2,820	6,087	6,100	1.00
D120	13,109[c]	2,820	15,929	13,360	0.84

[a] Calculated buckling pressures from Table 4.

[b] Calculated from Equation 1.

[c] Sum of buckling pressure for inside and outside liner.

Table 6. Predicted Failure Pressures by Lame Equations

Specimen Designation	Predicted Failure Pressure (psi)	Experimental Failure Pressure (psi)	Experimental / Predicted
I020	2,413	2,810	1.16
I060	3,568	3,480	0.98
I120-1	5,275	4,630	0.87
I120-2	5,275	3,450	0.65
ϕ060	3,400	3,605	1.06
ϕ120-1	4,923	4,910	1.00
ϕ120-2	4,923	4,260	0.87
D060	5,165	6,100	1.18
D120	8,476	13,360	1.58

FINDINGS

1. The reinforced concrete sphere having a 20-mil-thick steel liner (percent reinforcement of 1.8) showed essentially no improvement in structural behavior over unreinforced concrete spheres.

2. Reinforced concrete spheres having 60-mil-thick steel liners (liner-thickness-to-total-wall-thickness ratio of approximately 0.06) and having percentages of steel reinforcement between 5.5 and 11.9 showed improvements in structural behavior over unreinforced spheres. Average increases in the failure pressures over unreinforced spheres were 26% for inside or outside liner reinforcement and 117% for double liner (liner on inside and outside) reinforcement.

3. Reinforced concrete spheres having 120-mil-thick steel liners (liner-thickness-to-total-wall-thickness ratio of approximately 0.10) and having percentages of steel reinforcement between 11.1 and 23.9 showed substantially higher failure pressures than those for unreinforced spheres. Average increases in failure pressures over unreinforced spheres were 44% for inside liner reinforcement, 63% for outside liner reinforcement, and 374% for double liner reinforcement.

4. For a nominal 12% reinforcement, the reinforced concrete sphere having a double liner showed an increase in strength of 32 and 25% over the reinforced spheres having an inside or outside liner, respectively.

5. The failure pressures of reinforced concrete spheres can be predicted with an average 10% accuracy for single liner reinforced spheres and 40% accuracy (on conservative side) for double liner reinforced spheres using Lame classical equations.

CONCLUSIONS

There appears to be structural value to reinforcing concrete spherical hulls with steel liners that have a thickness/total wall thickness ratio greater than 0.02 but less than 0.06, because higher external pressures can be resisted by the lined spheres than by the concrete or steel spheres individually. It is recommended that liner reinforcement be placed on both the inside and the outside of the concrete sphere because this type of sandwich construction is more effective than reinforcing only the inside or the outside of the wall.

Appendix A

FAILED SPECIMENS

Figures A-1, A-2, and A-3 show the reinforced concrete spheres after being hydrostatically loaded to failure. Three types of failure are shown by the specimens: failure of the equatorial joint, failure by buckling of the liner, and failure by yield of the liner. Table 2 in the main text categorizes the different types of failure for each specimen.

(a) I020.

(b) I120-1.

(c) I060.

(d) I120-2.

Figure A-1. Postfailure views of specimens having internal liner reinforcement.

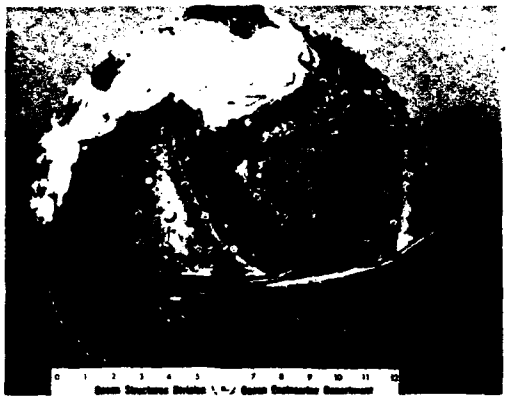

(a) O060.

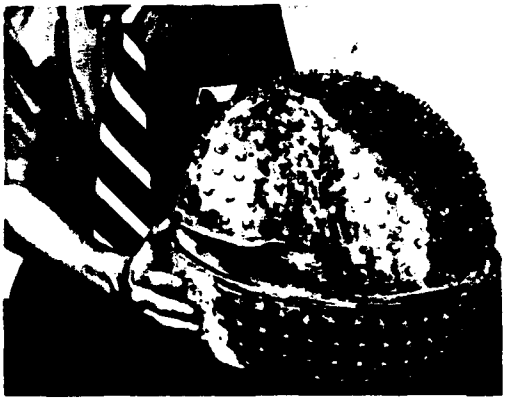

(b) O120-2.

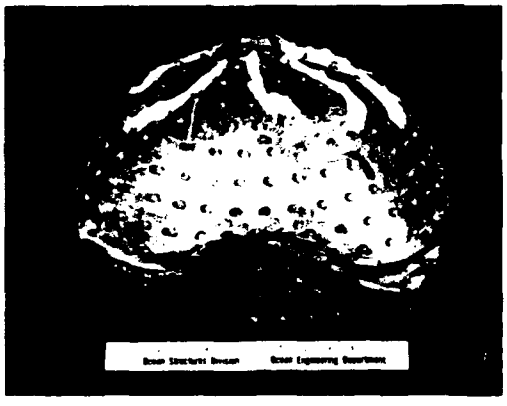

(c) O120-1.

Figure A-2. Postfailure views of specimens having external liner reinforcement.

(a) D060.

(b) D120.

Figure A-3. Postfailure views of specimens having double liner reinforcement.

Appendix B

LAMÉ EQUATIONS APPLIED TO MULTILAYERED SPHERES

Lamé's equations in their general form are:

$$\sigma_t = \frac{-p\, r_o^3 (r_i^3 + 2\, r^3)}{2\, r^3 (r_o^3 - r_i^3)} \qquad \text{(B-1)}$$

and

$$\sigma_r = \frac{-p\, r_o^3 (r^3 - r_i^3)}{r^3 (r_o^3 - r_i^3)} \qquad \text{(B-2)}$$

where σ_t = tangential stress

σ_r = *radial stress*

p = external pressure

r_i = internal radius

r_o = external radius

r = radius to point of examination

Using Equations B-1 and B-2 with the following elastic strain equations

$$\epsilon_t = \frac{1}{E}\left[\sigma_t - \nu(\sigma_t + \sigma_r)\right] \qquad \text{(B-3)}$$

and

$$\epsilon_r = \frac{1}{E}\left(\sigma_r - 2\nu\sigma_t\right) \qquad \text{(B-4)}$$

where ϵ_t = tangential strain

ϵ_r = radial strain

E = modulus of elasticity

ν = Poisson's ratio

enables one to calculate the stresses, strains, or pressures acting on the sphere.

As an example of how the equations apply to multilayered spheres, the appropriate equations are presented for a reinforced sphere with an outer liner.

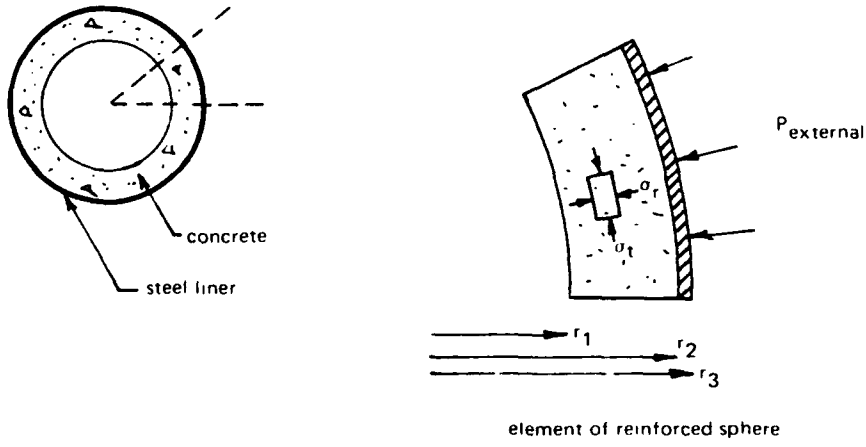

element of reinforced sphere

For the concrete sphere, $r_1 < r < r_2$

$$\sigma_t = \frac{-P_1 r_2^3 (r_1^3 + 2r^3)}{2r^3 (r_2^3 - r_1^3)} \qquad \text{(B-5)}$$

$$\sigma_r = \frac{-P_1 r_2^3 (r^3 - r_1^3)}{r^3 (r_2^3 - r_1^3)} \qquad \text{(B-6)}$$

$$\epsilon_t = \frac{1}{E_1} [\sigma_t - \nu_1 (\sigma_t + \sigma_r)] \qquad \text{(B-7)}$$

$$\epsilon_r = \frac{1}{E_1} (\sigma_r - 2\nu_1 \sigma_t) \qquad \text{(B-8)}$$

At interior surface where $r = r_1$

$$P_1 = -(\epsilon_t)_1 E_1 \left[\frac{2(r_2^3 - r_1^3)}{3r_2^3 (1 - \nu_1)}\right] \qquad \text{(B-9)}$$

For the steel sphere, $r_2 < r < r_3$

$$\sigma_t = \frac{-P_2 r_3^3 (r_2^3 + 2r^3)}{2r^3 (r_3^3 - r_2^3)} + \frac{P_1 r_2^3 (r_3^3 + 2r^3)}{2r^3 (r_3^3 - r_2^3)} \tag{B-10}$$

$$\sigma_r = \frac{-P_2 r_3^3 (r^3 - r_2^3)}{r^3 (r_3^3 - r_2^3)} + \frac{-P_1 r_2^3 (r_3^3 - r^3)}{r^3 (r_3^3 - r_2^3)} \tag{B-11}$$

$$\epsilon_t = \frac{1}{E_2} [\sigma_t - \nu_2 (\sigma_t + \sigma_r)] \tag{B-12}$$

$$\epsilon_r = \frac{1}{E_2} (\sigma_r - 2\nu_2 \sigma_t) \tag{B-13}$$

By equating $(\epsilon_t)_{2c}$ and $(\epsilon_t)_{2s}$, one obtains:

$$P_2 = P_1 \left[\frac{2(r_3^3 - r_2^3)}{3r_3^3 (1 - \nu_2)}\right] \left\{ \frac{r_3^3 + 2r_2^3}{2(r_3^3 - r_2^3)} (1 - \nu_2) + \nu_2 + \frac{E_2}{E_1} \left[\frac{r_1^3 + 2r_2^3}{2(r_2^3 - r_1^3)} (1 - \nu_1) - \nu_1 \right] \right\} \tag{B-14}$$

where P_1 = pressure acting on exterior of first layer (concrete)

P_2 = pressure acting on exterior of second layer (steel)

E_1 = modulus of elasticity of material in first layer (concrete)

E_2 = modulus of elasticity of material in second layer (steel)

$(\epsilon_t)_1$ = tangential strain on interior of first layer (concrete)

$(\epsilon_t)_{2c}$ = tangential strain on exterior of first layer (concrete)

$(\epsilon_t)_{2s}$ = tangential strain on interior of second layer (steel)

ν_1 = Poisson's ratio of material in first layer (concrete)

ν_2 = Poisson's ratio of material in second layer (steel)

r = radius to point of examination

r_1 = radius to interior of first layer

r_2 = radius to interior of second layer

r_3 = radius to exterior of second layer

A computer program, Figure B-1, was developed to calculate the stresses, strains, and pressures in each layer of the reinforced spheres. Initially, a small interior tangential strain is applied, and the Lamé equations are used to calculate the exterior pressure necessary to produce such a strain. Using the calculated pressures, the tangential and radial stresses and strains across the thickness of each material is calculated.

When the strain in the concrete or the steel reached 3,000 or 6,400 μin./in., respectively, the external pressure was defined as failure pressure.

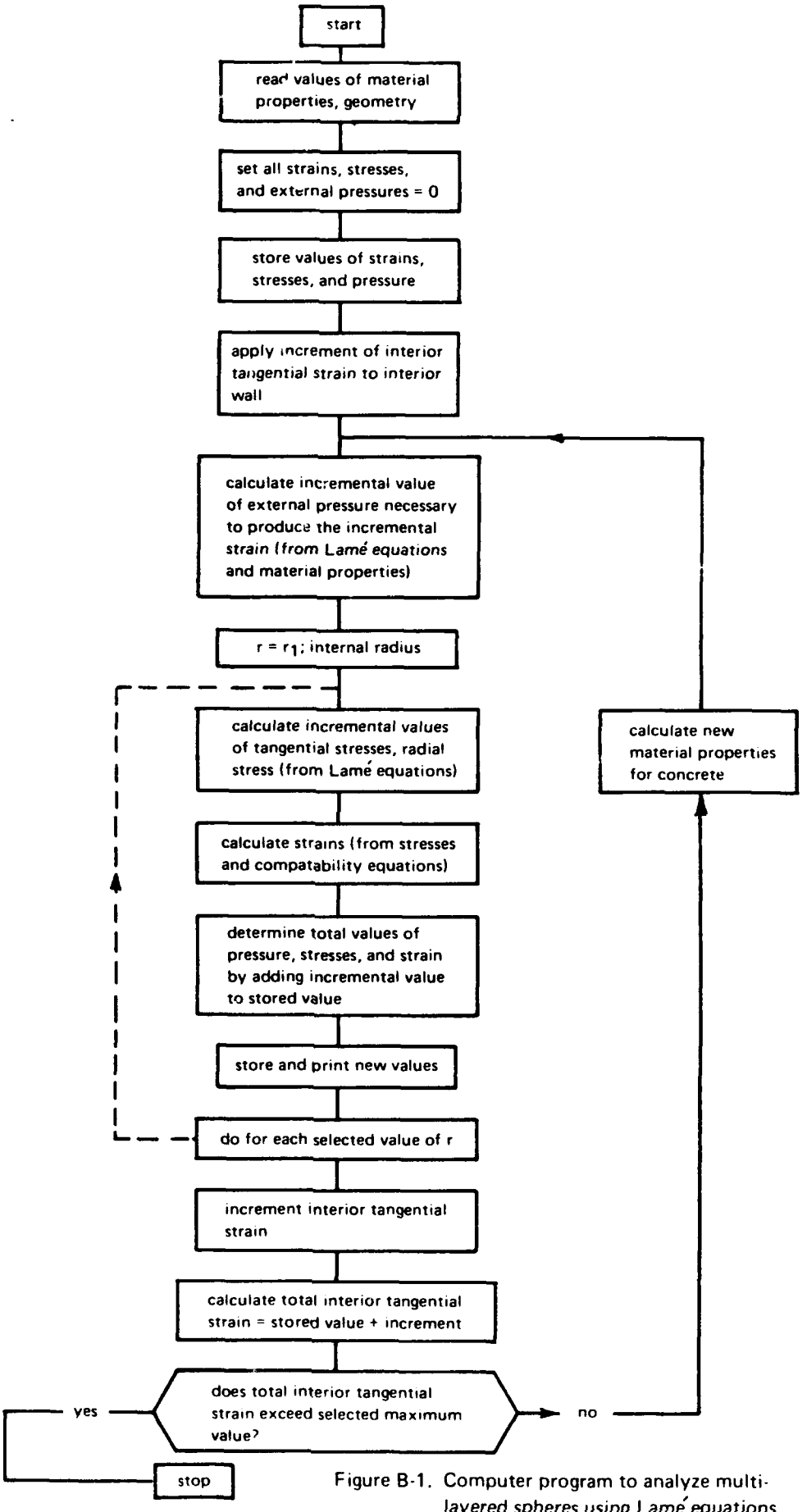

Figure B-1. Computer program to analyze multi-layered spheres using Lamé equations.

REFERENCES

1. Naval Civil Engineering Laboratory. Technical Report R-517: Behavior of spherical concrete hulls under hydrostatic loading, pt. 1. Exploratory investigation, by J. D. Stachiw and K. O. Gray. Port Hueneme, Calif., Mar 1967. (AD 649290)

2.———. Technical Report R-547: Behavior of spherical concrete hulls under hydrostatic loading, pt. 2. Effect of penetrations, by J. D. Stachiw. Port Hueneme, Calif., Oct 1967. (AD 661187)

3.———. Technical Report R-588: Behavior of spherical concrete hulls under hydrostatic loading, pt. 3. Relationship between thickness-to-diameter ratio and critical pressures, strains, and water penetration rates, by J. D. Stachiw and K. Mack. Port Hueneme, Calif., Jun 1968. (AD 835492L)

4.———. Technical Report R-679: Failure of thick-walled concrete spheres subjected to hydrostatic loading, by H. H. Haynes and R. A. Hoofnagle. Port Hueneme, Calif., May 1970. (AD 708011)

5.———. Technical Report R-735: Influence of stiff equatorial rings on concrete spherical hulls subjected to hydrostatic loading, by L. F. Kahn and J. D. Stachiw. Port Hueneme, Calif., Aug. 1971. (AD 731352)

6.———. Technical Report R-774: Behavior of 66-inch concrete spheres under short and long term hydrostatic loading, by H. H. Haynes and L. F. Kahn. Port Hueneme, Calif., Sep 1972. (AD 748584)

7. H. H. Haynes and L. F. Kahn. "Experimental studies on concrete spherical shells under hydrostatic loading," paper presented at Symposium on Hydromechanically Loaded Shells, International Association for Shell Structures, Honolulu, Hawaii, Oct. 10-15, 1971. (Preprint no. 8-7; proceedings to be published 1973)

8. David Taylor Model Basin. Report 1713: The elastic buckling strength of near-perfect deep spherical shells with ideal boundaries, by M. A. Krenzke. Washington, D.C., Jul 1963. (AD 416057)

9. Naval Civil Engineering Laboratory. Technical Report R-740: Influence of end-closure stiffness on behavior of concrete cylindrical hulls subjected to hydrostatic loading, by L. F. Kahn. Port Hueneme, Calif., Oct 1971. (AD 732363)

DISTRIBUTION LIST

SNDL Code	No. of Activities	Total Copies	
–	1	12	Defense Documentation Center
FKAIC	1	10	Naval Facilities Engineering Command
FKNI	6	6	NAVFAC Engineering Field Divisions
FKN5	9	9	Public Works Centers
FA25	1	1	Public Works Center
–	9	9	RDT&E Liaison Officers at NAVFAC Engineering Field Divisions and Construction Battalion Centers
–	291	291	NCEL Special Distribution List No. 11 for persons and activities interested in reports on Ocean Engineering

Naval Civil Engineering Laboratory
HYDROSTATIC LOADING OF CONCRETE SPHERICAL HULLS REINFORCED WITH STEEL LINERS (Final), by H. H. Haynes, G. L. Page, and R. J. Ross
TR-785 27 p. illus April 1973 Unclassified

1. Reinforced concrete spheres 2. Underwater structures I. 3.1610-1D

Nine model concrete spheres reinforced with steel liners located on the inside, outside, or both inside and outside were tested to failure under hydrostatic loading. The quantity of reinforcement varied from 1.8 to 23.9% by area; for this range of reinforcement, the spheres showed increases in failure pressure from 0 to 374% over that of unreinforced concrete spheres (2,810 psi). Using a nominal 12% reinforcement, it was found that the best reinforcing method was to place liners on both the inside and outside of the wall.

Naval Civil Engineering Laboratory
HYDROSTATIC LOADING OF CONCRETE SPHERICAL HULLS REINFORCED WITH STEEL LINERS (Final), by H. H. Haynes, G. L. Page, and R. J. Ross
TR-785 27 p. illus April 1973 Unclassified

1. Reinforced concrete spheres 2. Underwater structures I. 3.1610-1D

Nine model concrete spheres reinforced with steel liners located on the inside, outside, or both inside and outside were tested to failure under hydrostatic loading. The quantity of reinforcement varied from 1.8 to 23.9% by area; for this range of reinforcement, the spheres showed increases in failure pressure from 0 to 374% over that of unreinforced concrete spheres (2,810 psi). Using a nominal 12% reinforcement, it was found that the best reinforcing method was to place liners on both the inside and outside of the wall.

Naval Civil Engineering Laboratory
HYDROSTATIC LOADING OF CONCRETE SPHERICAL HULLS REINFORCED WITH STEEL LINERS (Final), by H. H. Haynes, G. L. Page, and R. J. Ross
TR-785 27 p. illus April 1973 Unclassified

1. Reinforced concrete spheres 2. Underwater structures I. 3.1610-1D

Nine model concrete spheres reinforced with steel liners located on the inside, outside, or both inside and outside were tested to failure under hydrostatic loading. The quantity of reinforcement varied from 1.8 to 23.9% by area; for this range of reinforcement, the spheres showed increases in failure pressure from 0 to 374% over that of unreinforced concrete spheres (2,810 psi). Using a nominal 12% reinforcement, it was found that the best reinforcing method was to place liners on both the inside and outside of the wall.

Naval Civil Engineering Laboratory
HYDROSTATIC LOADING OF CONCRETE SPHERICAL HULLS REINFORCED WITH STEEL LINERS (Final), by H. H. Haynes, G. L. Page, and R. J. Ross
TR-785 27 p. illus April 1973 Unclassified

1. Reinforced concrete spheres 2. Underwater structures I. 3.1610-1D

Nine model concrete spheres reinforced with steel liners located on the inside, outside, or both inside and outside were tested to failure under hydrostatic loading. The quantity of reinforcement varied from 1.8 to 23.9% by area; for this range of reinforcement, the spheres showed increases in failure pressure from 0 to 374% over that of unreinforced concrete spheres (2,810 psi). Using a nominal 12% reinforcement, it was found that the best reinforcing method was to place liners on both the inside and outside of the wall.

Naval Civil Engineering Laboratory
HYDROSTATIC LOADING OF CONCRETE SPHERICAL HULLS REINFORCED WITH STEEL LINERS (Final), by H. H. Haynes, G. L. Page, and R. J. Ross
TR-785 27 p. illus April 1973 Unclassified

1. Reinforced concrete spheres 2. Underwater structures I. 3.1610-1D

Nine model concrete spheres reinforced with steel liners located on the inside, outside, or both inside and outside were tested to failure under hydrostatic loading. The quantity of reinforcement varied from 1.8 to 23.9% by area; for this range of reinforcement, the spheres showed increases in failure pressure from 0 to 374% over that of unreinforced concrete spheres (2,810 psi). Using a nominal 12% reinforcement, it was found that the best reinforcing method was to place liners on both the inside and outside of the wall.

Naval Civil Engineering Laboratory
HYDROSTATIC LOADING OF CONCRETE SPHERICAL HULLS REINFORCED WITH STEEL LINERS (Final), by H. H. Haynes, G. L. Page, and R. J. Ross
TR-785 27 p. illus April 1973 Unclassified

1. Reinforced concrete spheres 2. Underwater structures I. 3.1610-1D

Nine model concrete spheres reinforced with steel liners located on the inside, outside, or both inside and outside were tested to failure under hydrostatic loading. The quantity of reinforcement varied from 1.8 to 23.9% by area; for this range of reinforcement, the spheres showed increases in failure pressure from 0 to 374% over that of unreinforced concrete spheres (2,810 psi). Using a nominal 12% reinforcement, it was found that the best reinforcing method was to place liners on both the inside and outside of the wall.

Naval Civil Engineering Laboratory
HYDROSTATIC LOADING OF CONCRETE SPHERICAL HULLS REINFORCED WITH STEEL LINERS (Final), by H. H. Haynes, G. L. Page, and R. J. Ross
TR-785 27 p. illus April 1973 Unclassified

1. Reinforced concrete spheres 2. Underwater structures I. 3.1610-1D

Nine model concrete spheres reinforced with steel liners located on the inside, outside, or both inside and outside were tested to failure under hydrostatic loading. The quantity of reinforcement varied from 1.8 to 23.9% by area; for this range of reinforcement, the spheres showed increases in failure pressure from 0 to 374% over that of unreinforced concrete spheres (2,810 psi). Using a nominal 12% reinforcement, it was found that the best reinforcing method was to place liners on both the inside and outside of the wall.

Naval Civil Engineering Laboratory
HYDROSTATIC LOADING OF CONCRETE SPHERICAL HULLS REINFORCED WITH STEEL LINERS (Final), by H. H. Haynes, G. L. Page, and R. J. Ross
TR-785 27 p. illus April 1973 Unclassified

1. Reinforced concrete spheres 2. Underwater structures I. 3.1610-1D

Nine model concrete spheres reinforced with steel liners located on the inside, outside, or both inside and outside were tested to failure under hydrostatic loading. The quantity of reinforcement varied from 1.8 to 23.9% by area; for this range of reinforcement, the spheres showed increases in failure pressure from 0 to 374% over that of unreinforced concrete spheres (2,810 psi). Using a nominal 12% reinforcement, it was found that the best reinforcing method was to place liners on both the inside and outside of the wall.

Unclassified

Security Classification

DOCUMENT CONTROL DATA - R & D

Security classification of title, body of abstract and indexing annotation must be entered when the overall report is classified)

1. ORIGINATING ACTIVITY *(Corporate author)*

Naval Civil Engineering Laboratory
Port Hueneme, California 93043

2a. REPORT SECURITY CLASSIFICATION

Unclassified

2b. GROUP

3. REPORT TITLE

HYDROSTATIC LOADING OF CONCRETE SPHERICAL HULLS REINFORCED WITH STEEL LINERS

4. DESCRIPTIVE NOTES *(Type of report and inclusive dates)*

Final; July 1969 – June 1971

5. AUTHOR(S) *(First name, middle initial, last name)*

H. H. Haynes, G. L. Page, and R. J. Ross

6. REPORT DATE	7a. TOTAL NO. OF PAGES	7b. NO. OF REFS
April 1973	27	9

8a. CONTRACT OR GRANT NO.	9a. ORIGINATOR'S REPORT NUMBER(S)
b. PROJECT NO. 3.1610-1D	TR-785
c.	9b. OTHER REPORT NO(S) *(Any other numbers that may be assigned this report)*
d.	

10. DISTRIBUTION STATEMENT

Approved for public release; distribution unlimited.

11. SUPPLEMENTARY NOTES	12. SPONSORING MILITARY ACTIVITY
	Naval Facilities Engineering Command Washington, D.C. 20390

13. ABSTRACT

Nine model concrete spheres reinforced with steel liners located on the inside, outside, or both inside and outside were tested to failure under hydrostatic loading. The quantity of reinforcement varied from 1.8 to 23.9% by area; for this range of reinforcement, the spheres showed increases in failure pressure from 0 to 374% over that of unreinforced concrete spheres (2,810 psi). Using a nominal 12% reinforcement, it was found that the best reinforcing method was to place liners on both the inside and outside of the wall.

14 KEY WORDS	LINK A		LINK B		LINK C	
	ROLE	WT	ROLE	WT	ROLE	WT
Concrete						
Underwater construction						
Pressure-resistant structures						
Reinforced concrete						
Steel liners						
Continuous liners						
Spherical structures						
Inside steel liner						
Outside steel liner						
Double steel liner						
Hydrostatic pressure						
Failure pressures						
Stresses						
Strains						
Lamé equations						
Compressive strength						